Effect of clay and material additives on forward combustion of crude oil

Safar, Fadhel S. A.

Award date:
1987

Awarding institution:
University of Bath

EFFECT OF CLAY AND MATERIAL ADDITIVES

ON FORWARD COMBUSTION OF CRUDE OIL

Submitted by Fadhel S.A. Safar

for the degree of Doctor of Philosophy

of the University of Bath

1987

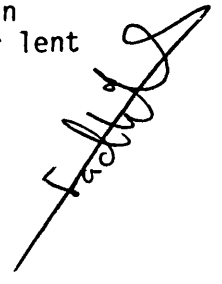

ProQuest LLC
789 East Eisenhower Parkway
P.O. Box 1346
Ann Arbor, MI 48106-1346

Dedicated to the author's parents

ACKNOWLEDGEMENTS

I am sincerely grateful to Dr. M. Greaves for his supervision and valuable assistance during the course of this study. My thanks are also extended to Dr. R.W. Field for his co-operation and keen interest in the progress of the work.

I gratefully acknowledge the scholarship from the Kuwait Oil Company and the Study Leave Committee members. Appreciation is expressed to the Production Development Group management. The financial and technical support of the British Petroleum Research Centre (Sunbury-on-Thames) is very much appreciated.

I am grateful to the technicians of the University of Bath - Mr. Tom Walton, Mr. Geoffrey Venn and Mr. John Bishop - for their beneficial assistance at various times. I also wish to thank Dr. Salah Ali for his reviewing and useful discussions. I am grateful to fellow postgraduate students for discussions and encouragement. I should also like to thank Mrs. Paula Keilthy for typing the thesis.

Finally, I owe a great debt of gratitude to my family for their prayers and moral support, and to close friends for their best wishes.

ABSTRACT

The effect of additives in the *in situ* combustion operation has been studied using a combustion tube apparatus equipped for use with air and enriched air up to 35% oxygen. The range of additives included Kaolin (also in acidised form), amorphous silica, natural core material, ferric oxide and nickel chloride. Experiments were made on three crude oils, namely, Maya Isthmus, Maya, and Cold Lake. A weight ratio of crude oil to sand of 7% wt provided an oil saturation of 36.7% -42.4%. The porosity of mixture varied from 29.1 - 39.6%. A total of 20 combustion tube experiments were conducted at a maximum pressure of 50 psig and an air flux of 14.57 $m^3(st)/m^2hr$.

Different amounts of clay and amorphous silica were added to the sand mixture ranging up to 15% wt, in order to investigate the influence of the increased surface area on the *in situ* combustion parameters. Consumption of fuel increased as the percentage amount of clay or amorphous silica increased. A higher fuel consumption was achieved using amorphous silica, compared with Kaolin. The nature of the surface area also has a significant effect on the fuel consumption process. For example, the surface area of Kaolin is changed when treated with sulphuric acid, and the higher fuel consumption was achieved under these conditions.

Light Maya Isthmus crude oil (32.4° API) was not able to support a self-sustained combustion front unless the sand pack contained a minimum of 3% wt Kaolin. The medium and heavy crude oils, Maya (22.1° API) and Cold Lake (10.2° API), were however able to sustain stable combustion without the presence of additives. Lower Fars reservoir material also enables stable combustion to be propagated.

Incorporation of the metal compounds ferric oxide and nickel chloride, into the sand matrix produced an increased fuel consumption, but reduced the combustion peak temperature.

Oxygen enrichment to 35% oxygen achieved faster spontaneous ignition, higher combustion temperature and earlier oil recovery.

Nomenclature

°API	American Petroleum Institute gravity: $°API = \frac{141.5}{\text{specific gravity}} - 131.5$.
AFR	Air fuel ratio, m^3 (st)/kg
AOR	Air oil ratio, m^3 (st)/m^3
Cal/g CH_x	Calorie per one gram of fuel
Cal/g sand	Calorie per one gram of sand
COFCAW	Combination of forward combustion and water-flooding
DSC	Differential scanning calorimetry
DTA	Differential thermal analysis
EOR	Enhanced oil recovery
GFR	Gas fuel ratio, m^3/kg
GOR	Gas oil ratio, m^3/kg
LTO	Low temperature oxidation
M	1000 English Engineering Units
m^3 (st)	Standard cubic meter
OOIP	Original oil in place
SEM	Scanning electron microscope
So_i	Initial oil saturation
TGA	Thermogravimetric analysis
WAR	Water air ratio, m^3/Mm^3 (st)
WGR	Water gas ratio, m^3/Mm^3 (st)
Wt	Weight

CONTENTS

CONTENTS (Contd)

CHAPTER 1

Introduction

The term Enhanced Oil Recovery refers to any method used to recover more oil from a petroleum reservoir than would be obtained by primary recovery. In primary recovery the natural reservoir energy is utilised to drive the oil. It may involve evolution of gas from solution, expansion of free gas, and oil influx of natural water, or gravity force.

Secondary oil recovery involves the introduction of energy into a reservoir by injecting gas, water, or chemicals under pressure. The added energy may stimulate the movement of oil, providing additional recovery at increased rates. In addition, the thermal potential of the reservoir can be increased by injecting heat, either directly (steam, hot water), or by generation *in situ*.

In situ combustion is the process of injecting air (or oxygen) into an oil reservoir through selected injection wells first to create communication within the reservoir, and then igniting the crude oil so that a combustion front is propagated towards the production well.

The idea of using underground combustion in order to recover hydrocarbons dates back to the Russian scientist Mendeleev who, in 1888, proposed a method for underground gasification of coal to produce combustible gases (Farouq Ali, 1967). In 1920, in Ohio, USA, a production well was stimulated by initiating combustion in the wellbore by means of oil impregnated materials. The first field test of underground combustion was conducted in the USSR, during 1932-1938. In 1953, the Magnolia Petroleum Company reported laboratory and field test information on the *in situ* combustion process. Shortly afterwards, Grant and Szasz (1954) published results on the "heat wave " process, wherein some of

the produced flue gas is reinjected. Walter (1957) reported on a field test in Illinois involving a combination of steam drive and *in situ* combustion process. Since that time, considerable investigation of the *in situ* combustion process has taken place and many variations of the basic process have been devised.

The process of *in situ* combustion may be operated either in the forward or reverse combustion mode. The latter involves propagation of the combustion front in a direction opposite to that of the gas flow, and is mainly applicable to tar sands. In forward combustion, the combustion front propagates in a direction concurrent to the oxidant stream, *i.e.*, the burning front moves from the injection well to the production well. The *in situ* combustion projects may be either dry or wet, according to whether water is simultaneously injected with the air [Langues and Beeson (1965), Dietz and Weijdema (1968), Parrish *et al.* (1969), and Hughes (1985)].

The operation of *in situ* combustion processes involves initiating air injection into the oil reservoir, as shown in Figure 1.1. Crude oil near the injection well begins to oxidise, and if the rate of oxidation is rapid, ignition occurs spontaneously. If, however, the oxidation rate is too slow, ignition can be achieved by downhole heating on preheating the air.

Following ignition, continuous air injection causes the burning front to move out through the reservoir towards the production well. Combustion gases, together with evaporated liquids, flow ahead and are produced with other fluids. Heat generated at the burning front vaporises formation water, which develops a steam zone downstream. Water from the combustion reactions also contributes to this steam zone. Appreciable quantities of oil are displaced from the steamed region, leaving a relatively low oil

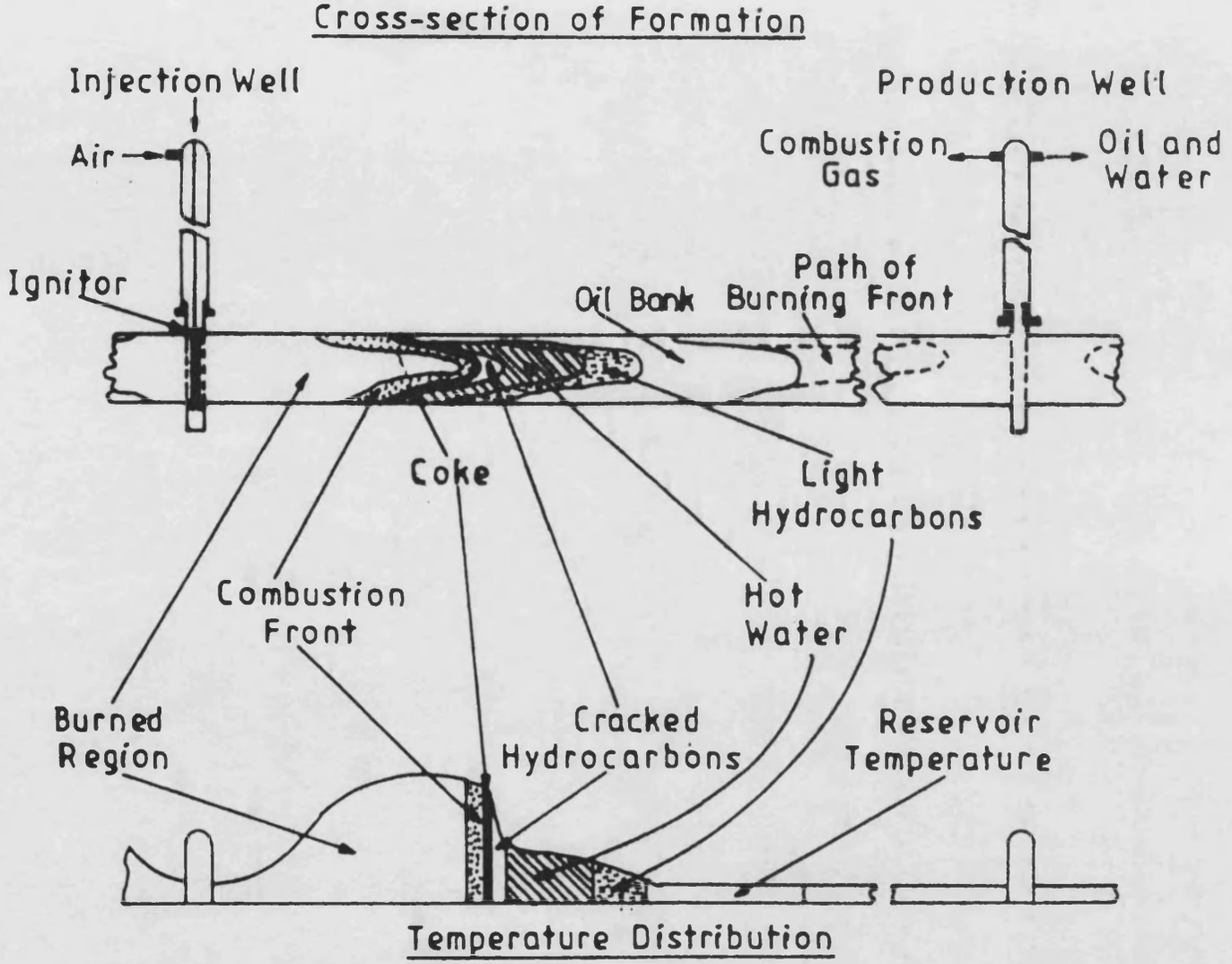

Figure 1.1 Schematic diagram of *in situ* combustion process [P.D. White (1985)].

saturation to be overtaken by the burning front. The high temperature generated at the combustion front vaporises and also cracks the oil, leaving mainly a coke-like residue to be burned, which is formed from the heaviest and least valuable part of the crude oil. Steam condenses in the cooler region of the reservoir and causes the combusting gases to concentrate in the upper region of the structure. Because of this effect, there is a tendency also for the combustion front to follow the gas path. The extent to which the combustion front sweeps the upper part of the oil zone must therefore be recognised in applying *in situ* combustion. When the heat front arrives at the production well, the production rate usually increases due to the reduction in oil viscosity. Figure 1.2 shows the effect of temperature on fluid viscosity, indicating that a very significant change in heavy oil viscosity can be achieved at relative low temperatures. The change is much less dramatic for the lighter oils and water.

Extensive investigations have been carried out in the laboratory in order to understand the mechanism and chemical reactions governing the *in situ* combustion process [Wilson *et al.* (1958), Berry and Parrish (1960), Showalter (1963), Gottfried (1965), and Dabbous and Fulton (1974)]. One of the major objectives of *in situ* combustion experiments has been to relate the fuel deposition and fuel consumption to other parameters of the process [Martin *et al.* (1958), Alexander *et al.* (1962), Dew *et al.* (1965), and Thomas *et al.* (1979)]. In order to define the physical limits of combustion and to delineate the process variables necessary for successful propagation of a combustion front, several investigators have carried out field pilot tests [Gates and Ramey (1958), Clark *et al.* (1965), and Parrish *et al.* (1974)].

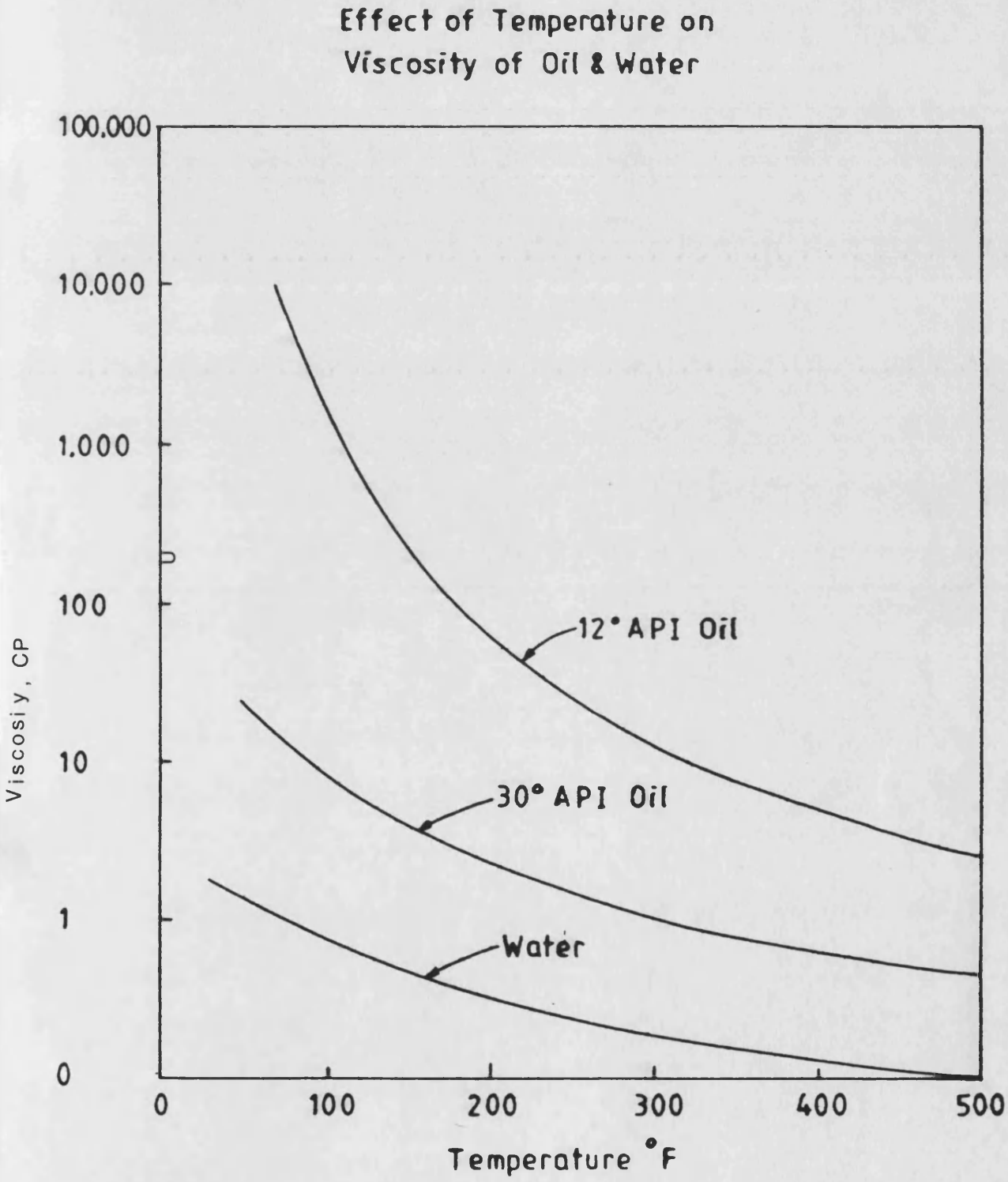

Figure 1.2 Effect of temperature on viscosity of oil and water (Computer Modelling Group, 1982).

Analysis of the reservoir sands has shown that fine particles are invariably present in the formation, often in sufficient quantities seriously to affect oil production. Fine particle solids derived from reservoir sediments and clays can have a wide size distribution and mineral composition [Hardey *et al.* (1972) and Buchwald *et al.* (1973)].

The main objective of the present study was to investigate in a quantitative manner the effect of clay additives on the *in situ* combustion process. These materials possess very high specific surface areas, relative to the surface of the host matrix. They can therefore significantly influence combustion kinetics and fuel laydown. In addition, clay additives and fine solid materials may be catalytically active, and therefore this effect was also investigated.

CHAPTER 2

Porous Media and Crude Oil Properties

The most important controlling factors of the *in situ* combustion process are the nature of the crude oil and reservoir porous media. This chapter is divided into two sections. The first deals with the role of clays in the *in situ* combustion process and the second section describes the characteristics of the crude oils.

2.1 Role of Clays in the *In Situ* Combustion Process

Clays are as grained, natural, earthy, argillaceous material. They are composed of alumina, silica, and water, together with iron, alkalies and alkaline earths. As shown in Figure 2.1, clay minerals consist of two relatively simple building units. These are the silica tetrahedral sheet and the alumina or magnesia octahedral sheet.

In addition to the clay minerals, some clays contain varying amounts of so-called non-clay minerals, typically quartz, calcite, feldspar and pyrite. They may also contain organic material and water-soluble salts.

All clays are negatively charged (Hower, 1974). The density of the negative charge can be measured by determining the number of positive charges required to neutralise the crystal. This is known as the cation exchange capacity of the clay and is expressed in milliequivalents (ME) of 100 grams of clay. Many properties, such as those concerned with optical and infrared characteristics, are particularly important for the identification of the clay minerals.

Other factors such as the crystallinity, surface area, catalytic activity, particle size of clays and solubility in acids and alkalies, may influence the properties of clay materials and may in most instances be more important than clay mineral composition.

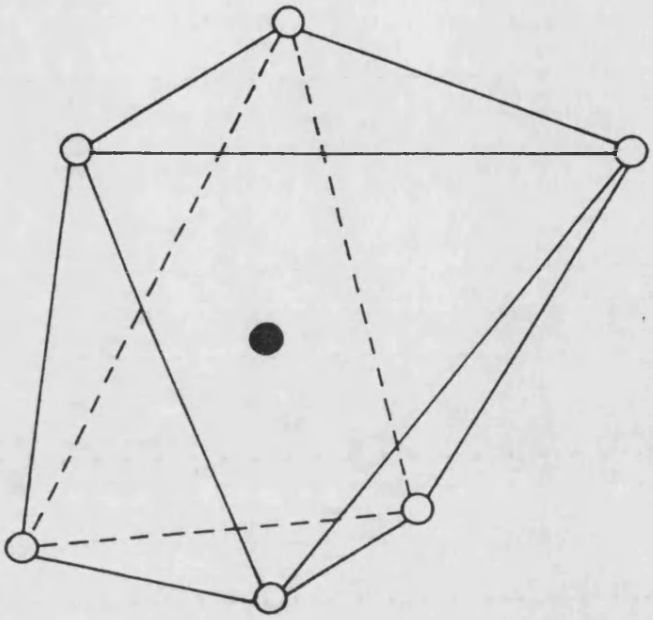

○ : Hydroxyls ● : Aluminium or Magnesium

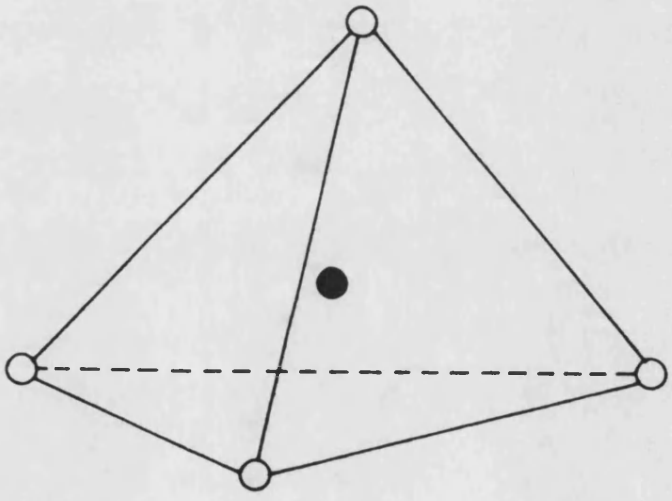

○ : Oxygen ● : Silicone

Figure 2.1 Chemical structure of clay mineral, from Grim (1962) "Applied Clay Mineralogy".

2.1.1 Clays in petroleum reservoir

A petroleum reservoir is a porous strata that is sufficiently permeable to allow fluids to move through it. Fine solid particles are present in the pore spaces of all sand stone reservoirs. Regardless of their origin, it has been recognised that these particles cause severe formation damage. This is because they are not held physically in place, but are free to migrate through the pores depending on the fluid motion and can concentrate at pore restrictions causing severe plugging and large reductions in permeability.

Mineral analysis [Hardy *et al.* (1972)] for May-Libby core material indicates that it contains 76% medium to coarse grain size sand, 13.5% silt and 10.5% clay. The clay fraction was kaolinite, but did contain some montmorillonite, illite, and chlorite. The minerals appeared to be well dispersed throughout the reservoir. Buchwald *et al.* (1973) analysed a reservoir rock which was unusually clean and consisted of 98.9% sand, 0.5% silt, and 0.6% clay. The silt and clay fractions consisted of kaolinite and montmorillonite in concentrations of about 35% each. The remainder minerals in these two fractions comprised illite, calcite, chlorite, quartz, feldspar, and siderite.

The total mineralogy of the host matrix can have a great influence on the process variables of an *in situ* combustion process, especially for reservoirs which contain high gravity crude oils. Hardy *et al.* (1972) carried out a series of combustion tube tests with synthetic and also natural core matrices restored to post-waterflood saturations. An adiabatic combustion tube 5" in diameter and 42" long, was used in the tests. The synthetic matrix consisted of a mixture of 95 wt % Penn sands and 5 wt % kaolin clay. In tests using this mixture there was some difficulty in

sustaining a combustion front. The natural core material was crushed before being packed into the combustion tube and the original saturations of oil, water and gas were restored. No difficulty was observed in maintaining a vigorous combustion in the natural core material. Data from these tests and from *X*-ray and chemical analysis of the matrix and crude oil indicated that the *in situ* combustion process variables of this high gravity crude oil (40° API) are greatly influenced by the mineral composition of the host matrix.

Using Differential Thermal Analysis (DTA), Burger and Sahuquet (1972), studied the kinetics of oxidation reactions involved in crude oil burning. They found a significant difference between burning crude oil in a porous medium consisting of natural rock containing clay and porous media composing only ground silica. In the natural matrix, a higher oxidation temperature was obtained, and larger amounts of oxygen were consumed and larger amounts of CO and CO_2 were also produced. The differences in the two sets of results are shown in Figures 2.2 and 2.3, and believed to be due to the catalytic effect of clays, or the large surface area, or both.

Ejiogu *et al.* (1978) found that a natural core could deposit sufficient fuel to sustain combustion, even when the residual oil saturation was as low as 28.9% at high water:air ratio [2.73×10^{-3} m^3/m^3 (st)]. He suggested that it was important to obtain a mineral analysis of pre- and post-burn samples, for possible correction of carbon dioxide generated by decarbonation of such minerals as calcite, dolomite, and siderite when using natural core.

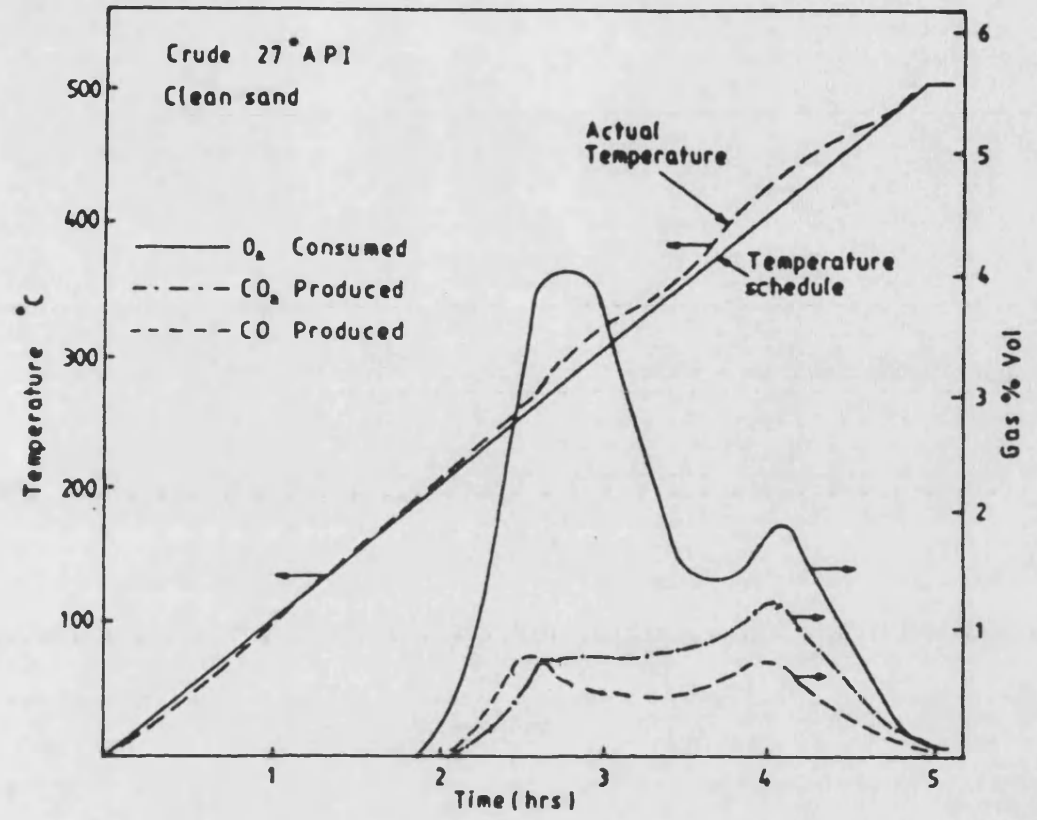

Figure 2.2 Oxidation of crude oil in a clean sand [Burger and Sahuquet (1972)].

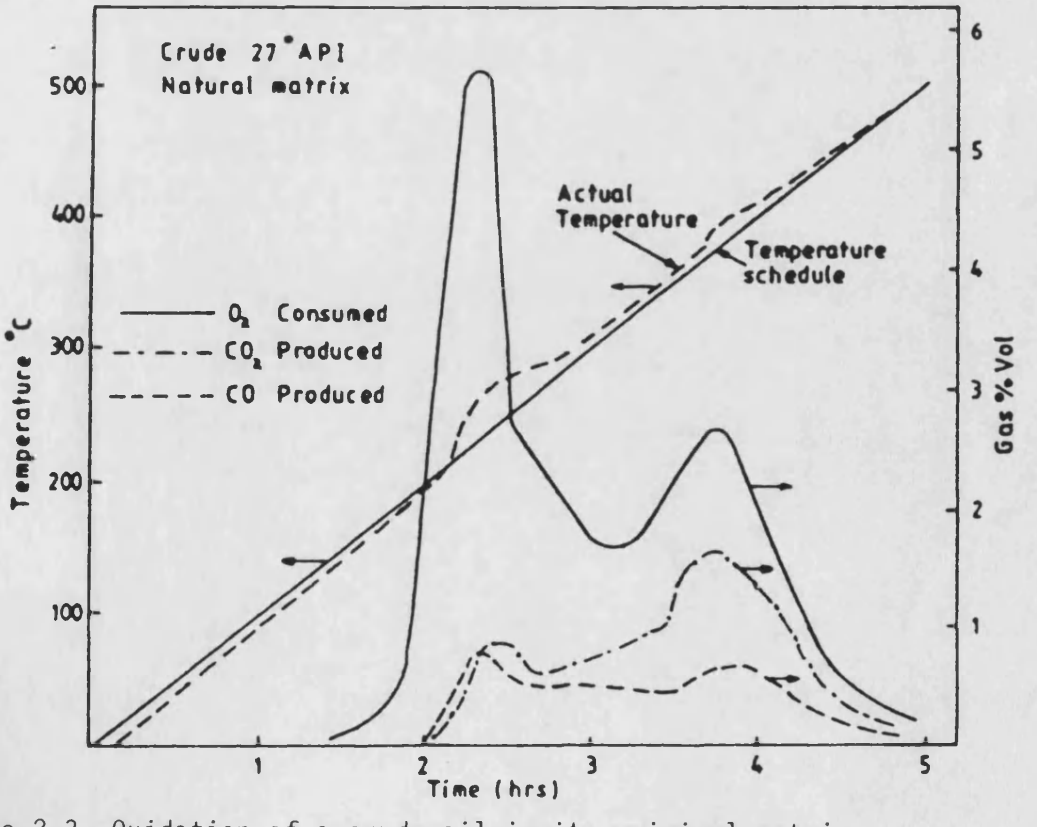

Figure 2.3 Oxidation of a crude oil in its original matrix [Burger and Sahuquet (1972)].

2.1.2 Surface area of clays

Specific surface area is defined as the surface of the pore channels per unit bulk volume. The specific surface area is dependent upon the number, shape, size and length of the pore channels.

Sand formations contain a relatively large amount of fine particles, some of which can be dislodged by flow of fluids. Table 2.1 gives data showing the magnitude of the surface area of some clay minerals. The specific surface area of a particular clay mineral varies with particle size distribution, particle shape and the presence of crakcs and pores in the sample.

The specific surface area of clay minerals has a significant effect on *in situ* combustion parameters, as discussed by Poettman *et al.* (1967). They deduced that the surface area of clays had a direct effect on fuel deposition characteristics of high-gravity, paraffin-based crude oil. Their results showed that with a high oil saturation of approximately 70%, relatively low temperature (117 °C), and air flux of 0.1 cm^3/cm^2 second (12 scf/h-sq.ft.), maximum fuel deposition (3.65%wt carbon/rock) was obtained. Also, the minimum fuel required to initiate a combustion wave was found to be about 1% by weight. Given these conditions, sufficient time is necessary to promote the deposition of carbon on sand.

Guvenir (1980) studied the effect of kaolin content on dry forward combustion of Iola crude oil. Four combustion runs were conducted with clay content varying from 0-15 wt %. In one combustion run, amorphous silica powder was used. This is an inert material with a relatively large surface area (1.42 m^2/g). Thus, the objective in this case was to determine whether clay had a catalytic effect on the process or the

Table 2.1 Specific surface area of some clay minerals (Grim, 1959).

	Heat* treatment (°C)	Loss in weight (%)	Specific surface area (m^2/gm)
Kaolinite	30	-	15.5
	200	0.2	15.3
	500	12.7	18.1
	700	14.3	16.5
	900	14.6	1.5
Illite,	30	-	97.1
	200	0.4	92.2
	500	5.8	91.6
	700	7.7	80.4
Montmorillonite	30	-	15.5
Halloysite	30	-	43.2

*Heated at temperature given until no further weight loss.

effect was due to its large surface area. Guvenir concluded that the surface area of the kaolinite was the major contributing factor responsible for fuel deposition. Figure 2.4 shows how fuel deposition increases with clay content.

Vossoughi *et al.* (1982) investigated the effect of surface area using both combustion tube tests, thermogravimetric analysis (TGA) and differential scanning calorimetry (DSC). Their results show a minimum specific surface area is required for any particular crude oil in order to establish a self-sustained combustion front in clean, unconsolidated sand packs.

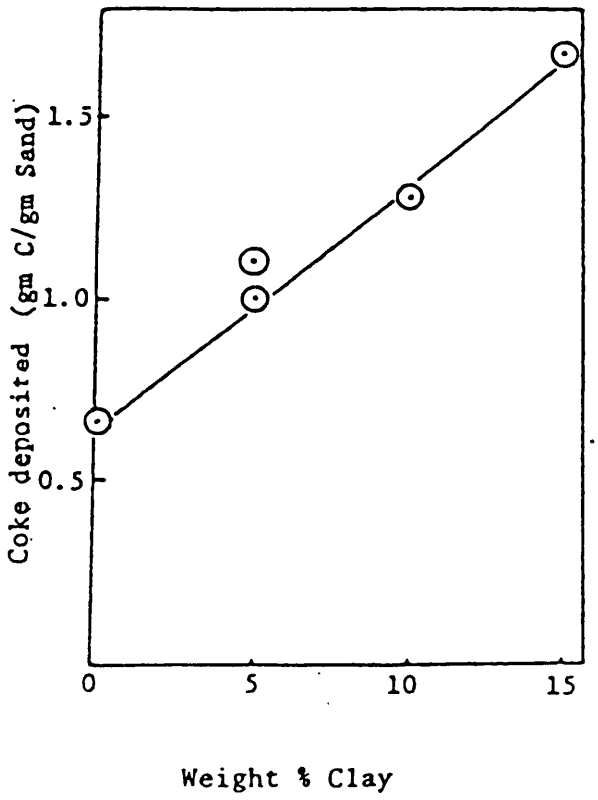

Figure 2.4 Fuel deposition *versus* clay content of sand (Guvenir, 1980).

Dabbous and Fulton (1974) found that the rock surface area affected the reaction rate constants for oxygen consumption. In particular, they noticed that the rock mixture with the highest surface area gave the largest carbon oxide conversion. This suggested that the initial carbon oxidation reaction is a heterogeneous surface reaction. Fassihi and Brigham (1981) also studied the effect of the rock surface area on the combustion process. They found that using a sand mixture instead of natural core gave different values in the reaction parameters. An analysis showed that the sand grains were much finer in the original core than in the sand mixture.

A study by Drici and Vossoughi (1985) investigated the effect of surface area on crude oil combustion. TGA and DSC were performed on crude oil alone and in the presence of clays, silica and alumina with variable specific surface areas. They found that crude oil combustion is influenced not only by the clays, but also by any granular material with high specific surface area. Additional tube runs were performed by Vosoughi et al. (1985) with finer sand grains having specific surface areas of 0.0317, 0.112 and 0.3332 m^2/g. A strong sustained combustion front was observed only in the run with the greatest specific surface area. It was concluded, therefore, that a minimum surface area is necessary for there to be sufficient laydown of fuel by the coking process.

2.1.3 Catalytic additives

The rates and activation energy of many reactions are affected by materials which are neither reactants nor products. Such materials are called catalysts. They may slow down the reactions, in which case they are called negative catalysts, or they may speed up the reactions, in which case they are called positive catalysts (El-Shoubary, 1981). Reactions

with solid catalysts usually involve high energy rupture or high energy synthesis of materials and these reactions play an important role in many industrial processes, *e.g.*, the production of methanol, ammonia, sulphuric acid and many other petrochemicals (Levenspiel, 1972).

In a situation where a number of chemical reactions are possible, a catalyst may affect the rate of all, or just some, of them and this property of catalysts is called selectivity, *i.e.*, the ability to direct reactions along certain paths and enhance rates of reaction. Another characteristic of a catalyst is that only comparatively small numbers of active catalytic sites are required to produce a large reaction effect.

During catalytic cracking processes, carbonaceous material gradually accumulates on the surface of the catalyst according to a mechanism which involves initially adsorption of either the reactants or products, followed by chemical reaction of the adsorbed material to produce surface deposits of much lower volatility. The effect of a catalyst will differ from one component to another. Therefore, grouping the processes such as cracking, low temperature oxidation, coke combustion, *etc.*, is necessary.

In the catalytic cracking of petroleum fractions during refining, carbonaceous materials gradually accumulate on the surface of the catalyst. These deposits tend to lower the cracking activity of the catalyst and must be periodically removed by burning. The catalysts normally used have high surface areas and consequently adsorb significant amounts of hydrocarbons, even at elevated temperatures.

(a) Catalytic effect of clays:

It is known that clay materials generally possess catalytic properties towards various organic liquids. However, this property is not present to the same degree in all kinds of clay materials. Grim (1962) showed

that some structure aspects of the clay minerals remain in the catalysts after manufacture and that this is essential to the properties of the clay catalysts.

Some investigators have found that the presence of clay can have a dramatic effect on the *in situ* combustion process. Bousaid (1967) reported that the activation energy in the oxidation of crude oil decreased from 26,600 to about 20,000 Btu/lb mole for a porous medium containing 20 wt % clays. The fuel deposition was much greater for the porous medium containing a mixture of 80 wt % sand and 20 wt % clay, compared with no clay additives.

Fassihi (1980) studied the effect of clay content on forward combustion and carried out similar runs to Guvenir's (1980), but with different crude oil. The presence of clay had an effect on the frontal behaviour of the combustion zone in the porous media. The average front temperature of the combustion zone was higher when clay was present in the sand mixture. The oxygen utilisation efficiency also improved, but a considerable amount of coke was left unburned.

Vossoughi *et al.* (1983) observed a significant reduction in activation energy of the crude oil combustion resulting from addition of clay to the oil/sand mixture, which was attributed to the catalytic properties of the clay.

(b) Acid treatment of clays:

The first catalysts to be used industrially were natural clays of the bentonite type (Decroocq, 1984). They had to be activated by acid treatment, which considerably modified their physical and chemical properties. Surface area and porosity increased (as a result of the dissolution of some aluminium and magnesium atoms) and surface sites favouring

hydrocarbon cracked were formed by ion exchange. Grim (1962) suggested that the surface of kaolinite clay provides adequate catalytic activity to produce gasoline from hydrocarbons and it is only necessary to increase the surface area to produce a commercial product. Acid activation of montmorillonite followed by leaching serves to increase the surface area and porosity, and to decrease the particle density. The surface area is increased from about 20 to more than 300 m^2/g in the finished catalyst.

The solubility of the clay minerals in acids varies with the nature of the acid, the acid concentration, the acid to clay ratio, temperature, and the duration of the treatment. Also, the solubility of the various clay mineral groups varies greatly. This is because individual groups exhibit different degrees of crystallinity, so that the solubility increases as the degree of crystallinity decreases. The solubility would, of course, tend to increase with smaller particle size. In general, clay minerals are more soluble in sulphuric acid than in hydrochloric acid. The treatment is sufficient for substantially complete removal of adsorbed alkalies and alkaline earths. The exchangeable cations are replaced by hydrogen. The proton penetrates the octahedral part of the montmorillonite lattice displacing octahedral magnesium, iron, and aluminium, in about that order. The protons from the acid probably join with oxygens in the octahedral unit to form hydroxyls, thereby freeing the octahedral cations. Magnesium, aluminium and iron proceed from octahedral positions to exchange sites and then into solution at a rate and to a degree depending on treatment procedure, *e.g.*, acid dosage, acid concentration, temperature, and time. Following acid treatment, the clay is washed to eliminate alkalies and calcium, and to reduce the iron content. This enables the desired magnesium and aluminium composition to be developed. Table 2.2 shows the extraction of alumina from various clay minerals with sulphuric acid.

Table 2.2 Extraction of alumina from various clay minerals with sulphuric acid [Grim (1959)]

Clay mineral	Aluminium extracted, % total aluminium present		
	Clay dried at 130 °C	Clay calcined at 800 °C*	Pressure digestion at 155 °C†
Kaolinite	3	100	70
Anauxite	9	95	-
Halloysite	63	100	98
	50	96	-
	90	-	-
	78	100	100
Illite	11	52	87
Smectite	87	28	85
	33	19	93
Mascovite	17	29	-

*Determination made after boiling 0.5 g of sample in 35 cc of 20% solution of sulphuric acid for 1 h.

†Clay dried at 130 °C, then digestion of 0.5 gm sample in 35 cc of 20% solution of sulphuric acid for 1 h.

Different authors have described the procedure for treatment of clays with acids. In this study, the kaolin has been prepared according to the method described by Mills (1949) and will be outlined in the next chapter.

Generally, a substantial increase in surface area is necessary to develop adequate commercial catalytic properties, but there is no direct correlation between the amount of surface and catalytic activity (Grim, 1962), *i.e.*, a material with a high surface area is not necessarily a satisfactory catalyst. However, Milliken *et al.* (1955) reported surface areas of 150 to 200 m^2/g for halloysite and kaolinite after treatment with acid. No investigation has studied the effect of clay after acid treatment on the *in situ* combustion process.

Drici and Vossoughi (1985) carried out extensive work on the effect of the matrix on fuel deposition and activation energy. The effect of clays, silica and alumina were studied and they are classified as solid acid catalysts. They concluded that the catalytic activities of clays are related to their acid site density and acid strength. Activation energy decreases with increasing number of acid sites, which would favour LTO and thus promote fuel deposition. Dabbous and Fulton (1974) showed that increasing catalyst site density and acid strength favours an increased rate of coke formation. This is very important when combustion is applied to light oil reservoir when fuel deposition may be a limiting factor (White, 1985).

2.2 Crude Oil Characteristics

The composition of petroleum can vary with the depth of an individual reservoir formation. It will also depend on the location and age of the oil. Crude oil is defined by Hobson (1984) as a naturally occurring mixture consisting predominantly of hydrocarbons, together with sulphur, nitrogen, and oxygen derivatives of hydrocarbons. The main hydrocarbon constituents of crude oils are shown in Figure 2.5 and Table 2.3.

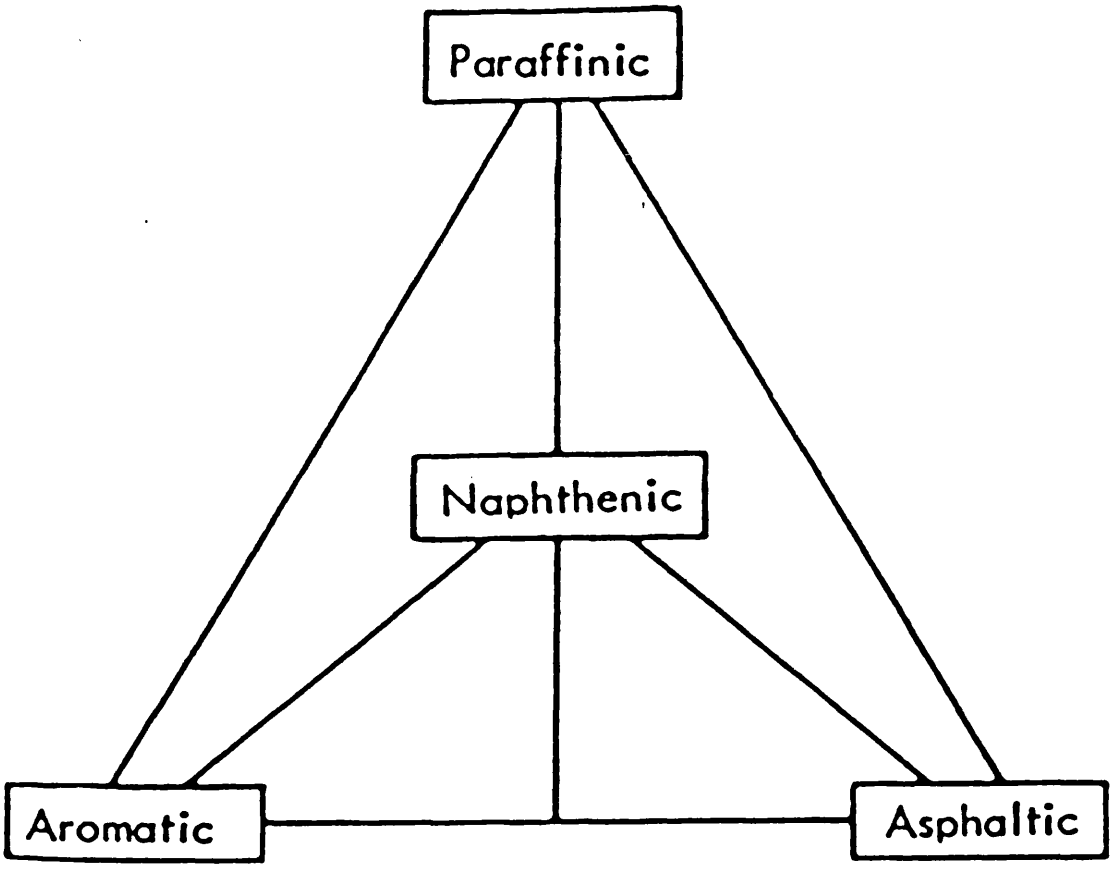

Figure 2.5 Composition diagram for petroleum from "The Chemistry and Reaction of Petroleum", by J.G. Speight (Marcel Dekker Inc.) 1980.

Table 2.3 Petroleum classification according to chemical composition [from the above source (see Figure 2.5)]

Class of crude	Composition of 250-300 °C fraction				
	% Porosity	% Naphth.	% Arom.	% Wax	% Asphalt
Paraffinic	46-61	22-32	12-25	1.5-10	0-6
Paraffinic naphthanic	42-45	38-39	16-20	1-6	0-6
Naphthanic	15-26	61-76	8-13	trace	0-6
Paraffinic-naphthanic-aromatic	27-35	36-47	26-23	0.5-1	0-10
Aromatic	0-8	57-78	20-25	0-0.5	0-20

2.2.1 Oxidation of crude oil

Reactions between oxygen and hydrocarbons at temperatures below 350 °C are termed low temperature oxidation (LTO) reactions. These are characterised either by the absence of cabron oxides, or low levels of carbon oxides in the effluent gases. In other words, more oxygen reacts with the oil in place than can be accounted for in the produced gases. As the temperature of hydrocarbon oxidation is raised above 350 °C, increasing quantities of products are formed. According to Alexander *et al.* (1962), partial oxidation of crude oil during *in situ* combustion significantly influences the behaviour of the crude oil-water system in the zones preceding the combustion zone. This consequently, has an effect on the amount and characteristic of the fuel available for combustion. They asserted that LTO is generally undesirable because of adverse effect on the viscosity and distillation characteristics of the crude. Displacement of oil in the reservoir by the *in situ* combustion is ultimately controlled by the

physical properties and distillation characteristics of the crude. The results are in agreement with those of Tadema (1959), who used DTA to study the thermal effects of mixtures of various oils and sands. The study showed that there are two distinct combustion which occur at approximately 270 °C and 400 °C. Analysis of the exhaust gas showed that oxygen was taken up near the 270 °C peak and a coke-like residue was formed. Only a small part of the oxygen could be found as carbon dioxide or carbon monoxide. A small percentage is taken up by the residue and the major part reacts to form water. At the high temperature peak, mainly CO_2 and some CO are formed and little water was produced. No residue remained.

Bousaid (1967) studied the oxidation of crude oil in unconsolidated porous media and obtained an expression for the burning rate of carbon as a function of carbon concentration, oxygen partial pressure and combustion temperature. The carbon burning rate for the two types of crude oil gave a first order reaction with respect to both carbon concentration and oxygen partial pressure. While the activation energy was similar for the two crudes examined, the presence of clay decreased the activation energy.

Bae (1977) studied the thermo-oxidative behaviour of crude oils using DTA and TGA. In his experiments, the crude oil used ranging from 6-38 °API gravity at pressures of 50,500 and 1000 psig using nitrogen and air atmospheres. In the curves from the DTG runs, two peaks usually occurred. The first peak started just below 205 °C (400 °F), signalling the onset of low temperature oxidation. A second peak appeared around 370 °C (700 °F) and when the temperature reached 482 °C (900 °F), the reaction was complete. Bae concluded that the availability of oxygen at low temperature drastically changed the quantity and the quality of the fuel laydown.

The kinetics of both low temperature oxidation of crude oils, occurring below 250 °C, and high temperature combustion reaction of the coke left behind after thermal cracking of the crude was used to obtained rate equations for the overall rate of LTO reactions. The reaction order was dependent upon the crude, but independent of the properties of the porous media.

In the study of Kharrat and Vossoughi (1985) using DSC and TGA, the first step was to identify the oxidation behaviour of the crude oils. The shape of the curves obtained in all cases indicated the occurrence of four distinct transitions during the process. These transitions are distillation, low temperature oxidation, and first and second combustion/ cracking reactions (Figures 2.6 and 2.7).

Both low temperature and high temperature reactions have an effect on the viscosity and distillation characteristics of crude oil. Martin *et al.* (1958) emphasised that LTO increases oil viscosity and alters the distillation characteristics of crude oil. Another study concerning a high API gravity of oil of 32.1-44.3° was conducted by Sterner and Wertman (1967). Their results confirmed that *in situ* combustion is applicable to both asphaltic and paraffinic-based high gravity oils under suitable conditions. Okandan *et al.* (1982) pointed out that LTO causes a decrease in the API gravity of oil. It significantly increases the amount of fuel available for combustion.

A recent study by Lerner *et al.* (1985) outlines the effects caused by LTO on the vaporisation of the oil, changes in oil volatility resulting from coking and changes in oil properties. Changes in viscosity and vaporisation characteristics of the oil, due to low temperature oxidation, can significantly affect *in situ* combustion performance. It is believed

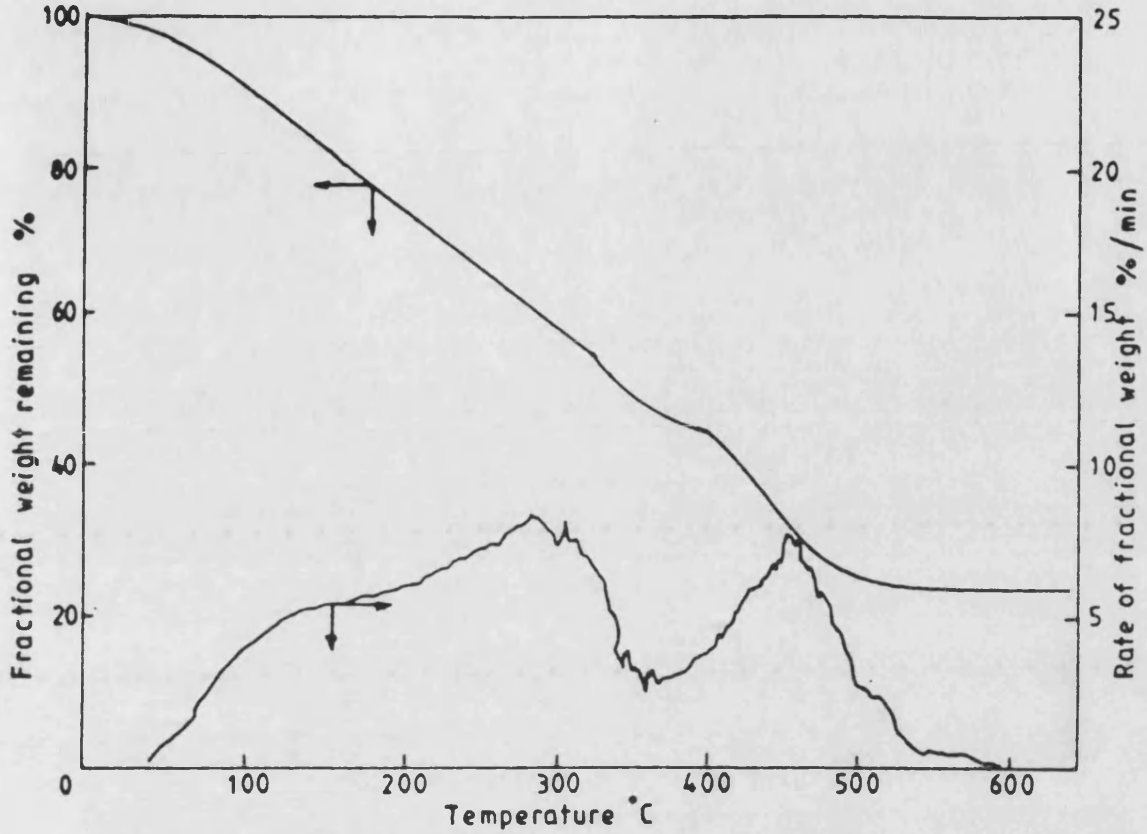

Figure 2.6 TGA and DTG curves of Moran reservoir core in dynamic air purge [Kharrat and Vossoughi (1985)].

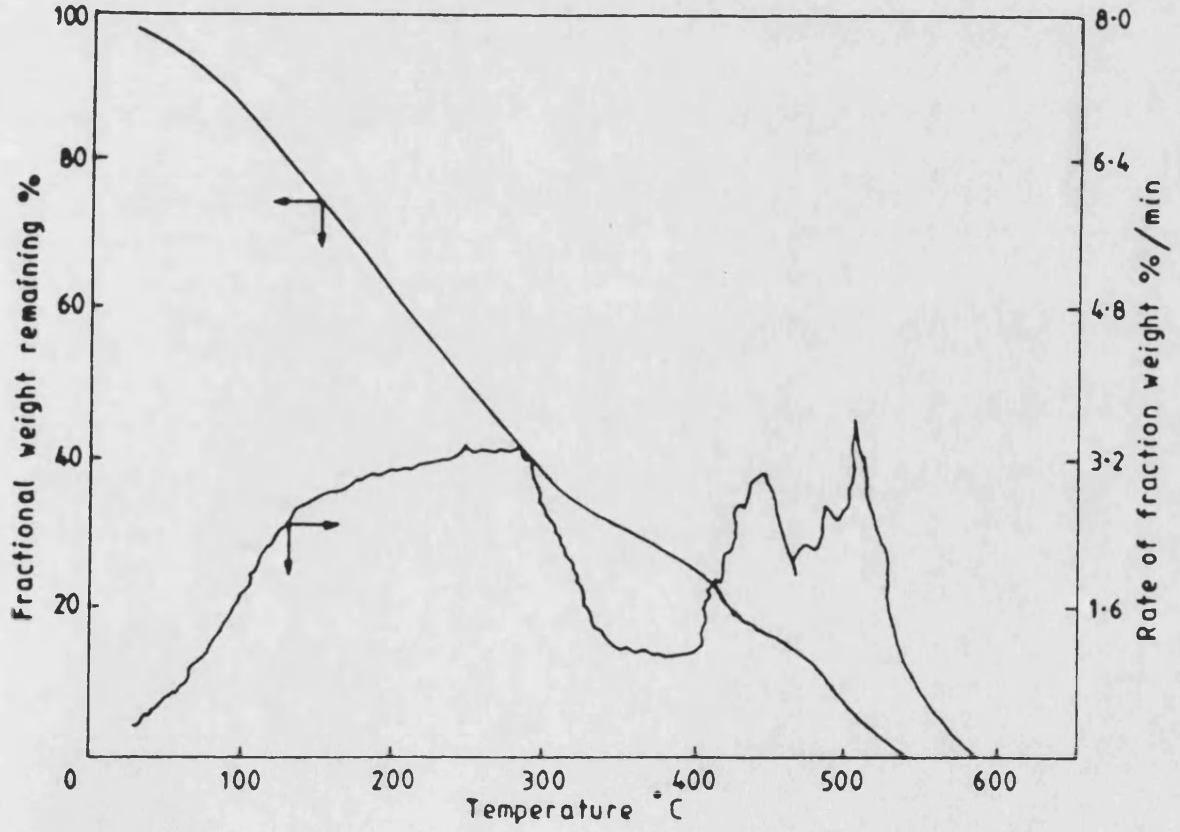

Figure 2.7 TGA and DTG curves of Moran crude oil in dynamic air purge [Kharrat and Vossoughi (1985)].

that light crudes are more susceptible to LTO than are heavy oils. Crawford (1968) has listed some of the products of LTO as alcohols, aldehydes, ketones, acids and peracids. He concluded that aldehydes promote the reaction.

In 1981, Lee *et al.* mixed two crude oil fractions in order to study the feasibility of representing the crude oil by only two fractions. It was established that a two fraction scheme gives a set of results fairly close to that predicted by the original oil scheme.

2.2.2 Minimum crude content

The minimum crude oil content required for a self sustained combustion was found (Kharrat and Vossoughi, 1985) by applying an energy balance over a unit bulk volume of the rock in the vicinity of the combustion front:

$$W_{min} = \frac{\rho_b C_b \Delta T_{min}}{\Delta H} \qquad (1)$$

where

$$\rho_b C_b = (1-\psi)\rho_s C_s + \psi \rho_g C_g \qquad (2)$$

$\Delta T_{min} = T_{min} - T_A$, T_{min} and T_A are the required minimum front temperature and the known temperature and ΔH is the heating value of crude; ψ = porosity, ρ = density of gas, C_b, C_s, and C_g are respectively, the specific heat of bulk, solid and gas.

The temperature at which the total crude oil sample was consumed was considered to be the required minimum front temperature, T_{min}. This temperature was obtained by conducting a series of TGA and DSC runs. The ΔH value of the sample was determined from the area under the DSC curve. The value of ρ_b, C_b is calculated from equation (2) by ignoring $\rho_g C_g$. The oil content of the reservoir, W_R, was calculated by the equation

$$W_R = s_o \rho_o \psi \qquad (3)$$

where s_o is the oil saturation, ρ_o is the oil density, and ψ is the

porosity of the reservoir. Reservoirs with W_R greater than, or equal to W_{min}, were considered feasible candidates for *in situ* combustion.

A successful combustion tube run for crude oil has been reported by Vossoughi *et al.* (1982), in which a sand pack with 7 wt % crude oil was used.

Burger *et al.* (1985) considered the minimum oil content to be between 8 and 12 volume % for steam injection applications and 7% for *in situ* combustion.

2.2.3 Metallic additives

Petroleum contains a small amount of metal compounds such as copper, iron, nickel, vanadium, magnesium and calcium. Tables 2.4 and 2.5 show the ranges of such elements in the petroleum and the metals content of different curde oils. The sand matrix may also contain other metal compounds, *e.g.*, siderite, magnetite and iron.

Zinc, calcium and magnesium are present in the crude oil in the form of organometallic soaps possessing surface-active properties. These are adsorbed at the water-oil interface and act as emulsion stabilisers. Vanadium, copper, nickel and iron appear as a different class and are present as oil soluble compounds (Speight, 1980).

The term cracking is applied to the process of decomposition of hydrocarbons or of petroleum fractions, by the action of heat (thermal cracking), or by heat in the presence of suitable catalysts (catalytic cracking). The products resulting from the decomposition are of a lower molecular weight than the feed stock, and are mainly olefinic in character. Many of the catalytic effects are observed in catalytic cracking processes, can be related to the presence of certain non-hydrocarbon impurities in crude oil [Medley and Cooley (1960)].

Table 2.4 Ranges of principal trace elements found in petroleum

Element	Range in Petroleum (ppm)
Cu	0.2 - 12.0
Ca	1.0 - 2.5
Mg	1.0 - 2.5
Ba	0.001 - 0.1
Sr	0.001 - 0.1
Zn	0.5 - 1.0
Hg	0.03 - 0.1
Ce	0.001 - 0.6
B	0.001 - 0.1
Al	0.5 - 1.0
Ga	0.001 - 0.1
Tl	0.001 - 0.4
Zr	0.001 - 0.4
Si	0.1 - 5.0
Sn	0.1 - 0.3
Pb	0.001 - 0.2
V	5.0 - 1500
Fe	0.04 - 120
Co	0.001 - 12
Ni	3.0 - 120

Table 2.5 Metals content of various crude oils

Source	Metals (ppm) Fe	Ni	V	Cu
East Texas	3.2	1.7	1.2	0.4
West Texas	5.1	4.8	7.9	0.4
Mirando	7.6	1.9	1.4	0.6
Jackson	4.4	1.8	0.9	0.2
Scurry County	3.4	1.0	0.8	0.2
Wilmington	28.0	46.0	41.0	0.6
Santa Maria	17.0	97.0	223.0	0.3
Kettleman	24.0	35.0	34.0	0.4
Ventura	31.0	33.0	49.0	1.1
Tibu-Petrolea	1.6	9.0	60.0	0.9
Kuwait	0.7	6.0	22.5	0.1
Mid-Continent	3.8	4.2	7.9	0.3
Kansas	5.8	5.8	20.8	0.4
Morocco		0.8	0.6	0.1
Redwater	3.4	10.6	4.5	0.1

Metallic additives may shift the rate determining step from fuel combustion towards middle temperature reactions. Burger and Sahuquet (1982) presented a set of experimental results. A 2000 ppm of copper derivative was added to the oil (Figure 2.8) and 1 wt % nickel oxide was added to the sand in another case (Figure 2.9).

In the presence of metallic additives (a) the oxidation reactions occur at noticeably lower temperatures due to lower activation energy, and (b) fuel availability and air requirements are increased, due to greater coke formation.

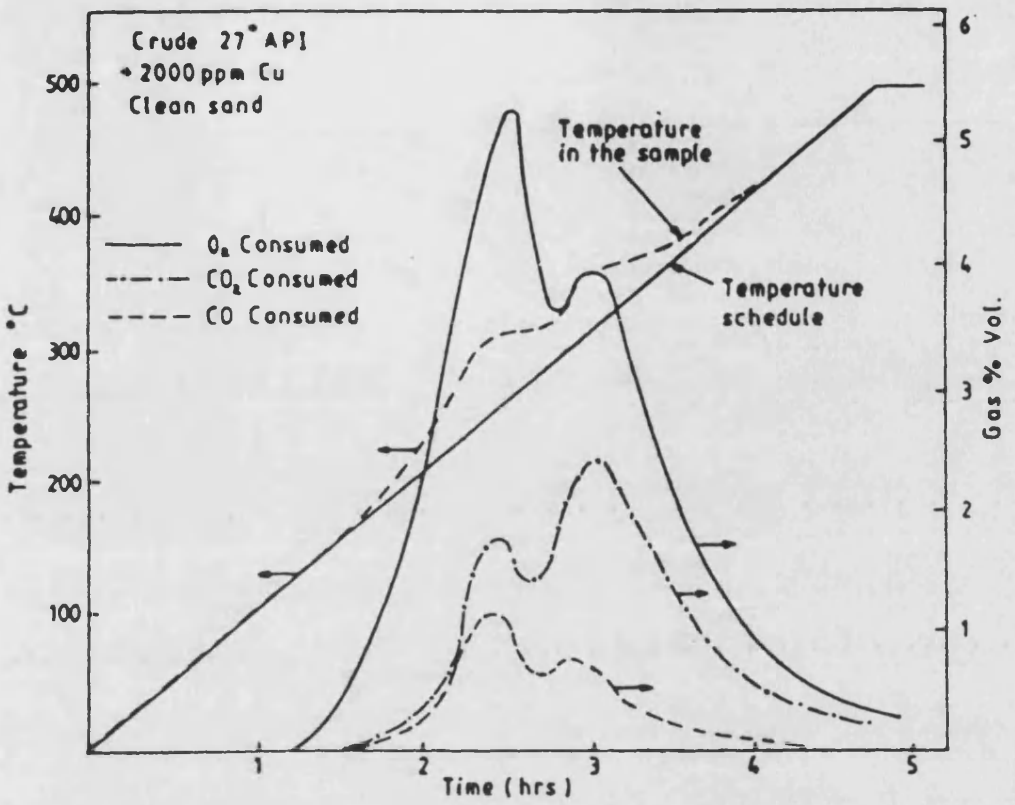

Figure 2.8 Oxidation of crude oil containing a copper additive in a clean sand.

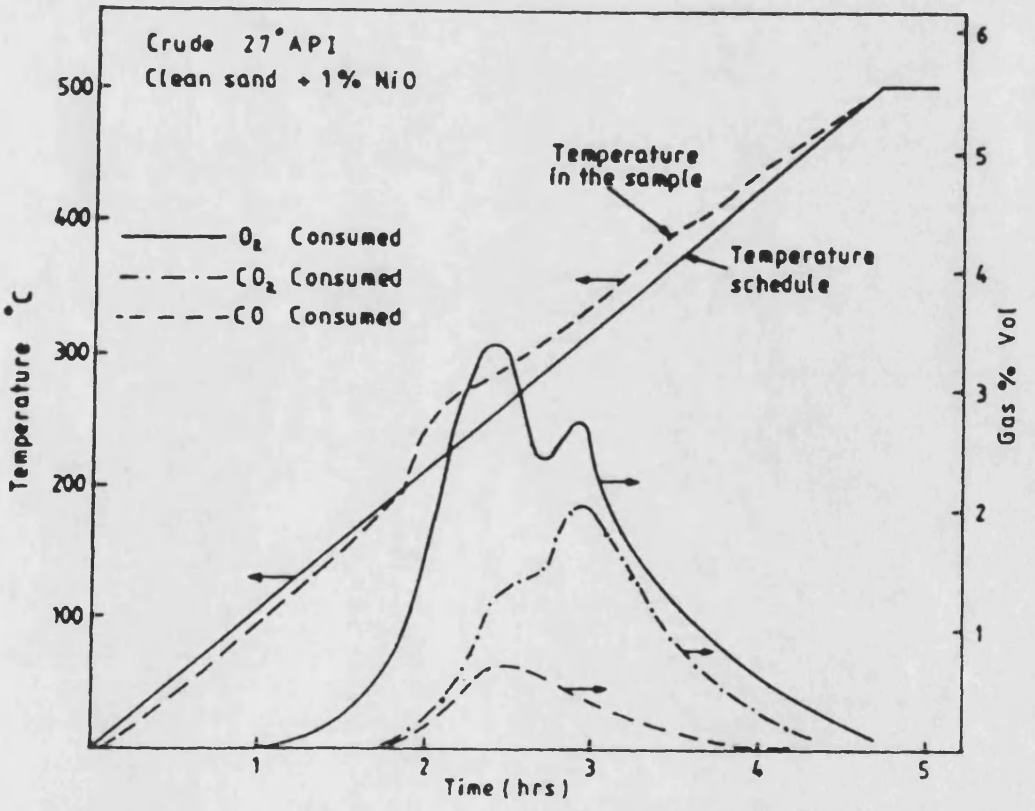

Figure 2.9 Oxidation of crude oil in a clean sand with addition of nickel oxide.

The analysis of oxidation data for a French oil presented by Fassihi *et al.* (1984) showed that addition of 2000 ppm of copper to the sand mixture lowered the activation energy by approximately 50%. Because of this profound dependency of the kinetic parameters on the matrix compounds, all combustion studies, as stated by Fassihi, should be conducted with the parent cores. If this is not possible, the matrix should be analysed to see whether metallic and clay additives are present. It is felt that the existence of clay, or a very fine matrix, in a light oil reservoir may lead to a successful combustion project in a field. Fassihi concluded that metallic additives have a catalytic effect on the oxidation reactions and that clays increase fuel deposition by promoting adsorption.

Drici and Vossoughi (1985) studied crude oil combustion in the presence of titanium, ferric, nickel, cupric, vanadium and chromium oxides. Differential scanning calorimetry and thermogravimetric analyses were applied to the crude oil combustion in the presence and absence of the metal oxides. It was found that the effect of titanium oxide was similar to that of silica and alumina. The fractional amount of heat released in the lower temperature region increased with increasing quantities of the titanium oxide and attaind a maximum level. The coke combustion peak shifted slightly to the lower temperature region and became smaller. Vanadium, nickel and ferric oxide behaved similarly in enhancing the endothermic reactions. The effect of a small amount of metal oxides (about 1% by weight) on the crude oil combustion in the presence of silica powder was insignificant. However, the same amount of metal oxide affected the DSC curves produced from the combustion of the crude oil/sand mixture significantly. Therefore, when there is a large surface area, *e.g.*, when silica is present, the surface reactions are predominant and are unaffected by the small amount of metal oxide present.

CHAPTER 3

Equipment and Experimental Procedures

Figure 3.1 shows a diagram of the *in situ* combustion assembly used in this study. Table 3.1 contains a listing of the equipment items shown in Figure 3.1. The main parts of the *in situ* combustion assembly are described in section 3.1. Sections 3.2 and 3.3 discuss the preparation procedures and operating conditions for the experiments.

3.1 Equipment

The combustion apparatus consists of combustion tube, product separation train, gas sampling and associated measurement instrumentation. A detailed description of the equipment is given by Al-Shalabe (1985).

The combustion tube consists of a high pressure jacket and thin walled combustion tube. The combustion tube is surrounded with one band heater at the top of the tube to provide ignition. A tape heater is wrapped around the combustion tube wall to maintain a near adiabatic condition during the run. Twelve thermocouples were welded at different levels onto the combustion tube wall. A further twelve thermocouples were positioned along the central axis of the sand pack by means of a thermocouple probe.

The separator and the condenser were used to collect the condensed liquid products. Gaseous components which could not be condensed in the separator were mostly condensed in the condenser, due to cold water circulation. At the bottom of both, there were shut-off valves to liquid sampling containers which could be utilised to collect liquid samples during the combustion runs. In order to improve the condensation of the liquids associated with the produced gases, a third separator was inserted in an ice bath.

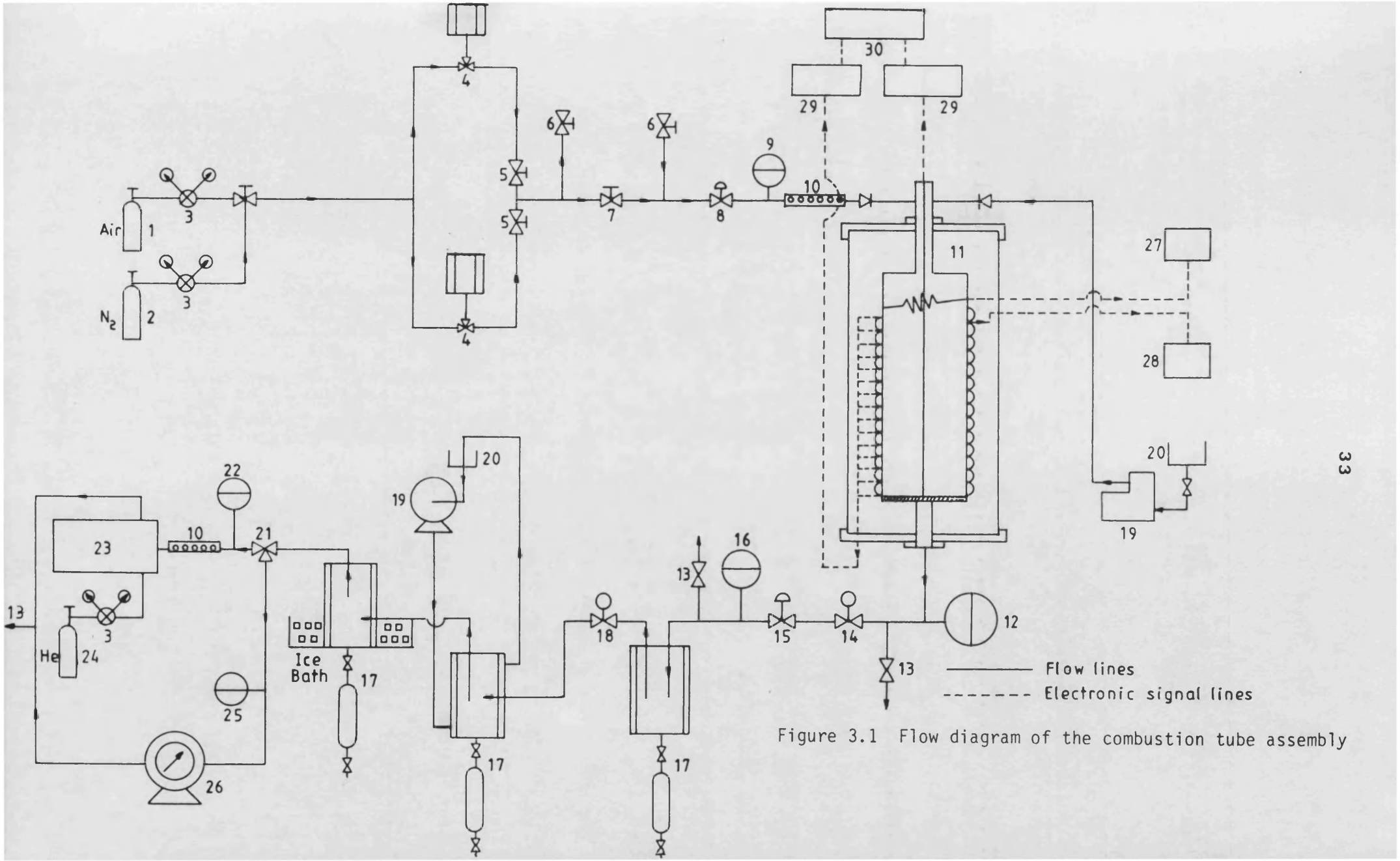

Figure 3.1 Flow diagram of the combustion tube assembly

Table 3.1 List of equipment shown in Figure 3.1

1. Compressed air cylinder
2. Compressed nitrogen cylinder
3. Two stage regulators
4. Gas flow meters
5. Shut-off valves
6. Inlet and outlet control valves
7. Air by-pass valve
8. Air-water pressure regulator
9. Combustion reactor inlet pressure gauge
10. Filter
11. Combustion tube and pressure jacket assembly
12. Pressure control gauge
13. Gas exit lines
14. Combustion reactor back pressure regulator
15. Pressure regulator
16. Separator inlet pressure gauge
17. Separators
18. Separator back pressure regulator
19. Water pump
20. Water source
21. Three-way valve
22. Chromatograph inlet pressure gauge
23. Gas chromatograph
24. Helium compressed cylinder
25. Wet test meter inlet pressure gauge
26. Wet test meter
27. Band heater controller
28. Preheater power regulator
29. Selector unit
30. Digital temperature display

The water injection system consists of a metering pump which delivers water directly to the top inlet of the combustion tube. A non-return valve is installed in the water line to prevent back flow of the gases into the metering pump. In order to control the pressure of the injected water to the combustion tube, a back pressure regulator (Series 30-10, provided by Scientific Glass Engineering) was installed to the discharge line of the water metering pump.

A Pye Unicam series low gas chromatograph fitted with a thermal conductivity detector head was used to analyse the composition of the gases produced. The analysis of gases is completed within a few minutes using the CTR column, which is packed with a blend of pore pack polymers in the inner column and molecule sieve 13X in the annular space. A gas filter packed with 'Indicating Drierite' was installed for the gas chromatograph, in order to filter out any non-gaseous components which may be carried by the produced gas, and to reduce the pressure of the gas samples before they are sent for analysis to the gas chromatograph.

3.2 Preparation Procedures

Seventeen combustion runs were reported, in which different additives have been used. These included runs with clay (kaolin),amorphous silica, ferric oxide, and nickel chloride. In addition to these, three combustion tests were made using natural core matrix from the Lower Fars formation of the Kuwait oil field. Three different crude oils were used in the experiments, namely Maya Isthmus (Mexico), Maya (Mexico) and Cold Lake (Canada), as described in Table 3.2. The combustion tube was operated in a vertical position in order to avoid gravity segregation effects, which would occur if mounted in a horizontal position. The combustion tube was prepared for an experimental run by mixing the sand, water and oil manually in a container in atmospheric pressure and at room temperature to yield the desired fluid saturation distribution. The weight

Table 3.2 Physical and chemical properties of crude oil

	Maya Isthmus[a]	Maya[a]	Cold Lake[b]
Gravity, °API	32.4	22.1	10.2
Density, gm/cm^3	0.8649	0.921	0.9986
Viscosity, CS+	at 40 °C, 11.42 at 100 °C, 8.71	at 10 °C, 406 at 20 °C, 203	at 20 °C, 200,000 at 100 °C, 80
Pour point, °C	15[c]	-27	not available
Sulphur, wt %	1.51[c]	3.91	4.4
Carbon residue, wt %	8.08[d]	11.0	13.6
Asphaltenes, wt %	not available	9.4	15.9
Vanadium, ppm	67.1[d]	267	164
Nickel, ppm	14.8[d]	52	62
C_1-C_4, wt %	not available	1.3	not available
H/c atomic ratio	not available	not available	1.491

[a]British Petroleum Research Centre, Sunbury-on-Thames. Middlesex

[b]Speight (1981) 'The Desulphurisation of Heavy Oils and Residues'

[c]*Oil and Gas J.*, V.81, N. 43, P. 88, 24th October, 1983.

[d]*Ibid.*, data for topped oil.

ratio of crude oil to sand mixture provided an oil saturation of 36.7-42.4%. The weight ratio of water to sand mixture, also, gave a water saturation of 5.93-9.37%. The porosity of the mixtures varies from 29.1-39.6%.

The above mixture is tamped carefully into the tube. Three to four grams of linseed oil is poured on the sand face. This was done because the high reactivity of this oil yields a fast and uniform ignition. The top end of the combustion tube is tightened. All the lines are connected, the electric switches turned on, and the necessary valves are opened. Nitrogen is injected at about 0.5 lit/min through the tube to get a complete displacement of the air. The heating tape is turned on to raise the temperature of the pack. Then the band heater is turned on to raise the temperature of the inlet face of the sand pack until the ignition zone has reached about 340-350 °C (about 650 °F). At this time, air injection is commenced at a flow rate of 0.8 lit/min (48 x 10^{-3} m^3 (st)/h), which provide an air flux of 14.57 m^3 (st)/h m^2. Inlet air pressure was set at 50 psig. Ignition is confirmed both by the temperature increasing of the inlet face of the sand and by the increase in carbon dioxide, the appearance of carbon monoxide and a decrease in oxygen in the exit gas. The produced gases are analysed by gas chromatography every 15 minutes and the gas volume is measured by the wet test meter. Produced liquids were collected from the sampling cylinders every hour. The wall and axial combustion temperatures were recorded as a funtion of time every 30 minutes. In case of wet combustion tests, water injection at a constant rate of 50 x 10^{-6} m^3/h [WAR = 1.0 m^3/Mm^3 (st)]

was commenced once the stabilised combustion front had travelled a distance of two thermocouple positions.

The run is terminated when the last thermocouple from the production end has reached a temperature of about 300 °C (572 °F). This is necessary in order to avoid coke formation on the mesh screen at the bottom of the tube, and prevent fire break-through in the production line. Air injection is switched to nitrogen injection and the sand pack is allowed to cool. All heaters and other electric devices are turned off. Lines to the top of the combustion tube are disconnected. The combustion tube is opened and the sand pack is removed. Analysis of the data was begun. This included analyses of the liquids produced, and a complete material balance of all material originally packed into the combustion tube. Samples from the combustion zone were weighed and then heated to determine the fuel remaining on the sand. The produced liquids were separated into oil and water by a centrifuge and each fraction was weighed. In those cases where emulsion had formed, a known quantity of toluene was added before centrifuging.

Information regarding the clay (kaolin) and amorphous silica types used are given in Tables 3.3 and 3.4.

3.3 Operating Conditions

A particular clay to sand ratio was selected for each individual run and the average surface area is given in Table 3.5. The experimental conditions for the combustion tube runs are shown in Table 3.6.

The effect of surface area on the crude oil combustion was studied using a wide range of specific surface areas. The experimental runs were conducted using mixtures of sand with 0, 2, 5, 10 and 15 wt %

Table 3.3

Analysis of clay (kaolin)

Shape	powder
Specific surface area	12-14 m^2/gm
Loss on drying	0.9%
Loss on ignition	12.7%
Chloride	< 350 ppm
Heavy metal	< 20 ppm
Arsenic	< 2 ppm
Soluble matter	4.6 mg/g
Coarse particles	0.3 mg/g
Fine particles	76.2%

Supplied by Dearborn Chemicals Ltd.

Table 3.4

Analysis of amorphous silica

Shape	Powder
Specific surface area	2.0216 m^2/gm
particle size distribution	0.5-10 micron
Approximately 80% between	1-5 micron
Chemical composition	SiO_2 approximately 99%

Nature: a mixture of microcrystalline and amorphous particles

Supplied by Sigma Chemical Company

Table 3.5 Specific surface area of sand pack

Composition of sand pack	Specific surface area (m^2/gm)
100% silica sand	0.130
2% clay + 98% silica sand	0.387
3% clay + 97% silica sand	0.516
5% clay + 95% silica sand	0.774
10% clay + 90% silica sand	1.417
15% clay + 85% silica sand	2.061
2% amorphous silica + 98% silica sand	0.167
5% amorphous silica + 95% silica sand	0.224
10% amorphous silica + 90% silica sand	0.317
13.75% amorphous silica + 86.25% silica sand	0.387

Table 3.6 Initial experimental runs conditions

Sand	Silica sand (Buckland Sand) Mesh size used = 52 Surface area = 0.13 m^2/gm
Clay type	Kaolin (surface area = 12-14 m^2/gm)
Amorphous silica	Powder (surface area = 2.016 m^2/gm)
Oil to (sand + clay) ratio	7.0% wt
Water to (sand + clay) ratio	2.0% wt
Pressure (maximum)	50 psig
Gas flow rate	0.8 lit/min = 48 x 10^{-3} m^3(st)/h
Gas flux	14.57 m^3(st)/m^2 h
WAR (for wet combustion runs)	1.0 m^3/Mm^3(st)

respectively, of clay kaolin. The experiments were conducted with fixed WAR 1.0 m^3/Mm^3. The composition of the sand mixture was varied as shown in Table 3.7. Porosity of the porous media and oil saturations is shown in the same table. After these runs, it was decided to change the composition of the mixtures by substituting clay (kaolin) with amorphous silica. The purpose of adding amorphous silica was to study the catalytic effects of clay on the *in situ* combustion process, and to see if a similar behaviour could be obtained when amorphous silica, which possesses a relatively large surface area, is added to the sand mixture. The compositions chosen for this investigation are given in Table 3.8. A 13.75% weight amorphous silica was mixed with 86.25% weight silica sand to give an average surface area of 0.387 m^2/gm, which is equivalent to the surface area provided when 2% weight clay is mixed with 98% silica sand (see Table 3.5). The porosity and oil saturation of these sand packs are included in table 3.8.

Three experimental runs were conducted to find the minimum clay content in the sand mixture, which is necessary to self-sustain the combustion front. In these runs, 1, 2 and 3 % weight of clay (kaolin) respectively, were added to the sand mixtures with Maya Isthmus crude oil. In the first two runs, a combustion front could not be sustained, while in the third run, No.10 (3% kaolin), a self-sustained combustion front was obtained. The initial conditions for this experimental run are given in Table 3.9.

Table 3.10 shows the properties of sand mixture when Cold Lake crude oil is used with silica sand only. This experiment was conducted to show that for heavy crude oil, self-sustained combustion fronts could be established in the absence of kaolin in the sand pack mixture.

Table 3.7 Sand mixture characteristics of clay runs

Run No.	Composition of sand pack	Crude oil type	type of combustion	Porosity (%)	Oil saturation (%)
1	100% silica sand	Maya	wet	36.0	40.0
2	2% clay + 98% silica sand	Maya	wet	33.70	39.5
3	5% clay + 95% silica sand	Maya	wet	33.80	40.35
4	10% clay + 90% silica sand	Maya	wet	35.79	40.92
5	15% clay + 85% silica sand	Maya	wet	36.89	40.0

Table 3.8 Sand mixture characteristics of amorphous silica runs

Run No.	Composition of sand pack	Crude oil type	Type of combustion	Porosity (%)	Oil saturation (%)
6	2% amorphous silica + 98% silica sand	Maya	wet	29.20	40.40
7	5% amorphous silica + 95% silica sand	Maya	wet	28.34	38.12
8	10% amorphous silica + 90% silica sand	Maya	wet	29.96	40.33
9	13.75% amorphous silica + 86.25% silica sand	Maya	wet	35.25	40.77

Table 3.9 The properties of sand mixture for Run 10

Crude oil gravity, °API	32.4
Type of combustion	dry
Porosity, %	33.0
Clay content, % weight	3
Oil saturation, %	36.65

Table 3.10 The properties of sand mixture for Run 11

Crude oil gravity, °API	10.2
Type of combustion	wet
Water air ratio, m^3/Mm^3(st)	1.0
Porosity, %	31.92
Clay content, % weight	0
Oil saturation, %	39.59

A natural core from the Lower Fars formation of Kuwait oil field has been studied. The core was old and contained aged hydrocarbons of approximately 18.0 °API gravity. Data concerning this core and the experimental conditions are shown in Table 3.11. The oil saturation was measured and found to be approximately 20%. Evidently, the relatively low saturation was affected by exposed storage over a long period. This is undesirable, and fresh cores recommended for future experimental study.

Comparison of the sieve analysis for the core sand and the Buckland sand is shown in Table 3.12. The natural core was analysed using *X*-ray diffraction and was found to contain 95% quartz, and approximately 5% weight clays and fines. It was packed into the combustion tube with restored saturation of oil and no difficulty was experienced in maintaining a combustion front.

Table 3.11 Data summary of natural core and experimental run conditions (Run 12)

Formation*	Lower Fars
History of core*	1982
Depth*	770-800 feet
Description*	Sand, fine-medium grained, loose, rounded, very good porosity (36.48%), oil saturated.
Specific gravity of initial oil in place*	Approximately 18.0 °API
Core mineral content, %	5
Oil originally in pack, gm	140
Oil saturation in pack, %	20
Porosity of pack, %	40
Air flux, $m^3(st)/m^2$ h	14.57
Water air ratio, $m^3/Mm^3(st)$	1.0

Table 3.12 Sieve analysis of natural core and silica sand

Sieve sand	Natural core, %	Buckland silica sand, %
30	56.16	10.50
52	22.04	37.90
60	7.23	6.90
100	9.57	40.40
pan	5.00	4.30
	100	100

*Data provided by Kuwait Oil Company, Geological Department.

In Run 13, a mixture of 25% weight of natural core and 75% weight of silica sand has been made with Maya crude oil. The clay and silt content in this mixture was approximately 1% and the conditions for this run are given in Table 3.13.

Three combustion tube tests were made using 35% oxygen, with a constant (O_2 + N_2) flux of 14.57 m^3(s.t)/m^2 h. The purpose was to provide an understanding of the effect of oxygen enrichment. The conditions for these runs are given in Table 3.14.

As mentioned previously, crude oils and sand matrix usually contain a trace amount of metals, typically vanadium, nickel and iron. Parker (1963) found that the combustion temperature can be decreased and the combustion reaction can be speeded up by the addition of iron-containing compounds to sand matrix. Three experimental runs have been conducted to investigate the effect of ferric oxide and nickel chloride additives. The technical information of these two additives are reported in Table 3.15. These metal compounds used were in the form of fine powders. In Run 19, 1% weight of ferric oxide added to the sand mixture in addition to 2% clay (kaolin) already mixed with the silica sand. The experimental conditions are shown in Table 3.16.

Grim (1962) mentioned that the surface of kaolin clay provides adequate catalytic activity for the oxidation of hydrocarbon, and it is only necessary to activate the clay to produce a commercial product. Acid treatment of the clay is required using sulphuric acid. In this investigation, the kaolin sample was placed in a beaker, together with sulphuric acid. The sample is leached for a few minutes and heated to 150 °C for approximately two hours. After acid treatment, the mixture was washed with distilled water repeatedly, and the sample was finally dried.

Table 3.13 Sand pack properties and experimental condtions for Run 13

Sand mixture	75% wt silica sand + 25% natural core
Clay content	1% from the natural core (L. Fars)
Crude oil gravity, °API	22.1
Water air ratio, m^3/Mm^3(s+)	1.0
Oil saturation of pack, %	37.93
Porosity of pack, %	32.8
Oxygen in injected gas, %	21

Table 3.14 Condition of experiments conducted with 35% O_2

	Run 14	Run 15	Run 16
Crude oil gravity, °API	22.1	10.2	22.1
Type of combustion	dry	wet	wet
Water air ratio, m^3/Mm^3(s+)	0	1.0	1.0
Oil saturation of pack, %	39.46	39.53	39.01
Porosity of pack, %	30.07	31.92	29.51
Clay content, %	5	0	1*

*The clay content is from the natural core. The sand mixture for this contains 75% silica sand + 25% natural core.

Table 3.15 Propertis of nickel chloride and ferric oxide

nickel chloride*	$NiCl_2.6H_2O$	
	Minimum purity	99%
	Copper	< 0.002%
	Iron	< 0.005%
	Lead	< 0.001%
	Zinc	< 0.001%
	Water insoluble	< 0.001%
ferric oxide†		
	Iron(III) oxide	Fe_2O_3
	Molecular weight	159.69
	Minimum assay	95%
	Maximum limits of impurities loss at 600 °C	1%
	Water soluble matter	1%
	Arsen (as)	
	RT: room temperature	18-30 °C

*Provided by Hopkin & Williams Ltd., Chadwell Heath, Essex

†Supplied by BDH Chemicals Ltd., Poole.

Table 3.16 Experimental conditions for metallic additive runs

	Run 17	Run 18	Run 19
Crude oil gravity, °API	22.1	22.1	22.1
Water:air ratio, $m^3/Mm^3(s+)$	1.0	1.0	1.0
Oil saturation in pack, %	42.4	40.5	38.6
Porosity of pack, %	39.6	37.5	30.9
Clay content, %	0	0	2
Metallic additives content, %	1†	1*	1†

A mixture of 1% weight of kaolin treated with sulphuric acid and silica sand is packed into the combustion tube. A fast, self-sustained combustion front was obtained. The experimental conditions are shown in Table 3.17.

Table 3.17 Experimental conditions for Run 20 using kaolin treated with acid

Crude oil gravity, °API	22.1
Water:air ratio, $m^3/Mm^3(s+)$	1.0
Oil saturation, %	37.37
Porosity of pack, %	33.72
Clay content (after treated with acid), %	1

*Nickel chloride

†Ferric oxide

CHAPTER 4

Clay and Amorphous Silica Additives

Introduction

The *in situ* combustion process is affected by the inclusion of clays and other mineral compounds, which are incorporated into the sand matrix. In this study, the specific additives of interest are kaolin and amorphous silica, both of which have a high specific surface area. These material additives can have an important influence on the behaviour of the combustion process.

Twelve combustion tube runs using Maya Isthmus, Maya, and Cold Lake crude oils, were carried out to investigate the effect of kaolin and amorphous silica addition in the sand pack. The investigations concentrated on the effect of varying the amount of additive in the sand pack, the effect of acidising the kaolin, and the minimum level of kaolin necessary to sustain the combustion front.

The measured parameters for the *in situ* combustion experiments include the temperature profiles along the sand pack, fuel consumption, combustion front velocity, carbon combustion rate, and air requirement. In addition, the characteristics and properties of kaolin, amorphous silica, and acidised kaolin were studied using scanning electron microscopy (SEM), mineral composition analyses and catalytic activity.

4.1 Temperature Profiles

Figures 4.1 to 4.12 show the temperature profiles established along the length of the sand pack, covering twelve experiments (Runs 1-11, and 20). The detailed temperature data for each combustion experiment are given in Appendix A. Temperature profiles taken at various times show the high temperatures behind the combustion front, the peak temperature of the combustion front and the rapid change in temperature

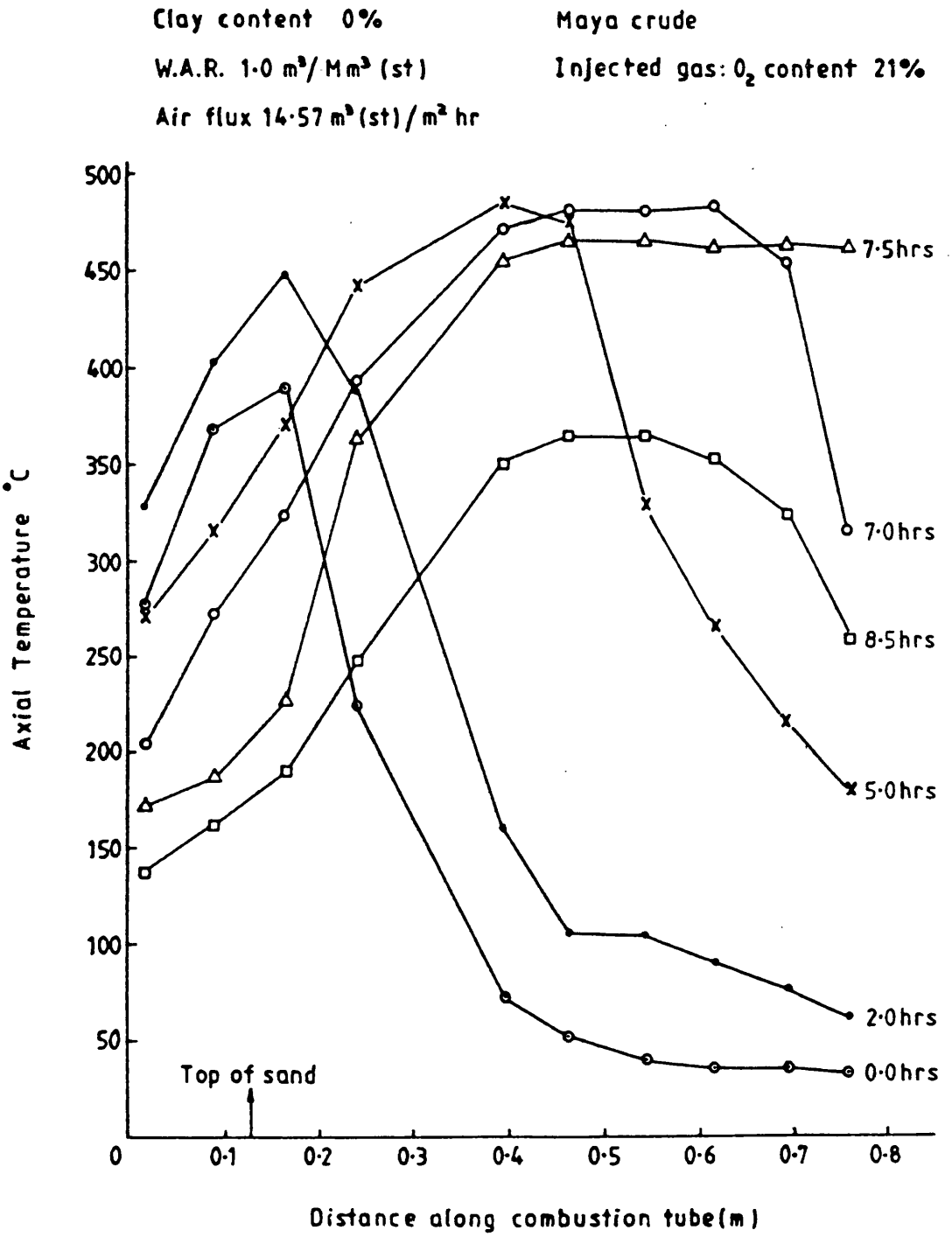

Figure 4.1 Temperature profile through combustion tube (Run 1)

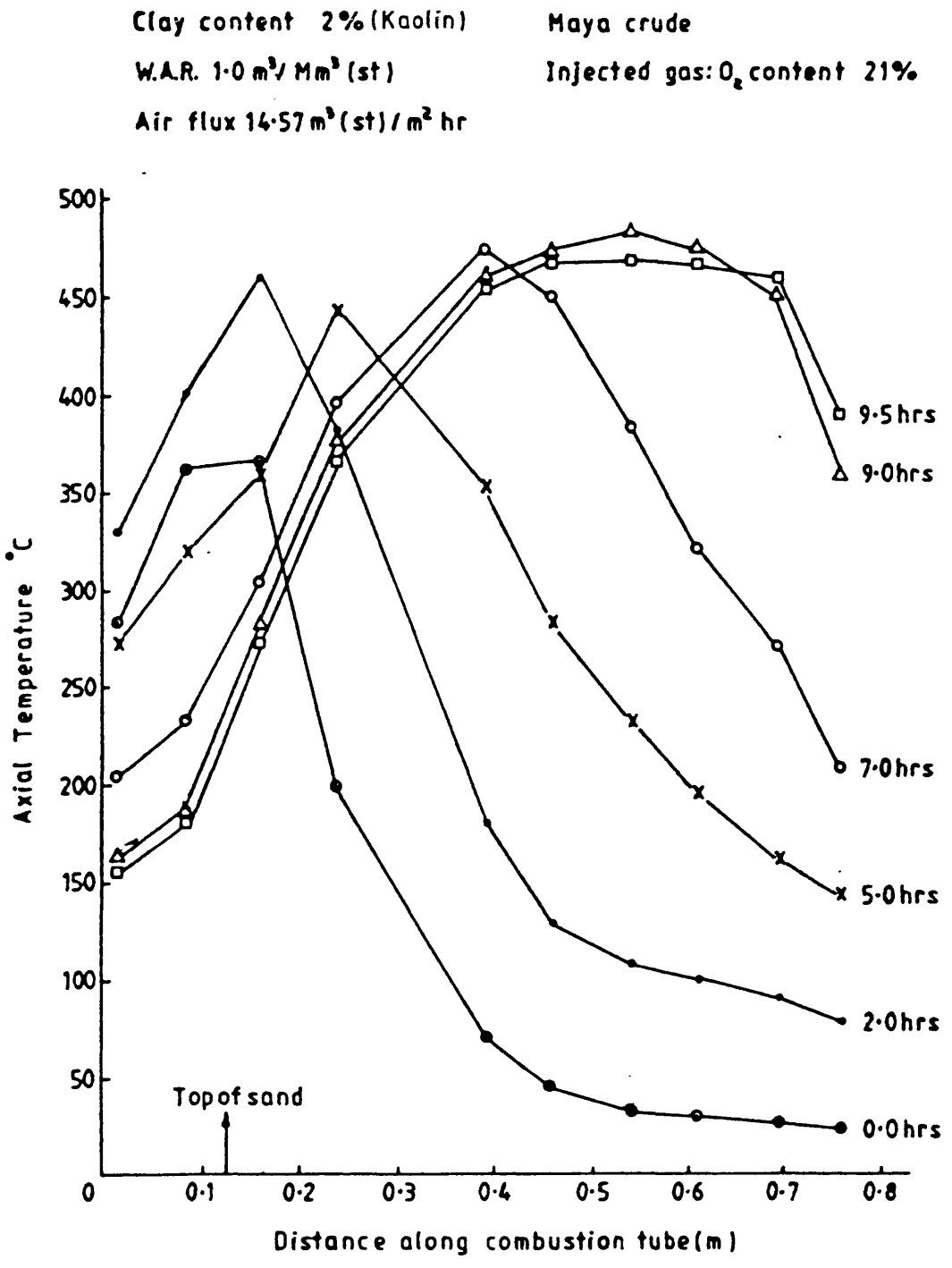

Figure 4.2 Temperature profile through combustion tube (Run 2)

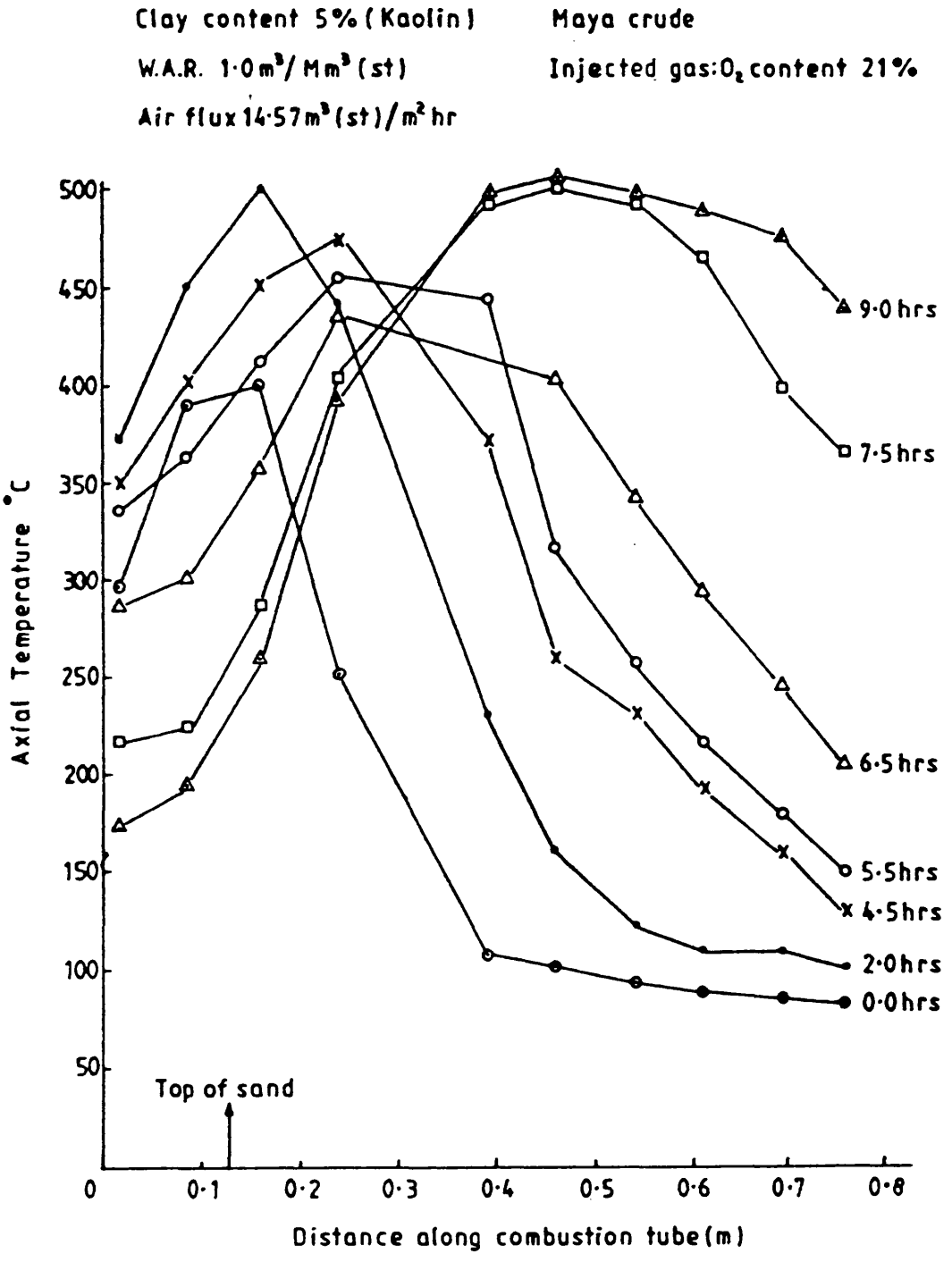

Figure 4.3 Temperature profile through combustion tube (Run 3)

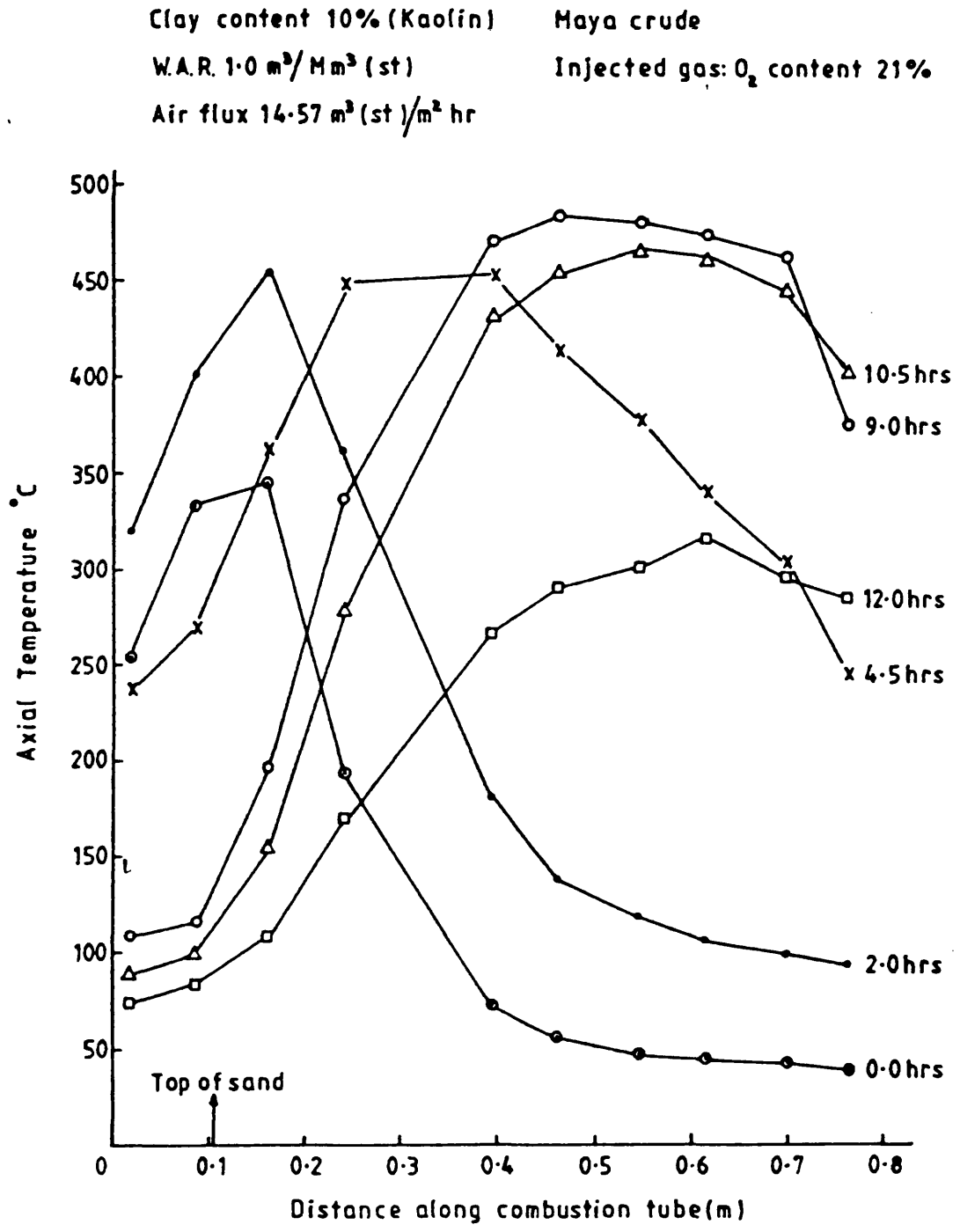

Figure 4.4 Temperature profile through combustion tube (Run 4)

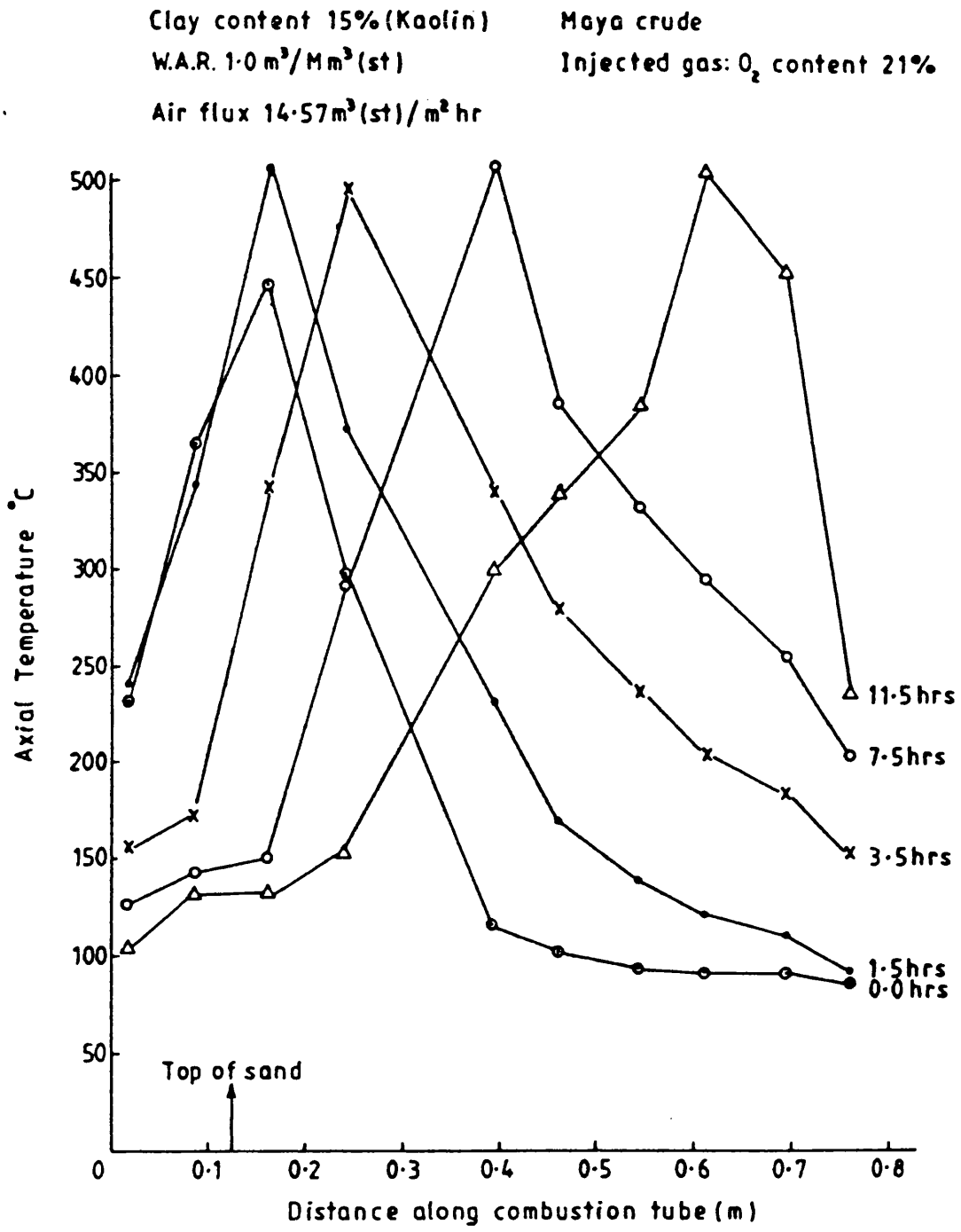

Figure 4.5 Temperature profile through combustion tube (Run 5)

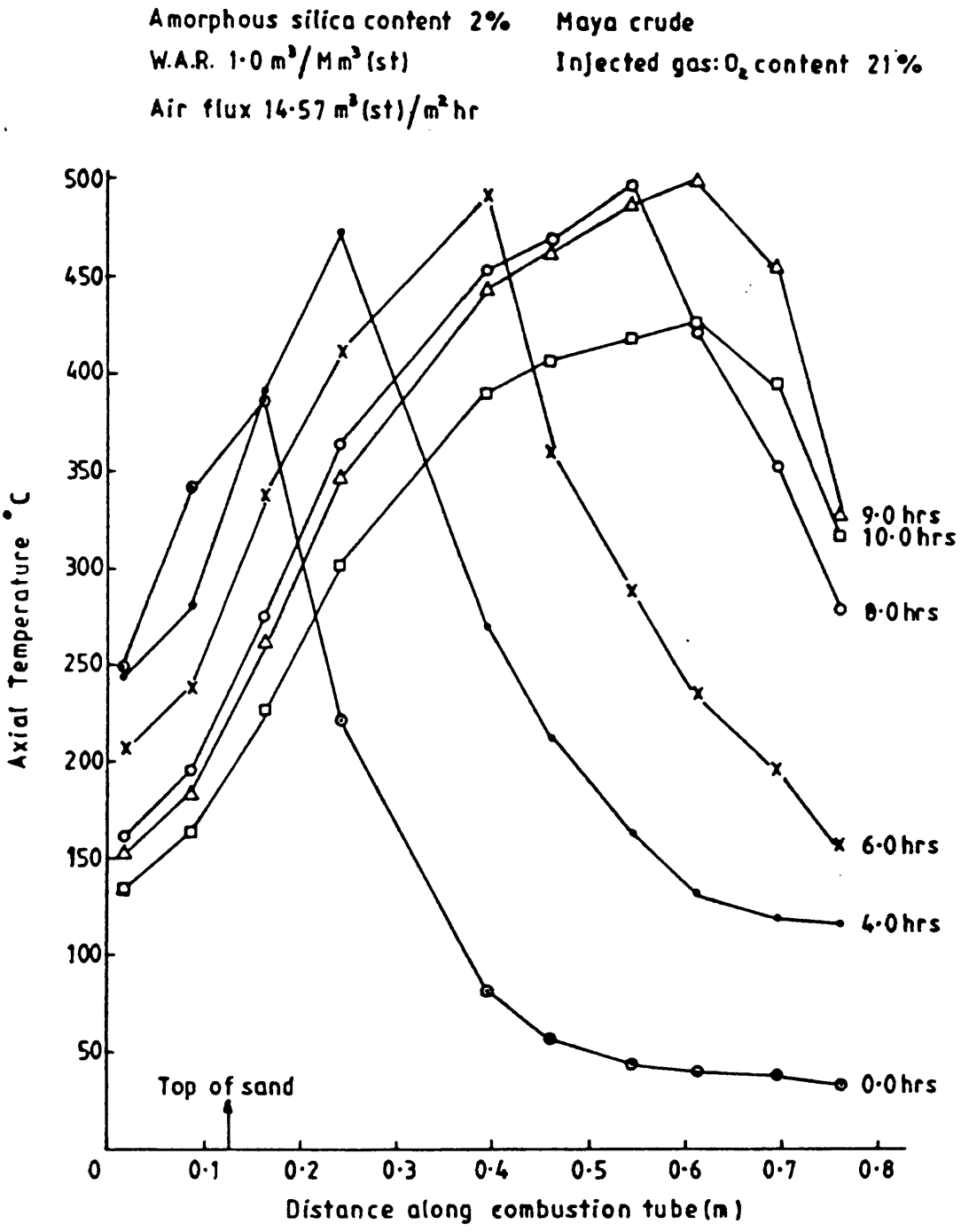

Figure 4.6 Temperature profile through combustion tube (Run 6)

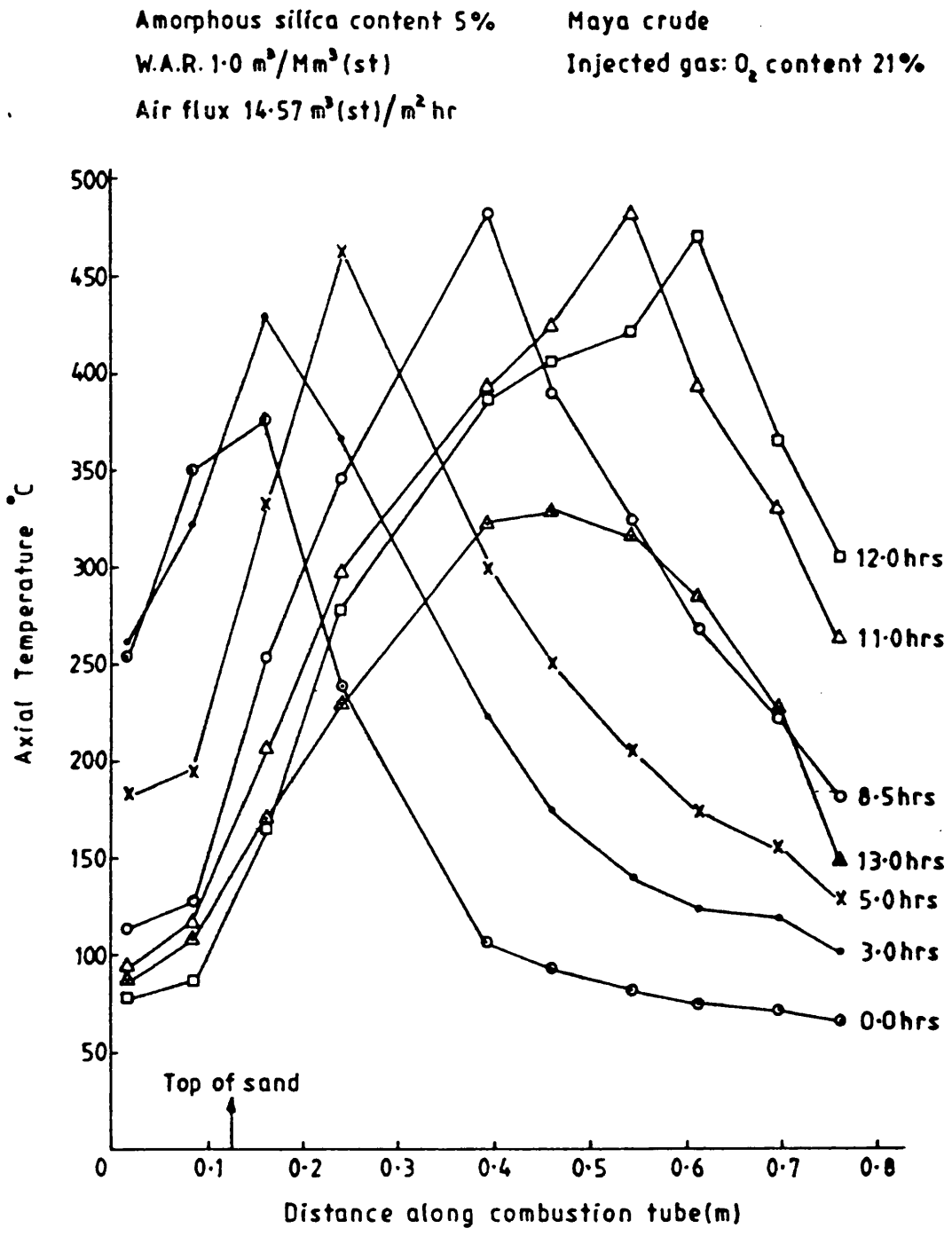

Figure 4.7 Temperature profile through combustion tube (Run 7)

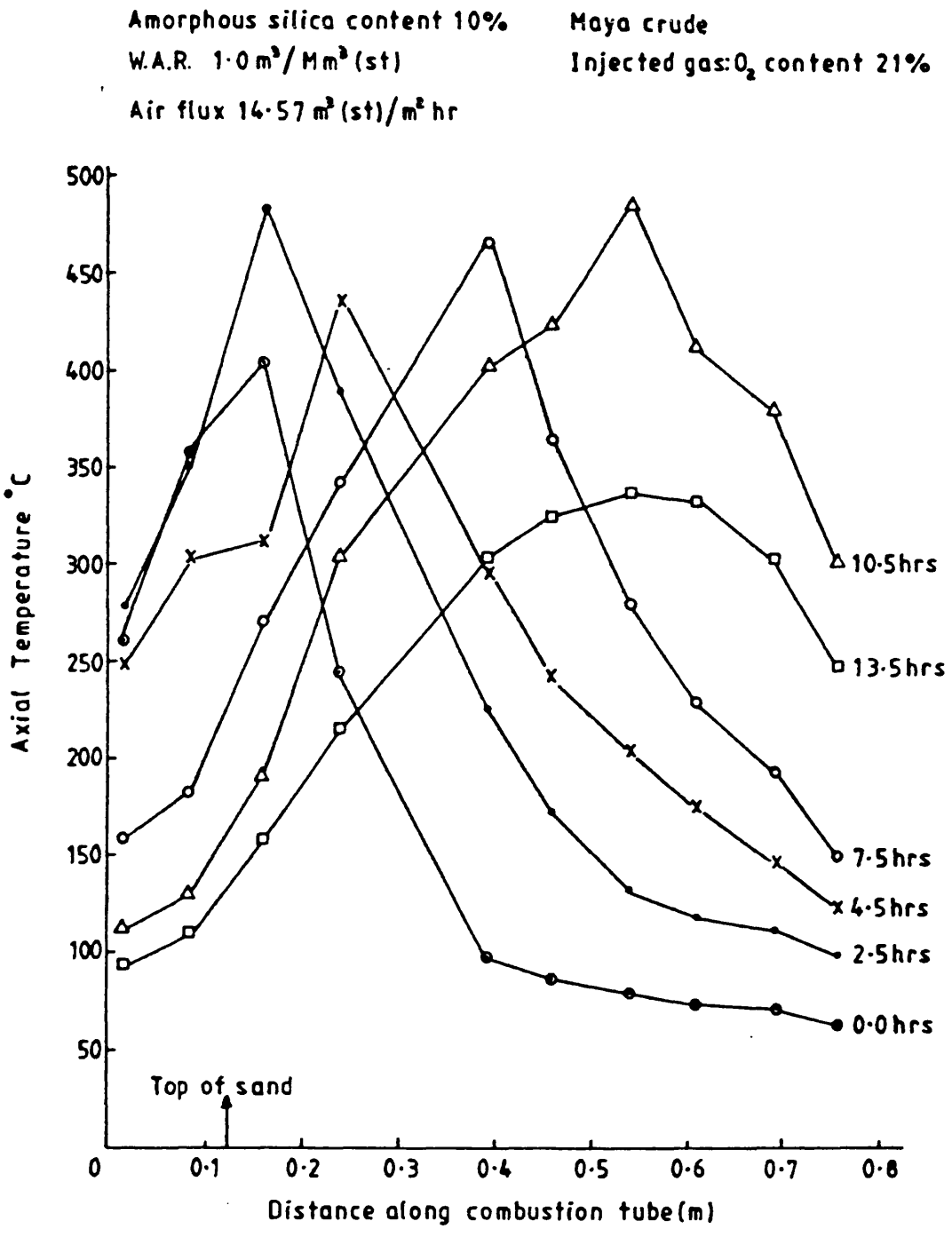

Figure 4.8 Temperature profile through combustion tube (Run 8)

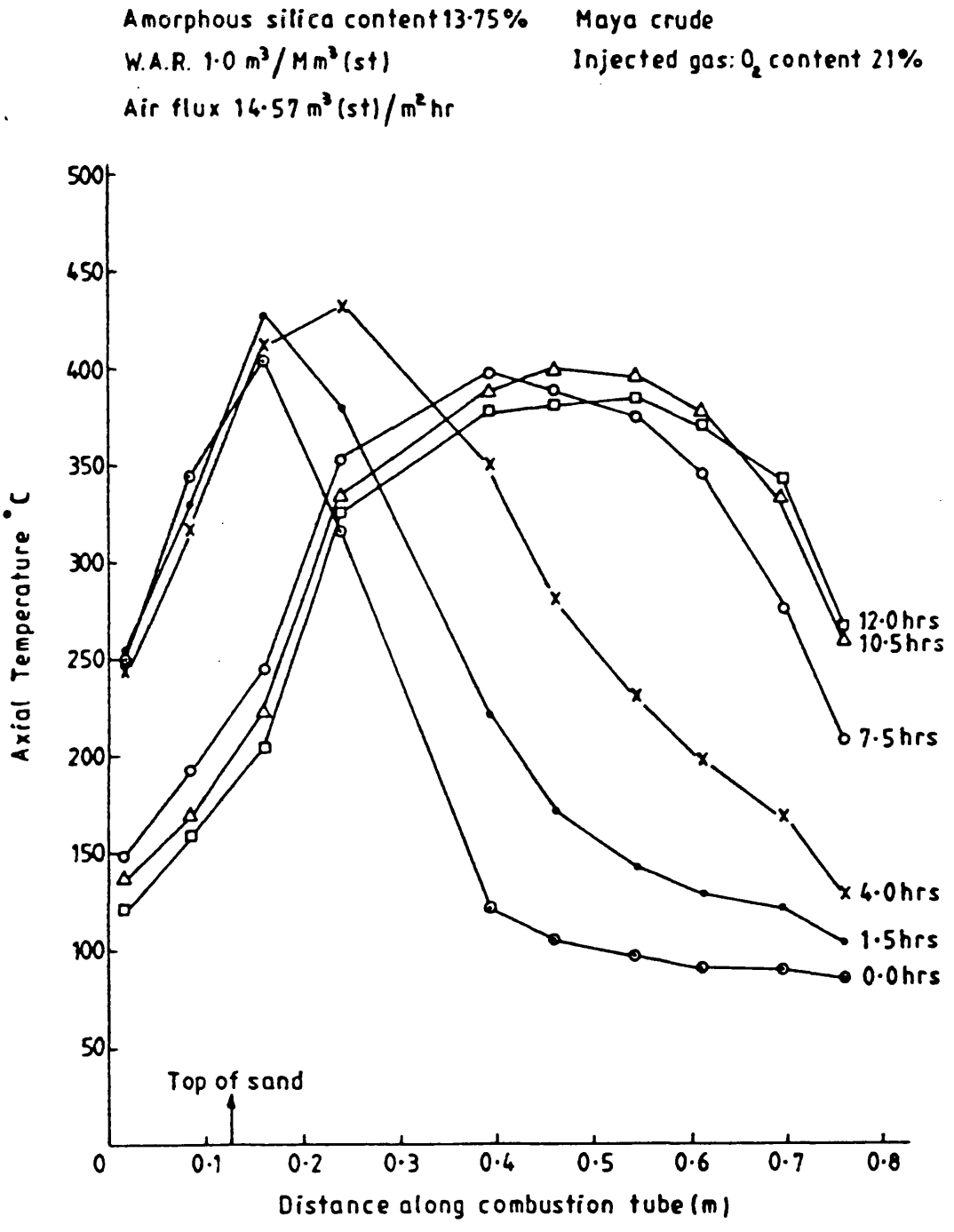

Figure 4.9 Temperature profile through combustion tube (Run 9)

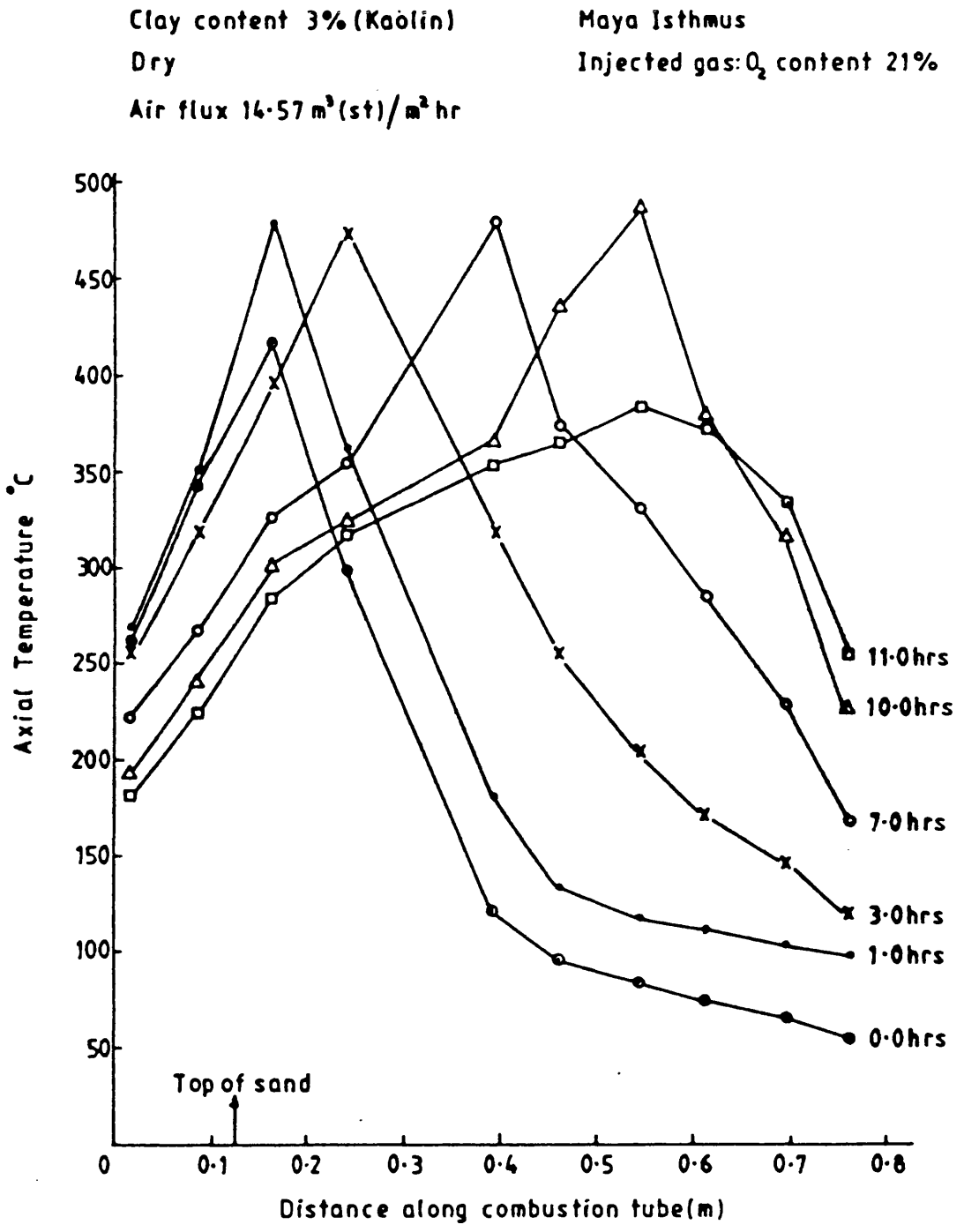

Figure 4.10 Temperature profile through combustion tube (Run 10)

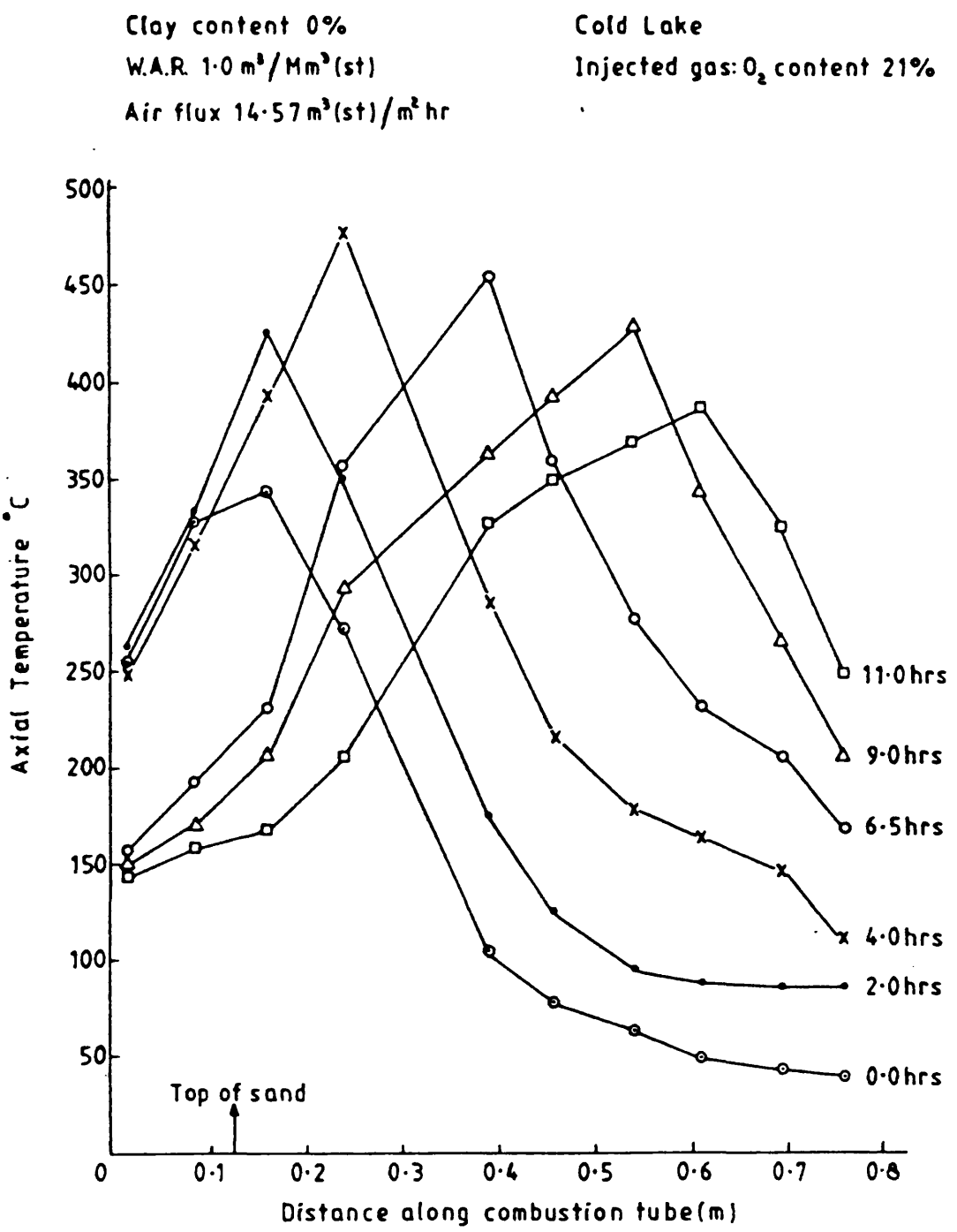

Figure 4.11 Temperature profile through combustion tube (Run 11)

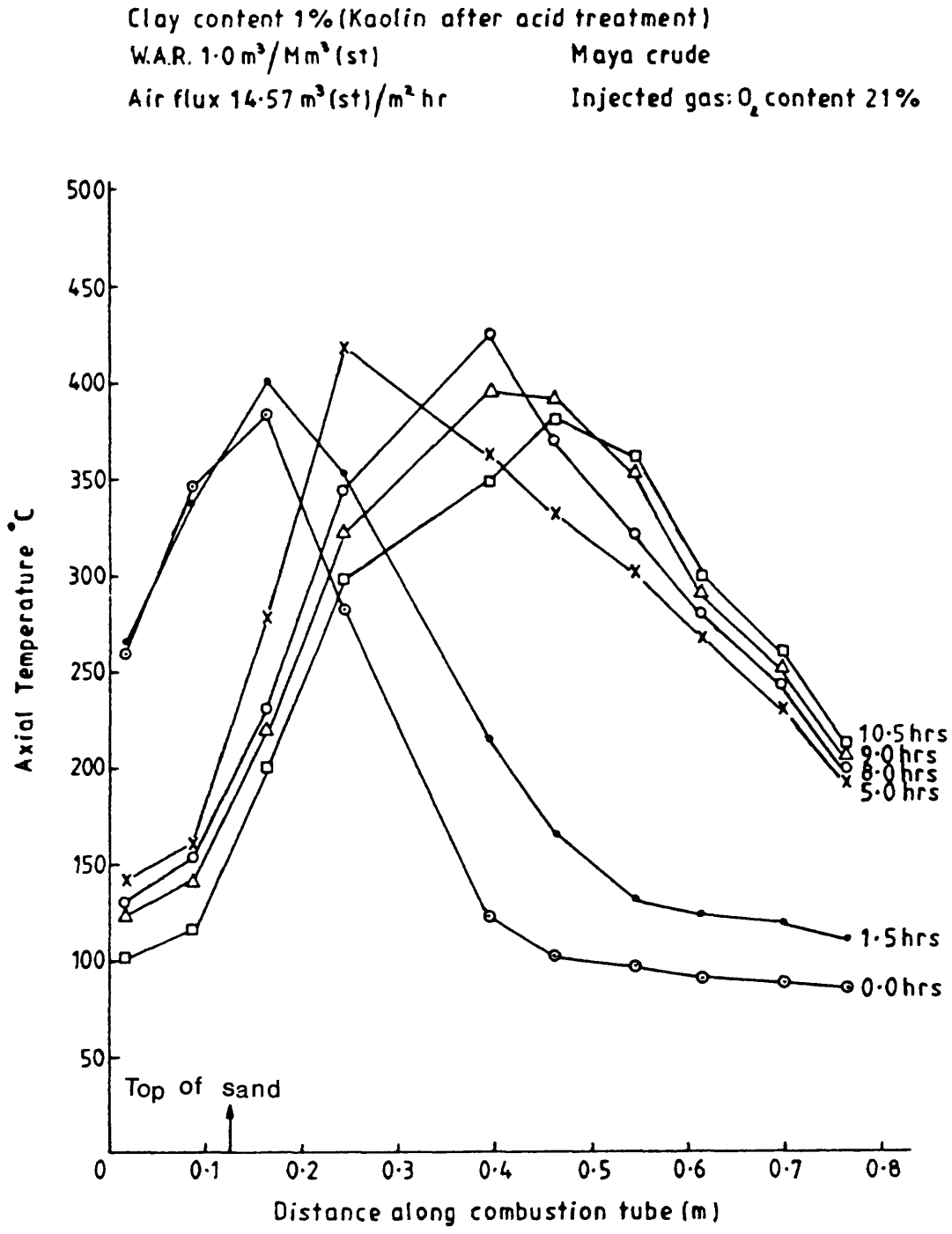

Figure 4.12 Temperature profile through combustion tube (Run 20)

through and ahead of the reactive zone. The peak temperatures observed along the axis of the sand pack provide a good basis for estimating the combustion front position.

The variation in peak temperature, as the combustion front moves through the sand pack, is partly due to heat losses from the combustion zone. Most of the heat generated by exothermic reaction is converted downstream of the combustion front, but a significant heat loss can also occur radially through and along the combustion tube wall. The peak combustion temperatures are dependent on fuel properties and composition, as well as air flux. Therefore, any change in these factors will also lead to variation in peak temperature.

In Figures 4.2, 4.3, 4.8 and 4.9 (Runs 2, 3, 8 and 9), the initial high temperature occurring two to four hours after ignition is mainly due to the preheating effect of the top band heater tube. However, the peak temperature tends to increase throughout each run by 2-7%. Convected heat transfer by the air and water vapour passing through the burnt upstream section of the bed is mainly responsible for this effect, transferring heat downstream of the combustion zone.

Initially, the temperature of the sandpack is raised approximately 50 °C. The top band heater is then used to increase the temperature of the top section of the sandpack to about 330 °C, in order to achieve ignition of the crude oil. Air injection is commenced at this point. These effects are demonstrated in Figure 4.1, for example, where the eventual onset of ignition (top of the sandpack) occurs at approximately 380 °C. Figure 4.1 (Run 1) shows that a self-sustained combustion front in the range 450-470 °C moves slowly downstream, reaching a maximum temperature of 480 °C at 5 hours after ignition.

In Runs 2, 3 and 4 (Figures 4.2, 4.3 and 4.4 respectively), the shape of the tmeperature profile is the same as that for Run 16 (Figure 4.1). During these wet combustion runs, however, the profile becomes steeper behind the combustion zone.

On the other hand, the shape of the temperature profile in Figure 4.5 (Run 5) shows a different trend to the other runs. This is most probably due to the presence of 15% kaolin in the sandpack which leads to a higher fuel consumption, and hence a higher combustion peak temperature. However, at the combustion front, the heating tape was not capable of generating a high enough temperature and so the combustion temperature drops sharply ahead of the front.

The shape of the temperature profiles in Figures 4.6, 4.7 and 4.8 exhibits a similar trend for which a different percentage of amorphous silica was used. However, the temperature profiles during Run 9 (Figure 4.9) are different and represent a more distinctive combustion steam zone formed at 7.5, 10.5 and 12 hours after ignition. These are relatively the same as those obtained in Run 20 (Figure 4.12).

A drop in combustion peak temperature was observed at the end of Runs 10 and 11 (Figures 4.10 and 4.11). This is attributed to the severe problems which were encountered towards the end of the run when heat losses became large due to conduction through the tube bottom flange.

The effect of adding clay (0, 2, 5, 10 and 15% kaolin) to the sand matrix is shown in Figures 4.1 to 4.5. The temperature profiles in these tests are quite similar, but the average peak temperature increases generally with clay content, which is due to the fact that clay material possesses a very high specific surface area which promotes fuel deposition. Increased fuel consumption (Table 4.3) gives rise to an increase in combustion temperature. However, a self-sustained combustion front was achieved in Run 1, when clay was absent. Evidently, therefore, sufficient thermal/catalytic cracking of Maya crude oil still occurs in this case.

Adding 2, 5 and 10% of amorphous silica to the sand pack produced no significant change in peak temperatures. During Runs 6, 7 and 8 (Figures 4.6 to 4.8), the average peak temperatures are 472, 469 and 472 °C, whereas an increase from 2 to 10% kaolin increased the average peak temperature by 15 °C.

When 13.75% amporphous silica is used (Run 9), the peak temperature after six hours from ignition reduced from 435 to 400 °C. This is attributed to a reduction in fuel consumption ahead of the combustion front. Hence, the combustion temperature is reduced.

Two other crude oils were used. Firstly, for Maya Isthmus crude oil (Run 10), a self-sustained combustion front was obtained when a minimum of 3% wt of kaolin was added to the sand pack. The combustion front temperature is virtually constant throughout the experiment at 486 °C, as shown in Figure 4.10. Secondly, for Cold Lake crude oil (Run 11), in which no clay additives were used, a self-sustained combustion front was obtained as well. Figure 4.11 shows that the combustion front temperature to decline as it approached the end of the sand pack. This is due to the low fuel laydown ahead of the combustion front, as explained previously for Run 9. Water injection can also exert an effect on the front temperature, if fuel availability is insufficient to maintain a high combustion temperature.

Figure 4.12 illustrates the effect when using 1% wt of kaolin which has been treated with sulphuric acid. In this case, the average peak temperature was only 415 °C. This low value could be due to the acidised kaolin acting as a catalyst, causing a reduction in the activation energy (Drici and Vossoughi, 1985) and shifting the reaction to a lower temperature.

A steam plateau is defined as a flat temperature region ahead of the combustion front. It is formed as a result of the combustion which generates heat as it moves through a porous medium. A narrow steam plateau is observed in Figures 4.2 and 4.4 (Runs 2 and 4 respectively), but a much more distinctive steam plateau occurs in Figures 4.1, 4.3 and 4.5 (Runs 1, 3 and 5 respectively). For Run 10 (Figure 4.10), the steam plateau which occurs after ignition is not fully established, but does stabilise at a temperature of 123 °C. A distinctive steam plateau is shown in Figure 4.12 (Run 20), as evidenced by the flat profile occurring 1.5 hours after ignition. The average temperature of the steam plateau is 120 °C.

4.2 Carbon Combustion Rate

The carbon combustion rate was calculated from cumulative plots of cabron burned against time. Figure 4.13 shows a typical carbon combustion profile for Run 5. Data for other experiments are given in Table 4.1. The instantaenous cumulative carbon burned for all runs is listed in Appendix B. The carbon combustion rate achieves a constant value shortly after the combustion front was fully established, typically one to two hours after ignition.

Figure 4.14 shows the carbon combustion rate when different amounts of clay (kaolin) and amorphous silica are used. This shows that the carbon combustion rate increases by approximately 0.05 gm/h/% clay. Carbon combustion rate does not change significantly in the presence of amorphous silica. However, Run 19 (13.75% amorphous silica) reveals a different behaviour. In this case, an appreciably low carbon combustion rate of 4.0 gm/h is achieved, and this is consistent with the lower peak combustion temperatuer of 431 °C (as discussed in the previous section) obtained in this run.

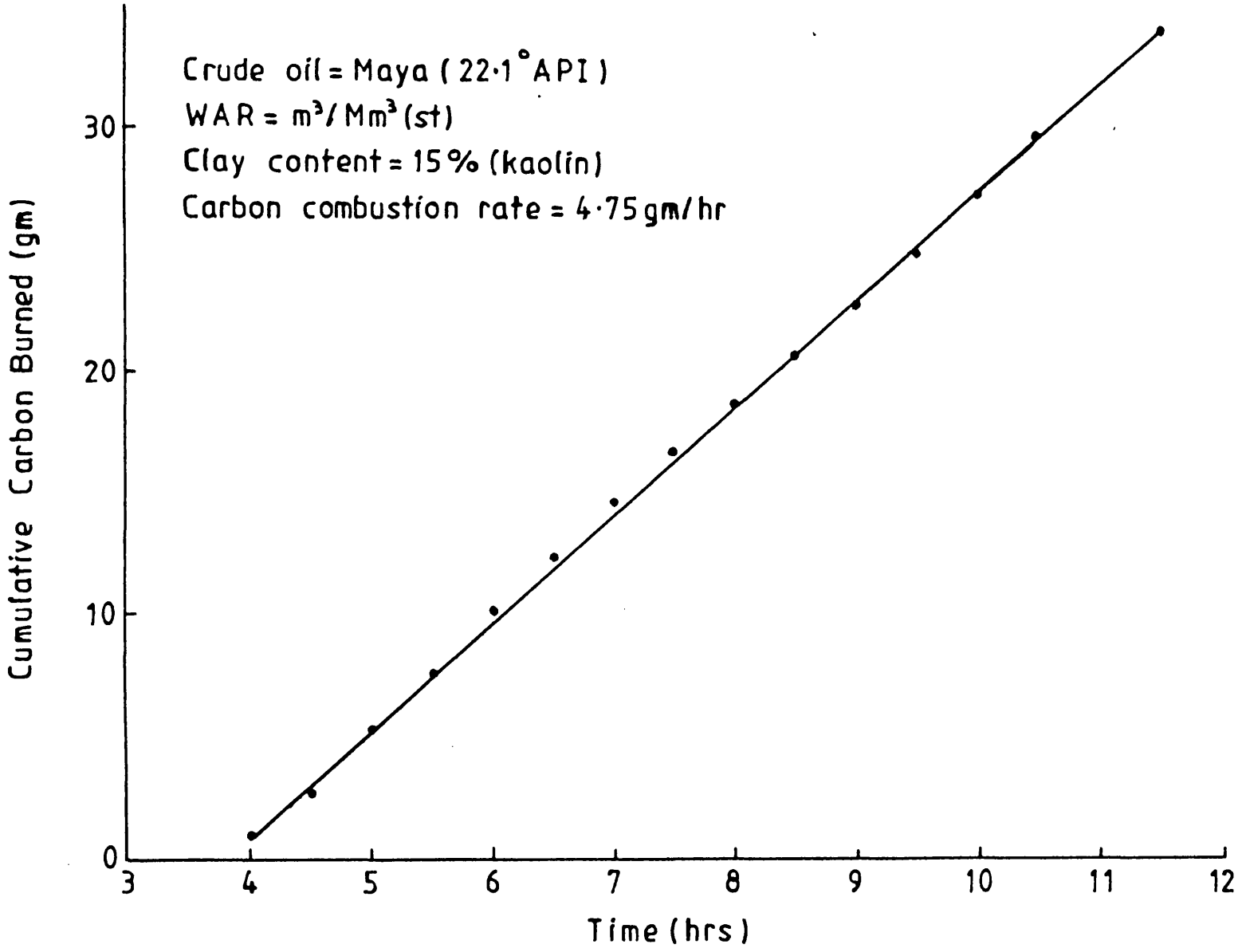

Figure 4.13 Typical carbon combustion rate curve (Run 5)

Table 4.1 Effect of Additives on Carbon Combustion Rate

Run No.	Crude Oil	WAR [m^3/Mm^3 (st)]	Additive Content	Carbon Combustion Rate (gm/h)
1	Maya	1.0	0%	4.0
2	"	1.0	2% kaolin	4.25
3	"	1.0	5% kaolin	4.25
4	"	1.0	10% kaolin	4.5
5	"	1.0	15% kaolin	4.75
6	Maya	1.0	2% amorphous silica	4.75
7	"	1.0	5% amorphous silica	4.75
8	"	1.0	10% amorphous silica	4.75
9	"	1.0	13.75% amorphous silica	4.0
10	Maya Isthmus	dry	3% kaolin	4.0
11	Cold Lake	1.0	0%	4.5
20	Maya	1.0	1% acidised kaolin	4.0
Guvenir (1980)	Iola (19.3 °API)	dry	0%	6.8
			5% kaolin	13.0
			10% kaolin	13.6
			15% kaolin	13.6
			15% amorphous silica	16.6
Al-Shalabe (1985)	Maya Isthmus	3.75	5% kaolin	2.24
		3.75	10% kaolin	3.08
		2.5	5% kaolin	3.27
		dry	10% amorphous silica	3.64
Adewusi (1986)	Maya	dry	8.4% kaolin	3.1
		6.3	8.4% kaolin	2.9

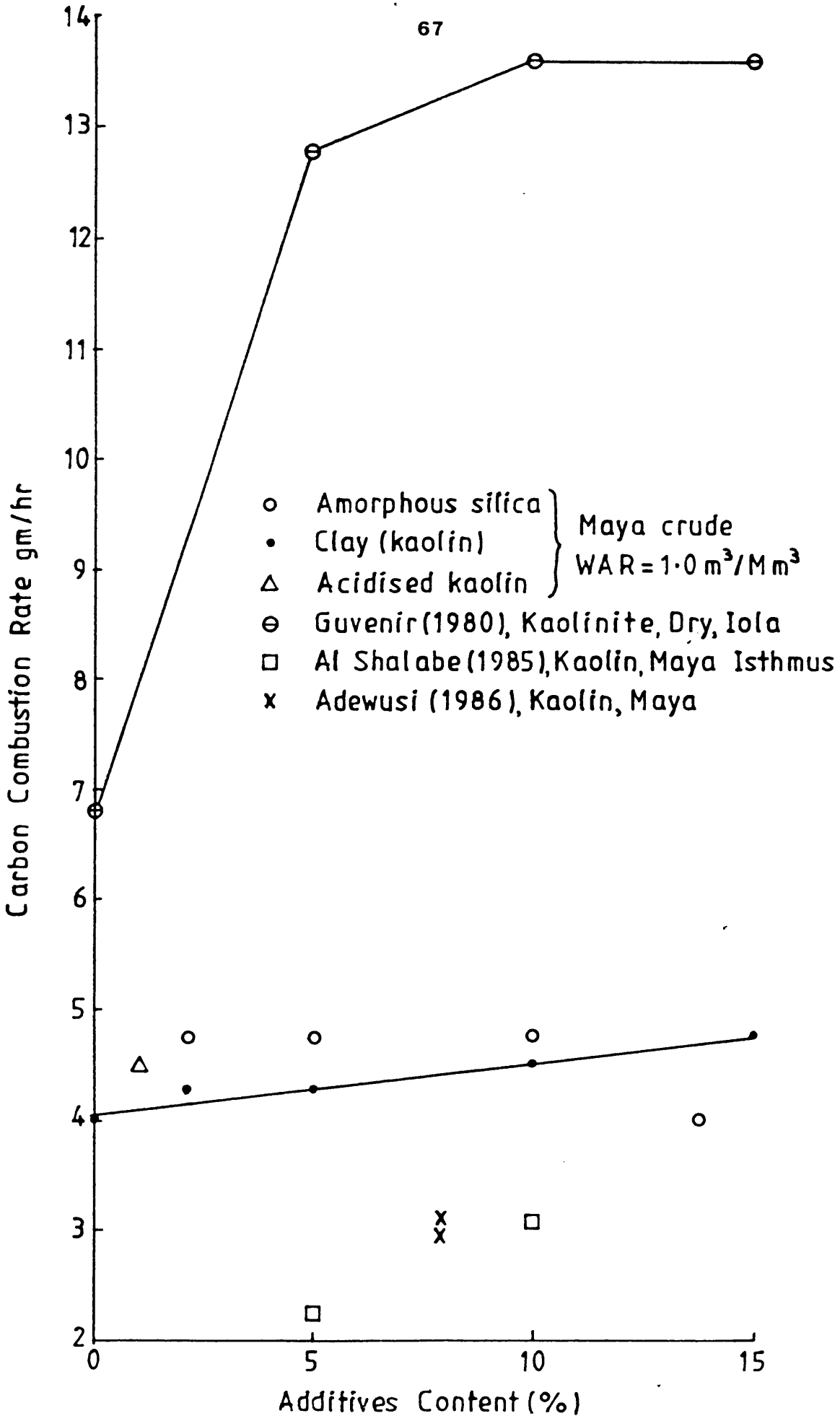

Figure 4.14 Effect of additives on carbon combustion rate

The carbon combustion rates obtained for Runs 1-11 and 20 lie in the range of 4.0-4.75 gm/h. Values obtained by Guvenir (1980), Al-Shalabe (1985) and Adewusi (1986) were respectively, 6.8-16.6 gm/h, 2.3-3.6 gm/h and 2.9-3.1 gm/h (Table 4.1). The results of Adewusi's work could have been affected by high heat losses, due to a thick wall combustion tube design. Guvenir's results are generally much higher than those obtained in the present work. Different equipment and operating conditions may be significant. Al-Shalabe carried out all of her experiments using the same equipment used in this work. However, she used a different oil to sand ratio (11.2%), which is probably the reason for her slightly lower carbon combustion rates. The oil to sand ratio used in the present work was 7%.

4.3 Combustion Front Velocity

The combustion front velocities which are obtained from the temperature profiles are listed in Table 4.2. Figure 4.15 represents a typical plot of front position *versus* time for Run 11. This demonstrates an overall linear trend.

The precision with which the front velocity can be estimated from the combustion temperature profile (peak temperatures) is very much influenced by the spacing of the temperature profiles. However, even though some localised inaccuracy is evident from the plot (Figure 4.15), a reasonable prediction is possible because of the averaging effect over the experiment.

Figure 4.16 shows the effect of clay content on the combustion front velocity. When up to 2% kaolin is used, there is a sharp fall in the combustion front velocity. At high concentrations, the velocity decreases at a constant rate, which is estimated to be 0.1 m/h/% clay. Using 1% acidised kaolin, however, the combustion front velocity is much lower compared with 1% unacidised clay. This is estimated to

Table 4.2 Effect of Additives on Combustion Front Velocity

Run No.	Crude Oil	WAR [m^3/Mm^3 (st)]	Additive Content	Combustion Front Velocity (m/h)
1	Maya	1.0	0%	0.11
2	"	1.0	2% kaolin	0.075
3	"	1.0	5% kaolin	0.0675
4	"	1.0	10% kaolin	0.0525
5	"	1.0	15% kaolin	0.0375
6	Maya	1.0	2% amorphous silica	0.06
7	"	1.0	5% amorphous silica	0.055
8	"	1.0	10% amorphous silica	0.046
9	"	1.0	13.75% amorphous silica	0.04
10	Maya Isthmus	dry	3% kaolin	0.04
11	Cold Lake	1.0	0%	0.0525
20	Maya	1.0	1% acidised kaolin	0.045
Guvenir (1980)	Iola (19.3 °API)	dry	sand only	0.055
			15% clay	0.033
			15% amorphous silica	0.052
Vossoughi *et al* (1985)	Iola (19.8 °API)	dry	15% silica powder	0.042
Al-Shalabe (1985)	Maya Isthmus	3.75	5% clay	0.1524
		3.75	10% clay	0.0965
		dry	10% amorphous silica	0.0558

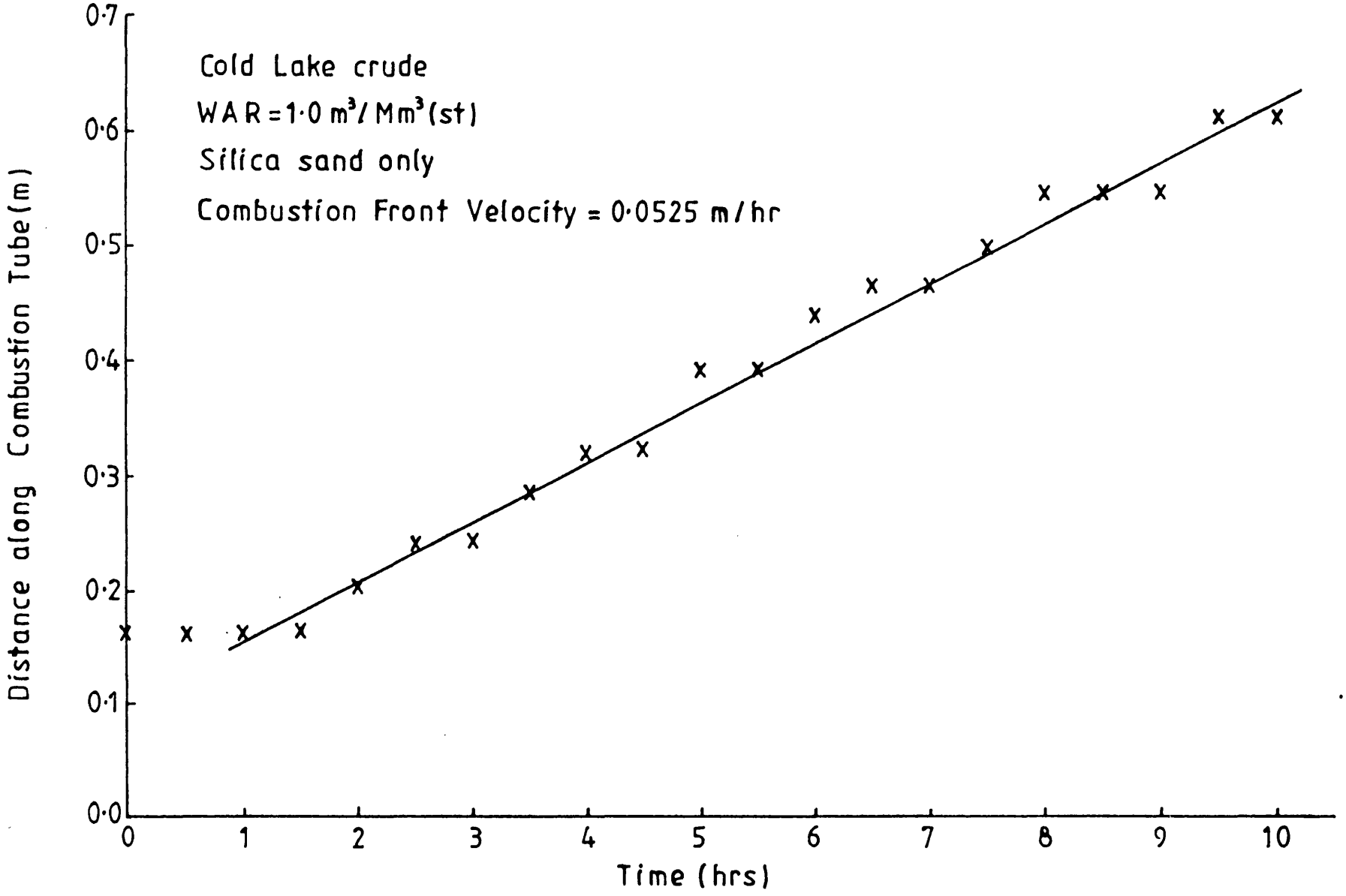

Figure 4.15 Combustion front velocity (Run 11)

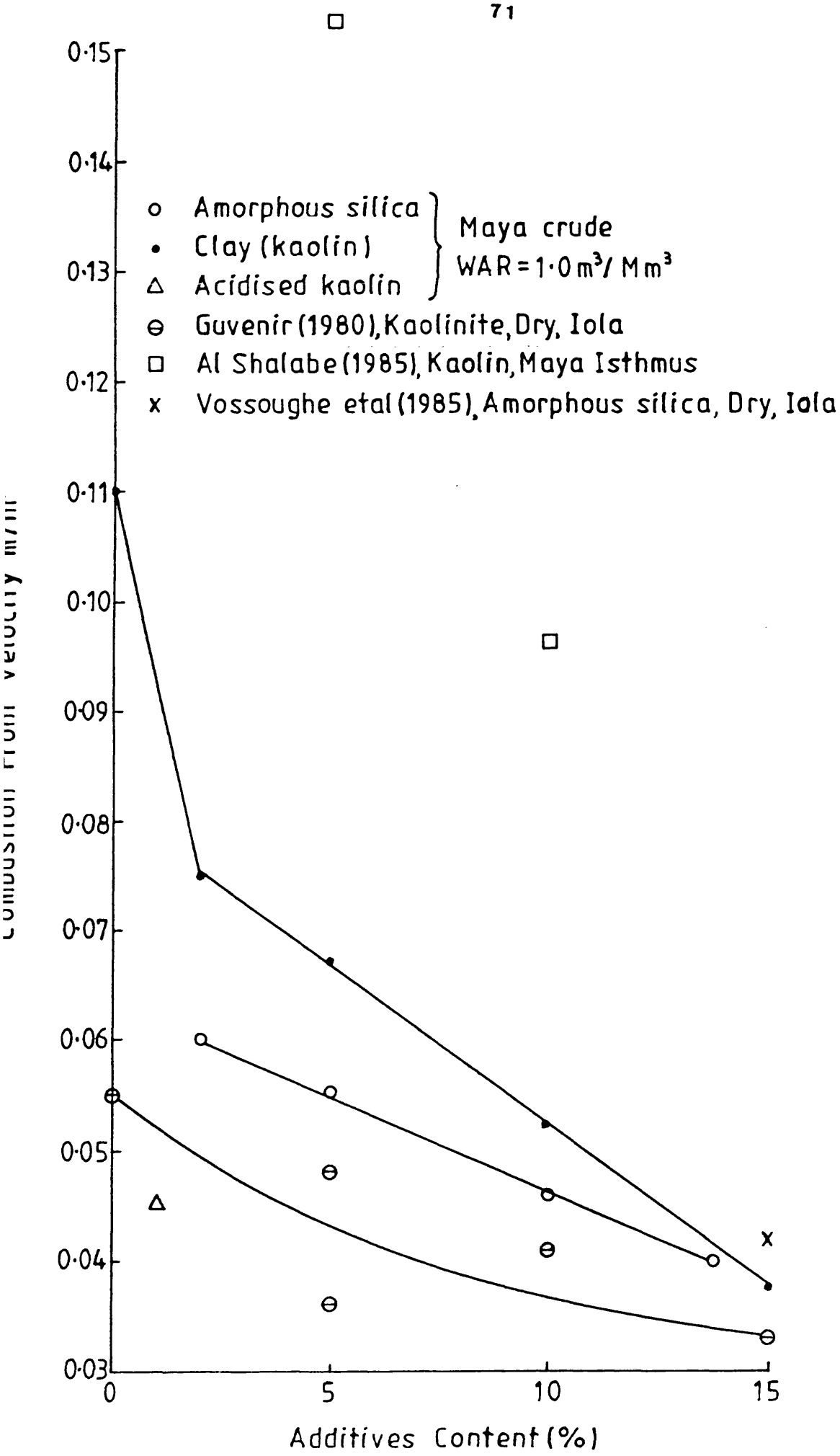

Figure 4.16 Effect of clay and amorphous silica on combustion front velocity

be 0.08 m/h.

For amorphous silica combustion runs (6 to 9), the combustion front velocity is lower than clays (Figure 4.16) and decreases with increased amounts of amorphous silica additives (0.14 m/h/% amorphous silica). This is due to the higher fuel consumption obtained with amorphous silica additives (see next Section).

The agreement between results obtained in the present work and those obtained by other studies (Table 4.2) is satisfactory. Figure 4.16 shows the values obtained by Guvenir (1980), which concluded that the combustion front velocity decreases with increasing clay content of the sand mixture. The only discrepancy in his work was the rather large difference observed for the two 5% clay runs. This was attributed to the difference in packing density.

Al-Shalabe (1985) observed similar trends for kaolin with Maya Isthmus crude oil (WAR of 3.75 m^3/Mm^3). The combustion front velocity decreased from 0.152 to 0.097 m/h when clay content was increased from 5 to 10% kaolin.

Values of combustion front velocity for amorphous silica in the present work are in the range 0.04-0.06 m/h. This range is consistent with values reported by Al-Shalabe (1985), Vossoughi *et al.* (1985) and Guvenir (1980) for 10 and 15% amorphous silica.

4.4 Fuel Consumption

The primary fuel for combustion is obtained from thermal cracking of the oil on the sand matrix. When residual oil in the steam zone is exposed to high temperature, carbon-rich with 'coke' is deposited on the sand surface. The amount of fuel present per unit bulk volume of reservoir is an extremely important parameter in combustion operations,

for it generally determines the air required to burn a unit bulk volume of reservoir. Fuel consumption then over the stabilised period is normally defined as follows:

$$\text{Fuel consumption } (kg/m^3) = \frac{\text{fuel burned (kgm)}}{\text{volume of combusted section } (m^3)}$$

Earlier *in situ* combustion studies concluded that oil gravity, original oil saturation, and rock properties (especially containing clay) had a major effect on fuel deposition (Mckay, 1982). Clays, which have a very large specific surface area, promote the deposition of a thin layer of carbon on the sand grains. As shown in Table 4.3 and Figure 4.17, a noticeable increase in fuel consumption results from the addition of clay to the sand pack. There is an overall linear relationship between clay content and fuel consumption and this can be represented simply by: fuel consumption = A (% kaolin) + B, where A = 0.55 and B = 12.5

On the other hand, amorphous silica, which has a specific surface area of 2 m^2/gm, compared with 12-14 m^2/gm for kaolin, also exhibits similar behaviour as kaolin, but represented a curve with concave shape (Figure 4.17). As shown in Table 4.3, the highest fuel consumption value of 29.43 kg/m^3 was obtained with acidised kaolin. This is attributed to the higher surface area of the acidised kaolin.

In Run 10 (dry), where Maya Isthmus crude oil was used and a minimum of 3% kaolin was added to the sand pack to sustain the combustion front, fuel consumption of 21.4 kg/m^3 is obtained. For Run 11 (WAR 1.0 m^3/Mm^3), in which Cold Lake crude oil and silica sand alone were used, a lower fuel consumption of 15.2 kg/m^3 is obtained. This is due to the effect of the water injected, which was believed to produce a substantial reduction in fuel consumption (Al-Shalabe, 1985).

Table 4.3 Effect of Additives on Fuel Consumption

Run No.	Crude Oil	WAR [M^3/Mm^3 (st)]	Additives Content	Fuel Consumption (kg/m^3)
1	Maya	1.0	0%	12.4
2	"	1.0	2% kaolin	14.3
3	"	1.0	5% kaolin	14.6
4	"	1.0	10% kaolin	17.9
5	"	1.0	15% kaolin	20.9
6	Maya	1.0	2% amorphous silica	16.22
7	"	1.0	5% amorphous silica	17.88
8	"	1.0	10% amorphous silica	19.91
9	"	1.0	13.75% amorphous silica	27.60
10	Maya Isthmus	dry	3% kaolin	21.42
11	Cold Lake	1.0	0%	15.19
20	Maya	1.0	1% acidised kaolin	29.43
Ejiogu *et al.*, (1978)	Pembina (37 °API)	dry	10% clay	26.14
		2.67	5% clay	18.81
Guvenir (1980)	Iola (19.3 °API)	dry	0%	2.54
			15% clay	6.41
			15% amorphous silica	4.80
			10% clay	4.9
Al-Shalabe (1985)	Maya Isthmus	3.75	5% clay	6.10
		3.75	10% clay	8.0
		dry	10% amorphous silica	18.57
		dry	5% clay	19.98

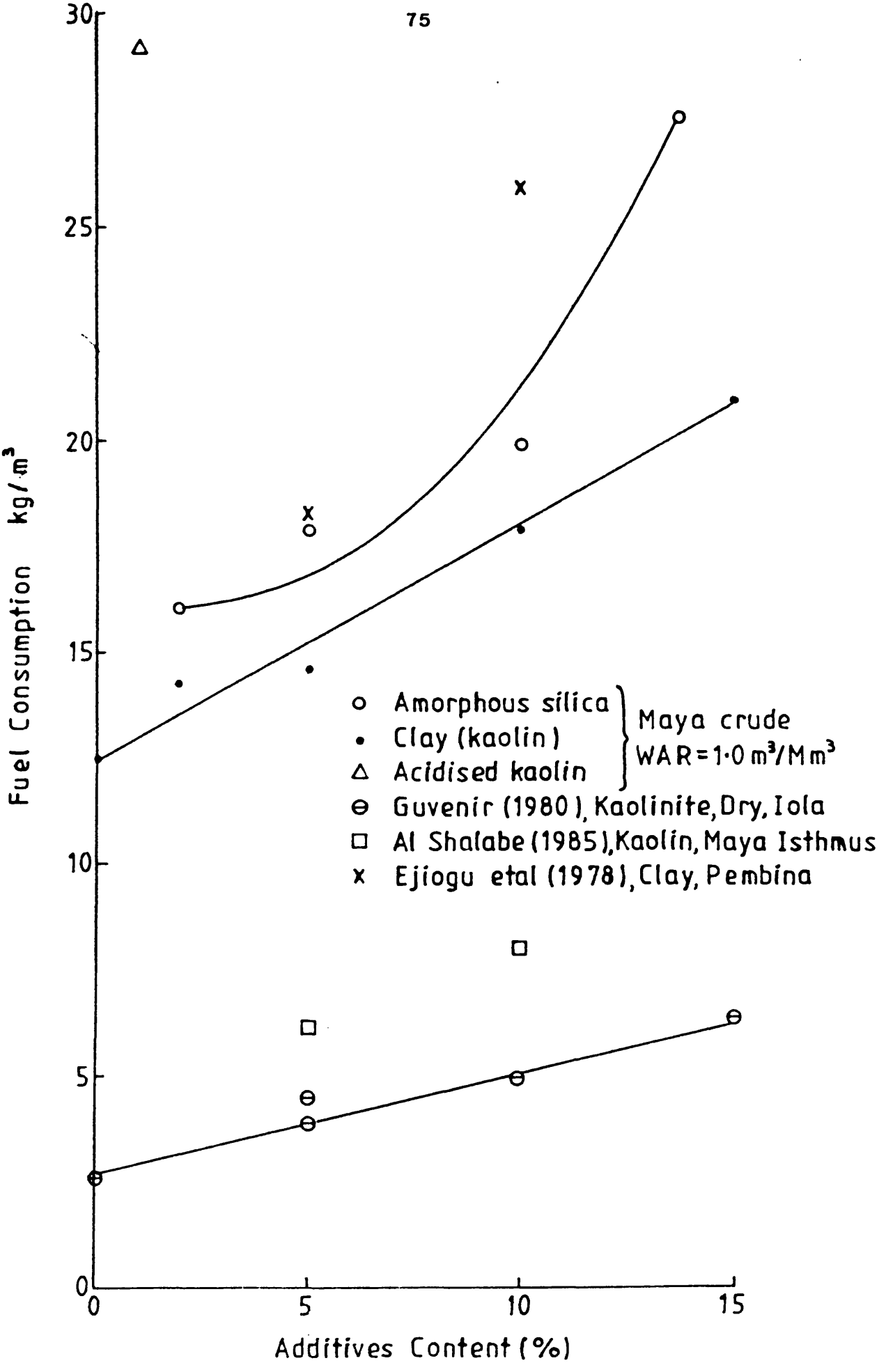

Figure 4.17 Effect of additivies on fuel consumption

The fuel consumption values reported in Table 4.3 for the present work are higher than those which were obtained by Guvenir (1980) and Al-Shalabe (1985). However, they compare favourably with those obtained by Ejiogu *et al.* (1979). In Guveiner's study, the fuel consumption in the sand mixture with 15% silica powder was almost equal to that in the sand mixture with 10% clay. Even though silica powder has a large surface area (1.5 m^2/g.), it is still smaller than the reported surface area of clay (2-20 m^2/g). The fuel consumption increased with increasing clay content. It was concluded that the large surface area of the clays is a major contributor to the fuel consumption process.

In Al-Shalabe's study the fuel consumption increased from 6.1 to 8.0 kg/m^3 when the clay content increased from 5 to 10% kaolin (Table 4.3). It can be seen that using 10% amorphous silica has a slightly lower value of fuel consumption than using 5% kaolin. This was attributed to the higher surface area of the kaolin (13 m^2/g) as against only 2 m^2/g for the amorphous silica.

4.5 Air Requirement

The amount of air required to propagate the combustion front through sands formation depends primarily on determined combustion requirements. Usually, it is defined as follows:

$$\text{air requirement } [m^3\ (st)/m^3] = \frac{\text{air consumed } [m^3\ (st)]}{\text{volume of combusted section } (m^3)}$$

Additionally, other quantities can be defined:

$$\text{air fuel ratio (AFR)} = \frac{\text{air consumed } [m^3\ (st)]}{\text{fuel burned (kg)}}$$

which relates amounts of air required to the fuel burned. An important economic indicator is the air to oil ratio:

$$\text{AOR} = \frac{\text{air consumed } [m^3\ (st)]}{\text{volume of oil produced } (m^3)}$$

The air requirement is based on a combustion efficiency of 100%, *i.e.*, all the oxygen injected is consumed. Table 4.4 reports the vlaues of air requirement, AFR and AOR obtained for Runs 1-11 and 20, where various amounts of kaolin and amorphous silica are used. The AFR values vary only very little over the range 9.17-11.10 m^3/m^3, which is consistent with Mckay's (1982) finding that AFR is relatively constant.

In Figure 4.18, the air requirement shows a gradual increasing trend as the percentage of kaolin increases, which is approximately linear. A similar trend is observed for amorphous silica up to about 10%, but the air requirement increases more markedly beyond this point. This is due to the larger fuel deposition, and consequently, greater air requirement to consume this fuel.

The effect of kaolin on AOR is similar to that for air requirement, but the data are much more scattered (Figure 4.19). In contrast, AOR increases very steeply beyond the 10% additive level when amorphous silica is used. Both air requirement and AOR are higher with amorphous silica compared with kaolin, which is due to the greater fuel consumption effect.

The highest air requirement value is achieved in Run 20, in which acidised kaolin was used. The exposure of the kaolin lattice when it is treated with acid enhances the specific surface area. Accordingly, fuel deposition is promoted and fuel consumption is increased.

The values of air requirement AOR and AFR in the present work and those obtained by other investigators are shown in Table 4.4. Showalter (1963) found that air requirement increases as heavier crude oil is used. Vossoughi *et al.* (1982) observed that air requirement

Table 4.4 Effect of Additives on Air Requirement, AFR and AOR

Run No.	Crude Oil	WAR [m^3/Mm^3 (st)]	Additives Content	Air Requirement [m^3 (st)/m^3]	AFR [m^3 (st)/kg]	AOR [m^3 (st)/m^3]
1	Maya	1.0	0%	130.3	10.5	1401.9
2	"	1.0	2% kaolin	153.5	10.7	1713.6
3	"	1.0	5% kaolin	162.77	11.1	1356.1
4	"	1.0	10% kaolin	191.4	10.7	1938.4
5	"	1.0	15% kaolin	199.27	9.51	1740.4
6	Maya	1.0	2% amorphous silica	158.7	9.78	1784.2
7	"	1.0	5% amorphous silica	180.8	10.11	1670.3
8	"	1.0	10% amorphous silica	200.3	10.06	1813.0
9	"	1.0	13.75% amorphous silica	302.2	10.95	3283.6
10	Maya Isthmus	dry	3% kaolin	246.06	11.49	2220.4
11	Cold Lake	1.0	0%	139.23	9.17	1620.7
20	Maya	1.0	1% acidised kaolin	328.1	11.13	2847.6
Showalter (1963)	11 °API	dry	3.6% clay	510	10.6	-
	17 °API	dry	3.6% clay	285	12.7	-
	30 °API	dry	3.6% clay	195	12.2	-
Vossoughi *et al.*(1982)	Iola (19.3 °API)	dry	0%	198.1	-	-
			5% clay	227.0	-	-
			10% clay	265.8	-	-
			15% clay	330.1	-	-
			15% amorphous silica	209.6	-	-
Ejiogu *et al.* (1978)	Pembina (37 °API)	dry	5% clay	189.9	10.1	2064.8
		2.67	10% clay	292.3	11.3	3389.3
Al-Shalabe (1985)	Maya Isthmus	3.75	5% kaolin	72.2	12.14	540.2
		3.75	10% kaolin	92.2	11.52	677.2
		dry	10% amorphous silica	182.6	9.83	1200.4

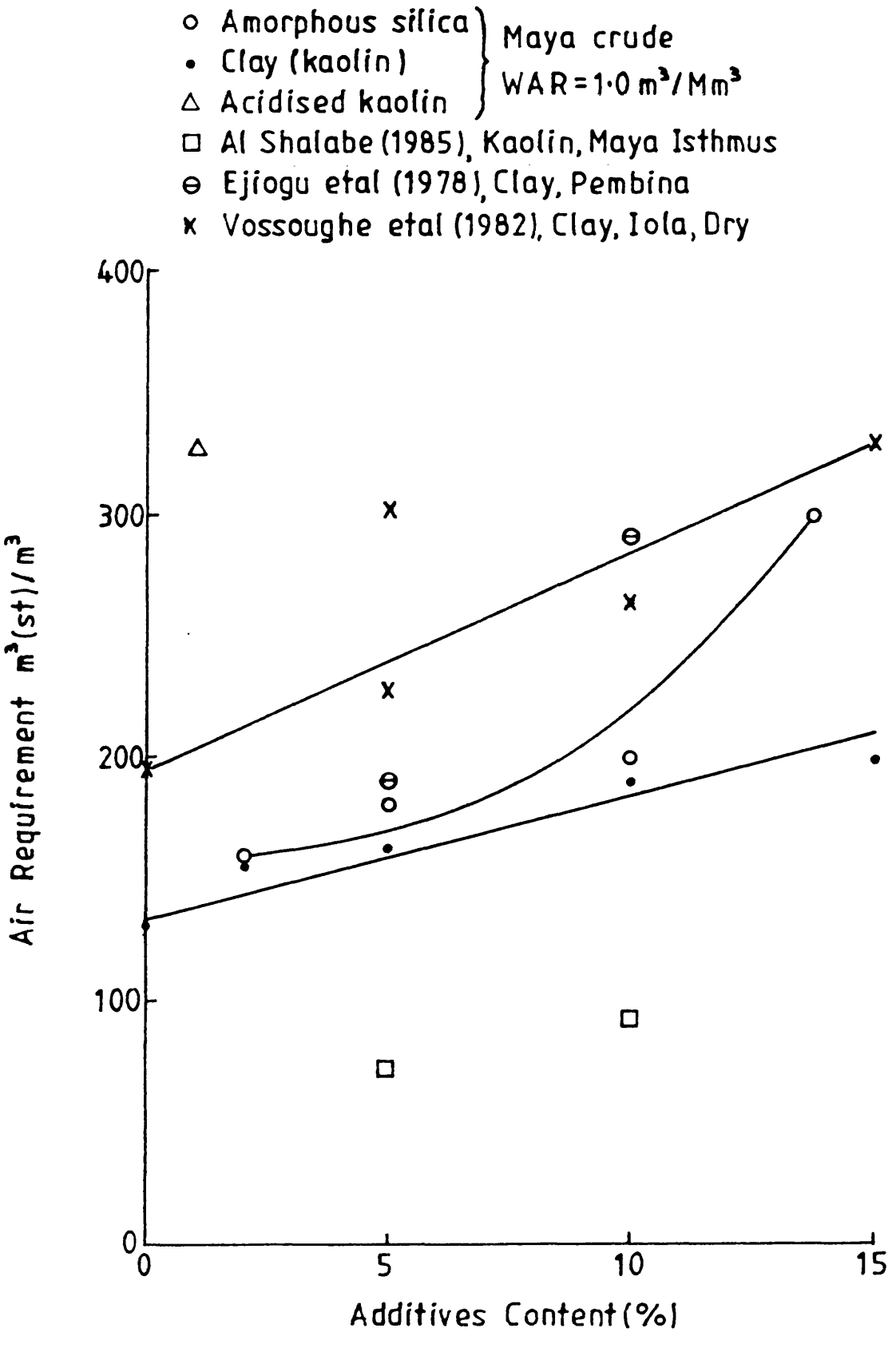

Figure 4.18 Effect of additives on air requirement

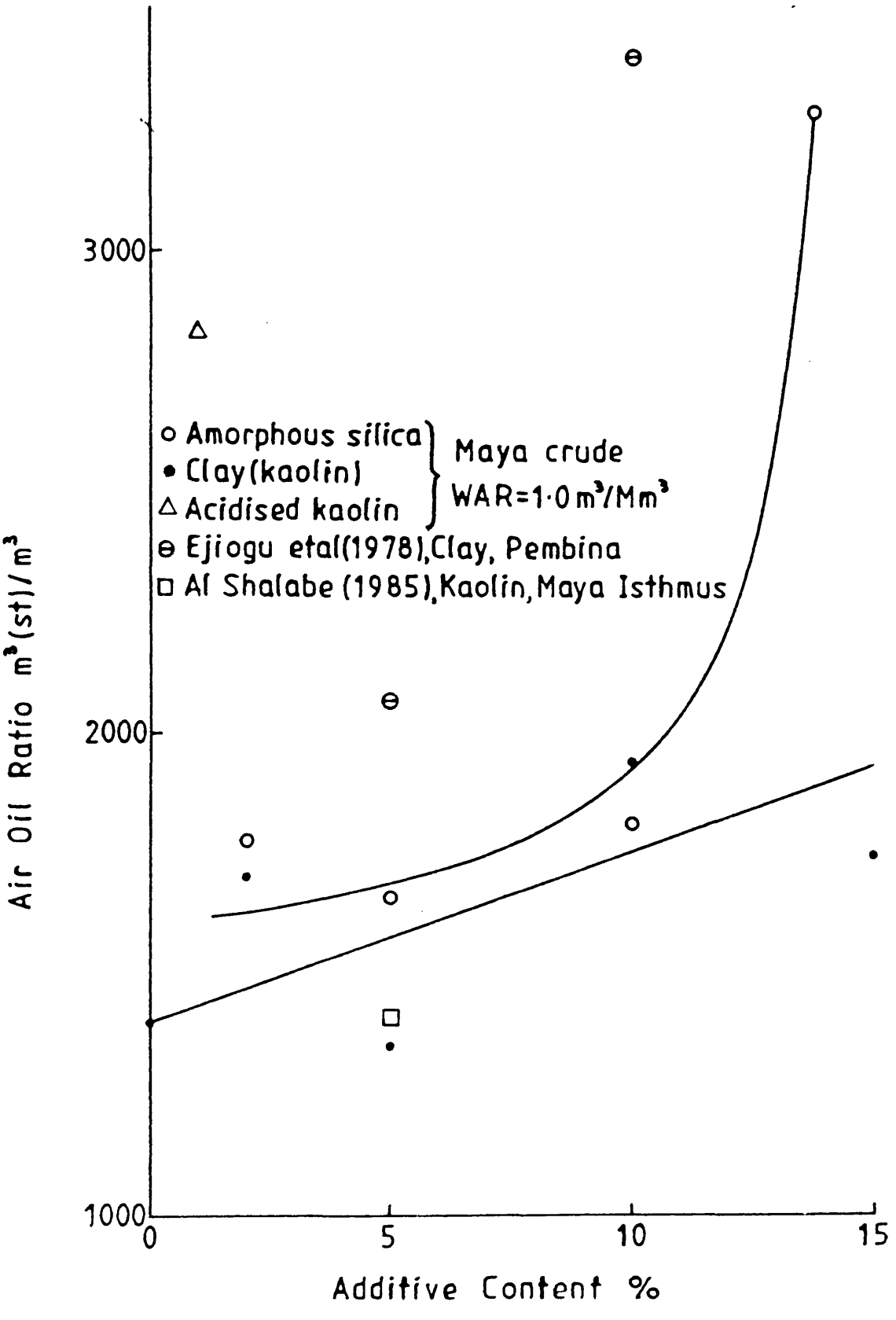

Figure 4.19 Effect of additives on AOR

increases with increasing clay content in the sand mixture. The only discrepancy is for the two 5% clay runs. As discussed earlier, sand pack density of the second run was larger than the first, which consequently produced a larger amount of fuel per unit length of the tube. This slowed down the combustion front, which, in turn, increased the air requirement. The air requirement of the mixture with silica powder was less than that of clay mixtures. Al-Shalabe (1985) also observed a similar effect of clay on air requirement that increasing the clay content from 5 to 10% increases the air requirmenet from 72 to 92 m^3/m^3 due to increased fuel availability.

4.6 Discussion

An increase in either the amount of kaolin or the amount of amorphous silica in the sand matrix increased fuel consumption. This gives rise to an increase in air requirment, carbon combustion rate and also combustion peak temperatures. The net process effect is a decrease in the combustion front velocity. Thus *in situ* combustion process is significantly influenced by the composition of the porous matrix when additives in the form of clays and amorphous silica are present.

The precise effects of porous medium in the *in situ* combustion process are complex and include both physical surface area influences as well as modification of reaction kinetics. The large surface area of the clay and amorphous silica materials is the major factor affecting the fuel consumption process. Although the surface area of kaolin (13 m^2/g) is higher than that of amorphous silica (2 m^2/g); more fuel being consumed in the latter case. This suggests that not only is the availability of the surface area important, but also the nature of the surface area has a very significant effect on the fuel consumption process.

The nature of surface area for kaolin and amorphous silica material has been studied by SEM. Figures 4.20 and 4.21 show details of the surface of these two materials using this technique. Amorphous silica has a granular shap with an open porous structure. Kaolin, on the other hand, has a flat, plate-like structure which is more closed, or tightly structured. The fuel deposition process in a porous media containing clays arises from cracking of the large hydrocarbon molecules within the intrapore space of the particles. It is expected, therefore, that kaolin will provide a greater diffusional resistance to oxygen, compared with amorphous silica. Thus more fuel should be consumed when amorphous silica is used, due to its lower resistance to oxygen diffusion. Buesse (1971) showed a similar behaviour by using quartz sand and glass-spheres in a number of combustion experiments. Similar observations have also been reported by Guvenir (1980) and Al-Shalabe (1985).

Certain mineral impurities, such as iron and nickel present in the porous media, could also affect the fuel content. The kaolin contains 330 ppm chloride and 20 ppm heavy metals (analysis supplied by Dearborn Chemicals Ltd.). The amorphous silica composition is approximately 99% SiO_2, with no precise understanding of what other compounds were present, but it is likely it contained amounts of iron and other metal compounds. These metals are known to deposit on the surface of porous substances and can interfere with reaction mechanics activity. The metal content of the clays and amorphous silica is, however, relatively small compared with that in the original heavy crude oil (see Chapter 3), but nevertheless they do contribute some effect in reducing the fuel consumption, as mentioned by Buesse (1971).

Figure 4.20 SEM photograph for kaolin at 2000 magnification.

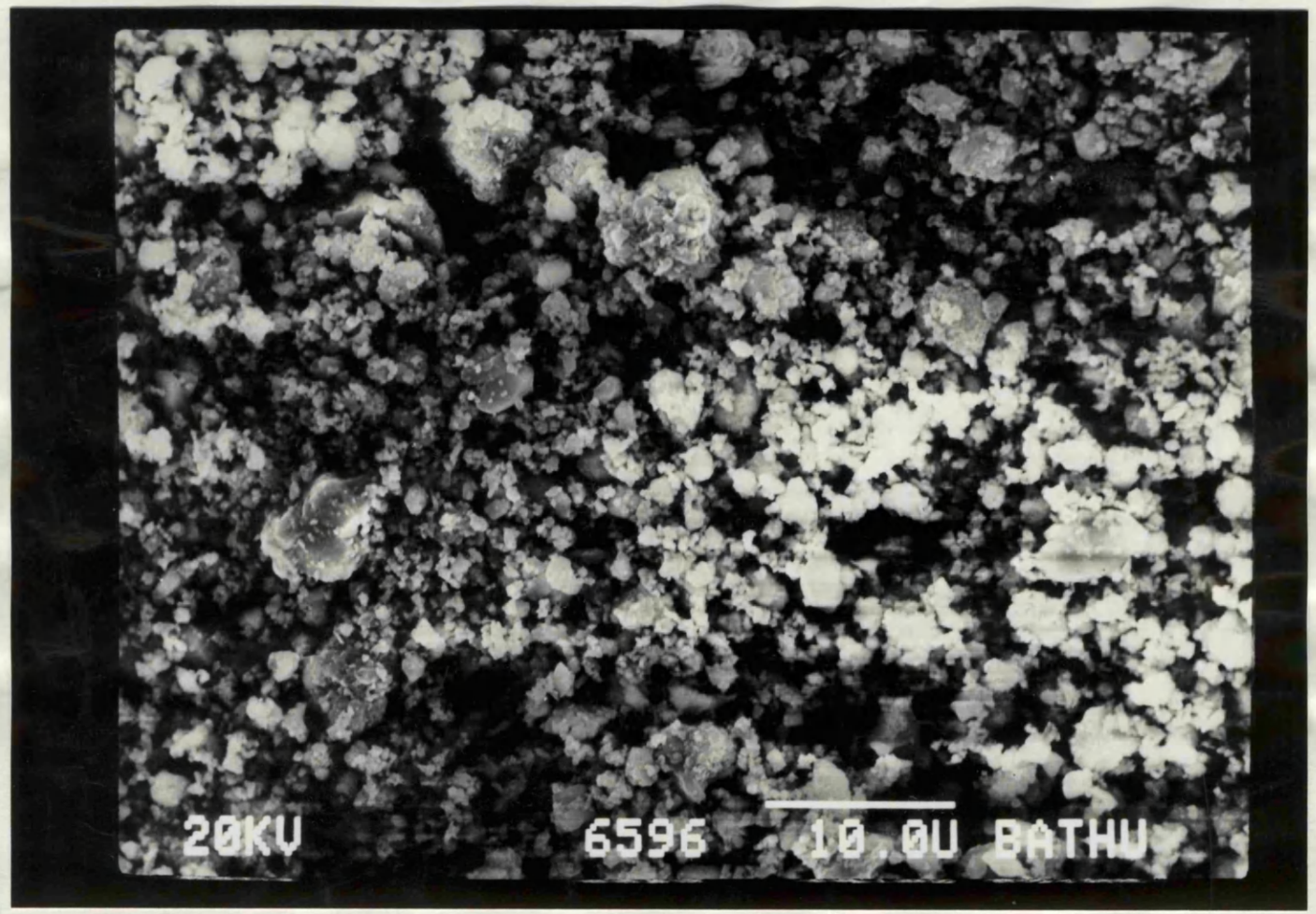

Figure 4.21 SEM photograph for amorphous silica at 2000 magnification.

Catalytic activity of clay plays an important role in the fuel consumption process. Amorphous silica is essentially an inert material. However, becuase of the nature of its structure (large surface area) and also included impurities, it does possess some catalytic activity. Grim (1962) stated that a catalyst with lower initial activity may be much more preferable than the one with a high initial activity. This is due to a very slow rate of decline in activity when either poisoning or fouling occurs. Thus, in the former case, fouling occurs in the *in situ* combustion process when coke deposits on the surface of the catalysts.

Acid treatment of kaolin increases its acidity (Decroocq, 1984), and also the surface area [due to dissolution of aluminium and magnesium compounds (Grim, 1962)]. It also changes the nature of the surface area. Figures 4.20 and 4.22 show the surface area of kaolin, before and after, the acid treatment. These physical and chemical changes occurring in the kaolin can therefore significantly affect the basic fuel deposition and combustion process in *in situ* combustion tests. This is demonstrated in the present experiment (Run 20) by high fuel consumption value when acidised kaolin is present.

As described earlier, one objective was to find the minimum amount of clay required to sustain steady combustion front. For Maya Isthmus crude oil (32.4 °API), the minimum amount of kaolin to sustain the combustion front was 3%. The corresponding average surface area for the sand pack is 0.516 m^2/g. For heavier crude oil, such as Maya (22.1 °API) and Cold Lake (10.2 °API), self-sustained combustion front was achieved without any kaolin addition. In these cases, the surface area is 0.13 m^2/g. Noting that all experiments were performed under the same conditions and that the sand pack contained similar oil saturation, it can be concluded that surface area determined whether a

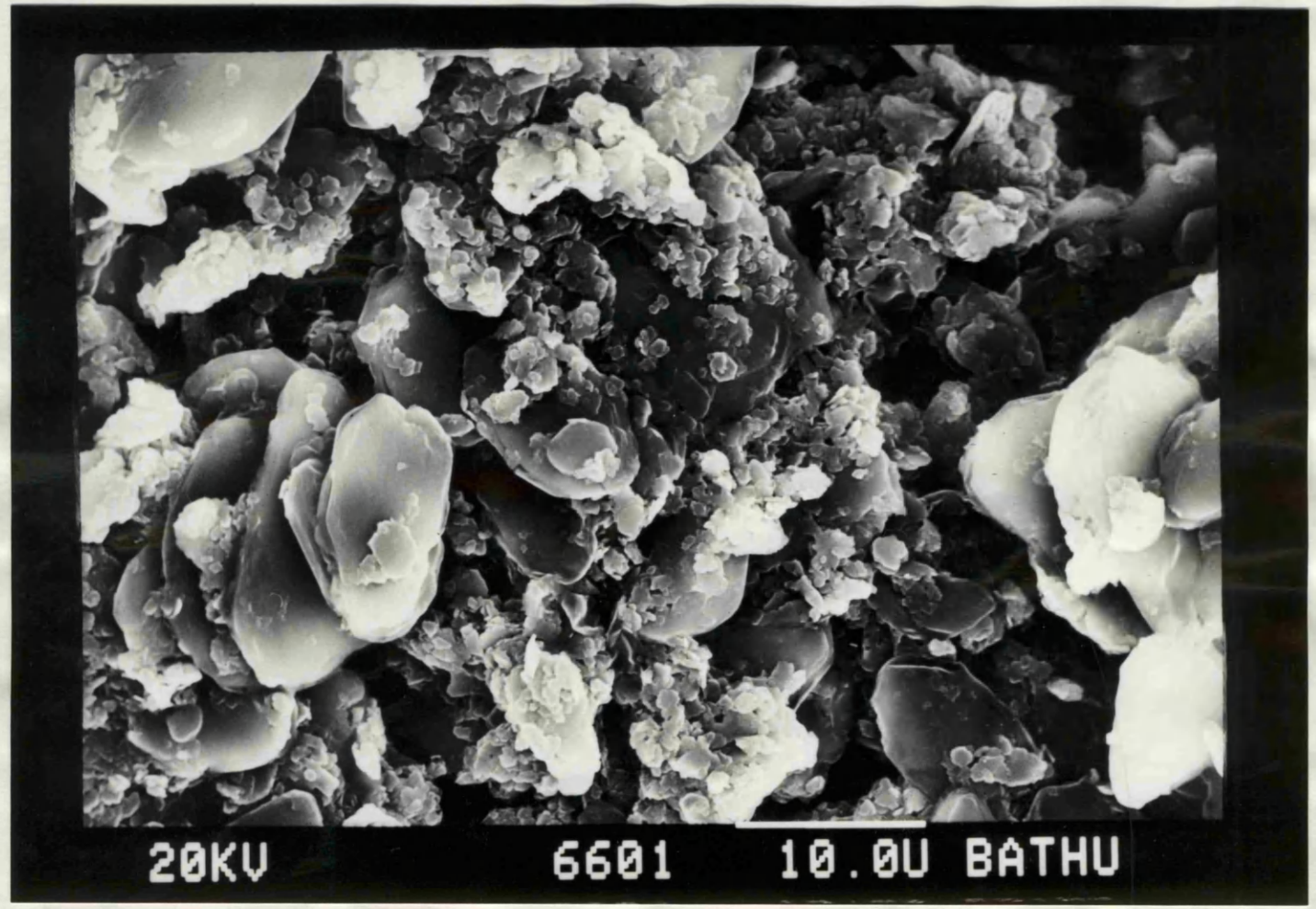

Figure 4.22 SEM photograph for acidised kaolin at 2000 magnification.

self-sustained combustion could be achieved in these experiments.

4.7 Conclusion

(1) The specific surface area of the porous medium or sand pack, importantly influences the process of fuel deposition and hence combustion front stability. This is most critical for light crude oils. In the case of Maya Isthmus crude oil, a minimum clay content of 3% was necessary to achieve stable combustion. Combustion of heavier crude oils is less critically dependent on clay content, as demonstrated by the ability to sustain stable combustion with Maya crude when the sand pack contained no clay. Therefore, crude oil gravity and chemical composition are important factors influencing *in situ* combustion behaviour.

(2) The additional surface area contributed by clay or amorphous silica additives, which at a level of only 2% kaolin, can increase the total surface area in the sand pack by 0.387 m^2/g (33%), results in a substantial increase in fuel deposition. The effect of additives, therefore, results in increased combustion temperatures, higher fuel consumption, and lower combustion front velocities, compared with experiments in a clean sand matrix.

(3) The physical structure and chemical properties of kaolin are modified by acidising with sulphuric acid. This has a significant effect on the fuel availability and causes an increase in fuel consumption.

CHAPTER 5

Effect of Oxygen Enrichment on Combustion Parameters

Introduction

The application of oxygen enrichment as a thermal recovery process for crude oils is believed to have a number of advantages over normal air combustion. In particular, higher displacement rate, lower gas velocities, increased mobility of the oil due to CO_2 solubility, and higher recovery factors. The use of oxygen enrichment showed improved combustion efficiency compared with air [Hansel *et al.* (1984), Leaute and Collyer (1984), Petit (1985), Garon *et al.* (1986) and Adewusi (1986)].

A description of a high pressure laboratory combustion tube system designed to operate with oxygen enrichment was presented by Hansel *et al.* (1984)]. Initial tests with the system utilised a light crude oil with a low value of oil in place and simulated reservoir conditions. The injected gas composition was varied from 21% and 95% oxygen. Only tests at 40% oxygen and above produced satisfactory combustion. Adewusi (1986) performed a number of experiments on Maya crude oil involving the use of oxygen enrichment to a level of 30 and 35% oxygen. Dry and wet combustion methods were examined. Hvizdos *et al.* (1983) have reported on a field project in the Forest Hill field in Texas. Results were encouraging, but analysis of data was difficult because of the short period of time oxygen was injected and because an air *in situ* combustion project was going on, on the adjacent patterns. Shu and Lu (1984) studied the potential benefit of CO_2 from oxygen combustion processes (Figure 5.1) in combustion tests.

5.1 Results and Discussion

In the present investigation, three experiments with enriched air were carried out. Runs 14-16 used a gas mixture of 35% oxygen

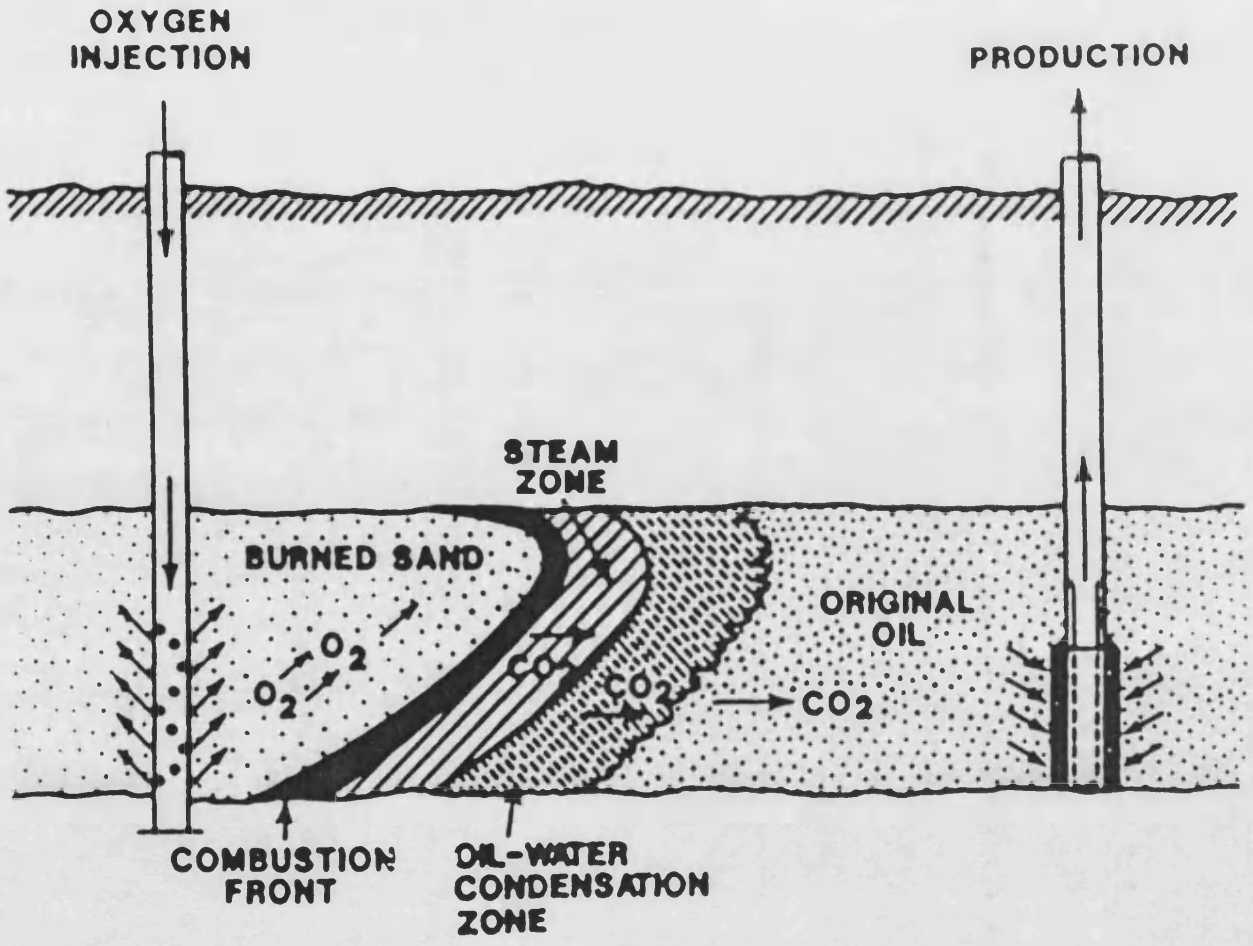

Figure 5.1 —Schematic of oxygen combustion process.

(Shu and Lu, 1984)

and 65% nitrogen at a gas flux of 14.57 m^3/m^2 h. Run 14 (dry combustion) was conducted with 5% kaolin and Maya crude oil. Run 15 was performed with silica sand and Cold Lake crude oil (WGR 1.0 m^3/Mm^3). Run 16 was involved with mixing 25% wt of Lower Fars core material with 75% wt silica sand to which Maya crude oil was added. For this run, the WGR was kept constant at 1.0 m^3/Mm^3. The conditions achieved in these tests are summarised in Table 5.1, alongside those of Runs 3, 11 and 13, in which no oxygen enrichment was used. Table 5.2 compares these results with those obtained by other investigators.

5.1.1 Temperature profile

Figures 5.2-5.4 show the respective temperature profiles for the combustion Runs 14-16. The maximum peak temperatures reached at the combustion front positions for Runs 15 and 16 are 483 and 505 °C, so are respecitvely 7 and 87 °C higher than the corresponding runs with air injection (Runs 11 and 13). The combustion peak temperature for Run 3 is higher than that for Run 14 by 24 °C. With the wet combustion method in Run 3, the combustion temperature increases due to the larger steam zone which is generated. The very large difference in combustion peak temperature between Runs 13 and 16 is due to the combination of oxygen enrichment and use of Lower Fars core material. The natural reservoir material is believed to promote the oxidation reaction. This trend of higher combustion peak temperature with oxygen enrichment agrees with the findings of Hansel *et al.* (1984) and Garon *et al.* (1986).

In Hansel *et al.*'s study, the combustion peak temperature for 30% oxygen was below 316 °C. This is relatively low for satisfactory combustion to be sustained. Peak combustion temperatures for 40-95% oxygen were in the range of 427-482 °C, which is the more normal situation observed for an air *in situ* combustion process. Garon *et al.* concluded

Table 5.1 Effect of oxygen enrichment on *in situ* combustion

	Run 3	Run 11	Run 13	Run 14	Run 15	Run 16
Crude oil	Maya	Cold Lake	Maya	Maya	Cold Lake	Maya
Additives Content	5% kaolin	0	1% L.Fars Core	5% kaolin	0	1% L.Fars Core
Injected gas: O2%	21	21	21	35	35	35
WGR m^3/Mm^3	1.0	1.0	1.0	0.0	1.0	1.0
Carbon combustion rate (gm/h)	4.25	4.5	3.5	7.0	7.25	7.0
Combustion front velocity (m/h)	0.0675	0.0525	0.035	0.0425	0.08	0.08
Fuel consumption (kg/m^3)	14.6	15.9	22.37	33.13	23.62	33.65
Oxygen requirement (m^3/m^3)	34.2	29.2	52	67.1	43.06	67.6
Oxygen oil ratio (m^3/m^3)	284.8	340.3	368.5	784.6	44.0	589.2
Oxygen fuel ratio (m^3/kg)	2.33	1.93	2.32	2.03	1.82	2.01
Total gas requirement (m^3/m^3)	162.8	139.2	247.6	191.7	123.1	193.2
Gas oil ratio (GOR) (m^3/m^3)	1356.1	1620.7	1754.6	224.2	1257.26	1683.4
Gas fuel ratio (GFR) (m^3/kg)	11.1	9.17	11.07	5.78	5.21	5.74
Peak temperature (°C)	485	476	418	461	483	505

Table 5.2 Effect of O_2 enrichment on combustion parameters

Author	Crude oil gravity (°API)	Gas flux ($m^3/h\ m^2$)	WGR (m^3/Mm^3)	Additives content	Injected gas % O_2	Carbon combustion rate (gm/h)	Fuel consumption (kg/m^3)	Combustion front vel. (m/h)	Total gas requirement (m^3/m^3)	GFR (m^3/kg)	GOR (m^3/m^3)	Peak temperature (°C)
Hansel *et al.* (1984)	31	18.3	dry	5% silica flour	21	NA	NA	0.063	NA	NA	3380.8	NA
					30			0.095			2313.2	316
					40		17.6	0.17	243	13.8	1067.6	427
					95		17.6	0.28	243	13.8	533.8	482
Leaute and Collyer (1984)	10.2	NA	dry	sand only	95	NA	31.2	0.098	67.5	2.2	635.6	570
Petit (1985)	13.8	19.1	dry	sand only	21	NA	26.9	0.067	298	11.1	NA	475
		8.02			50		31.3	0.06	131	4.2		463
		5.02			80		33.4	0.054	89.4	2.7		485
Garon *et al.* (1986)	13	NA	dry	NA	21	NA	26	NA	381	14.6	1428.6	480
					100		45		105	2.3	300	500
	13		4.8		21		27		309.5	11.5	761.9	455
			4.5		100		37		74	2.0	180	480
	25		dry		100		24		62	2.6	250	460
Adewusi (1986)	22.1	10.53	dry	8.4% kaolin	21	3.1	14.9	0.082	154.9	10.3	3567.3	399
		15.96	dry		30	6.2	25.3	0.068	194.6	7.7	4074	416
		16.63	dry		35	6.7	21.1	0.107	155.4	7.4	3473.1	424
		17.59	2.0		21	5.0	14.3	0.115	153.0	10.7	2485.4	418
		17.05	1.8		30	5.6	17.1	0.114	149.6	8.8	2939.1	400
		17.90	1.8		35	5.3	16.7	0.128	139.9	8.4	2643.3	414
Present work	10.2	14.57	1.0	silica sand only	21	4.5	15.9	0.053	139.2	9.2	1620.7	476
					35	7.25	23.6	0.08	123.0	5.2	1257.2	483
	22.1			25% L.Fars core	21	3.5	22.3	0.035	247.6	11.1	1754.6	395
					35	7.0	33.6	0.08	193.1	5.7	1683.4	507

NA = not available

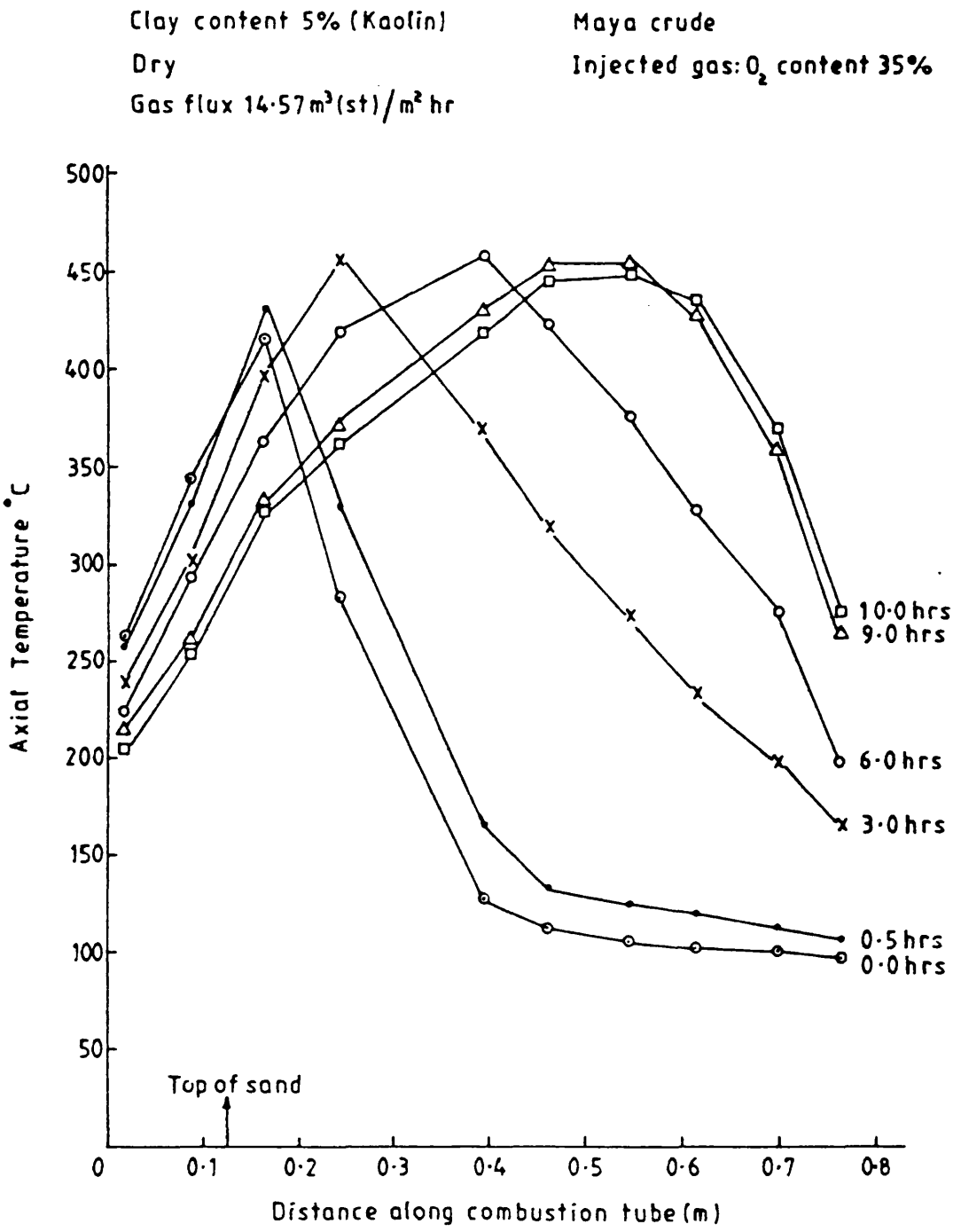

Figure 5.2 Temperature profile through combustion tube (Run 14)

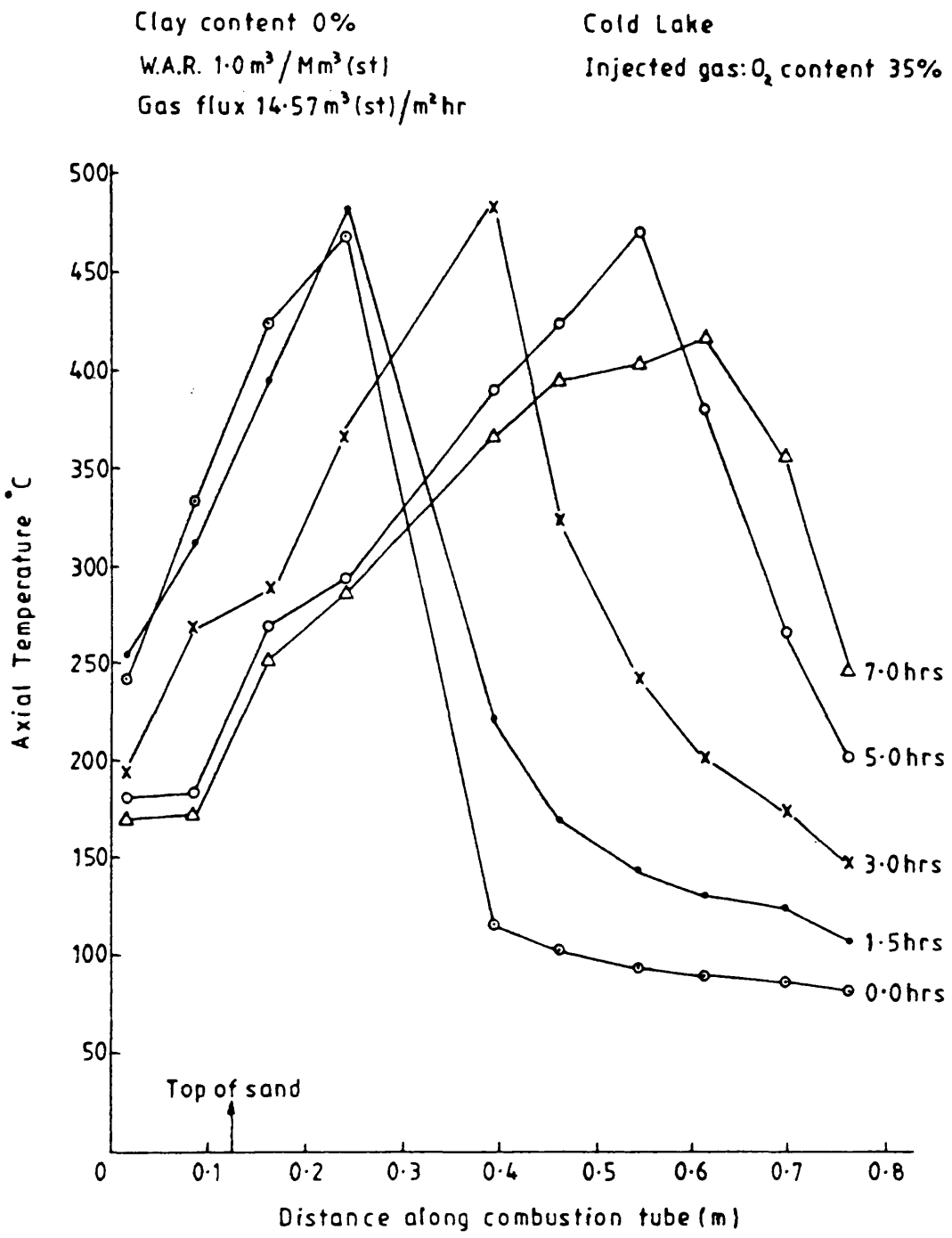

Figure 5.3 Temperature profile through combustion tube (Run 15)

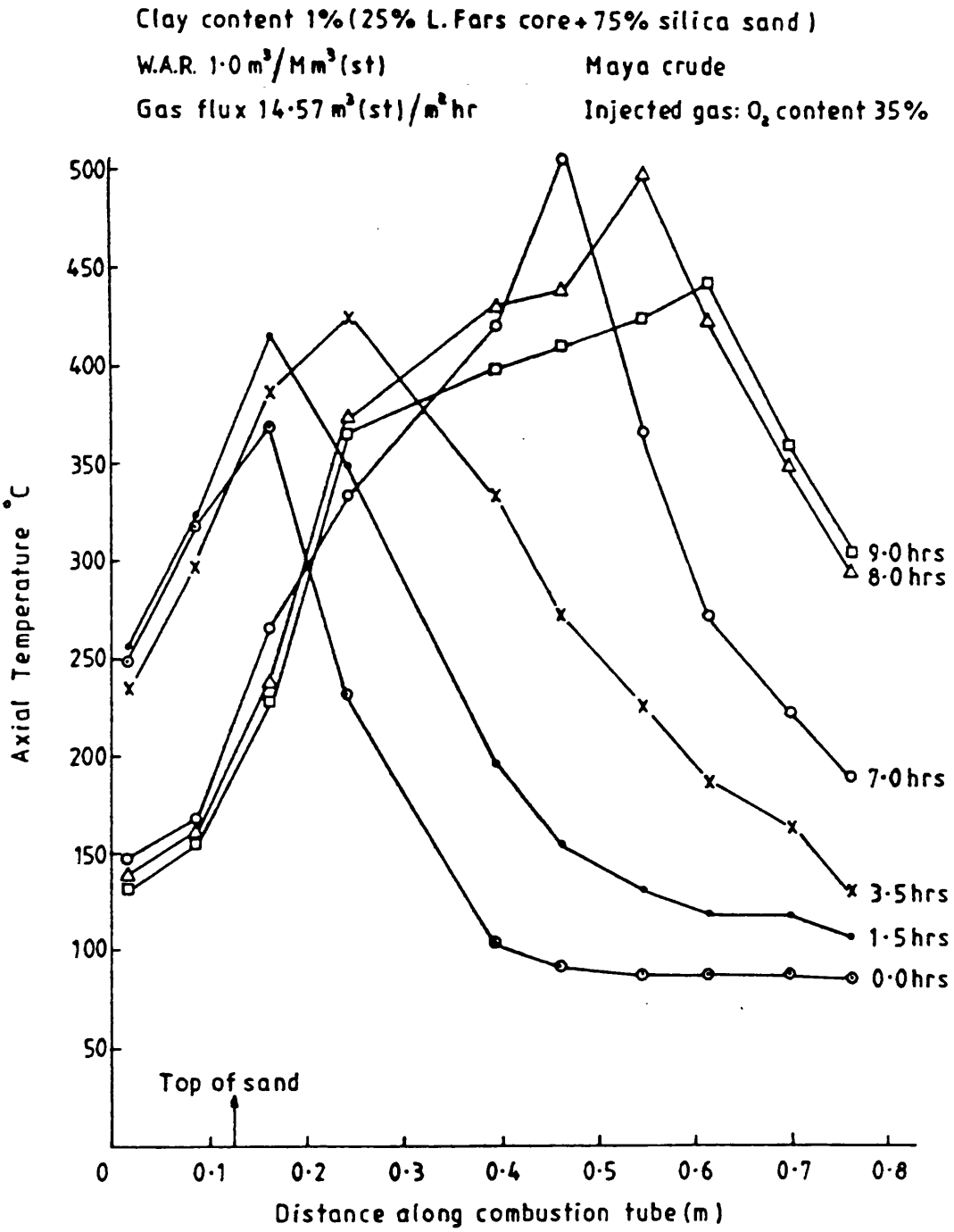

Figure 5.4 Temperature profile through combustion tube (Run 16)

that higher combustion temperatures result from greater fuel consumption during oxygen combustion. However, lower combustion temperatures were reported for a light crude oil of 25 °API even when the oxygen concentration reached 100% (Table 5.2).

Although Petit (1985) reported lower combustion temperatures with 50% oxygen enrichment than 21% oxygen, he did, in fact, observe an increase in the maximum temperature as oxygen enrichment increased to 80% oxygen. However, Adewusi (1986), who used the same Maya crude oil as in this study, obtained lower combustion temperatures. This is attributed to the larger heat losses increased in his combustion tube experiments. Leaute and Collyer (1984) achieved a very high combustion peak temperature (Table 5.2) with Cold lake crude oil of 570 °C, compared with a maximum value of 505 °C obtained in Run 16. The higher oxygen enrichment level of 95% oxygen used by them is mainly responsible for this.

The time to reach ignition for Runs 3, 11,&13-16 is shown in Table 5.3. It is lower for all cases involving oxygen enrichment. Also, the temperature of the top of the sand pack is shown in Table 5.3 and it is increased as oxygen concentration is increased, particularly for Runs 15 and 16. The temperature of the sand pack top in Run 3 is higher than that in Run 14, due to a larger steam zone which occurred with water injection. Therefore, in addition to higher combustion temperature, oxygen enrichment also leads to more rapid spontaneous ignition. Essentially this must be due to the higher concentration of oxygen available, causing more rapid oxidation of the oil and hence increased rate of temperature rise. Crookston *et al.*'s (1979) work showed that using pure oxygen, would significantly reduce the time for spontaneous ignition and ignition would occur closer to the injection well.

Table 5.3 Effect of oxygen enrichment on spontaneous ignition

	Run 3	Run 11	Run 13	Run 14	Run 15	Run 16
Temperature at the top of the sand pack at ignition time (°C)	390	335	350	380	375	360
Difference between gas injection and ignition times (h)	1.16	0.5	0.83	0.5	0.33	0.16
Crude oil	Maya	Cold Lake	Maya	Maya	Cold Lake	Maya
WGR (m^3/Mm^3)	1.0	1.0	1.0	0.0	1.0	1.0
Injected gas: O_2%	21	21	21	35	35	35
Additives content	5% kaolin	0	25% L.Fars core	5% kaolin	0	25% L.Fars core

In the oxygen enrichment tests, a distinctive steam plateau is achieved, as shown in Figures 5.2-5.4. Its length is approximately 0.2 m at an average temperature of 120 °C. Interestingly, Adewusi (1986) has reported a larger steam zone length for the same operating condition (*i.e.*, 0.102 m using 30 and 35% oxygen) compared with only 0.051 m using air. Compared with this work, the shorter length of the steam plateau in Adewusi's work is due to larger heat losses. Hansel *et al.* (1984) also reported a high steam temperature to be about 221 °C for 40 and 95% oxygen enrichment.

5.1.2 Carbon combustion rate

In Table 5.1 the enriched oxygen experiments (Runs 14-16) show a substantial increase in the carbon combustion rate compared with Runs 3, 11 and 13 (21% O_2). For Cold Lake crude oil (Runs 11 and 15), the increase is 38%, and in the Lower Fars core and Maya crude oil case (Runs 13 and 16), the increase is 50%. Adewusi (1986) also found an increase in carbon combustion rate when 30 and 35% oxygen was used (Table 5.2). In his experiments using 35% oxygen, the increase with dry combustion was higher by 54%, while with wet combustion it was only 6% higher compared with air. Adewusi concluded that the carbon combustion rate was affected by water injection when enriched air is used. However, this is not observed to be the case in the present results.

5.1.3 Combustion front velocity and fuel consumption

Combustion front velocity and fuel consumption values for 35% oxygen are higher than those using air (Table 5.1). Generally, increased oxygen concentration leads to a higher combustion temperature and hence an increased rate of combustion. However, with 35% oxygen enrichment, the combustion front velocity for dry combustion test (Run 14) shows a lower value than that for wet combustion (Run 3), in which 21% oxygen

is used. This behaviour is consistent with the higher values of total gas requirement and GOR achieved in Run 3.

The trend of combustion front velocity and fuel consumption with oxygen enrichment observed in the present work and other works is shown in Table 5.2. Hansel *et al.* (1984) used a light crude oil (31 °API) and reported a low fuel consumption of 17.6 kg/m^3 when using oxygen enrichments of 40-95%. The combustion front velocity increased as oxygen concentration was increased by 30, 40 and 95% oxygen. Leaute and Collyer (1984) used Cold Lake crude oil (10.2 °API) and achieved a fuel consumption of 31.2 kg/m^3. This is higher than the value of 23.6 kg/m^3 obtained in the present study (Run 15). This was expected, since they used a much higher oxygen enrichment level of 95% oxygen and dry combustion. In another study, Petit (1985) used a heavy crude oil (13 °API) and observed that the combustion front velocities were constant in time and tended to decrease slightly when the oxygen concentration was increased. However, this behaviour could be due to a change in gas flux.

Garon *et al.* (1986) who used a heavy crude oil of 13 °API, found that fuel consumption increased when the oxygen concentration was decreased, for both wet and dry combustion. Fuel consumption values in Garon *et al.*'s study are higher than those obtained in the present study. This is due to the better adiabatic temperature control in their work, which minimised the heat loss. They also found a lower fuel consumption with the lighter crude oil (25 °API), compared with the heavy crude oil (13 °API). For 100% oxygen this was approximately 45%. This behaviour is consistent with the low values of total gas requirement and combustion peak temperature.

Adewusi (1986) reported that the combustion front velocity increases dramatically beyond 30% oxygen enrichment due to greatly increased fuel consumption. The pattern of fuel consumption varied with oxygen enrichment in the range of 30-35% oxygen. This is attributed to the unfixed gas flux which affected the fuel consumption. For the same crude oil (°API), however, the fuel consumption values are lower than those obtained in the present work. This is probably due to higher heat losses increased in his experiments using a thicker walled combustion tube.

5.1.4 Total gas requirement

The oxygen requirement and oxygen oil ratio for oxygen enrichment tests (Runs 14-16) are higher than those of corresponding normal air runs (Table 5.1). This is due to the higher rate of fuel consumption commensurate with increased fuel availability, which has also been reported by Garon *et al.* (1986) and Petit (1985). Garon *et al.* observed an increase in oxygen requirement from 300-500 m^3/m^3 when oxygen concentration changed from 21 to 100% oxygen for dry combustion tests.

As shown in Table 5.1, the total gas requirement, gas fuel ratio (GFR), and gas oil ratio (GOR) for oxygen enrichment tests are lower than for air combustion. Comparing Runs 13 and 16, there is a decrease in gas requirement of 22% for a change in injected oxygen concentration from 21-35%. The GFR andGOR also decreased by 48% and 4% respectively. In Garon *et al.*'s (1986) dry combustion experiments, the gas requirement decreased by 72% when oxygen concentration was changed from 21-100% (Table 5.2). GOR and GFR values also decreased by 79% and 84% when oxygen concentration increased to 100% oxygen. However, with lighter crude oil (25 °API), the gas requirement and GOR decreased by 41% and 17% respectively for 100% oxygen, compared with heavy crude oil (13 °API).

Clearly, there is a broad measure of agreement between the results shown in Table 5.1 and others in Table 5.2, which are concerned with *in situ* combustion of heavy and light crude oils. On the other hand, experimental results are not identical because different operational conditions were used. However, in one case, where the same crude oil (22.1 °API) was used with 35% oxygen (Adewusi, 1986), there is a surprising difference with gas requirement. Adewusi's result is lower by 28%. This is attributed to the gas flux and WGR used in his study. Adewusi also found a continuous fall in total gas requirement and GFR with increasing oxygen concentration (Table 5.2).

Hansel *et al.* (1984) reported the gas requirements data for 40% oxygen and above of about 463 m^3/m^3 with no significant change with oxygen concentration. Below 40% oxygen, larger gas requirements were caused by unsatisfactory combustion which resulted in unreacted oxygen breakthrough. Although they used light crude oil (31 °API), the reduction trend of GOR with oxygen enrichment was remarkable.

Leaute and Collyer (1984) used Cold Lake crude oil, and the gas requirement, GFR and GOR obtained are lower than the values achieved in the present work for the same crude oil. This is considered to be reasonable, as they used higher oxygen enrichment of 95% oxygen. Petit (1985) also conducted oxygen enrichment experiments with heavy crude oil (13.8 °API). The gas flux varied over the range while oxygen flux was kept constant at 4.01 m^3/m^2 h. He reported that the total gas requirement decreased by 56 and 31% with oxygen enrichment of 21-50% oxygen and 50-80% oxygen, respectively. No GOR values were given.

From the above discussion, it can be concluded that oxygen enrichment causes a lower gas requirement and GOR, compared with air combustion. Oxygen combustion is thus more economically attractive, since less gas has to be compressed for the *in situ* combustion operation.

An economic study by Hvizdos *et al.* (1983) showed that the cost of a given mass of compressed oxygen is less than that of the equivalent quantity of air for large scale operations carried out under high pressure (Figure 5.5). This is particularly important in heavy oil reservoirs, in which there is increased fuel deposition and hence a greater gas requirement.

Table 5.2 lists the GFR values obtained by various authors and these are compared with those obtained in this study for both dry and wet combustion methods and for different types of crude oil. There is a considerable decrease in GFR values with oxygen enrichment, but constant values at 40% oxygen and above are obtained in Hansel *et al.*'s (1984) work, due to light crude oil used. In the present work, there is a reasonable agreement with the general trend exhibited by Leaute and Collyer (1984), Petit (1985) and Garon *et al.* (1986). They achieved very low values of GFR with high oxygen concentration of the range 50% oxygen and above. However, Adewusi (1986) used the same crude oil (22.1 °API) with 35% oxygen, but his GFR values are higher than those obtained in the present work. This is due to the lower fuel consumption in his work.

5.2 Conclusions

(1) The use of oxygen enrichment for *in situ* combustion produces a higher carbon combustion rate. It also achieves faster spontaneous ignition and higher combustion temperatures than with air combustion. The net effect is to increase the combustion front velocity and fuel consumption.

(2) With oxygen enrichment there is an overall reduction in the total gas requirement, GOR and GFR. A reduced gas requirement is a significant potential benefit in the *in situ* combustion

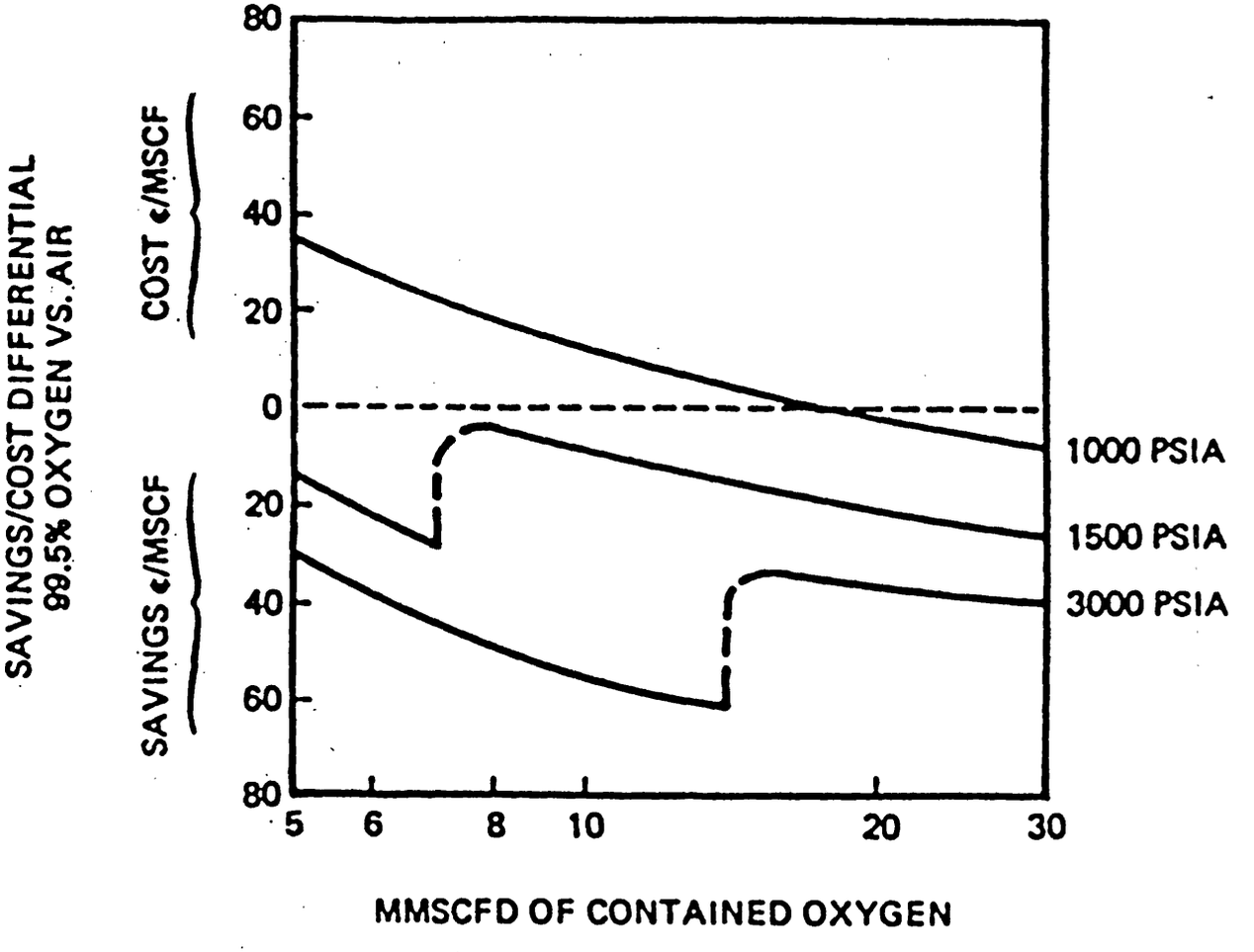

Figure 5.5 —Hvizdonian economics—oxygen vs. air costs.

recovery method since the cost of gas compression required is a major economic factor.

CHAPTER 6

Effect of Reservoir Core Material and Metal Compound Additives

Introduction

The mineralogy of the host matrix has a significant influence on the behaviour of the *in situ* combustion process. Various investigators (Fassihi, 1980; Guvenir, 1981; Al-Shalabe, 1985; and Adewusi, 1986) have, in fact, suggested that combustion parameters and reaction kinetics for a specific reservoir should be obtained using natural core material. Therefore, core material of varying grain size from the Kuwait Lower Fars reservoir was used in a number of experiments. This material was estimated to contain approximately 5% wt of fine silts and clays, an oil saturation of 20%, and crude oil gravity of 18 °API. The experimental results of runs cover the cases when 100% natural core material (Run 12) was used with no further oil saturation, and when a 25% mixture of core mateiral and 75% silica sand were used with Maya crude oil (Run 13). The effect of Lower Fars core material on the temperature profile, fuel consumption, carbon combustion rate, combustion front velocity, air requirements, AOR, and AFR was investigated.

Metals like vanadium, copper, iron, nickel, and their compounds are present in crude oils. The host sand matrix also contains other metal compounds such as pyrite, calcite, dolomite, siderite. It is believed that the presence of such metal compounds in crude oil or sand matrix provide a certain catalytic effect to the oxidation of hydrocarbons. Three experiments were carried out (17, 18 and 19) to investigate the effect of metal compounds; namely, ferric oxide and nickel chloride, on the crude oil combustion. Runs 17 and 18 contained 1% wt of ferric oxide and 1% wt of nickel chloride, respectively. Run 19 contained 1% wt of ferric oxide and 2% wt of kaolin. The results

of these experiments were compared with two other experiments, Runs 1 and 2 (detailed in Chapter 4).

6.1 Results

(A) Effect of natural core material.-Figures 6.1 and 6.2 show the temperature profiles for Runs 12 and 13. In Run 12, the combustion front propagated successfully, evidencing the ability of the natural core material to sustain the combustion process. It is observed that the combustion temperature starts to decrease towards the end of the combustion tube. This is due to the initial low oil saturation (20%) in the sand pack, so that there might be a region downstream of the combustion front with insufficient fuel to sustain combustion.

In Run 13 (Figure 6.2), the 1% of clays and silts was constituted from a mixture of 25% natural core material and 75% of silica sand. The temperature profiles are stable throughout the combustion period. The average temperature for Run 13 was 395 °C, whereas the average peak temperature for other runs (Runs 1-20) was higher than this. Most probably the presence of trace amounts of metal compounds in the natural compounds in the core material will reduce the average peak temperature due to the reduction in activation energy (Vossoughi *et al.*, 1982).

No steam plateau condition was observed during Run 12, but this did occur in Run 13 at a temperature of approximately 115 °C. The absence of steam plateau in Run 12 is attributed to the very low initial water saturation (almost zero), so that steam formation is entirely dependent on the combustion process.

As shown in Table 6.1, the data for Runs 12 and 13 exhibit a high fuel consumption. Consequently, the combustion front velocity is low and there is a high air requirement. The high fuel consumption

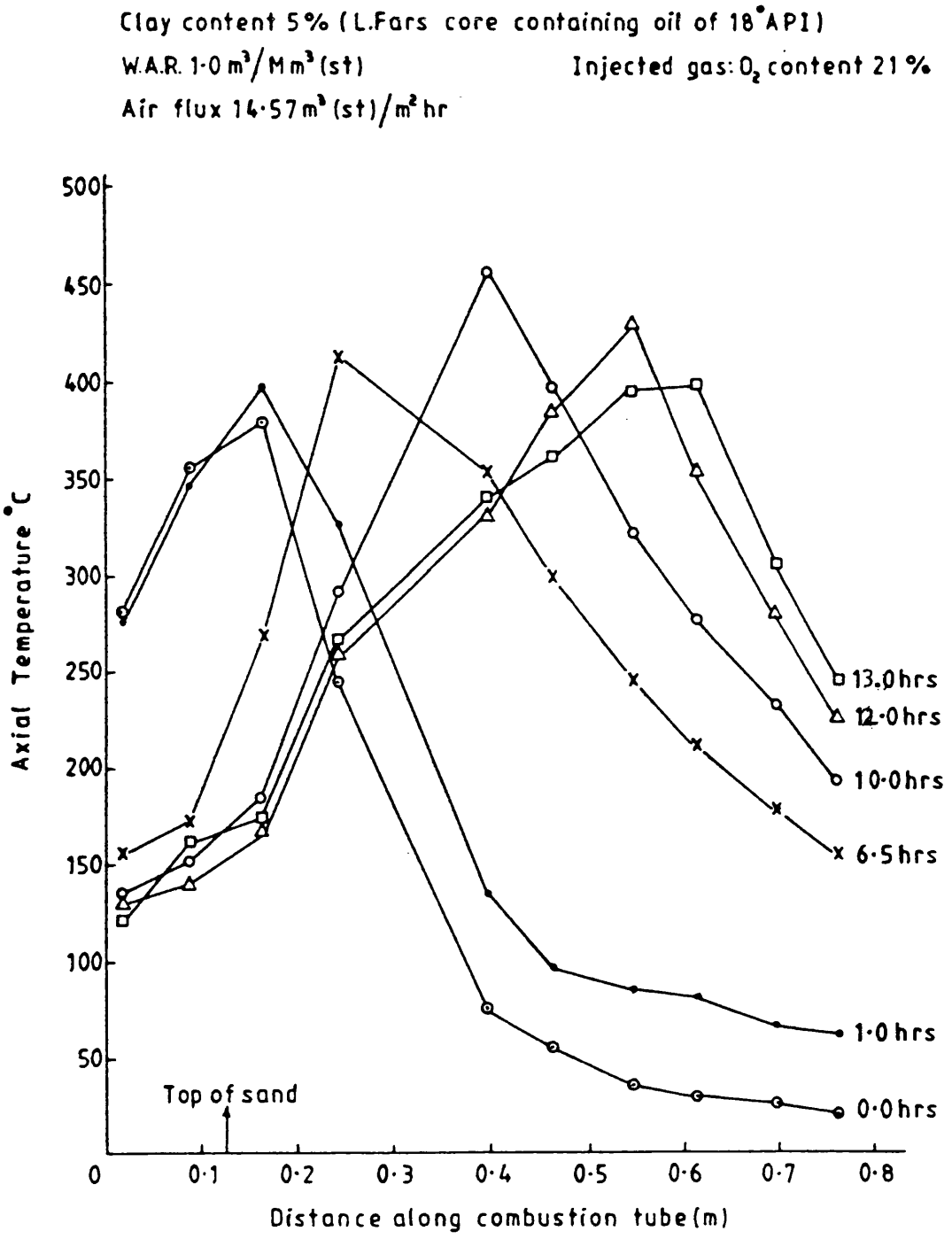

Figure 6.1 Temperature profile through combustion tube (Run 12)

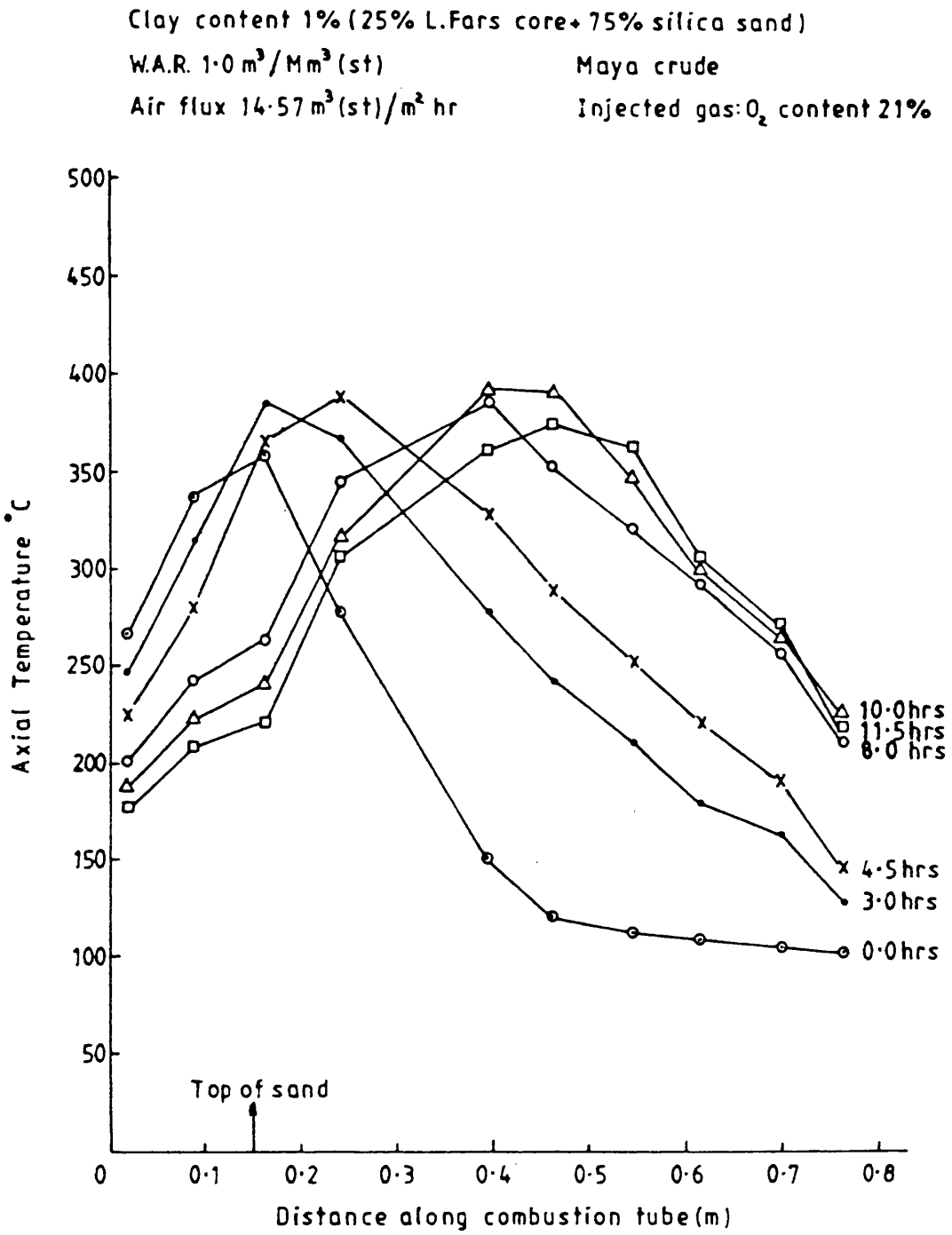

Figure 6.2 Temperature profile through combustion tube (Run 13)

with reservoir core material is due to the presence of natural clays and silts. These possess a high specific surface area and catalytic activity. The effect is emphasised in Run 12, which contains 100% core material. In the case of Run 13, the natural core material is present as a 25/75 sand mxiture, the reduced fuel consumption is compensated by the higher oil saturation (So_i = 37.9%).

The fuel consumption in Run 12 is 23.82 kg/m^3 and this represents 34.6% of the original oil in place. By comparison, Run 3, with a synthetic sand matrix and otherwise the same experimental conditions, gives a fuel consumption of only 14.6 kg/m^3, which is 10.29% of the original oil in place. This observation is consistent with Mckay's (1982) finding that natural rocks produce higher fuel consumption values than a synthetic silica sand matrix. Another study by Craig and Parrish (1969) also found that fuel consumption was higher using a natural Nellie Bly consolidated sand stone.

In Run 12, the high AOR value (Table 6.1) is due to low oil saturation (20%), which results in a relatively low oil recovery (51.1% OOIP). Therefore, a direct relationship exists between fuel consumption and oil recovery which agrees with the observation by Marten *et al.* (1958) work. The time required for the oil to be produced initially decreases as the initial oil saturation increases. Thus AOR is expected to increase as initial oil saturation decreases. Ejiogu *et al.* (1978) reported high AOR values (3688-3544 m^3/m^3), which he attributed to low initial oil saturation. The air requirement and AFR values obtained in the present work do not change appreciably with oil saturation.

The combustion results obtained with the Lower Fars core material are compared in Table 6.2 with those obtained in other studies which used other types of natural core material. There appears to be an

indication that both fuel consumption and air requirement increase with increasing WAR. However, the operating conditions (API, oil saturation, and pressure) are different, and no firm conclusions can be drawn. On the whole, there is a suggestion that fuel consumption and air requirement increased by using natural core material compared with synthetic matrices.

Table 6.1

Summary of data and results for natural matrix runs

	Run 12	Run 13
Crude oil	L.Fars	Maya
Oil saturation, %	20	37.93
Clays and silts (Lower Fars core)	5% wt	1% wt
WAR $m^3/M\ m^3$(st)	1.0	1.0
Pressure, bar	3.5	3.5
Peak temperature, °C	453	418
Fuel consumption, kg/m^3	23.82	22.37
Carbon combustion rate, gm/h	4.5	5.0
Combustion front velocity, m/h	0.0375	0.035
Air requirement, m^3 (st)/m^3	242.47	247.59
Air oil ratio, m^3 (st)/m^3	7456.0	1754.6
Air fuel ratio, m^3 (st)/kg	10.18	11.07

(B) Effect of metal compound additives.-Figures 6.3-6.5 show the temperature profiles obtained for Runs 17, 18 and 19. High peak temperatures were achieved almost at the middle of the combustion tube, particularly for Run 17 and also to a noticeable extent for Run 18. This is due to convective heat transport by the gas as it passes through the burnt upstream section of the bed. Water injection can enhance this behaviour, as it is a much more effective scavenger of the heat retained in the burnt section.

Table 6.2

Comparison of natural core results

Author	Core material	° API	oil (%) saturation	Pressure (bar)	WAR (m^3/Mm^3)	Fuel consumption (kg/m^3)	Air requirement (m^3/m^3)	AFR (m^3/kg)	AOR (m^3/m^3)
Burger and Sahuquet (1973)	Reservoir rock	27	45.7	36	1	22.8	250	10.9	-
	Silica sand	16	47.5	11	0	17.2	193	11.22	-
Ejiogu *et al* (1978)	Pembina (Alberta)	37	31.16	60	0.95	18.46	213.3	11.6	2047.1
Cady *et al* (1980)	Lloydminster (Alberta)	15.6	86	7	1.18	35.91	370	10.3	1671.6

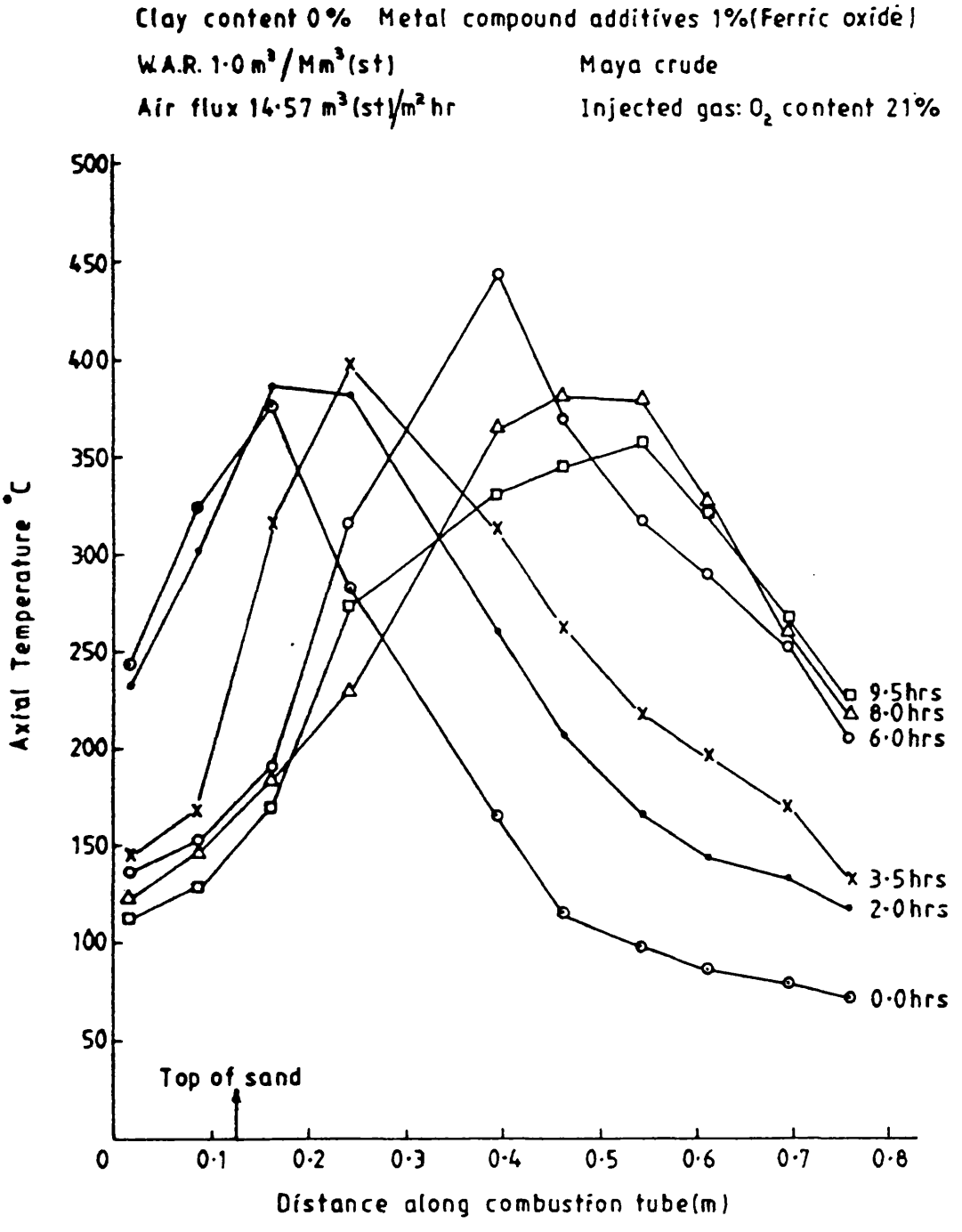

Figure 6.3 Temperature profile through combustion tube (Run 17)

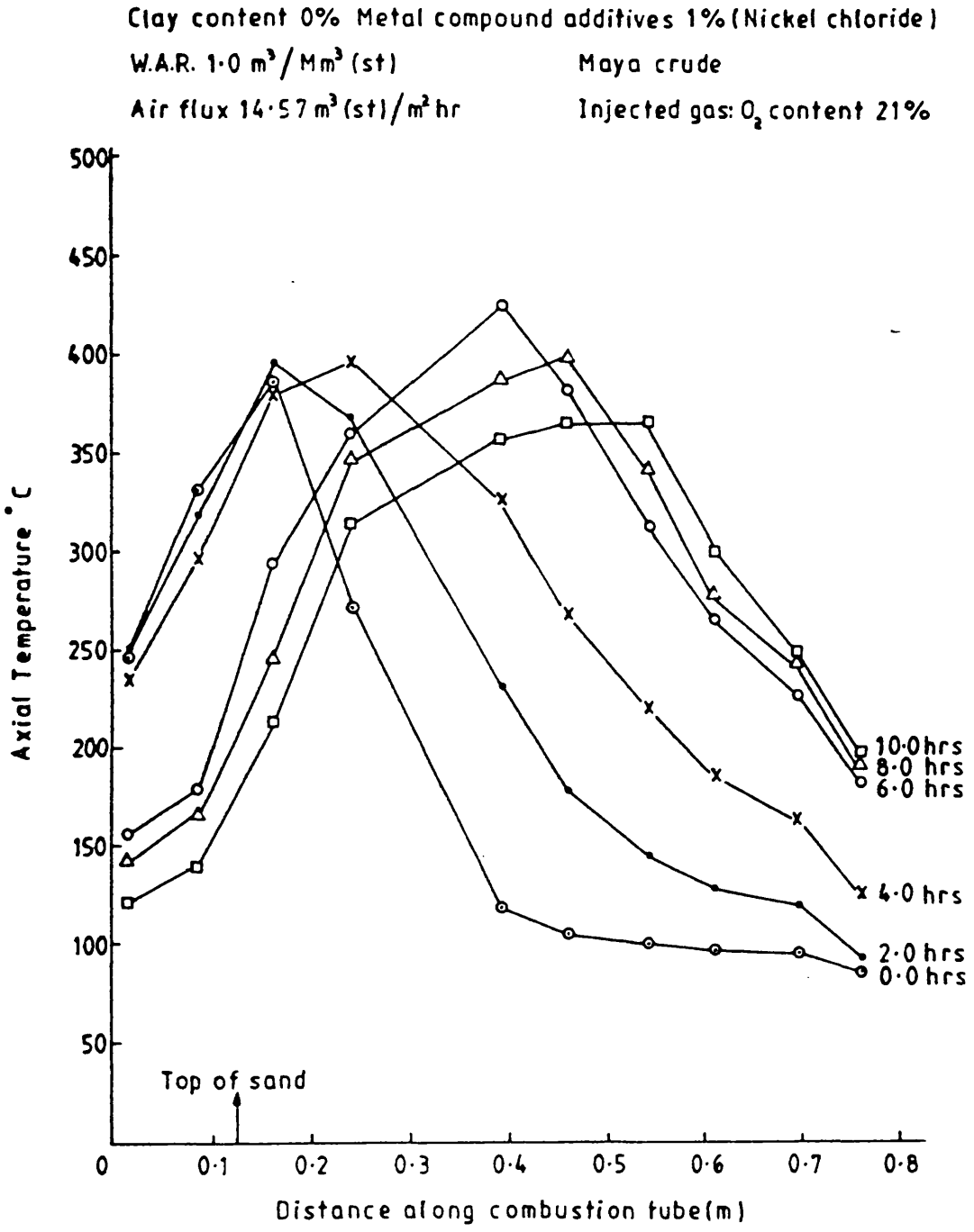

Figure 6.4 Temperature profile through combustion tube (Run 18)

Clay content 2%(Kaolin) Air flux 14·57m³(st)/m²hr
Metal compound additives 1%(Ferric oxide) Maya crude
W.A.R. 1·0m³/Mm³(st) Injected gas: O_2 content 21%

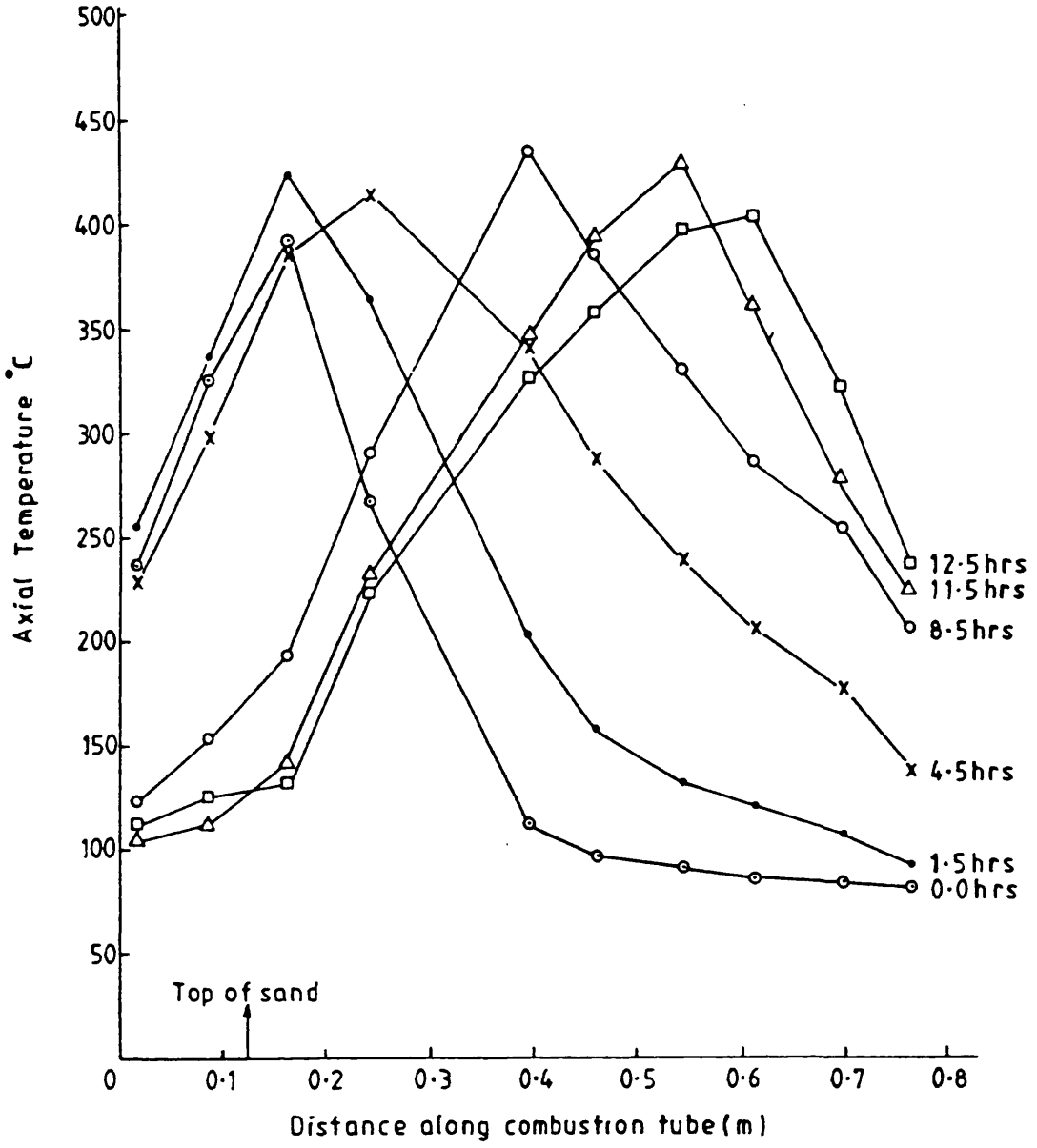

Figure 6.5 Temperature profile through combustion tube (Run 19)

There is a significant reduction in combustion temperature of approximately 30-50 °C for Runs 17, 18 and 19. The sand mixture in these runs contained ferric oxide and nickel chloride. On the other hand, Runs 1 and 2, which have the same initial conditions, but without any metal compounds present (Table 6.3), show no such effect. This accords with the work of Vossoughi *et al.* (1982), who showed that there is a lower activation energy in the petroleum combustion reaction due to the presence of metal compounds in the crude oil. An analysis of oxidation data for a French oil also showed that 2000 ppm of copper in the sand mixture lowered the activation energy by about 50%, reducing the combustion temperature (Fassihi *et al.*, 1984). Therefore, a reduction in the activation energy due to the presence of metal compounds acts to cause a reduction in the combustion temperature. This agrees with Drici and Vossoughi's (1985) results, showing that vanadium, nickel and ferric oxides enhanced endothermic reactions and shifted the combustion temperature to lower levels.

As shown in Figures 6.3-6.5, there is no steam plateau when metal compound additives are used. The lower combustion temperatures achieved in these experiments is responsible for this behaviour. Tests containing metal compounds (Runs 17, 18 and 19) achieved faster spontaneous ignition. This effect is thought to be caused by the catalytic activity of metal compounds which promote more rapid oxidation of the crude oil.

In Table 6.3, the combustion parameters obtained from Runs 1 and 2, which did not contain metal compounds are compared with Runs 17, 18 and 19. Higher values for fuel consumption, air requirement, and AOR, and lower values for combustion front velocity were obtained when metal compound additives were used. Run 19 (1% ferric oxide + 2% kaolin) gave increased values for the fuel consumption, air requirement, and AOR compared with Runs 17 and 18 (1% ferric oxide and 1% nickel

Table 6.3

Effect of metal compound additives on combustion runs

	Run 1	Run 2	Run 17	Run 18	Run 19
Crude oil	Maya	Maya	Maya	Maya	Maya
Additives content	0%	2% (kaolin)	1% ferric oxide	1% nickel chloride	1% ferric oxide + 2% kaolin
WAR, m^3/Mm^3 (st)	1.0	1.0	1.0	1.0	1.0
Peak temperature, °C	477	472	446	424	437
Fuel consumption, kg/m^3	12.4	14.3	21.9	24.0	29.87
Combustion front velocity, m/h	0.11	0.075	0.055	0.045	0.05
Air requirement, m^3 (st)/m^3	130.3	153.5	231.6	249.0	318.1
Air oil ratio, m^3 (st)/m^3	1401.9	1713.6	2046.4	2054.2	3795.1
Air fuel ratio, m^3 (st)/kg	10.5	10.7	10.6	10.4	10.7

chloride, respectively). Thus, it appears that the surface area effect of the clay play a more dominant role in this situation.

The effect of metal compounds on fuel consumption reported here is consistent with that reported by Fassihi and Brigham (1981), who analysed the results of Bardon and Gadelle (1977). They showed that the addition of metal compound additives to crude oils or sand matrices significantly increase the fuel consumption. Burger and Sahuquet (1972) also found an increase in fuel availability and air requirement in forward combustion when 2000 ppm of copper and 1% nickel chloride were added to crude oil and sand matrix, respectively.

6.2 Discussion

The core material from the Lower Fars reservoir contained crude oil gravity of 18 °API and 5% clays and silts. The average oil saturation was 20%, perhaps significantly lower than the fresh core, due to aging and exposure. Like other natural core, it contained a trace amount of metal compounds and organic material associated with the mineral constituents of the reservoir (Eltantaway and Arnold, 1973). These materials possess a high surface area, as well as catalytic activity, which promote the fuel laydown and sustain the combustion front.

The Computer Modelling Group (1982) have shown that the catalytic property of the rock matrix is strongly related to its composition. Drici and Vossoughi (1985),using surface areas ranging from 0.003 to 24.3 m^2/g, concluded, however, that the surface area of the additives affects crude oil combustion, regardless of their actual composition. It was seen in Chapter 4 that the nature of the surface area, as well as the availability of large surfaces, play an important role in determining the effectiveness of the additives.

An increase in initial oil saturation from 20% (Run 12) to 39.93% (Run 13) leads to a high fuel consumption value for the latter (22.37 kg/m^3). It seems that the fuel consumption for the *in situ* combustion process depends on initial oil saturation, as well as the type of the porous media. Alexander *et al.* (1962) also found that the fuel consumption increases as the initial oil saturation increases.

The reduction in combustion temperature, particularly for Run 13, which contained 25% core material and 75% silica sand, may be a result of low oxygen consumption due to the lower residence time for the oxygen in the combustion zone. This condition occurs when the combustion front overruns the mobile bank due to a lack of communication of the core material (Computer Modelling Group, 1982). A possible explanation for this behaviour is movement of clays and fine silts. Thus, increased oxygen flow downstream of the combustion front leads to further LTO reaction taking place. The residual hydrocarbon deposited on the sand matrix confirms the occurrence of LTO reactions. Ejiogu *et al.* (1978) also observed a reduction in combustion temperature when natural core material was used and they referred this behaviour to the hydrothermal reaction of the natural matrix at the high combustion temperatures.

Runs 17, 18 and 19, which contain metal compound additives (ferric oxide and nickel chloride) demonstrated great fuel consumption. Venuto and Habib (1979) stated that metals promote dehydrogenation and cyclisation reactions which lead to higher fuel consumption. Decrooq (1984) has reported specific surface areas for powdered solids catalysts in the range 102-200 m^2/g. Therefore, the question as to whether the metal compound additives effect is due to the possession of catalytic activity or whether it is due to their high specific surface area, or both, remains to be answered.

It is interesting to note that regardless of the catalytic activity of the metal compound additives, their surface area may play a major role in the fuel consumption process. An SEM photograph of ferric oxide crystal (Figure 6.6) shows that the solid particles are granular and the structure is more open and porous than the kaolin. The nature of the surface area for ferric oxide is thus more similar to that of amorphous silica. As discussed in Chapter 4, amorphous silica led to higher fuel consumption than the kaolin. Thus, surface areas, as well as catalytic activity, may be a major factor in determining the role that metal compound additives play in *in situ* combustion processes. An increase in fuel consumption and the reduction in combustion front velocity by approximately 50%, seems to confirm this.

The fact that metal compound additives shorten spontaneous ignition time, could be a valuable aid in *in situ* combustion field projects. This could be accomplished by injection of a solution of metal compounds into the reservoir, before injecting air. The type of metal compound additives to be used for the *in situ* combustion process need to be selected carefully. For example, amorphous SiO_2-ArO_3 is used as a catalyst in the cracking of heavy oil residues and tar liquids (Probstein, 1982). Zeolite (crystalline synthetic) is used to obtain specific hydrocarbon products (Venuto and Habib, 1979). The complete, or most satisfactory, oxidation of hydrocarbons seems to be with the use of metal oxides and also metal chloride additives.

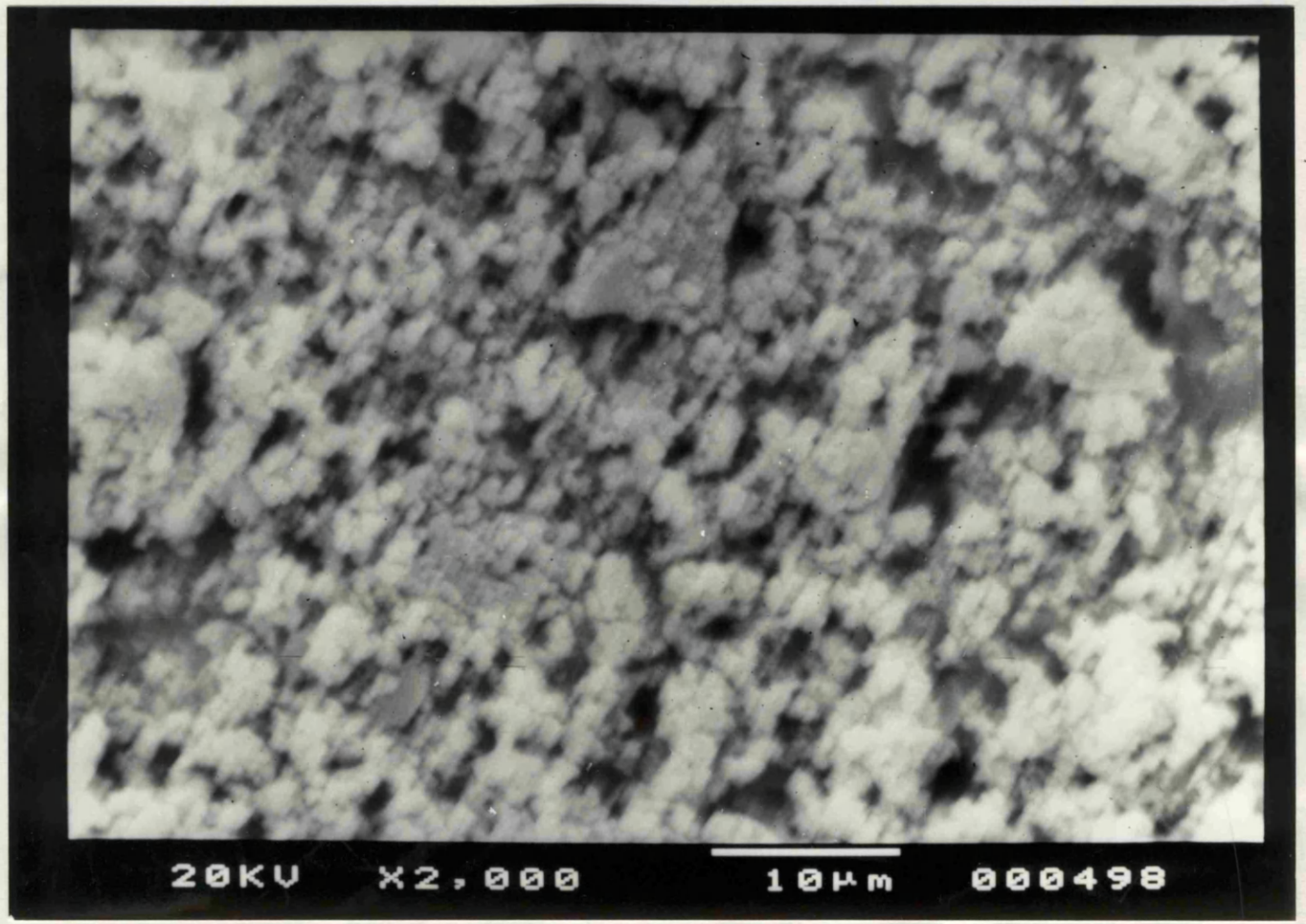

Figure 6.6 SEM photograph for ferric oxide 2000 magnification.

6.3 Conclusions

(1) Natural core material from the Lower Fars reservoir has a high specific surface area, as well as catalytic properties. For wet combustion, sufficient fuel is deposited to sustain the combustion front with a low initial oil saturation of only So_i = 20%.

(2) Detailed mineral analysis of the natural core is necessary, in order to evaluate systematically the effect of constituents such as metal compounds on the *in situ* combustion of crude oil.

(3) The addition of 1% ferric oxide and 1% nickel chloride to the sand pack acts to lower the combustion peak temperature by 31-35 °C and 53 °C respectively.

(4) Metal compounds possess a very large surface area and open porous structure which promotes fuel consumption, and increases air requirement and AOR. Additionally, faster spontaneous ingnition of crude oil was achieved. In practice, metal compound additives could be injected into the reservoir, prior to air injection, in order to achieve faster ignition.

CHAPTER 7

Effect of Additive Materials on Gas and Oil Production

The physical and chemical properties of crude oils undergo changes during combustion process. These changes arising from distillation, thermal cracking and LTO, may also be importantly influenced by the presence of additives such as Clay Kaolin, amorphous silica, natural core material and also metal compounds. An investigation of the effects of these material additives on composition of produced gas and oil was therefore made. The changes occuring to crude oil composition were identified from density measurements and oil viscosity trends. The effect of oxygen enrichment has also been investigated.

7.1 Produced Gas Composition

The measured gas composition profiles for Runs 1 to 20 are shown in Figures 7.1 to 7.20. They refer to the stabilised period of combustion, i.e. when the combustion front velocity is constant. Appendix B shows in tabular form the instantaneous composition of the produced gases for Runs 1 to 20. The overall gas and oxygen material balance is given in Appendix C.

At a temperature of 150°C or below, some oxygen will react with crude oil due to LTO reaction. This causes a small amount of CO and CO_2 to appear in the produced gas. At much higher temperature (430°C), the main products from the combustion reaction are CO and CO_2 and only a small amount of oxygen is left unreacted. When the combustion front nears the end of the sand pack, the CO and CO_2 concentration tends to decrease because of a reduction in fuel consumption brought on by lower fuel availability.

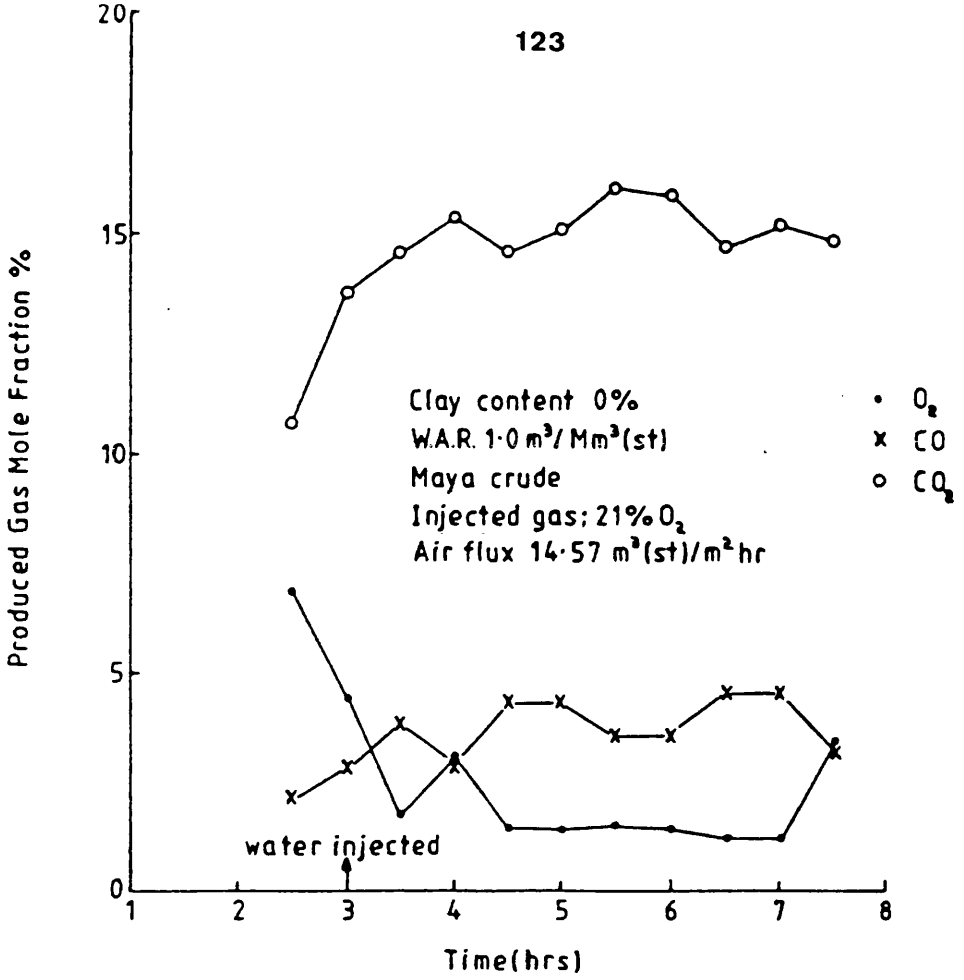

Figure 7.1 Produced gas composition (Run 1)

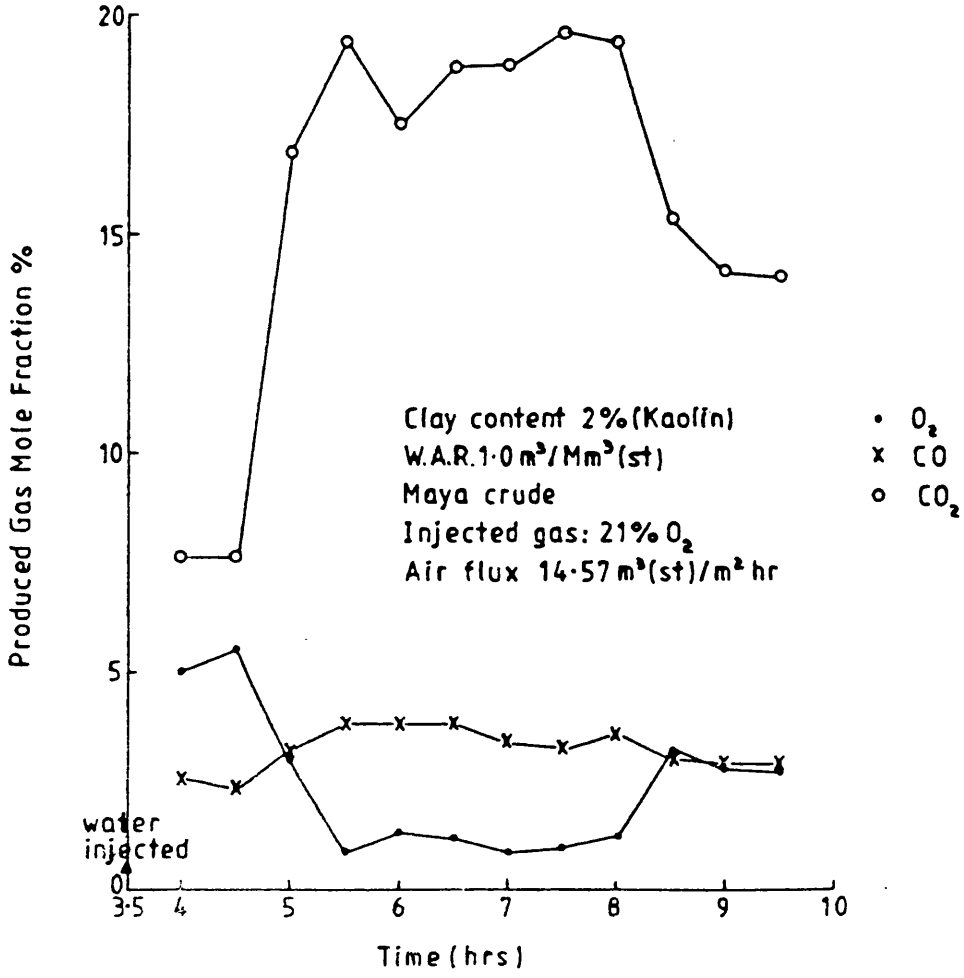

Figure 7.2 Produced gas composition (Run 2)

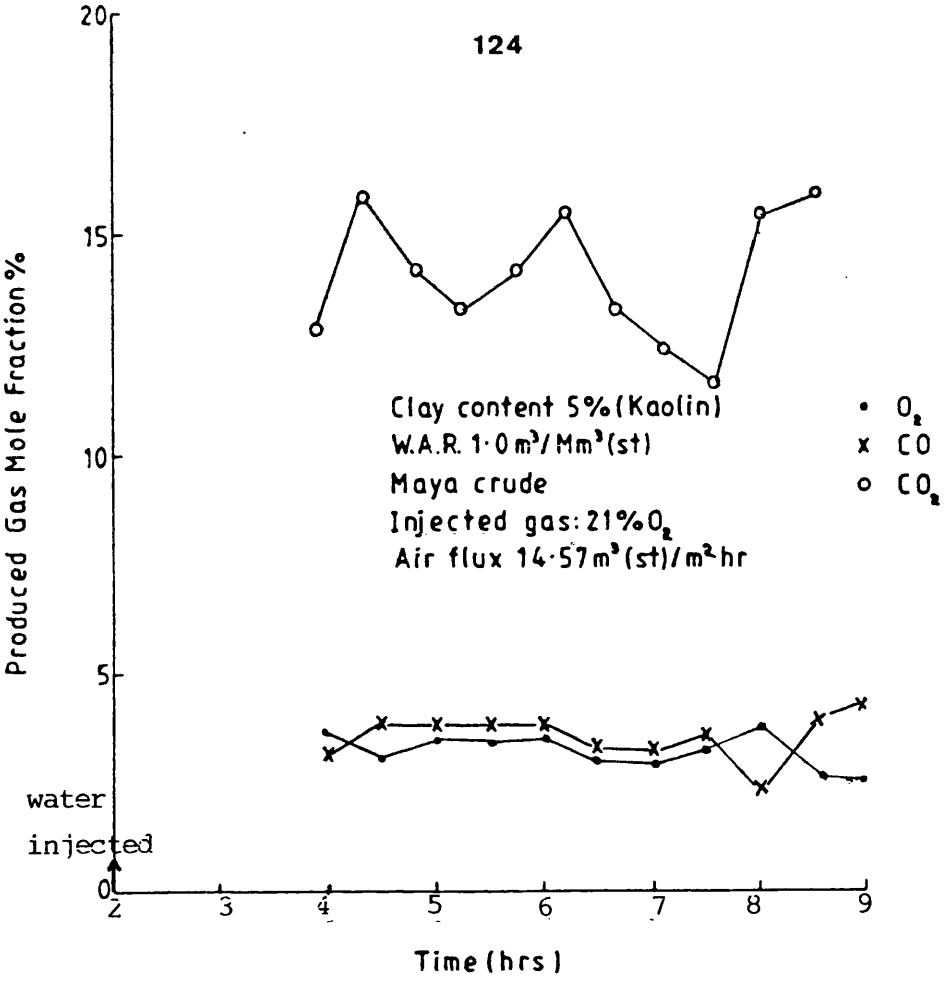

Figure 7.3 Produced gas composition (Run 3)

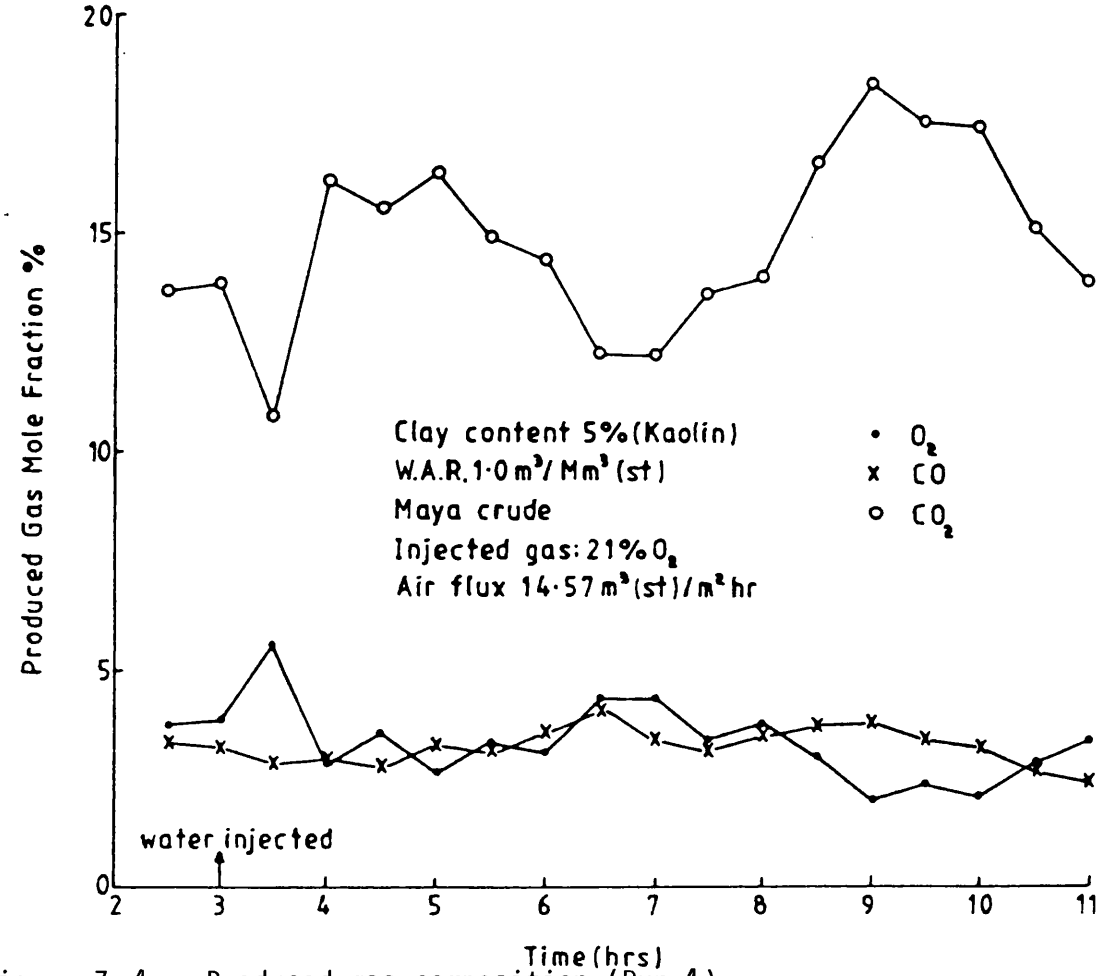

Figure 7.4 Produced gas composition (Run 4)

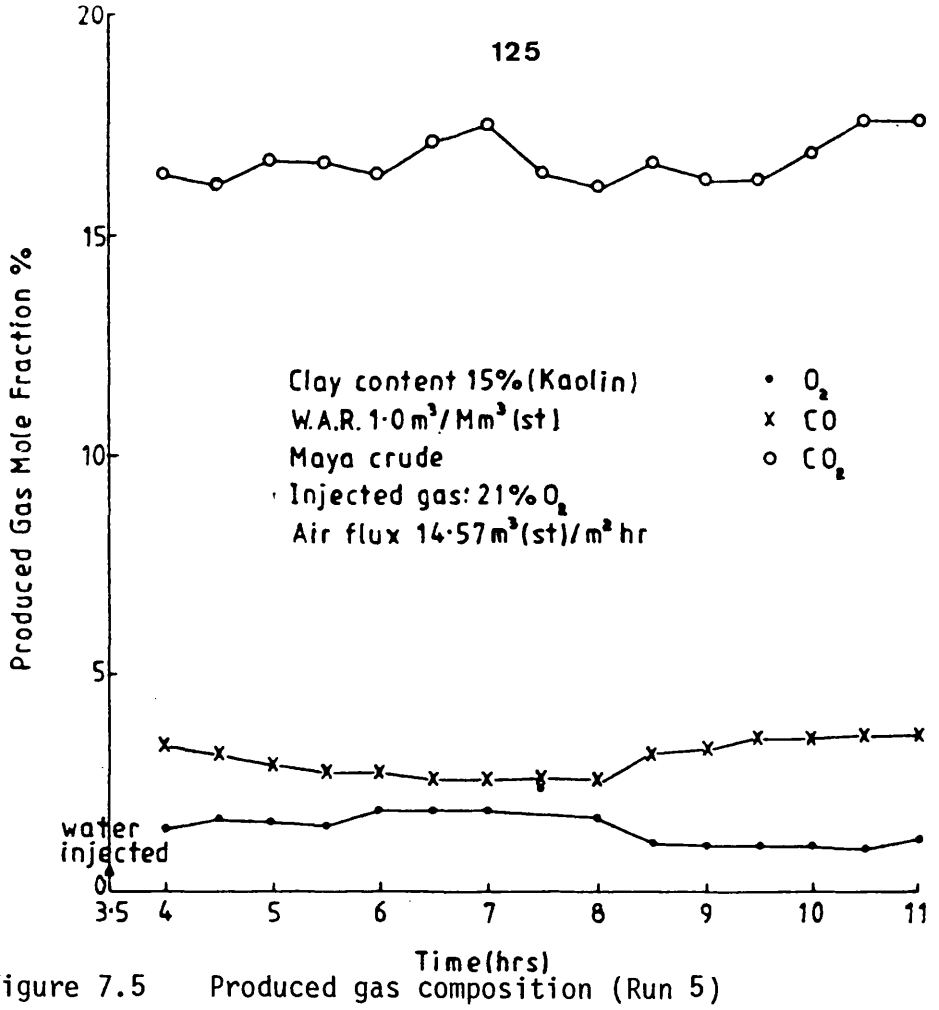

Figure 7.5 Produced gas composition (Run 5)

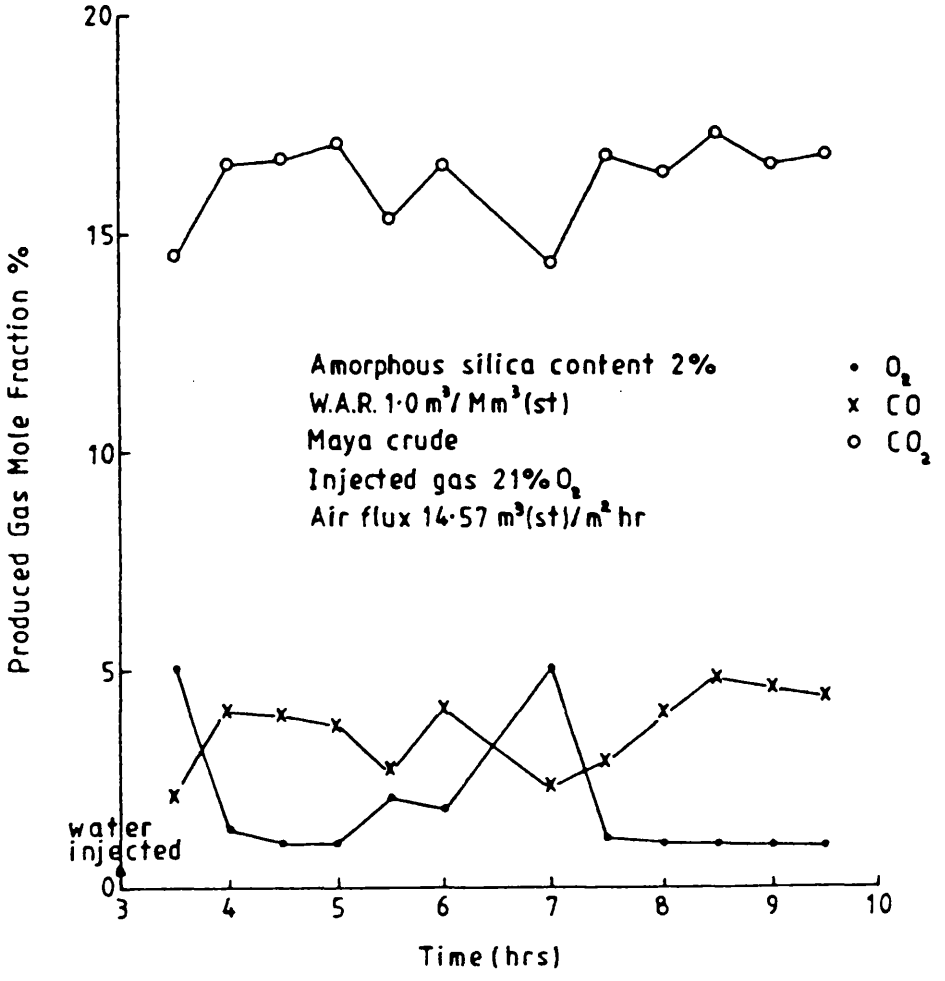

Figure 7.6 Produced gas composition (Run 6)

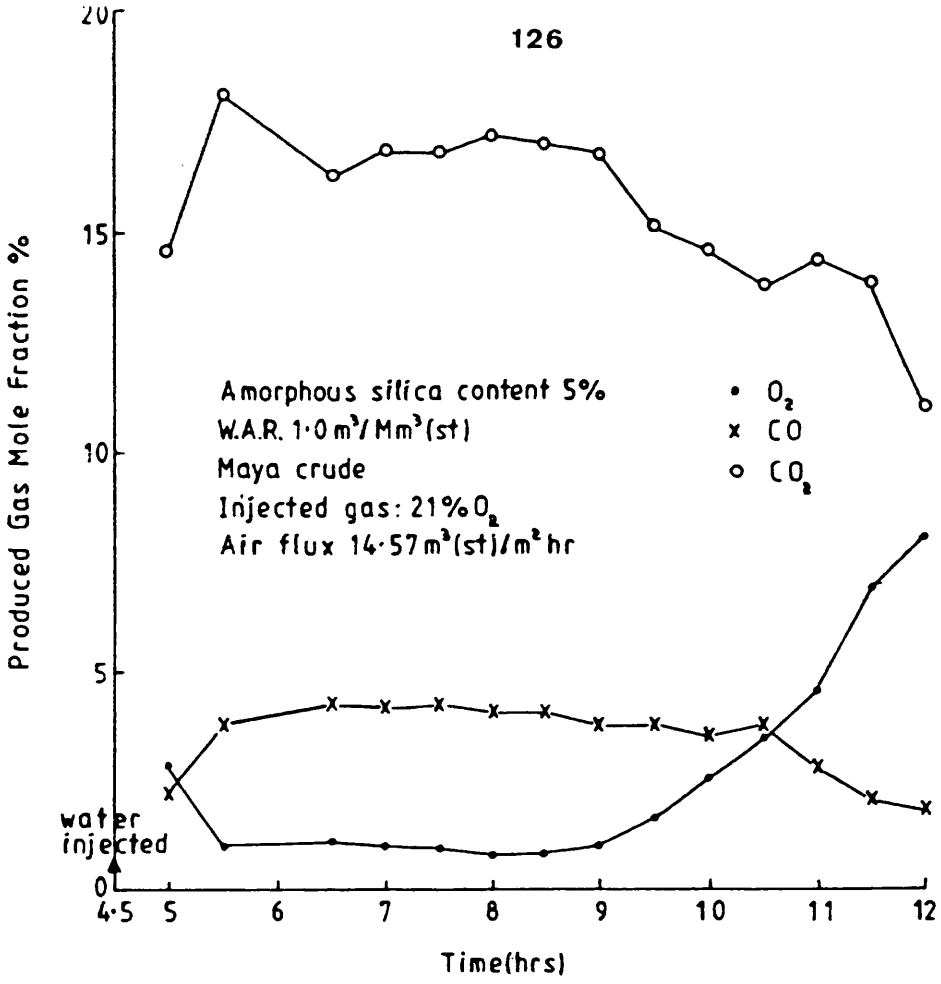

Figure 7.7 Produced gas composition (Run 7)

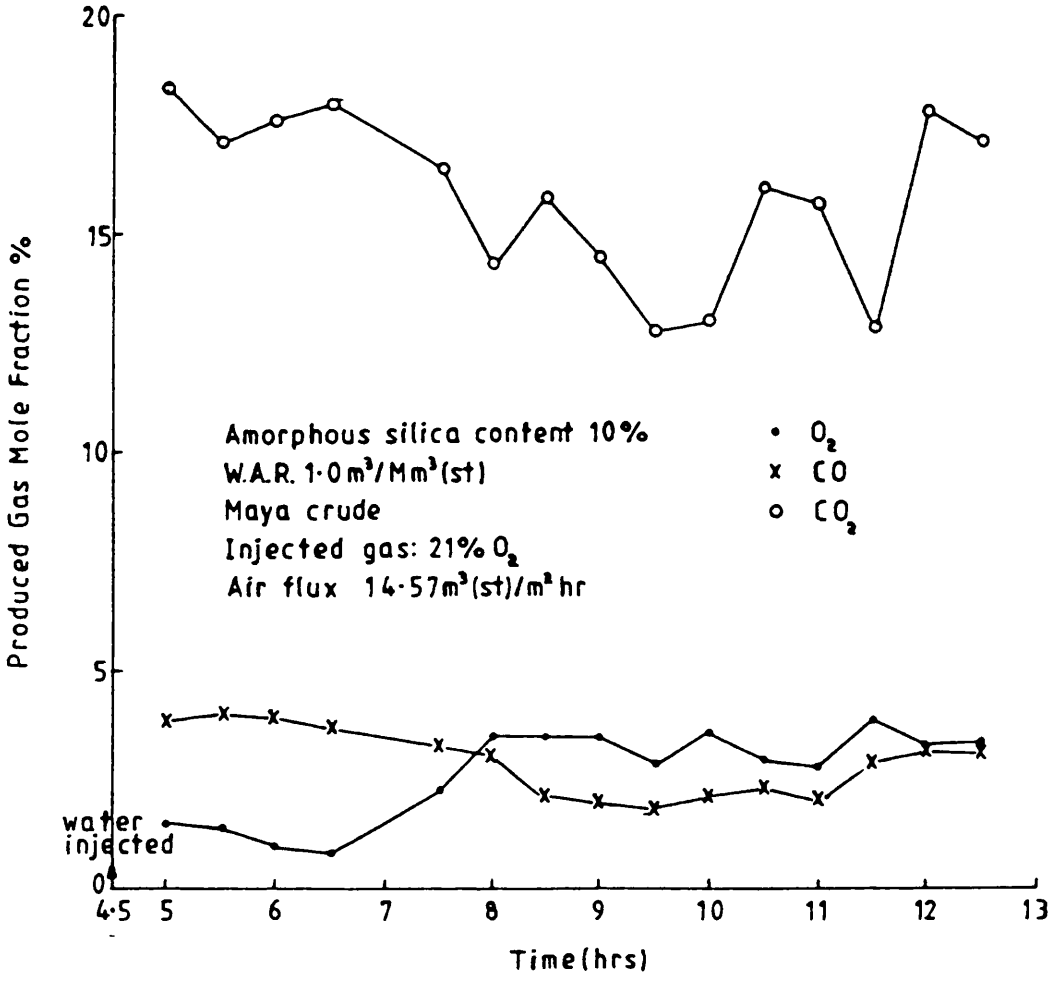

Figure 7.8 Produced gas composition (Run 8)

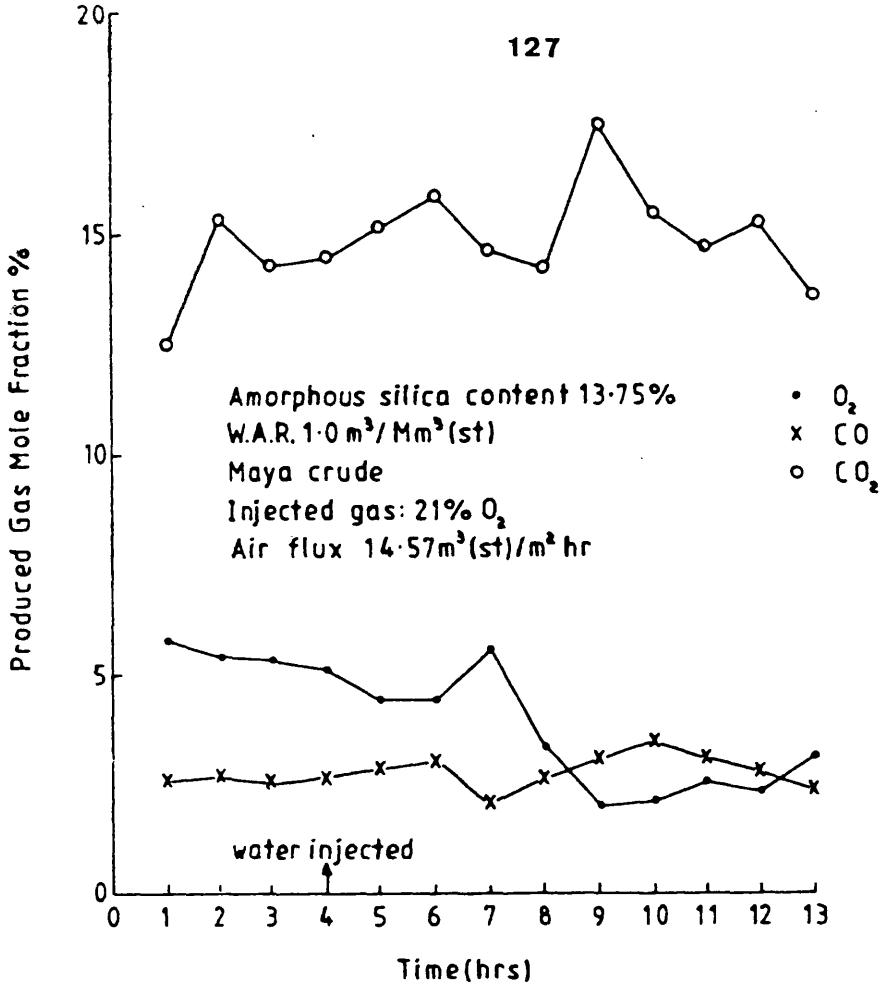

Figure 7.9 Produced gas composition (Run 9)

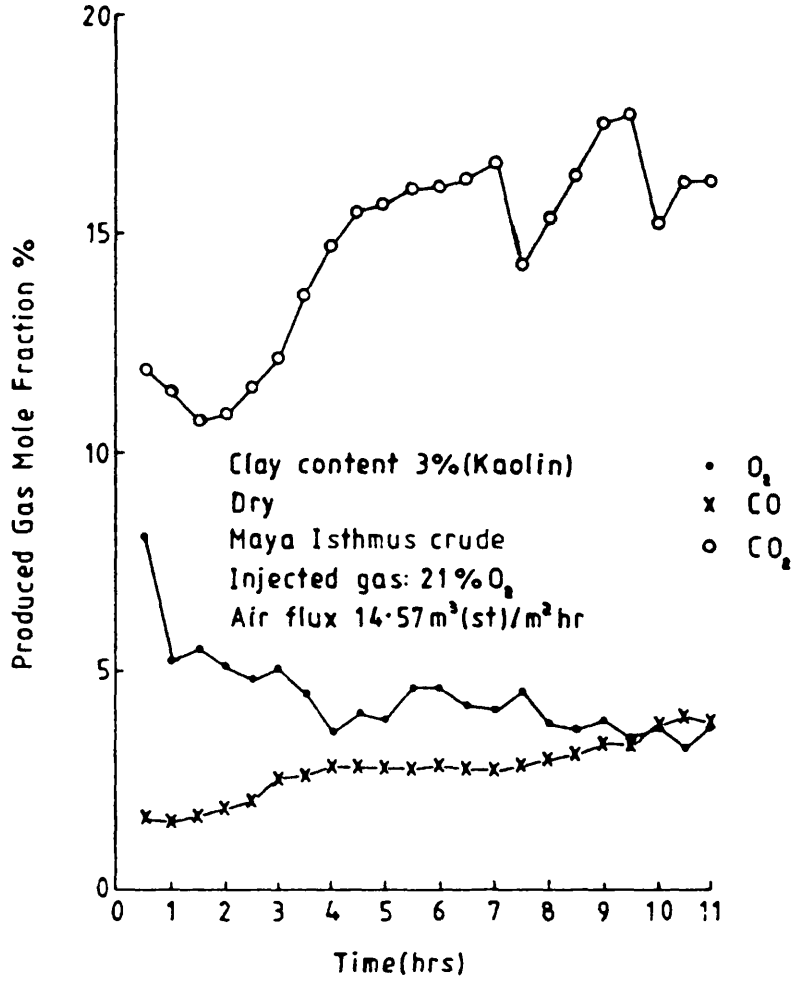

Figure 7.10 Produced gas composition (Run 10)

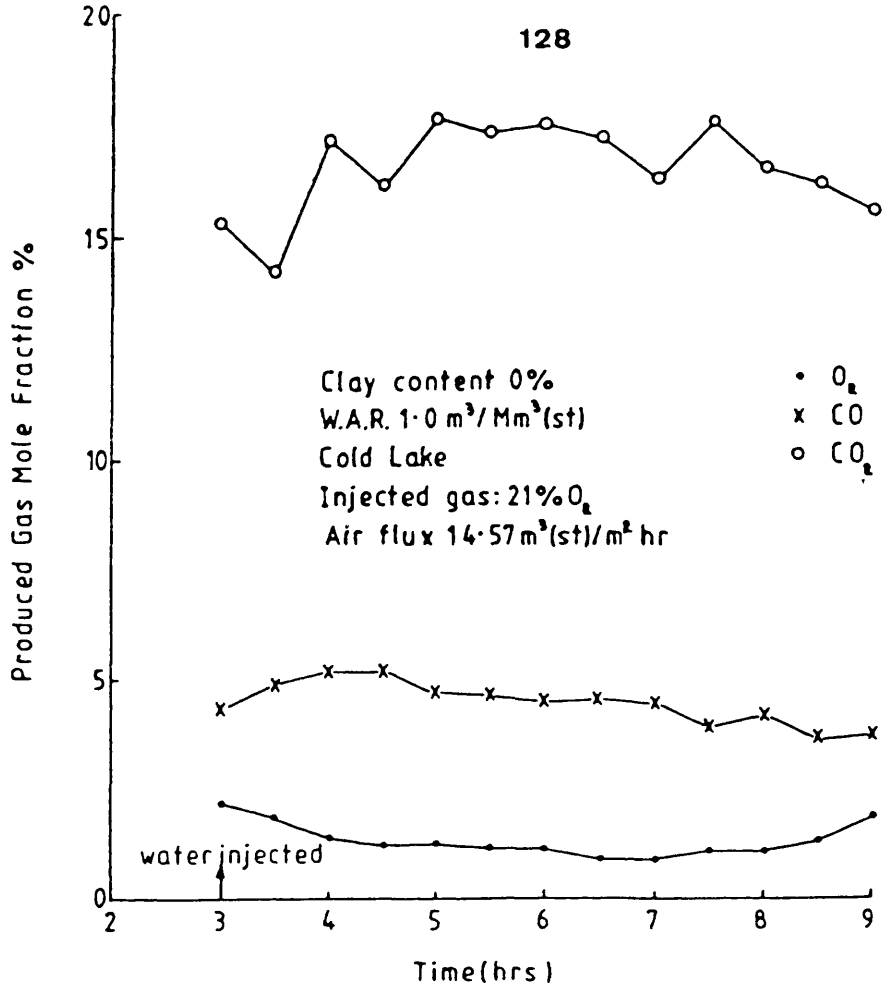

Figure 7.11 Produced gas composition (Run 11)

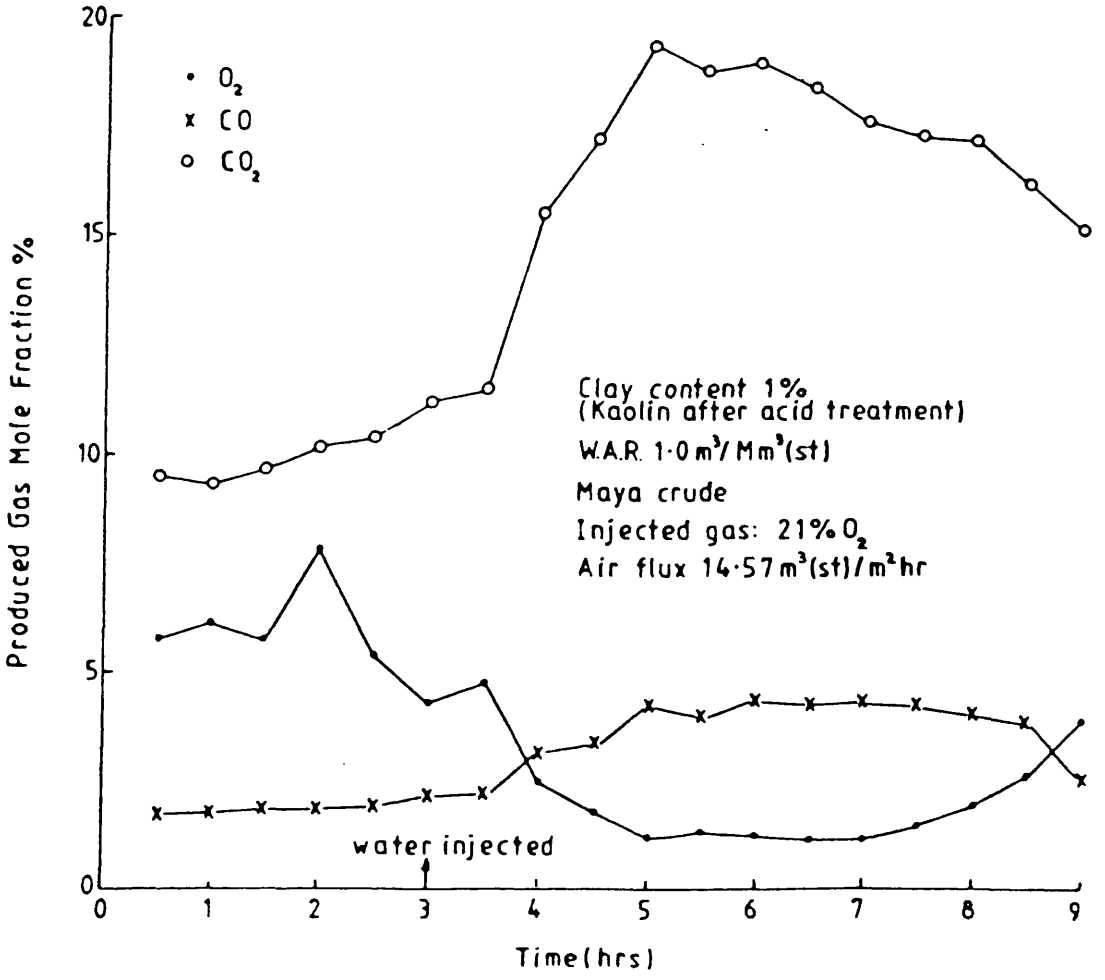

Figure 7.12 Produced gas composition (Run 20)

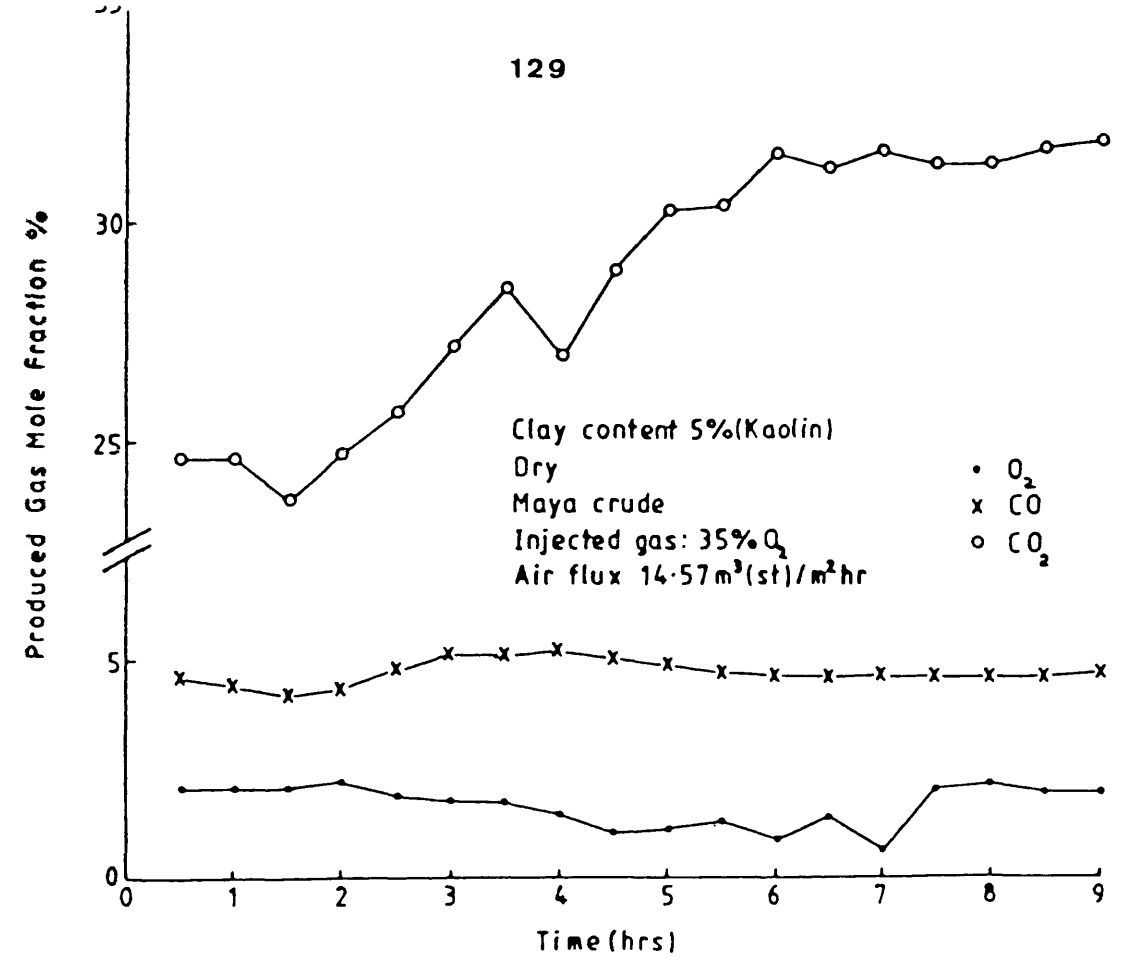

Figure 7.13 Produced gas composition (Run 14)

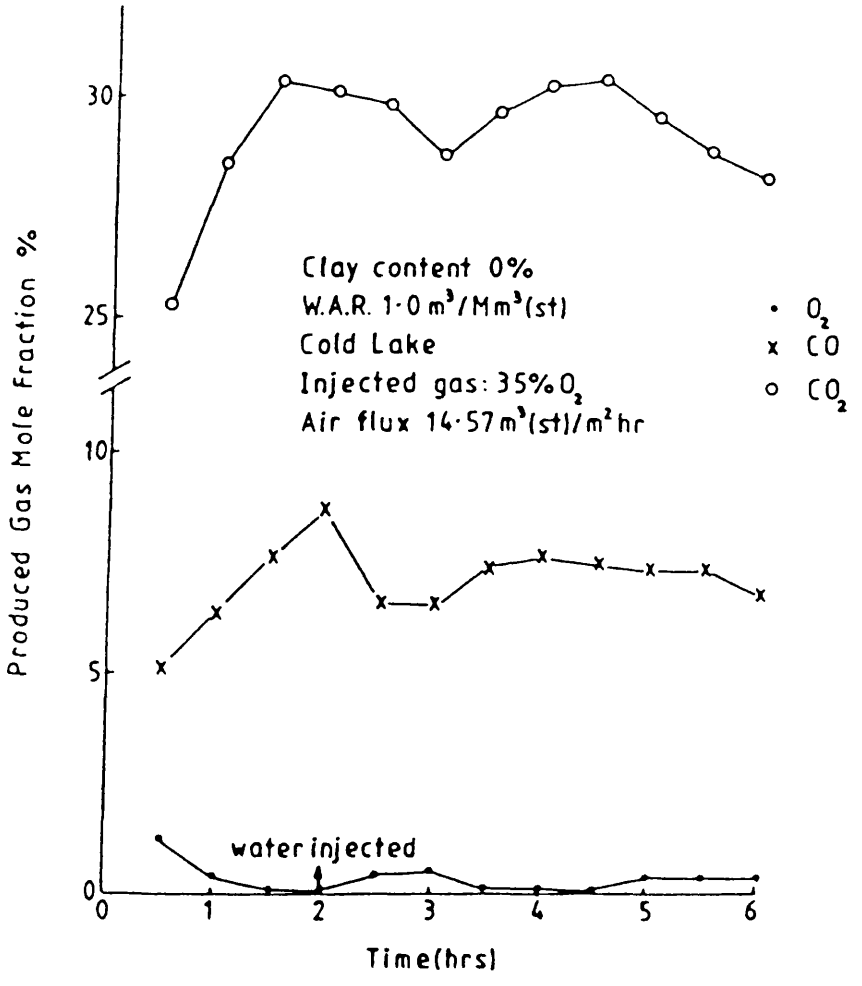

Figure 7.14 Produced gas composition (Run 15)

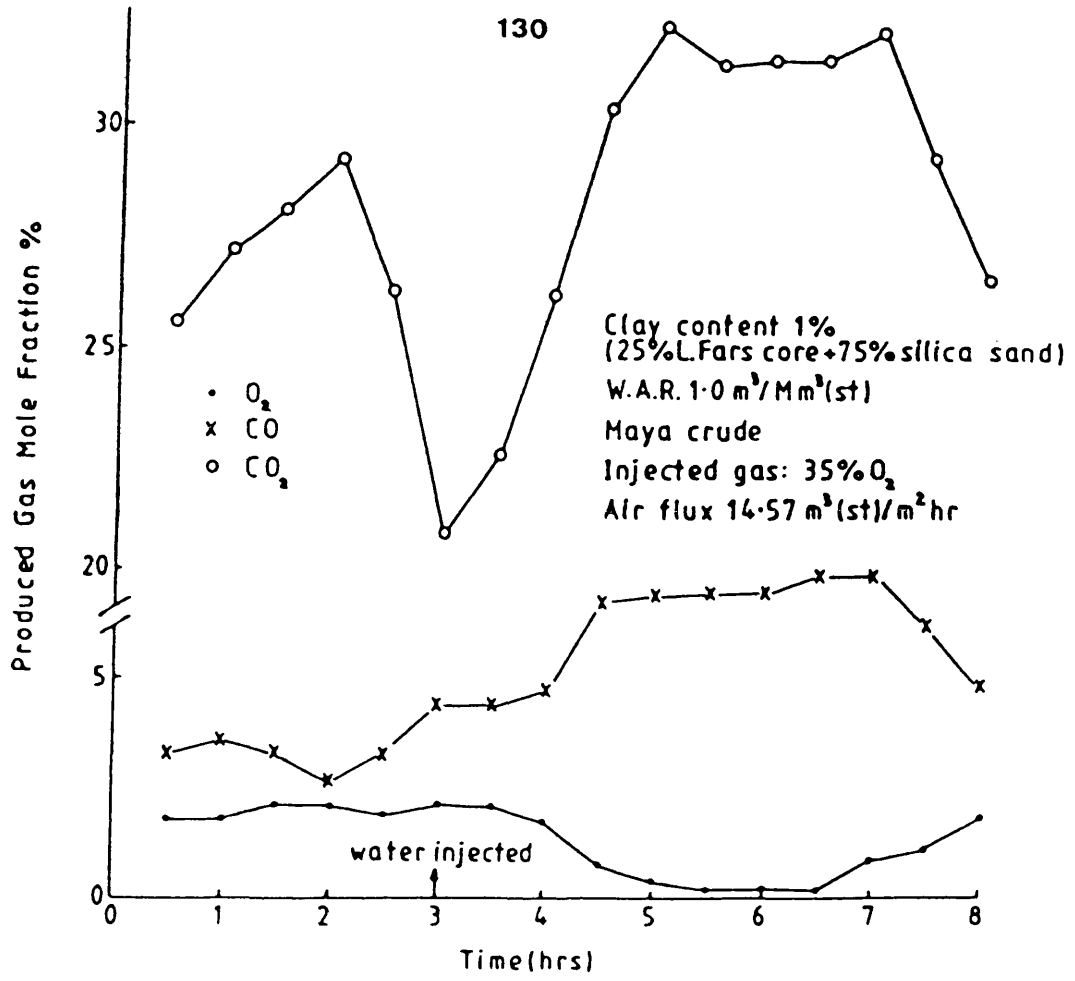

Figure 7.15 Produced gas composition (Run 16)

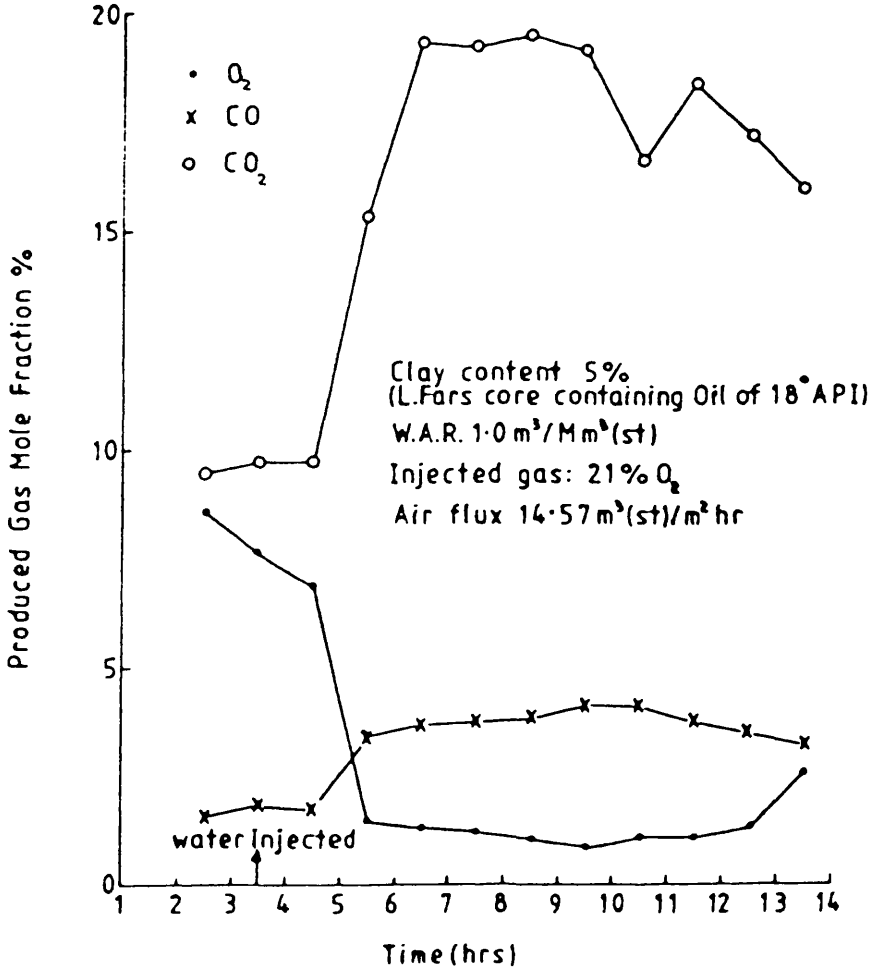

Figure 7.16 Produced gas composition (Run 12)

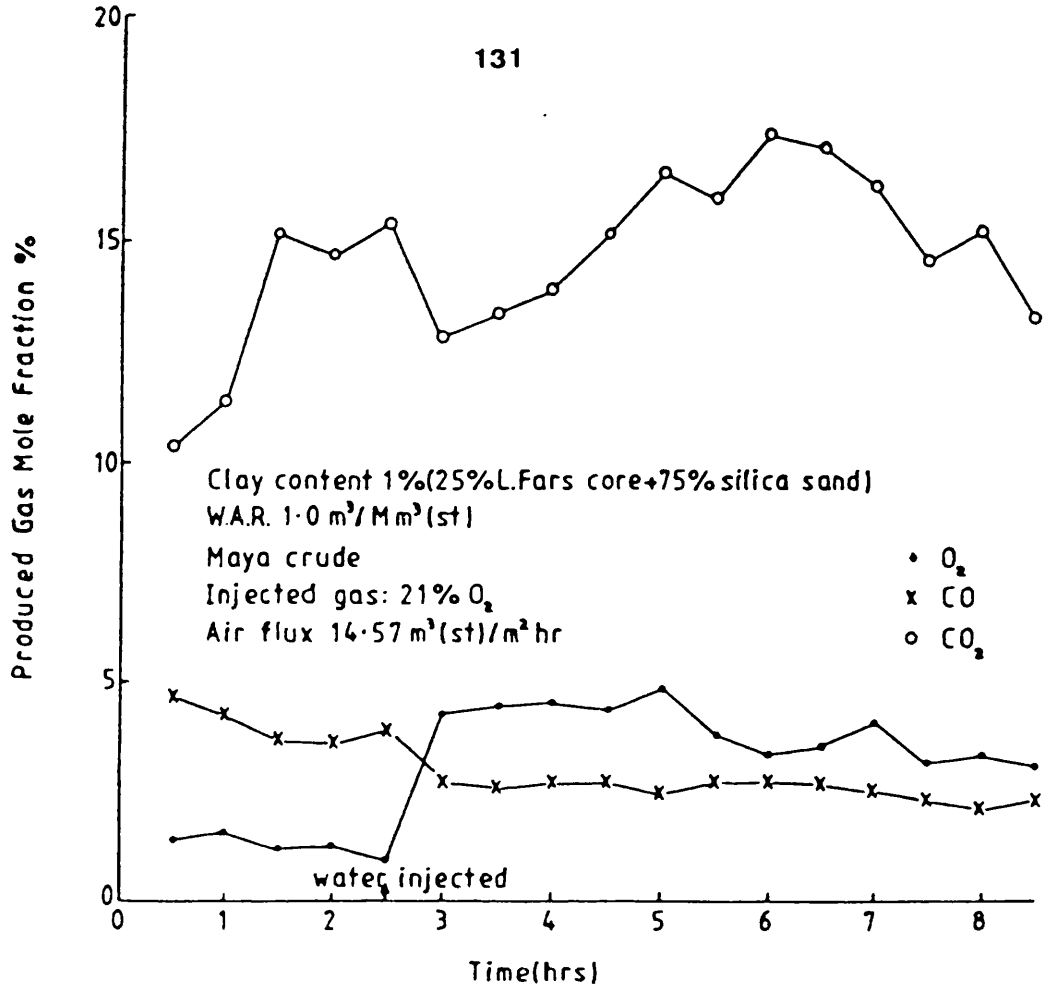

Figure 7.17 Produced gas composition (Run 13)

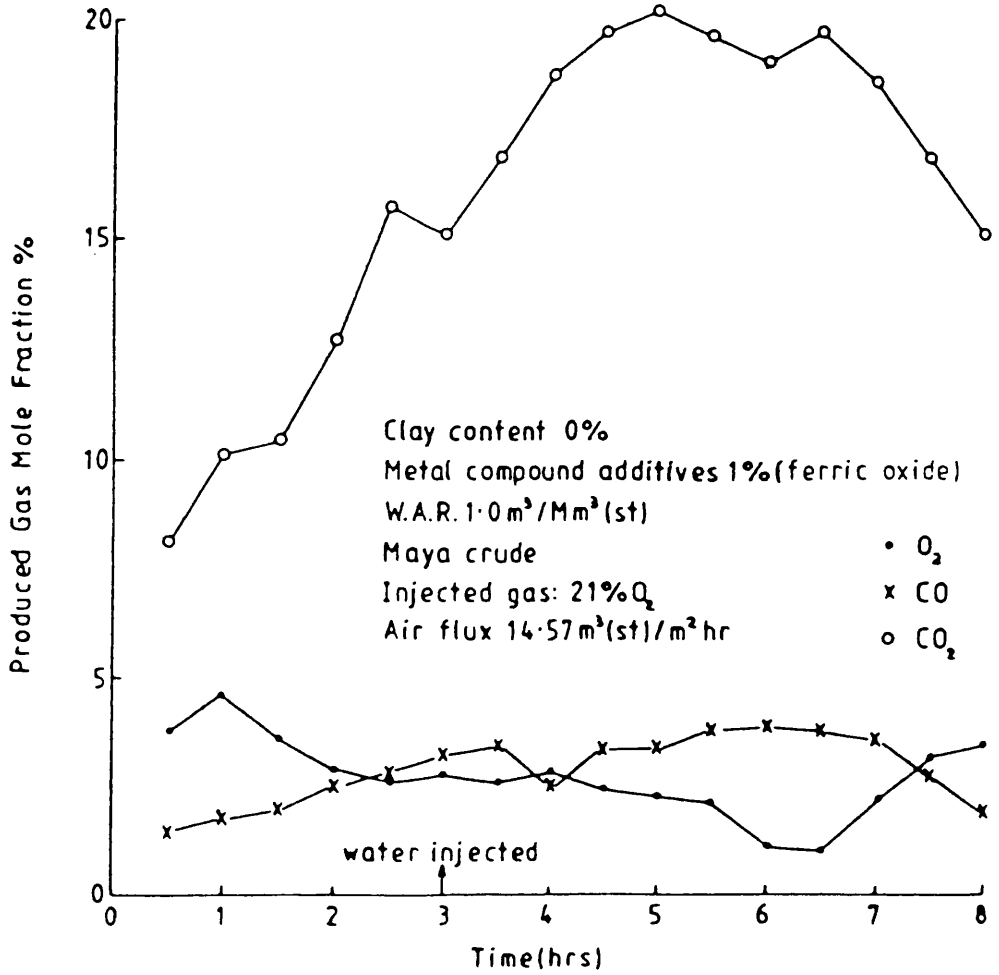

Figure 7.18 Produced gas composition (Run 17)

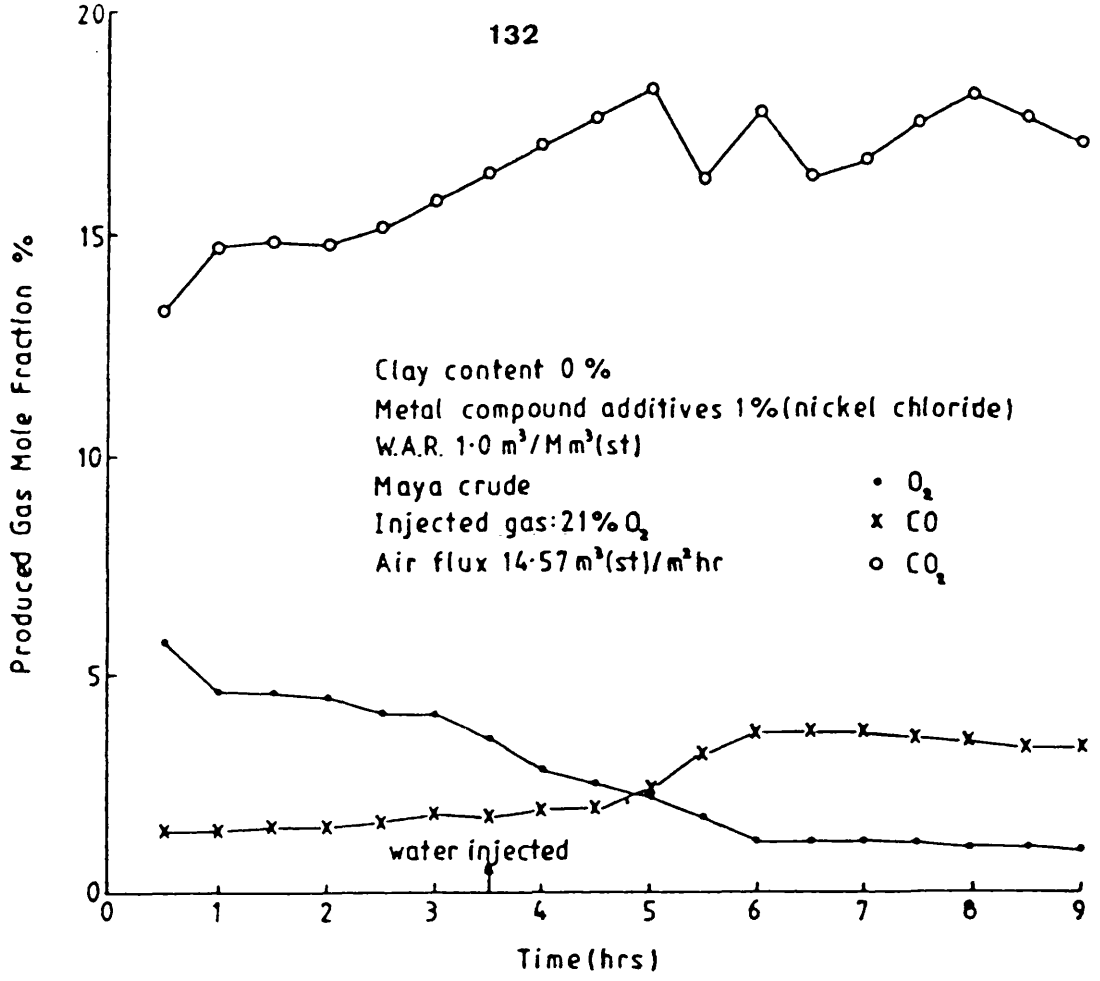

Figure 7.19 Produced gas composition (Run 18)

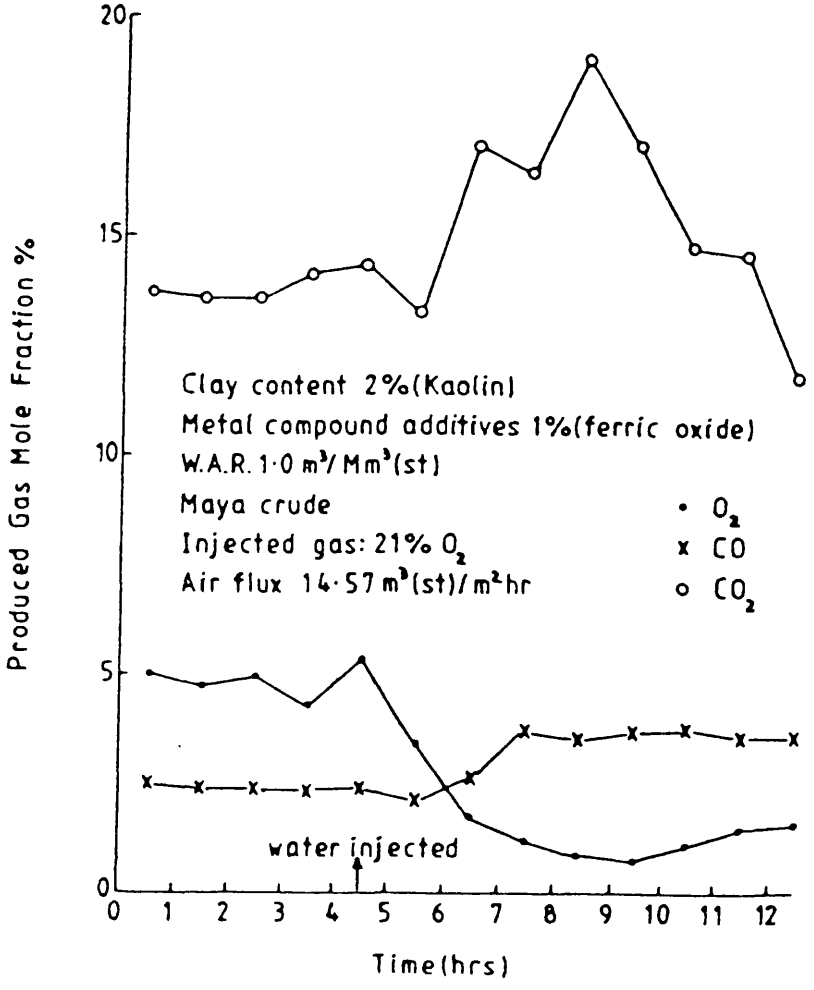

Figure 7.20 Produced gas composition (Run 19)

It is apparent in Figures 7.1 to 7.20, however, that there is considerable variability in the produced gas composition in a number of cases, especially regarding the CO_2 profile. There are additional effects due to the start of water injection, or because fuel availability becomes limited towards the end of a run. In order to provide a reasonable basis for comparing the effect of the additives, the average composition reported in Table 7.1 refers to the period in Runs 1-20 when the gas composition is most stable.

7.1.1 Effect of kaolin and amorphous silica

During Run 1 (Figure 7.1), with Maya crude oil, but no additives in the sand matrix, the variation exhibited by the gas profiles is small. For the stable period (between 4.5 to 7 h) the analysis of O_2, CO, and CO_2 shows mol fractions averaging 1.3, 4.2 and 15.5%, respectively. The low level of oxygen concentration in the produced gas indicates that most of the oxygen has been consumed by combustion.

In Run 2, 2% Kaolin was added to the sand matrix with Maya crude oil. In Figure 7.2, a fairly stable gas composition profiles is reached two hours after water injection and the composition of the produced gases averages 1.1% O_2, 3.6% CO and 19% CO_2 (Table 7.1). As the combustion front approaches the end of the combustion tube the CO_2 level decreases sharply and the O_2 level increases. Comparing with Run 1, the concentration of CO_2 produced is higher and O_2 concentration is lower by 18 and 15%, respectively. This is attributed to the presence of Kaolin in the sand pack.

In Run 3 (Figure 7.3), using 5% Kaolin and Maya crude oil, the produced gases contain 3.5% O_2, 4.1% CO and 15.6% CO_2. It is apparent that consumption of oxygen is incomplete. Also the CO_2 mol fraction is lower than that of Run 2 (2% Kaolin).

Table 7.1

Average Composition of Produced Gas

Run No.	Crude Oil	Method of Combustion	Additives Content	Injected Gas % O_2	mol %				
					O_2	CO	CO_2	CH_4	H_2
1	Maya	Wet	0%	21	1.3	4.2	15.5	0	0
2	"	"	2% Kaolin	21	1.1	3.6	19.0	Trace	0
3	"	"	5% Kaolin	21	3.5	4.1	15.6	Trace	Trace
4	"	"	10% Kaolin	21	3.3	3.3	16.0	0	0
5	"	"	15% Kaolin	21	1.6	3.3	16.9	0	0
6	"	"	2% amorphous silica	21	1.4	5.7	16.0	Trace	Trace
7	"	"	5% amorphous silica	21	1.1	4.1	16.8	0	0
8	"	"	10% amorphous silica	21	3.2	2.2	17.5	0	0
9	"	"	13.75% amorphous silica	21	4.8	2.6	15.0	0	0
10	Maya Isthmus	Dry	3% Kaolin	21	4.1	2.7	16.1	0	0
11	Cold Lake	Wet	0%	21	1.0	4.3	17.2	0.4	Trace
12	Lower Fars	"	5% additives from L. Fars	21	1.6	3.9	19.0	0	0
13	Maya	"	1% additives from L. Fars	21	4.0	2.6	16.2	0	0
14	"	Dry	5% Kaolin	35	1.3	4.7	34.8	Trace	Trace
15	Cold Lake	Wet	0%	35	0.24	7.5	29.8	0.2	Trace
16	Maya	"	1% additives from L. Fars	35	0.35	6.9	31.7	Trace	Trace
17	"	"	1% Ferric Oxide	21	1.5	3.6	19.6	0	0
18	"	"	1% Nickel Chloride	21	1.1	3.5	17.2	0	0
19	"	"	1% Ferric Oxide +2% Kaolin	21	1.1	3.6	17.0	0	0
20	"	"	1% Acidised Kaolin	21	1.2	4.1	18.3	0	0

With 10% Kaolin in Run 4 (Figure 7.4), the concentration of CO and CO_2 tends to increase generally over the combustion period. At midway of the combustion period the CO and CO_2 produced dropped to low values of 3.5 and 12%, respectively. The oxygen concentration is then 4.24% and it decreases to a low level of 2%. Although the CO_2 produced is higher than that of Run 1 (no additives), it is still lower than that of Run 2 (2% Kaolin).

During Run 5 (Figure 7.5), which included 15% Kaolin with Maya crude oil, very small variations are exhibited in the gas profiles. The O_2, CO and CO_2 compositions in the produced gases averaged 1.6, 3.3, and 16.9%, respectively.

For 2% amorphous silica (Run 6), the CO and CO_2 production followed the same trend (Figure 7.6). They are stabilised one hour after water injection and averaged5.7 and 16%, respectively. At the same time, the oxygen mol fraction is 1% and averaged 1.4% over the combustion period.

The product gas analysis for Run 7 (5% amorphous silica) is shown in Figure 7.7. The CO_2 concentration shows a reduced trend over the combustion period until it reaches a minimum level of 11% at the end of the test, while O_2 and CO concentrations show stable levels of 1.1 and 4.1% respectively (Table 7.1). Towards the end of the test, O_2 concentration increases to a level of 8% and CO concentration decreases to a level of 1.75%.

In Run 8, 10% amorphous silica is used. For the stabilisedperiod between 8.5 to 11 hr, the O_2 and CO_2 concentration averaged at 3.2 and 2.2% (Figure 7.8). The CO_2 concentration shows a decrease trend over

the combustion period with frequent variation, averaging 17.5%. This is higher than the CO_2 concentration in the previous runs at 2 and 5% amorphous silica.

Figure 7.9 presents the gas profile obtained with 13.75% amorphous silica (Run 9). The analysis of O_2, CO and CO_2 averages 4.8, 2.6, and 15%, respectively. The CO_2 concentration is smaller than those with lower amorphous silica content.

In Run 10 (Figure 7.10), which included 3% Kaolin with Maya Isthmus crude, the concentration of CO and CO_2 tends to increase generally and averages 2.7 and 16.1%, respectively. The O_2 concentration decreases gradually to a level of 3.5% at the end of the run. The composition of the O_2 averaged 4.1%

Figure 7.11 presents the gas profile for Run 11, using Cold Lake crude oil with no additives. One hour after water injection a fairly stable composition is observed (1.0% O_2, 4.3% CO, and 17.2% CO_2). Traces of methane and hydrogen were produced (Table 7.1), indicating some effect of visbreaking reactions for the heavy Cold Lake oil. This is consistent with Shu and Venkantesan (1983) work which reported a kinetic study of visbreaking data of Cold Lake bitumen at 260 - 325°C. It is well known that a thermal cracking of hydrocarbons produces lighter components of crude oil, while visbreaking produces heavier components.

Figure 7.12 shows the gas profiles for Run 20, in which 1% acidised Kaolin was used. The CO_2 concentration increases gradually and reaches a maximum level of 19%. At the same time, O_2

concentration decreases rapidly and stablises after two hours of water injection, at 1.2%. The CO_2 concentration obtained here is higher than those in Runs 3, 4, and 5 (5, 10 and 15% Kaolin).

Generally, when Kaolin and amorphous silica are present, the CO_2 concentration in the produced gases is higher than that with no additives in the sand matrix. For example, the CO_2 mol fraction increased as follows 15.6, 16, 16.9% with 5, 10 and 15% Kaolin content, respectively. This indicates the effect of increasing the surface area of the bed which leads to higher fuel deposition and hence greater production of CO_2. However, Run 2 (2% Kaolin) achieved a much higher concentration of CO_2 than in other runs (Table 7.1). Also, Run 9 (13.75% amorphous silica) obtained a lower value of CO_2 production than that in other runs. This is attributed to the fact that the large surface area of the sand pack/Kaolin or amorphous silica mixture produces LTO reactions ahead of the combustion front. This behaviour is responsible for the appearance of lower CO_2 mol fraction in the produced gases with increasing surface area of the pack.

7.1.2 Effect of oxygen enrichment

For the dry run (Run 14), a sand mixture containing 5% Kaolin and involving oxygen enrichment of 35% oxygen, the O_2 and CO production shows a fairly stable level of 1.3 and 4.7% (Figure 7.13). The CO_2 concentration value is very high compared with normal air injection run (Run 3) and shows an increasing trend. This is expected since the high oxygen flux promotes the oxidation reaction.

In Run 15, (Figure 7.14), Cold Lake crude oil with 35% oxygen enrichment were used. The CO and CO_2 concentration trends are similiar and both increased with oxygen enrichment by approximately 42% compared with Run 11 (Table 7.1). The slight decrease in CO and CO_2 mol fractions after 3 hours is due to cooling effect of the injected water.

During Run 16, where 25% Lower Fars core material and 35% oxygen enrichment were used, the CO_2 production first increases to a level of 29% and then falls sharply to 21% after water injection (Figure 7.15). The CO_2 level then increases quickly again, finally averaging 31.7%. Compared with Run 13, which used the same operating conditions but with air injection, the CO and CO_2 concentrations are higher and O_2 concentration is lower.

Clearly, oxygen enrichment has an appreciable effect on the composition of the produced gases in the *in situ* combustion process. The mol fractions of CO and CO_2 increased and the O_2 production decreased. The effects are due to more efficient combustion of fuel and hence greater conversion to CO and CO_2. Adewusi (1986) used the same crude (Maya) with oxygen enrichment of 30 and 35% oxygen. The CO and CO_2 mol fractions increased from 3.4 and 13% to 5.2 and 18%, respectively with 35% oxygen. These are much lower than the values obtained in the present work due to more heat losses in his experiments.

Other gases such as methane and hydrogen were produced with small amounts in all oxygen enrichment runs (Table 7.1).

7.1.3 Effect of natural core and metal compound additives

During Run 12 (Figure 7.16) which used 100% Lower Fars core material, the concentration of CO_2 began to increase to a level of 19% and decrease after 3 hours. At the same time, the composition of the O_2 and CO stabilised at 1.6 and 3.9% respectively. The level of CO_2 concentration is higher than those in all the runs, which used a synthetic sand mixture (Table 7.1). This effect is attributed to the clays and silts contained in the natural core material, which have a high specific surface area.

In Run 13, 25% Lower Fars core was mixed with 75% silica sand. The mol fraction of CO_2 is relatively low (10.5%) half hour after ignition (Figure 7.17). Later on, the CO_2 production starts to increase and reaches a level of 15%, then declines to 13%. The produced gases contain 4.0%O_2, 2.6%CO, and 16.2%CO_2. Compared with previous run (100% L. Fars reservoir rock), the produced CO and CO_2 are lower and O_2 production is higher, owing to the smaller percentage of natural core material used (25% L. Fars).

For 1% ferric oxide (Run 17, Figure 7.18) the level of CO_2 production is very low half hour after ignition and starts to increase rapidly. It averages at 19.6% which is higher than that obtained in Run 1 (no additives). This is due to the larger fuel consumption achieved with the presence of ferric oxide.

In Run 18, 1% nickel chloride is used. The CO_2 mol fraction increases gradually to a level of 18% and averages afterward at 17.2% (Figure 7.19). On the other hand, O_2 mol fraction decreases and CO increases gradaully and both average at 1.1 and 3.5% respectively. The CO_2 production obtained is also higher than that in Run 1.

Run 19 (Figure 7.20) used 2% Kaolin and 1% ferric oxide in the sand matrix. The CO_2 concentration increases to a high level of 19% and then falls sharply to a level of 11.5%. The average CO_2 production is 17% which is lower than that in Run 2 (2% Kaolin). This is possibly due to the combined effect that ferric oxide and Kaolin have on promoting LTO reaction ahead of the combustion front. The O_2 and CO mol fractions show a reverse trend to each other over the combustion period. Two hours after water injection their concentrations are stabilised and averaged 1.1 and 3.6% respectively.

7.2 Carbon Oxides Ratio

The average molar ratios of carbon oxides produced by oxidation reaction of crude oil for Run 1 to 20 are given in Table 7.2. These values are the average over the more stabilised part of the gas composition profile as shown in Figure 7.21 for Run 7. Appendix B provides the instantaneous CO/CO_2 ratio for Runs 1 to 20.

As shown in Table 7.2 and Figure 7.22, the CO/CO_2 ratio exhibits a very gradual reduction as the clay and amorphous silica content increases. This is due to increased fuel consumption. However, Run 2(2% Kaolin) demonstrates a lower value of CO/CO_2 ratio than Run 3 and 4 (5 and 10% Kaolin), and Run 9 (13.75% amorphous silica) gives higher value than in Run 8 (10% amorphous silica). This is due to LTO reaction as discussed in the previous section.

The relationship between CO/CO_2 ratio and clay content observed in the present work is consistent with Guvenir's (1980) results, which found that the CO/CO_2 molar ratio increased as the combustion front

Table 7.2

Carbon Oxides Ratio

Run No.	Crude Oil	Method of Combustion	Additives Content	Injected Gas % O_2	CO/CO_2 ratio	$\frac{CO+CO_2}{N_2}$ ratio
1	Maya	Wet	0%	21	0.27	0.25
2	"	"	2% Kaolin	21	0.19	0.29
3	"	"	5% Kaolin	21	0.26	0.25
4	"	"	10% Kaolin	21	0.22	0.23
5	"	"	15% Kaolin	21	0.19	0.26
6	"	"	2% amorphous silica	21	0.36	0.28
7	"	"	5% amorphous silica	21	0.24	0.27
8	"	"	10% amorphous silica	21	0.13	0.25
9	"	"	13.75% amorphous silica	21	0.17	0.22
10	Maya Isthmus	Dry	3% Kaolin	21	0.17	0.24
11	Cold Lake	Wet	0%	21	0.25	0.28
12	L. Fars	"	5% Clays from L. Fars	21	0.21	0.29
13	Maya	"	1% Clays from L. Fars	21	0.16	0.24
14	"	Dry	5% Kaolin	35	0.11	0.61
15	Cold Lake	Wet	0%	35	0.25	0.60
16	Maya	"	1% Clays from L. Fars	35	0.22	0.60
17	"	"	1% Ferric Oxide	21	0.18	0.30
18	"	"	1% Nickel Chloride	21	0.20	0.26
19	"	"	1% Ferric Oxide+2% Kaolin	21	0.21	0.26
20	"	"	1% Acidised Clay	21	0.22	0.28

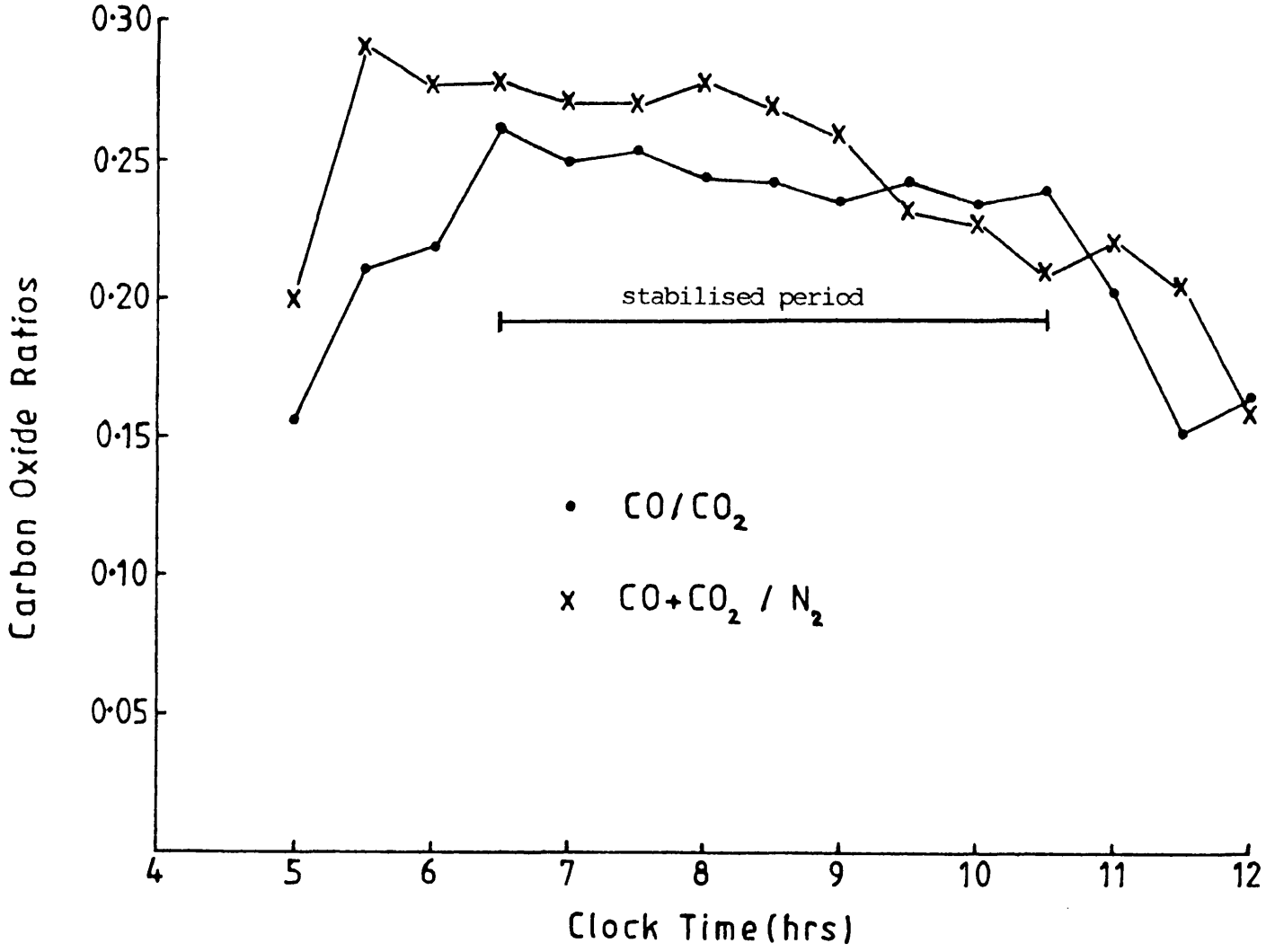

Figure 7.21 Carbon oxides ratio *versus* time (Run 7)

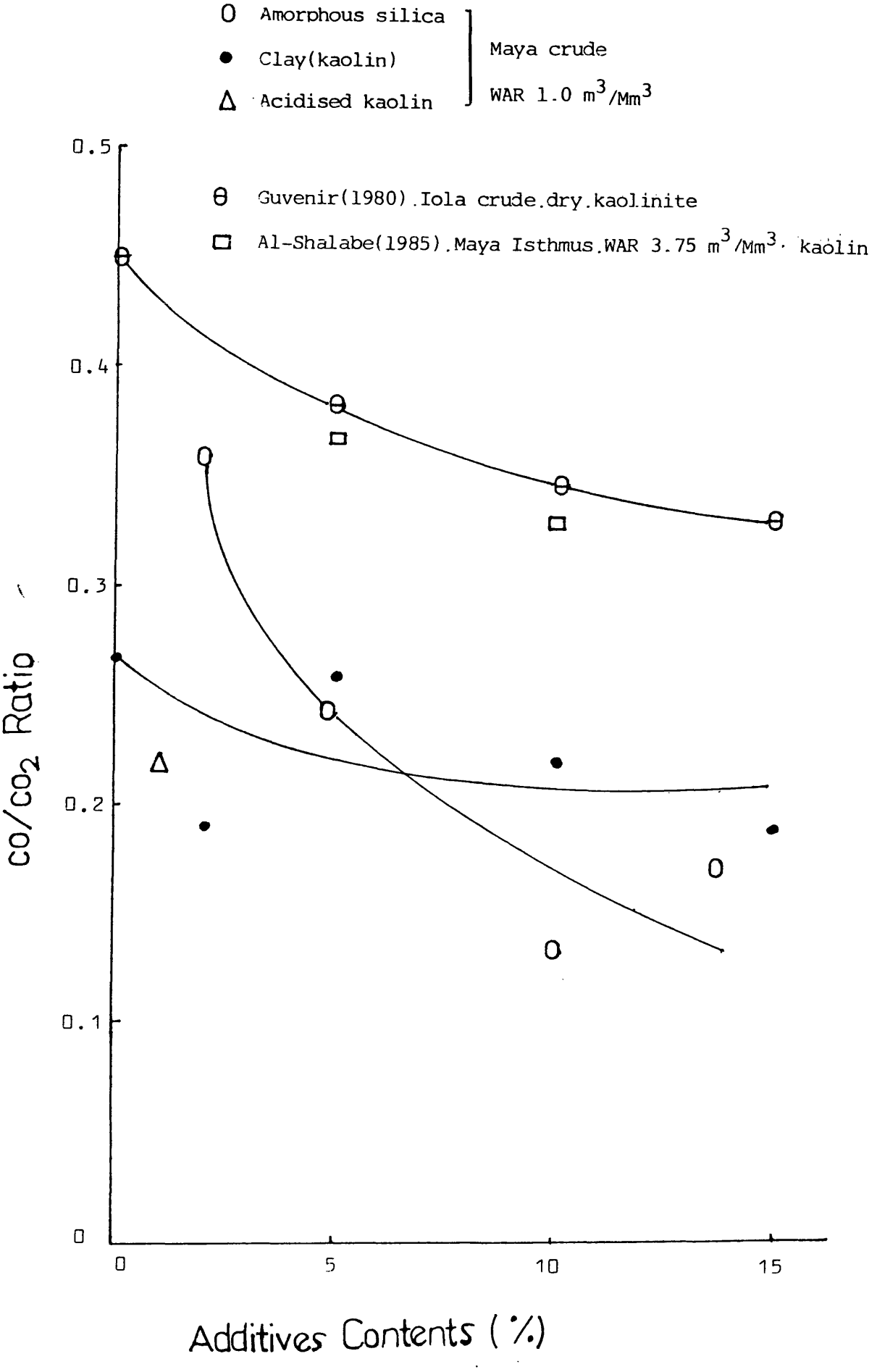

Figure 7.22 Effect of additives on CO/CO_2 ratio

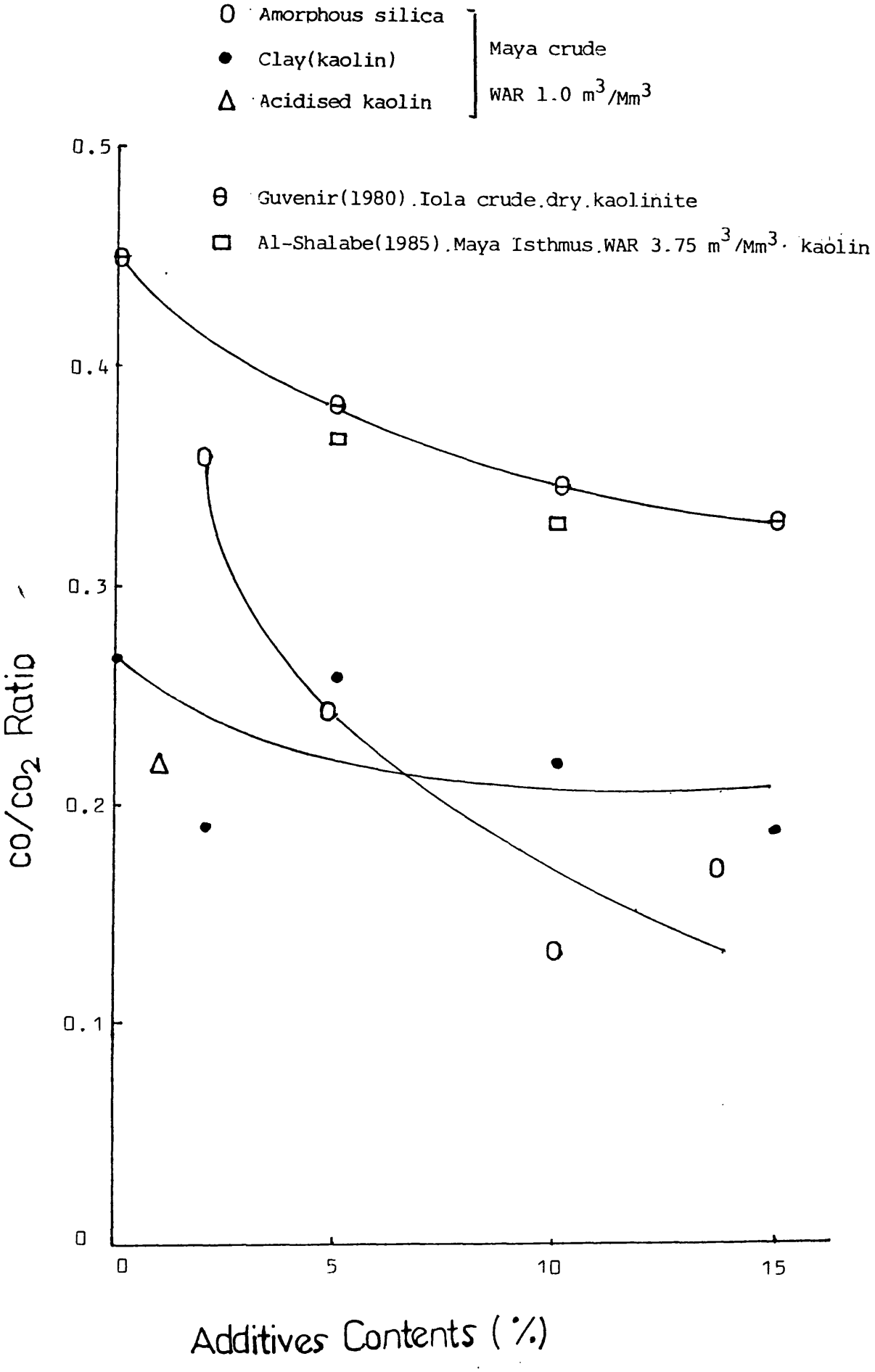

Figure 7.22 Effect of additives on CO/CO_2 ratio

Table 7.3

Carbon Oxides Ratio from *In Situ* Combustion Runs

Author	Crude Gravity °API	Additives Content	WGR m^3/Mm^3	Injected Gas $\%O_2$	CO/CO_2 Ratio	$\frac{CO+CO_2}{N}$ Ratio
Guvenir (1980)	19.3	0%	Dry	21	0.45	--
		5% Clay			0.38	--
		10% Clay			0.35	--
		15% Clay			0.33	--
		15% amorphous silica			0.36	--
Al-Shalable (1985)	32.4	5% Kaolin	Dry	21	0.2	0.23
		5% Kaolin	3.75		0.37	0.21
		10% Kaolin	3.75		0.33	0.21
		10% amorphous silica	Dry		0.194	0.25
Adewusi (1986)	22.1	8.4% Kaolin	Dry	21	0.26	0.2
				30	0.27	0.28
				35	0.29	0.3

moved from the 10% clay zone to the no clay zone (Table 7.3). Comparing with results obtained in the present work, Guvenir reported higher values due to different in operational conditions.

Al-Shalable (1985) also observed a reduction trend of CO/CO_2 ratio with Kaolin content (Table 7.3). She reported the lowest values of CO/CO_2 during a dry combustion run. This indicated preferential oxidation of carbon with conversion primarily to CO_2. Higher CO/CO_2 ratio was achieved during wet combustion with the same crude oil. The higher values of CO/CO_2 obtained in Al-Shalabe's study is consistent with the lower fuel consumption values in her work.

The CO/CO_2 ratio obtained with the Lower Fars Core material (Runs 12 and 13) and also the metal compound additives (Runs 17, 18 and 19) are lower than those obtained with the synthetic sand matrix (Run 3), and when no metal compound additives were present (Runs 1 and 2). While the $CO+CO_2/N_2$ ratio is higher for the same cases. This is attributed to the higher CO_2 production obtained with natural core and metal compound additives.

The CO/CO_2 ratio did not show any specific trend with oxygen enrichment as given in Table 7.2. But $\frac{CO+CO2}{N2}$ ratio increases significantly with 35% oxygen enrichment. This is due to the higher CO and CO_2 production. Adewusi (1986) also found an increase in $\frac{CO+CO2}{N2}$ ratio with 30 and 35% oxygen enrichment (Table 7.3).

7.4 H/C Ratio

The apparent H/C ratio of the fuel consumed is calculated from the analysis of produced gases for each combustion run as a function

of temperature. The relationship between the H/C ratio and the produced gas composition (Nelson and McNeil, 1961) is:

$$H/C = \frac{4\,[(YO2/YN2)\%\ N2 - \%O2 - \%CO2 - \%CO/2]}{[\%CO2 + \%CO]} \qquad (1)$$

Where YO_2 and YN_2 are the mol fraction of oxygen and nitrogen in the injected gas and $\%N_2$, $\%O_2$, %CO, and $\%CO_2$ are the mol fractions of the produced gases. This equation is based on the assumption that all the oxygen not observed in the exit gas had reacted to form water. This is not quite true because some oxygen is consumed in low temperature oxidation (LTO) reactions. Thus, the obtained H/C ratio is considered an apparent value.

Table 7.4 shows the average of the most stable values of H/C ratio of Runs 1 to 20. In some experiments negative values of H/C ratio occur and these are not reflected in the average values of H/C ratio. The computed H/C ratio is extremely sensitive to small errors in measurement. For example, in Run 1, the mol fractions of the produced gases are:

1.3% O_2, 4.2% CO, and 15.5% CO_2

The computed H/C ratio, according to eq.(1), is:

$$H/C = 0.45$$

If the concentration of CO_2 if increased by 5%, then CO_2 mol fraction becomes 16.32%.

Table 7.4

The H/C Ratio Results from *In Situ* Combustion

Run No	Crude Oil	WGR m^3/Mm^3	O_2% injected	Additives Content	H/C Ratio	Peak Temp.°
1	Maya	1.0	21	0%	0.45	480
2	Maya	1.0	21	2% Kaolin	1.38	485
3	Maya	1.0	21	5% Kaolin	0.56	500
4	Maya	1.0	21	10% Kaolin	0.48	495
5	Maya	1.0	21	15% Kaolin	0.22	509
6	Maya	1.0	21	2% amorphous silica	0.22	499
7	Maya	1.0	21	5% amorphous silica	0.29	488
8	Maya	1.0	21	10% amorphous silica	0.58	484
9	Maya	1.0	21	13.75% amorphous silica	0.45	431
10	Maya Isthamus	0.0	21	3% Kaolin	1.73	486
11	Cold Lake	1.0	21	0%	0.27	476
12	L. Fars Core	1.0	21	5% Clays of L. Fars Core	0.74	453
13	Maya	1.0	21	1% Clay of L. Fars Core	0.91	418
14	Maya	0.0	35	5% Kaolin	0.61	461
15	Cold Lake	1.0	35	0%	0.23	483
16	Maya	1.0	35	1% Clays of L. Fars Core	0.89	505
17	Maya	1.0	21	1% Ferric Oxide	1.27	446
18	Maya	1.0	21	1% Nickel Chloride	0.22	424
19	Maya	1.0	21	1% Ferric Oxide +2% Kaolin	0.57	437
20	Maya	1.0	21	1% Kaolin treated by acid	1.44	425
Guvenir (1980)	Iola (19.3 °API)	0.0	21	5% Clay	1.48	384
				10% Clay	1.35	419
				15% Clay	1.28	446
				15% amorphous silica	0.99	479
Al-Shalabe (1985)	Maya Isthumus	0.0	21	5% Kaolin	0.88	451
		3.75		5% Kaolin	1.63	451
		3.75		10% Kaolin	1.32	468
		0.0		10% amorphous silica	0.51	463
Adewusi (1986)	Maya	0.0	21	8.4% Kaolin	0.56	399
		0.0	30		0.69	416
		0.0	35		0.8	424
		2.0	21		0.49	418
		1.8	30		0.94	400
		1.8	35		2.04	414

Therefore from eq.(1):

$$H/C = 0.21$$

This ratio is lower by 53% than the original.

Therefore, the H/C ratio calculations are sensitive to any change in the level of CO_2 production. Fassihi and Brigham (1980) reported that when a lower H/C ratio is obtained, this indicates that more CO_2 are produced. Computer Modelling Group (1982) reported a very high CO_2 production of 30% for normal air *in situ* combustion with natural core material as shown in Table 7.5. They attributed this to the decomposition of carbonate materials which resulted in a negative H/C ratio.

The present results and other investigations results show that the H/C ratio decreases as the combustion peak temperature increases (Table 7.4). This is due to the increased fuel consumption and greater conversion of CO to CO_2. Fassihi *et al* (1984) also found that the H/C ratio decreased with an increase in combustion temperature.

As shown in Table 7.4, the H/C ratio decreases generally with increased Kaolin content. This is due to the increased amount of fuel consumption as the Kaolin content increased. Therefore, higher combustion peak temperature was achieved and lower H/C ratio obtained. This is supported by the lower H/C ratio achieved with amorphous silica which produced larger fuel consumption values than the Kaolin as discussed in Chapter 4. However, with higher amorphous silica content of 10 and 13.75% amorphous silica (Runs 8 and 9) the H/C ratio are higher than 2 and 5% amorphous silica (Run 6 and 7). This might be due to thermal cracking taking place with 2 and 5% amorphous

Table 7.5

Typical Product Gas Composition*

Core Decomposition Condition

CO_2	30.00
CO	1.50
O_2	0.00
N_2	68.00
H_2	0.00
C_1^+	0.39
H_2S	0.10
SO_2	0.01
COS	0.00
	100.00
$\left[\frac{CO_2 + CO}{CO}\right]$	21.00
[H/C]	-1.58
Air/Fuel[m^3(ST)/kg]	6.22

* Computer Modelling Group (1982)

silica, as the front approaches the coke zone. Although the trend of H/C ratio with clay content observed in the present work is in agreement with other investigations, the values obtained are generally lower (Table 7.4).

Guvenir (1980) showed that the H/C ratio decreases with increased clay content during dry combustion tests and pointed out the catalytic effect of clay on the H/C ratio. The lowest value of H/C ratio observed in his work was 0.9 with 15% amorphous silica. This is higher than most of the values obtained in the present work due to lower fuel consumption values obtained in his study (see Table 4.3).

Al-Shalabe (1985) observed that the H/C ratio for 10% Kaolin is lower than that for 5% Kaolin and the lowest value obtained for 10% amorphous silica case (H/C ratio = 0.51). This indicated preferential oxidation of carbon with a higher conversion to form CO_2 rather than CO. Compared with the results obtained here, Al-Shalabe's results are higher due to the lower fuel consumption.

As shown in Table 7.4, the H/C ratio shows a decreasing trend with oxygen enrichment. For example, H/C ratios for Run 11 and 13 (21% O_2) are 0.27 and 0.99 respectively, while for Runs 15 and 16 (35% O_2) they are 0.23 and 0.89. This is attributed to the higher combustion temperature achieved with oxygen enrichment. However, the H/C ratio for Run 14 (35% O_2) is lower than that for Run 3 (21% O_2). This is also due to the higher combustion temperature achieved in the dry combustion test (Run 14). Adewusi (1986) conducted experiments with oxygen enrichment of 30 and 35% oxygen and showed relatively low values of H/C ratio. But his results are still higher than those obtained in the present study due to lower combustion peak temperature achieved.

7.4 Oil Production

Figures 7.23-7.42 show the cumulative liquid production history and the specific gravity, the viscosity, and the rate of the oil produced over the combustion period for Runs 1 to 20. The dashed line in these figures represents the original crude oil density. The physical properties of the original crude and the produced oil for all runs are reported in Table 7.6. The overall liquid (oil and water) material balance is given in Appendix D.

The physical properties of the original crudes were taken from reference sources (Table 3.2). The specific gravity of the produced oil was measured by weighing the portions of oil collected during the experiments. These values were checked against the known specific gravities of the original crudes and the accuracy was found to be better than 4%. The viscosities of the produced oil were estimated from Figure 7.43 which represents the relationship between °API and viscosity at different temperatures.

Although toluene was used for separating emulsified water from the produced oil (generally about 40% of oil sample is toluene), the oil-water emulsions were not completely broken in some cases. This causes the produced oil to have a higher density than that of the original crude oil. Production of clay and material additives (due to very small particle size) also affected the density of the produced oil. Any value above the original crude density line is considered suspect and is discounted. These effects thus give rise to certain anomalous variations in the

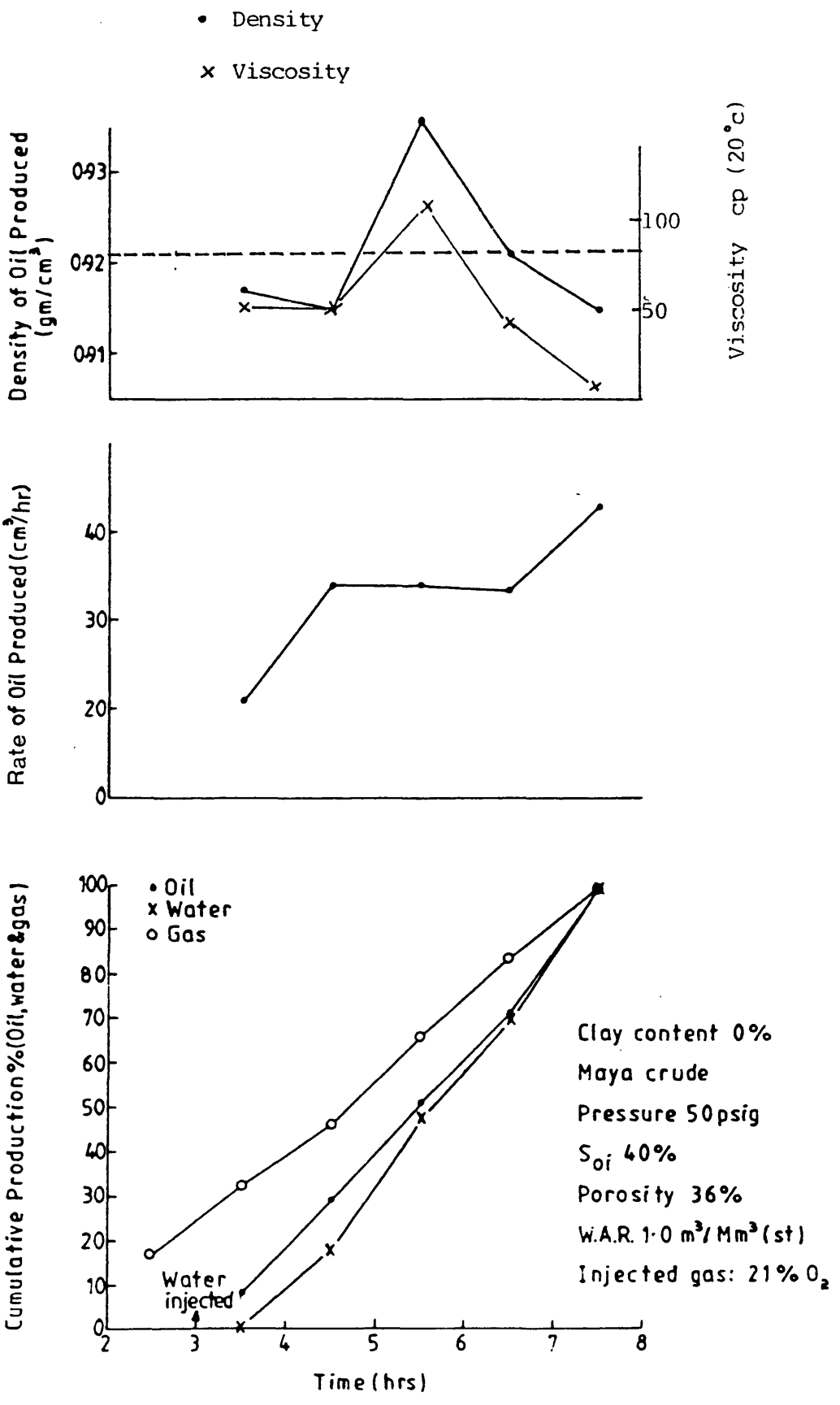

Figure 7.23 Production history (Run 1)

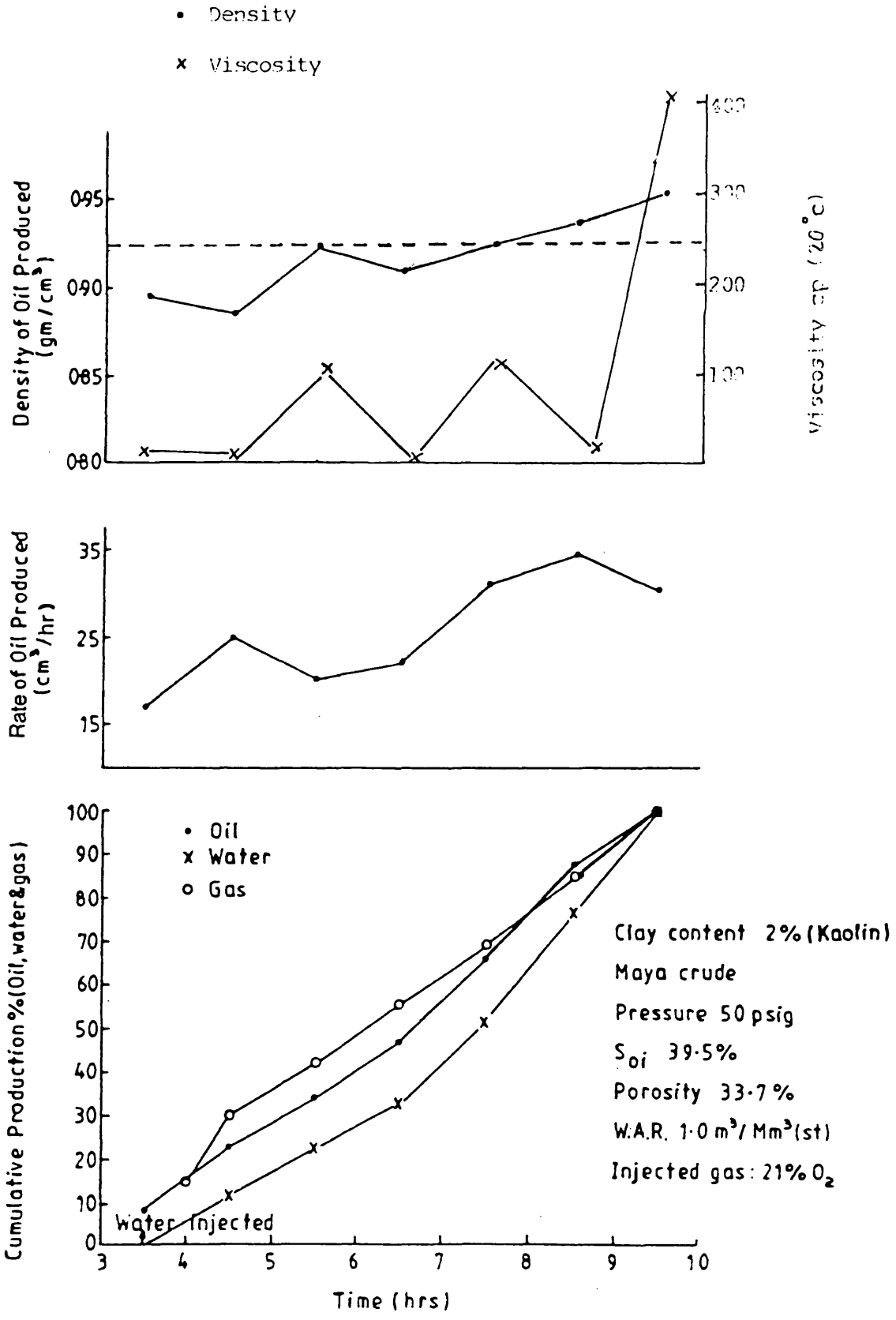

Figure 7.24 Production history (Run 2)

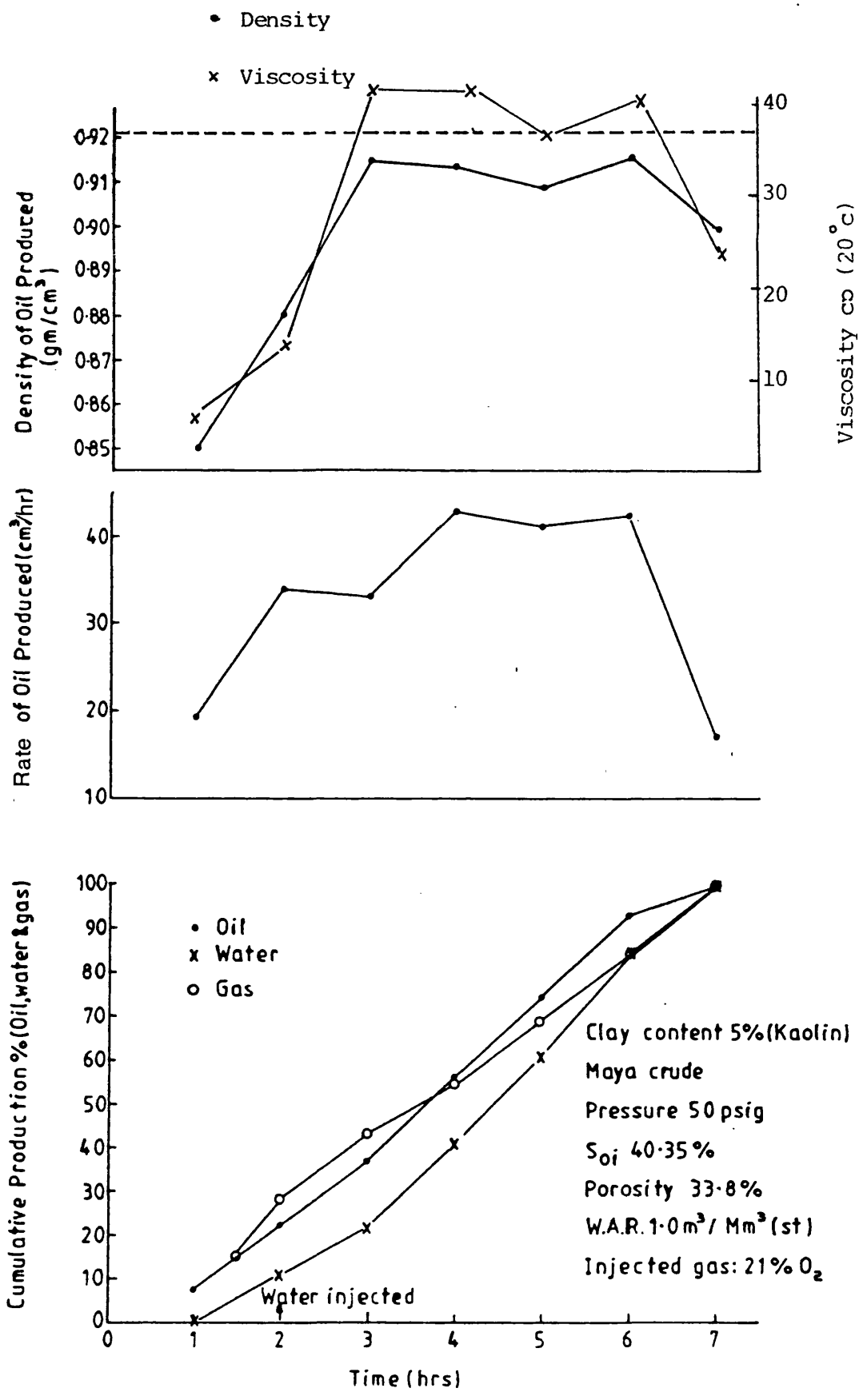

Figure 7.25 Production history (Run 3)

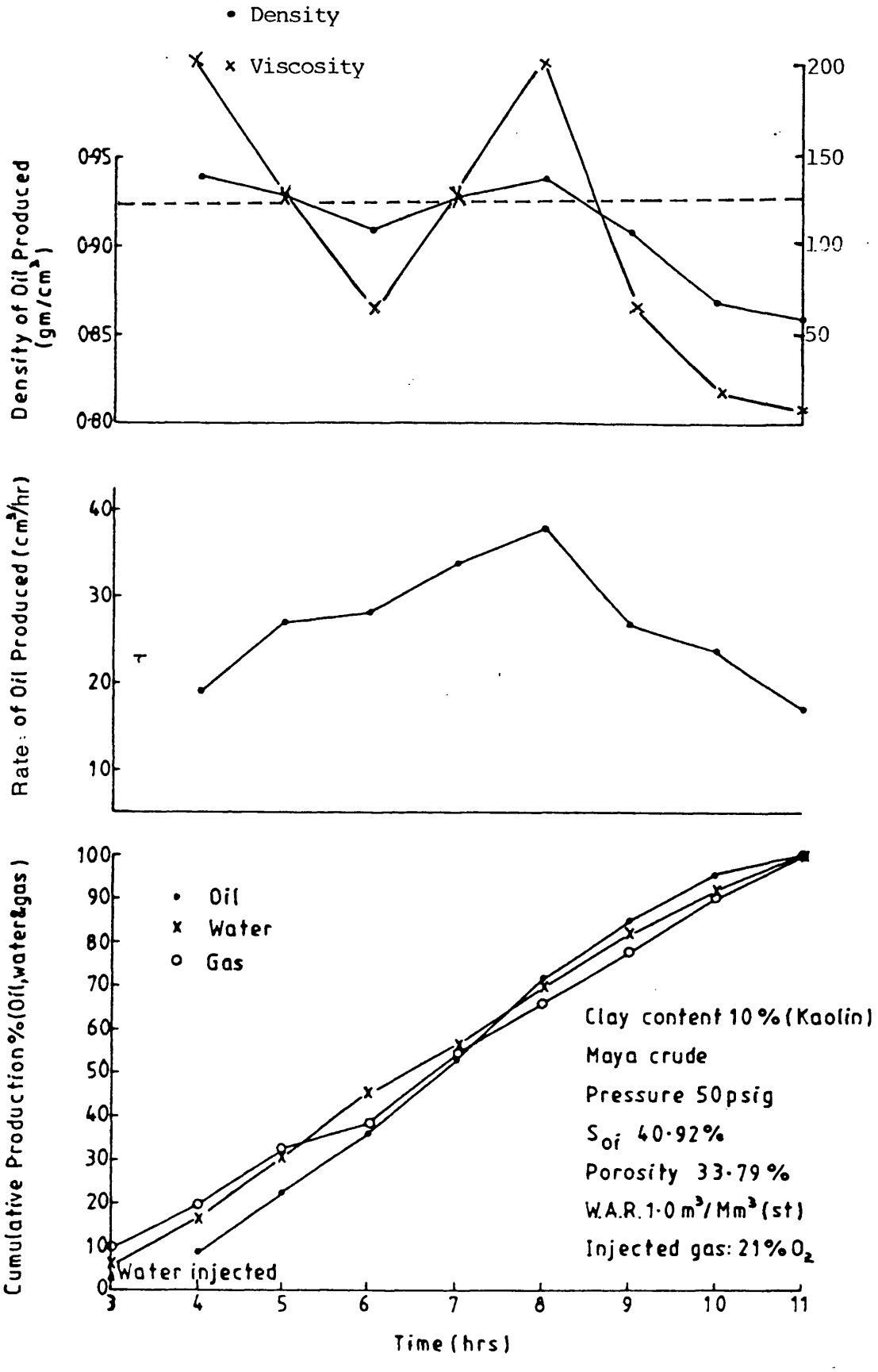

Figure 7.26 Production history (Run 4)

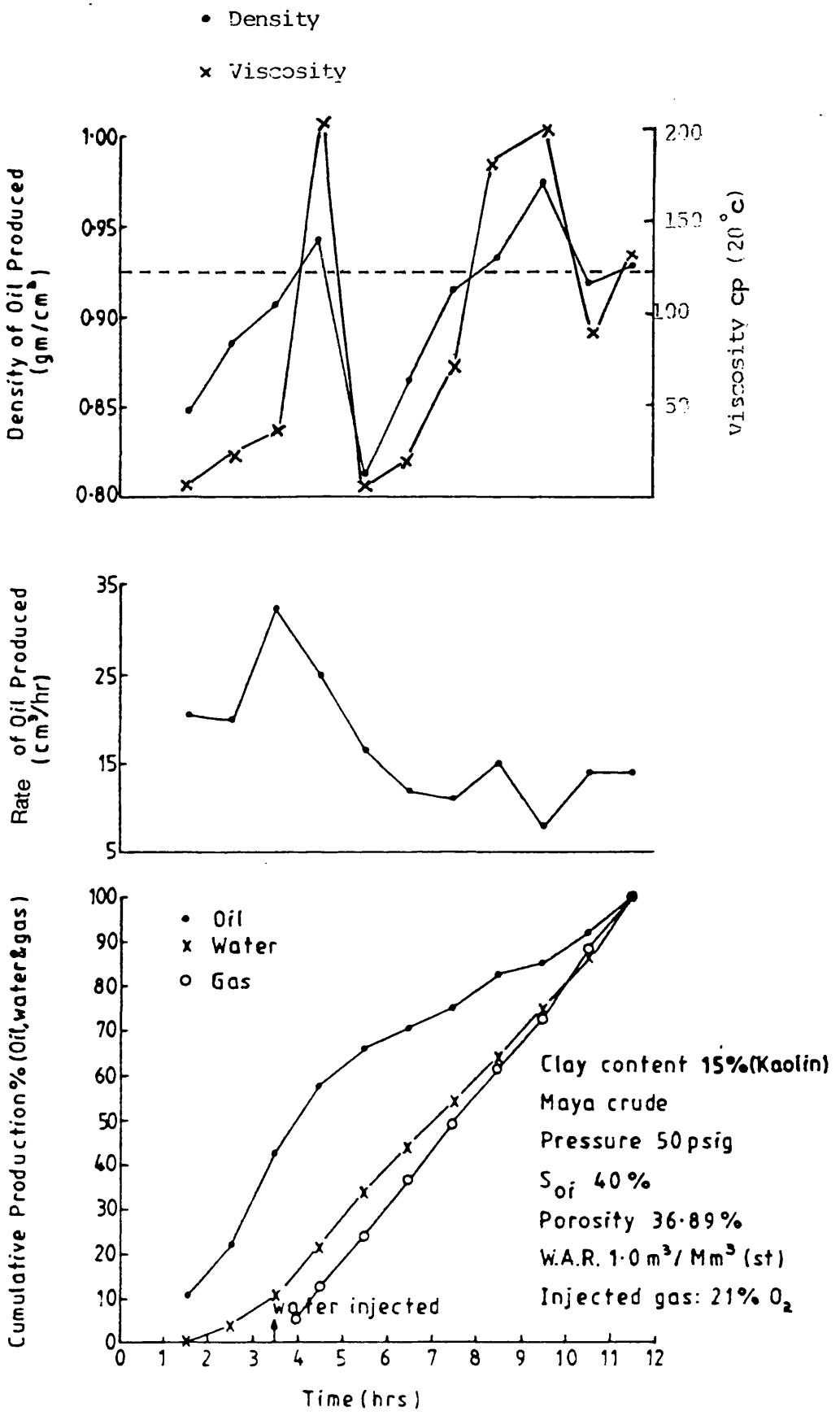

Figure 7.27 Production history (Run 5)

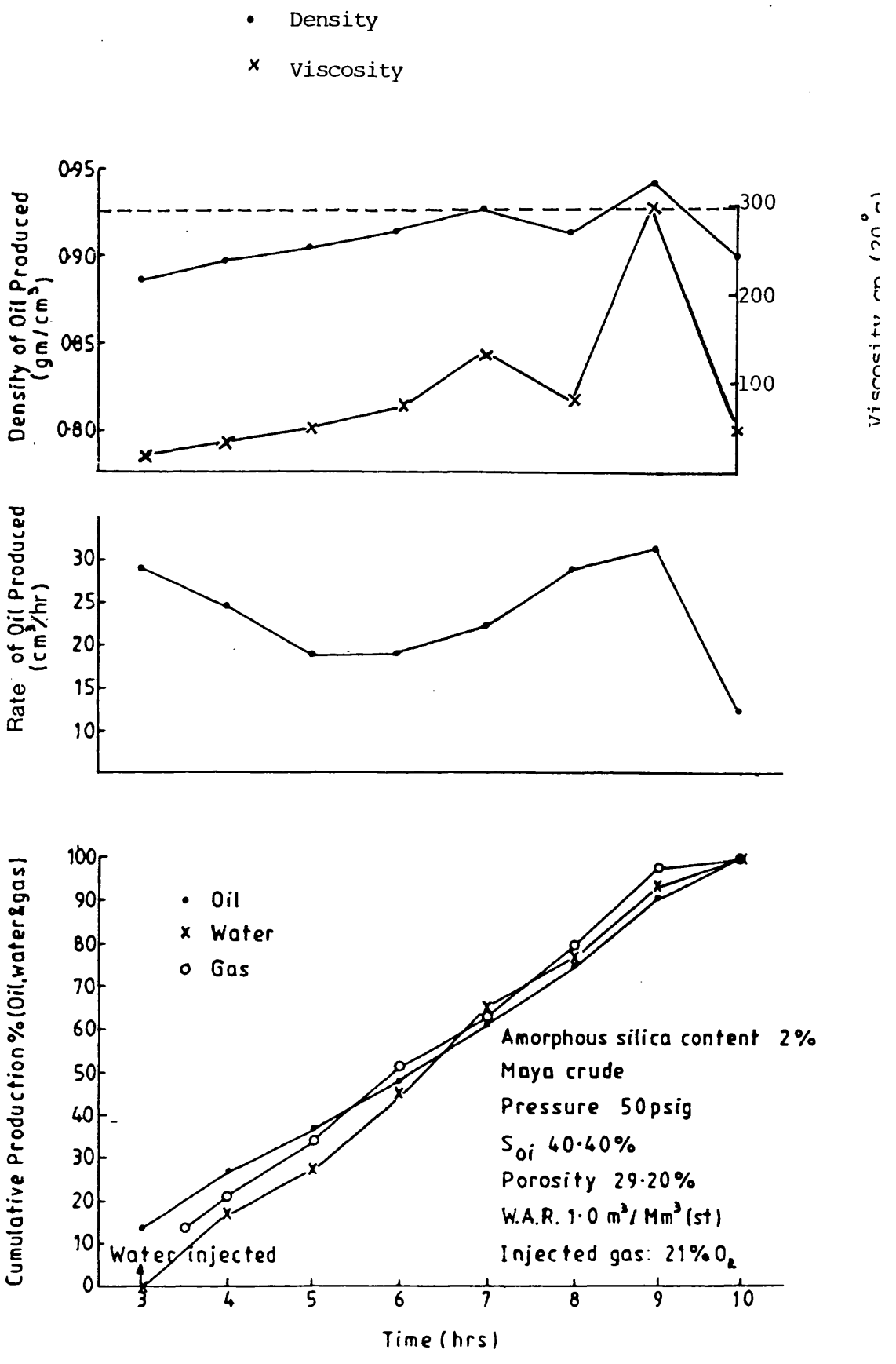

Figure 7.28 Production history (Run 6)

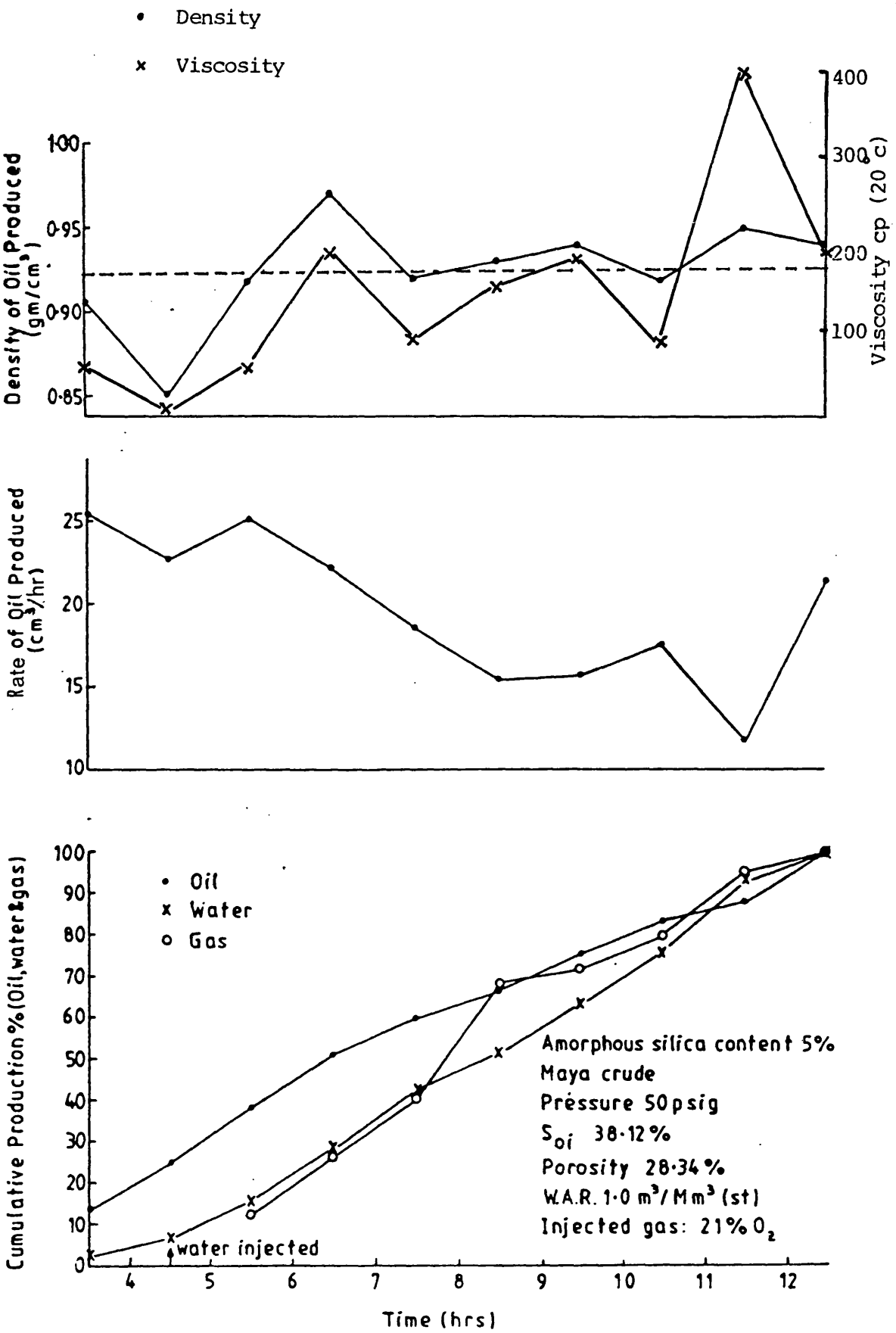

Figure 7.29 Production history (Run 7)

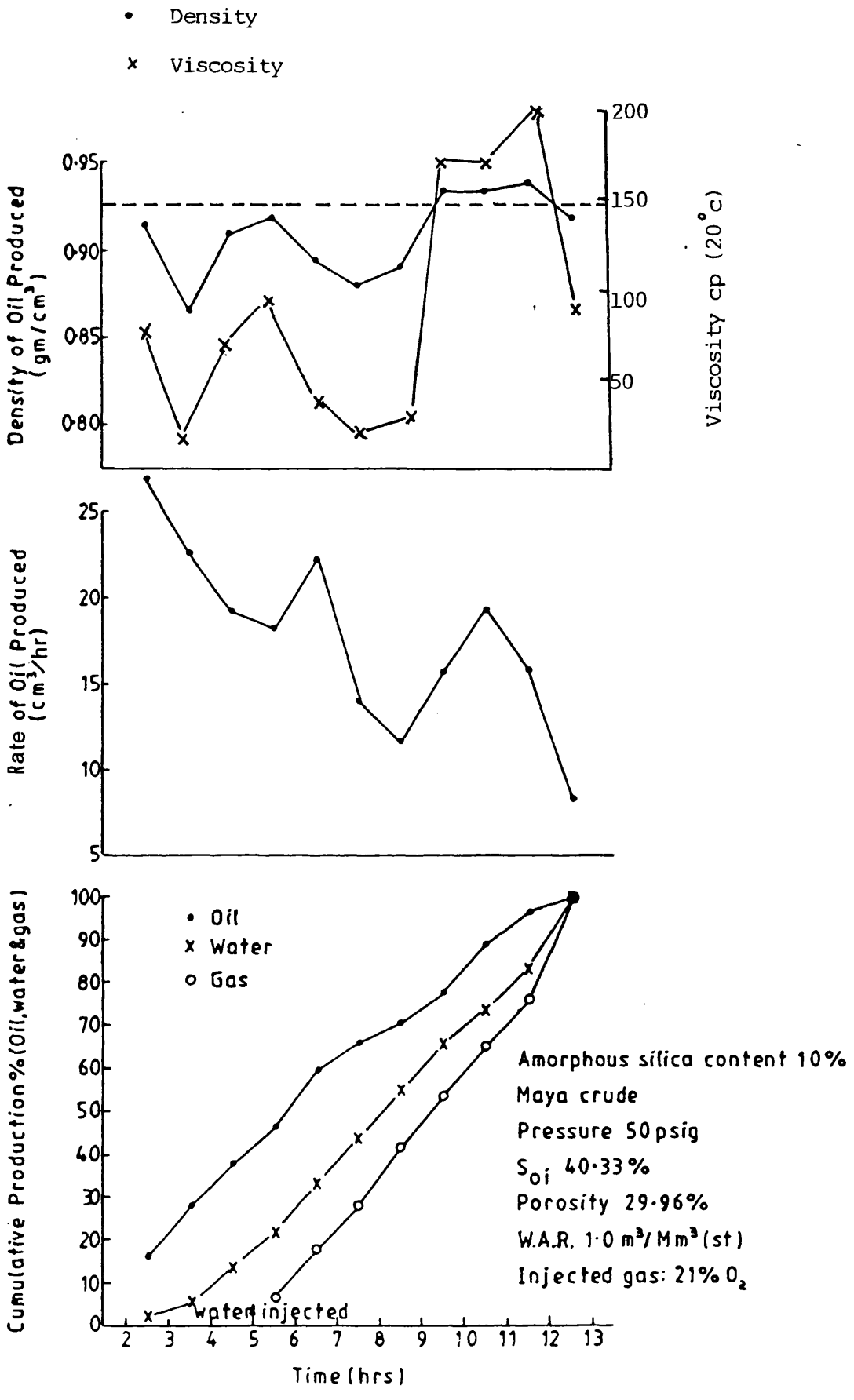

Figure 7.30 Production history (Run 8)

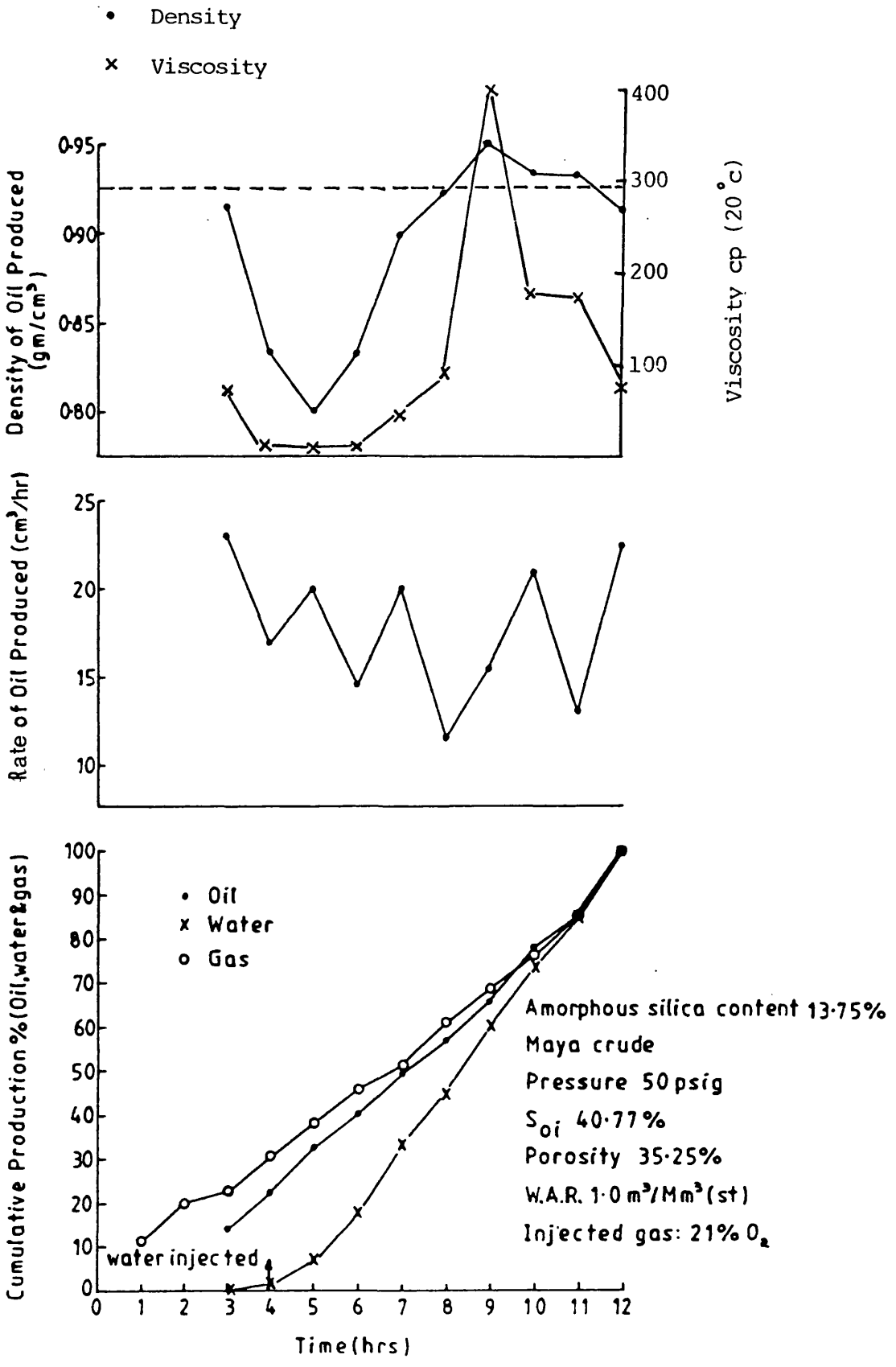

Figure 7.31 Production history (Run 9)

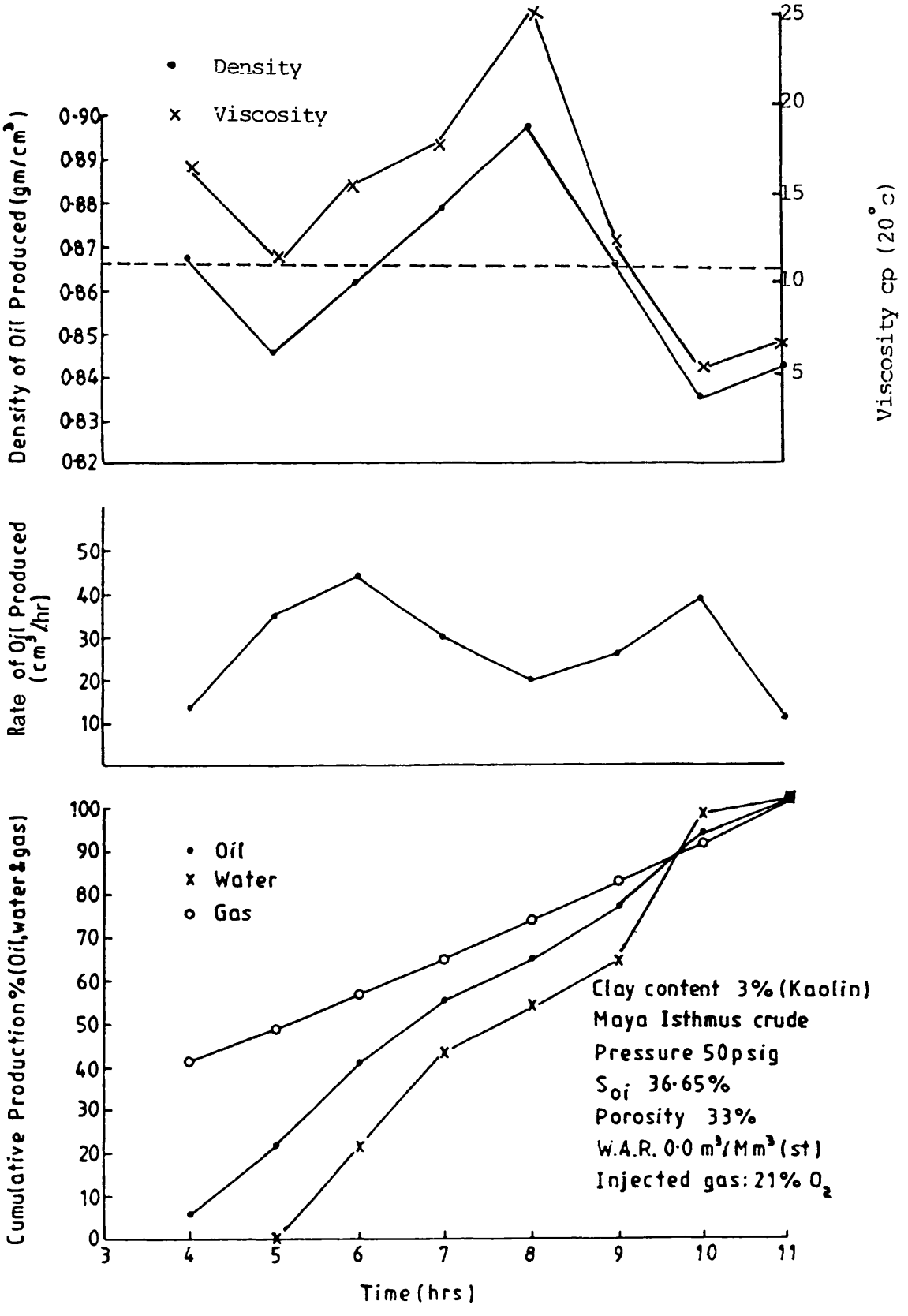

Figure 7.32 Production history (Run 10)

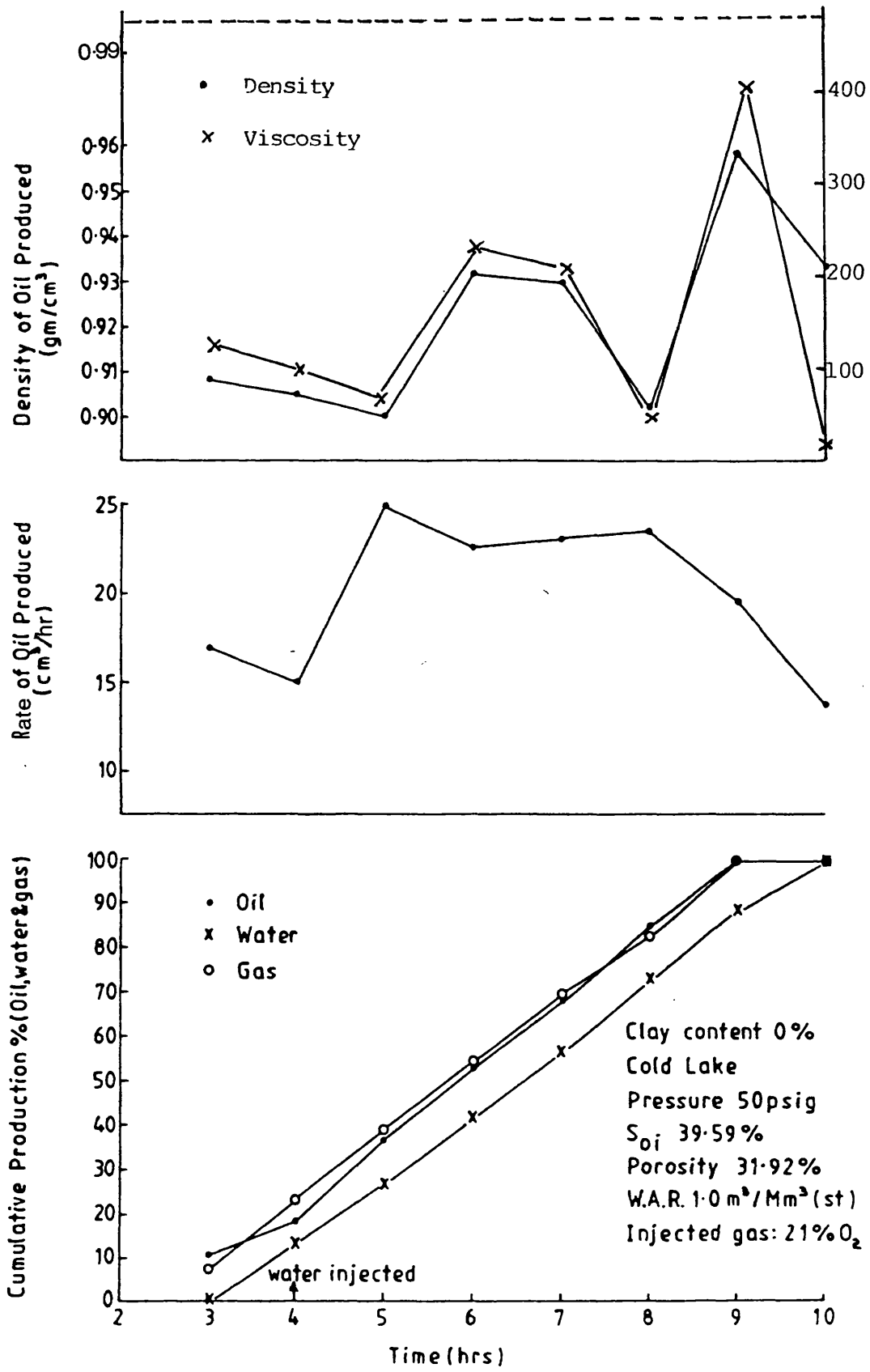

Figure 7.33 Production history (Run 11)

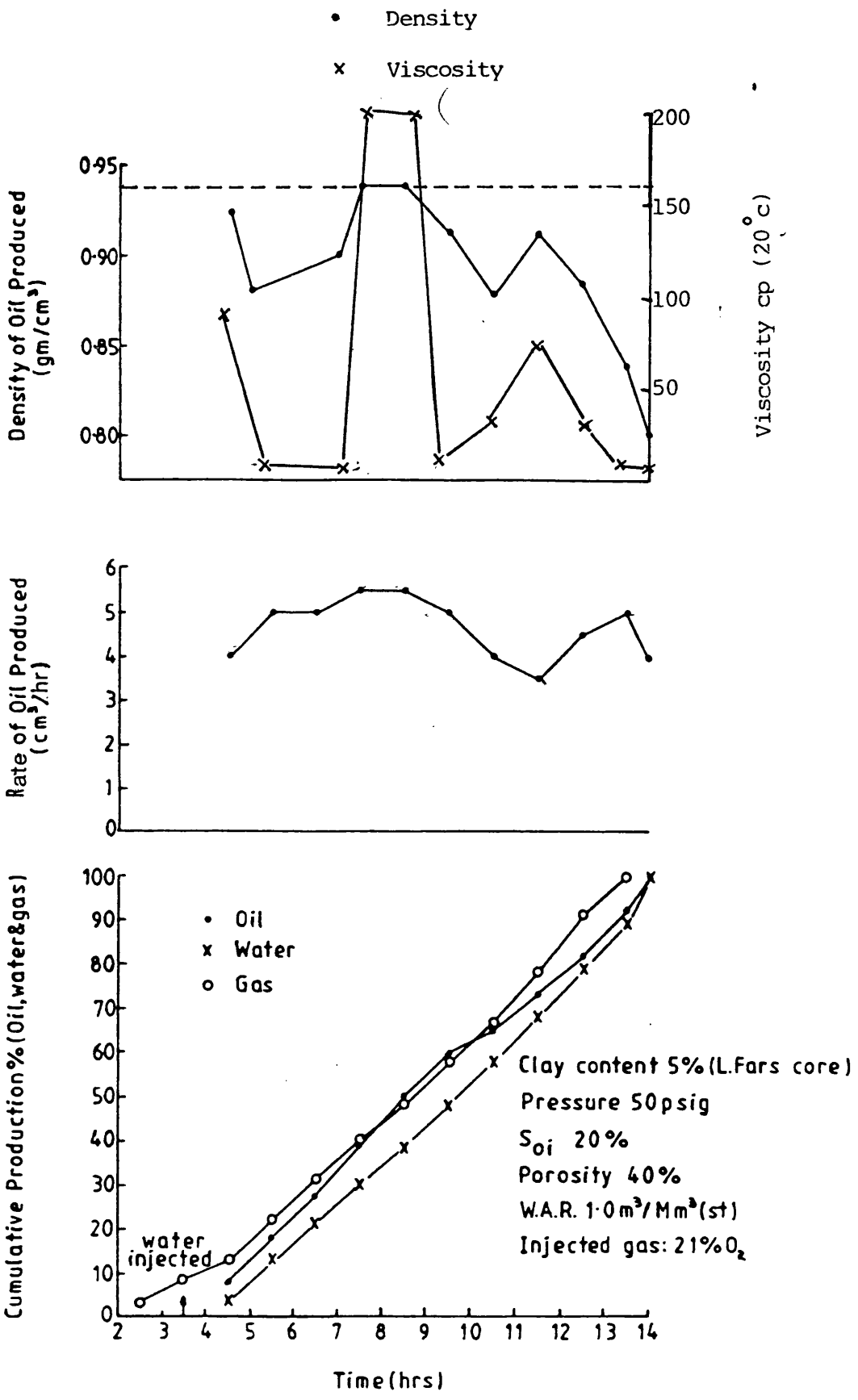

Figure 7.34 Production history (Run 12)

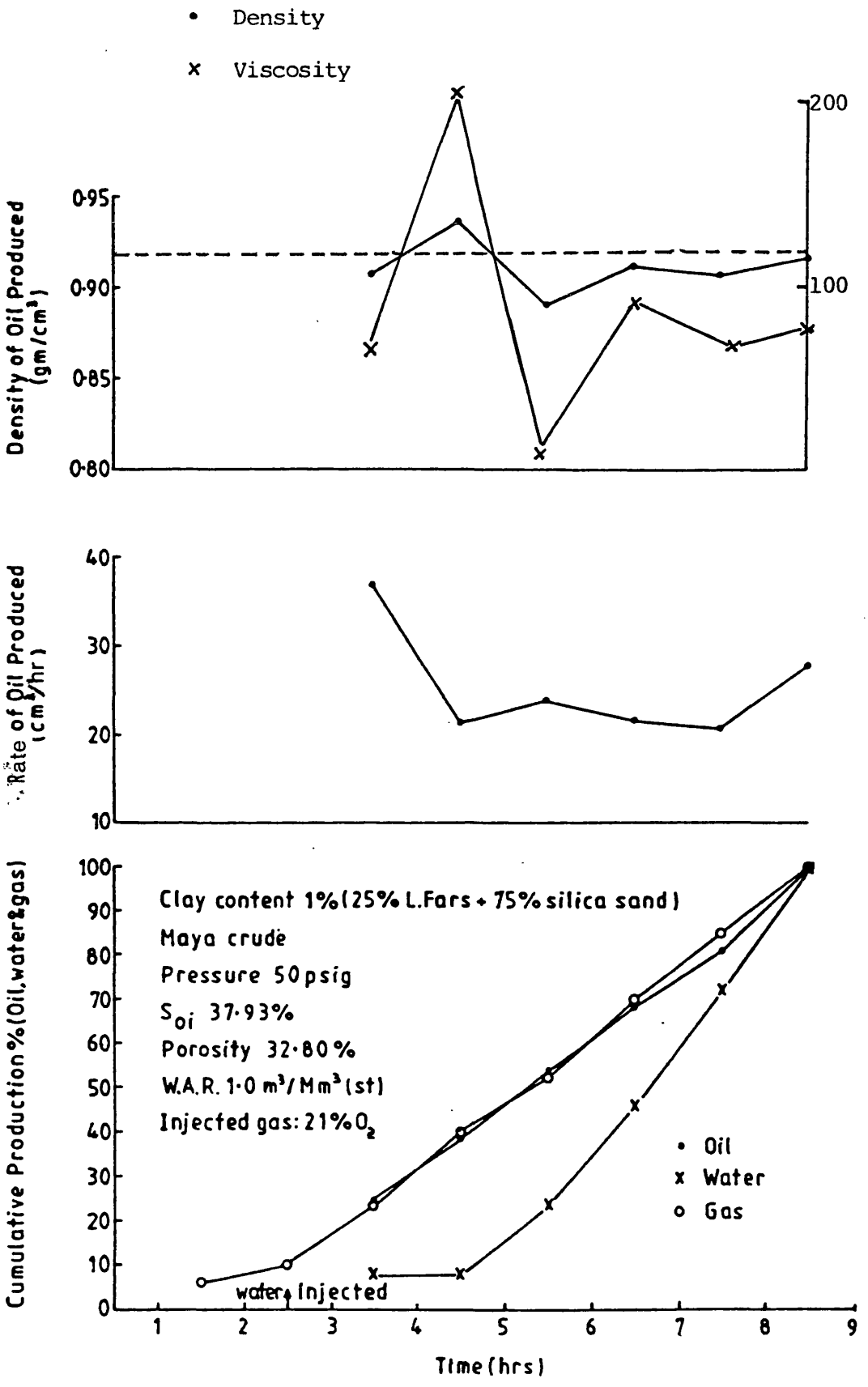

Figure 7.35 Production history (Run 13)

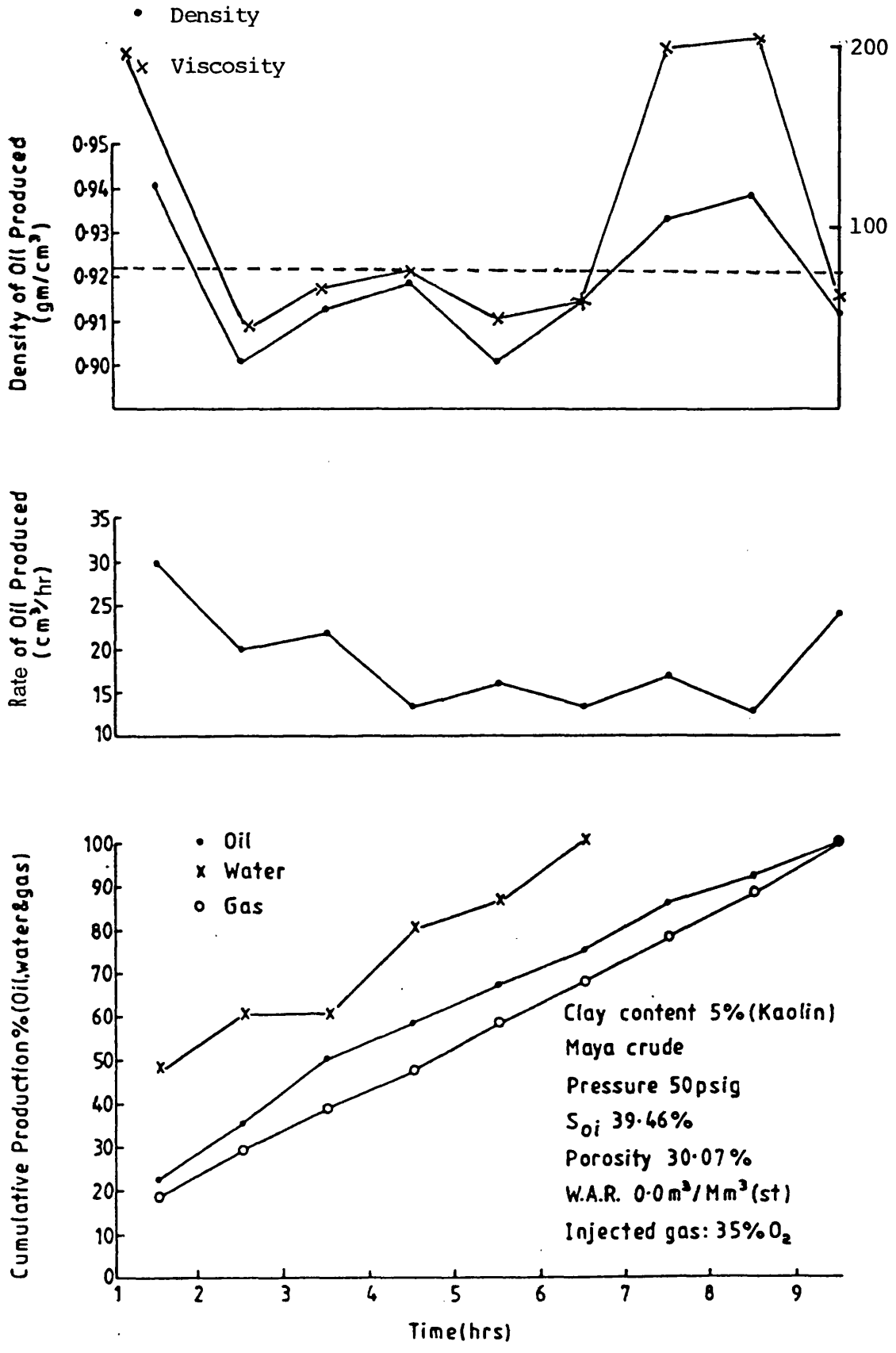

Figure 7.36 Production history (Run 14)

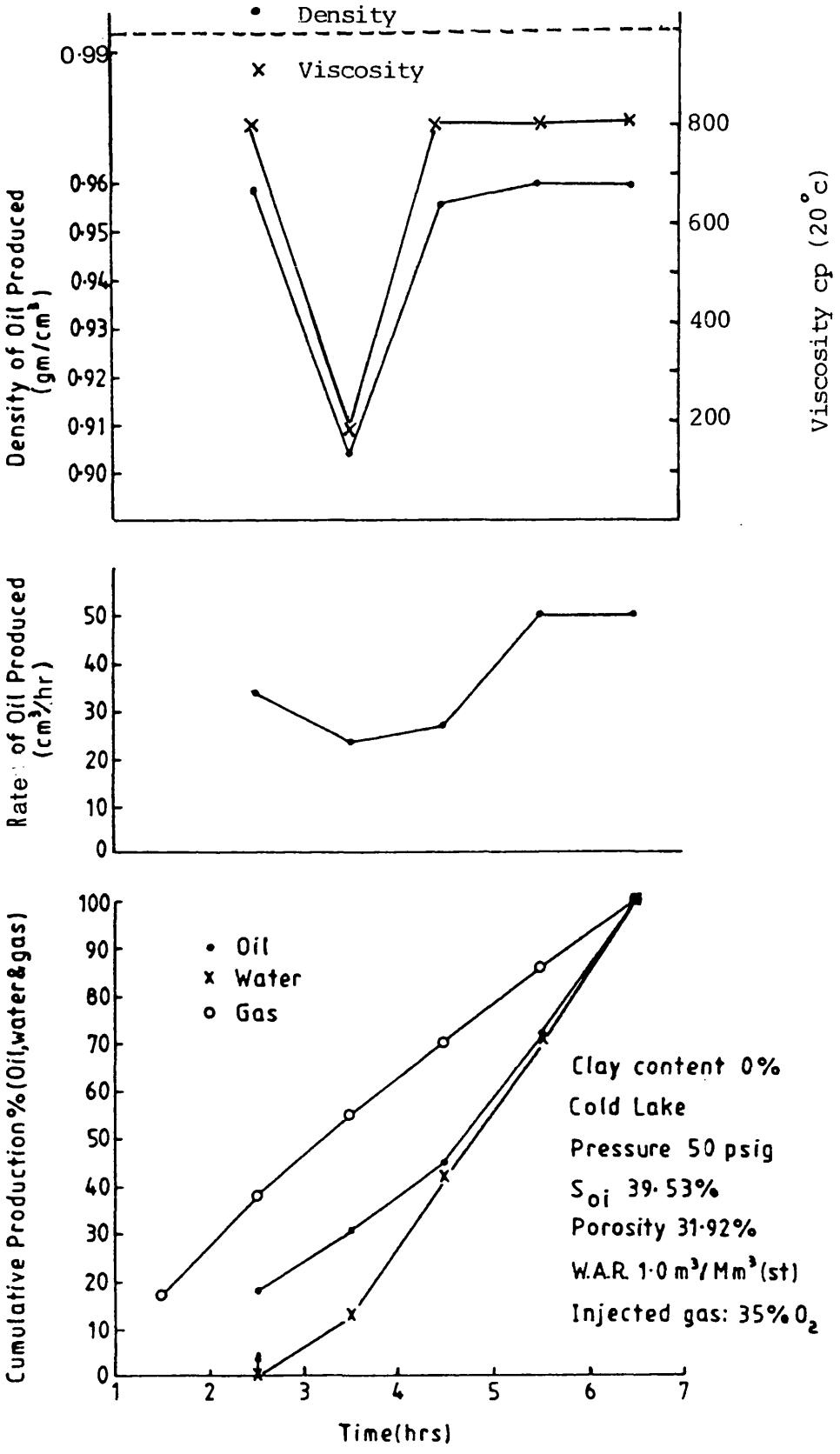

Figure 7.37 Production history (Run 15)

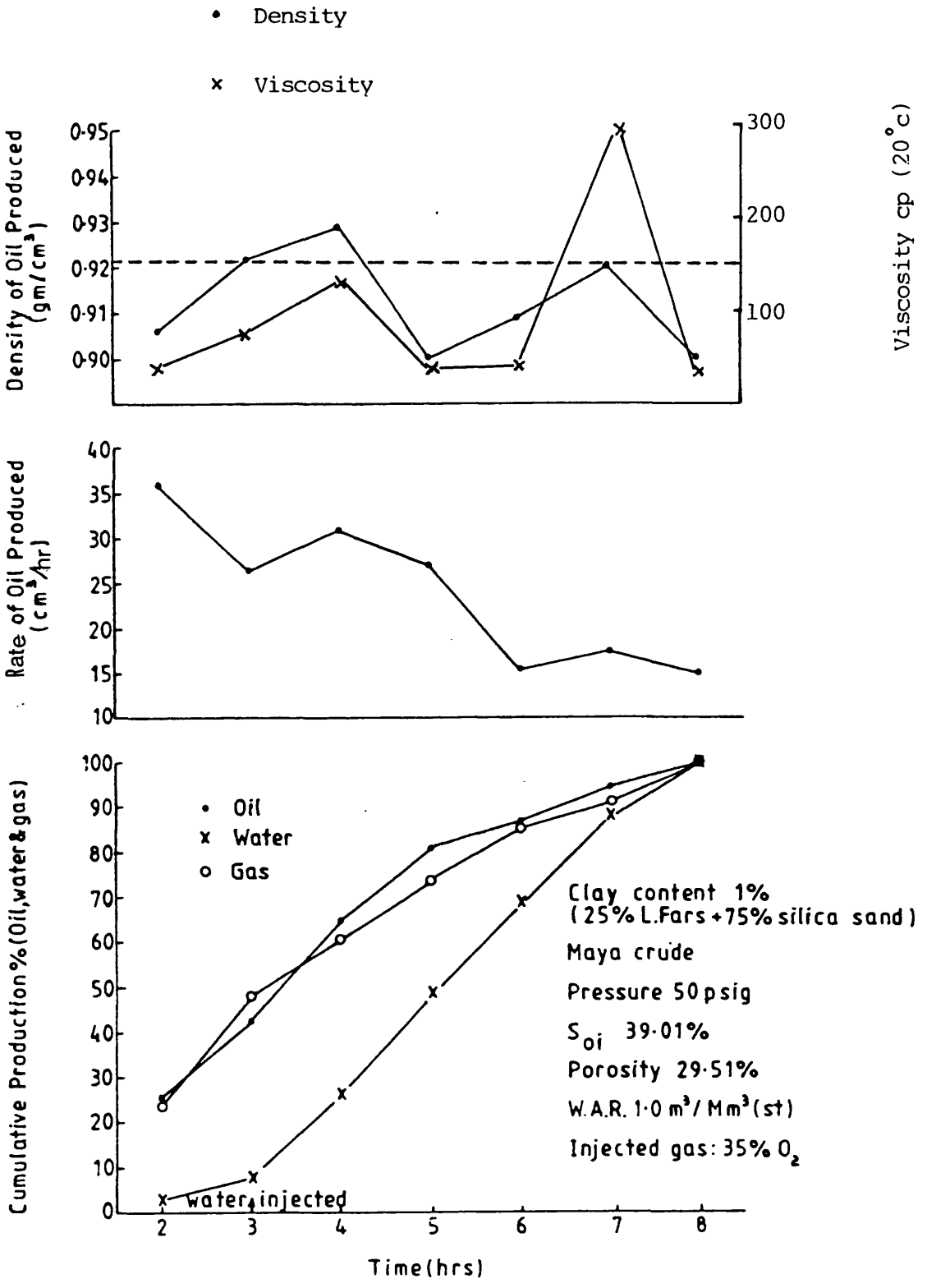

Figure 7.38 Production history (Run 16)

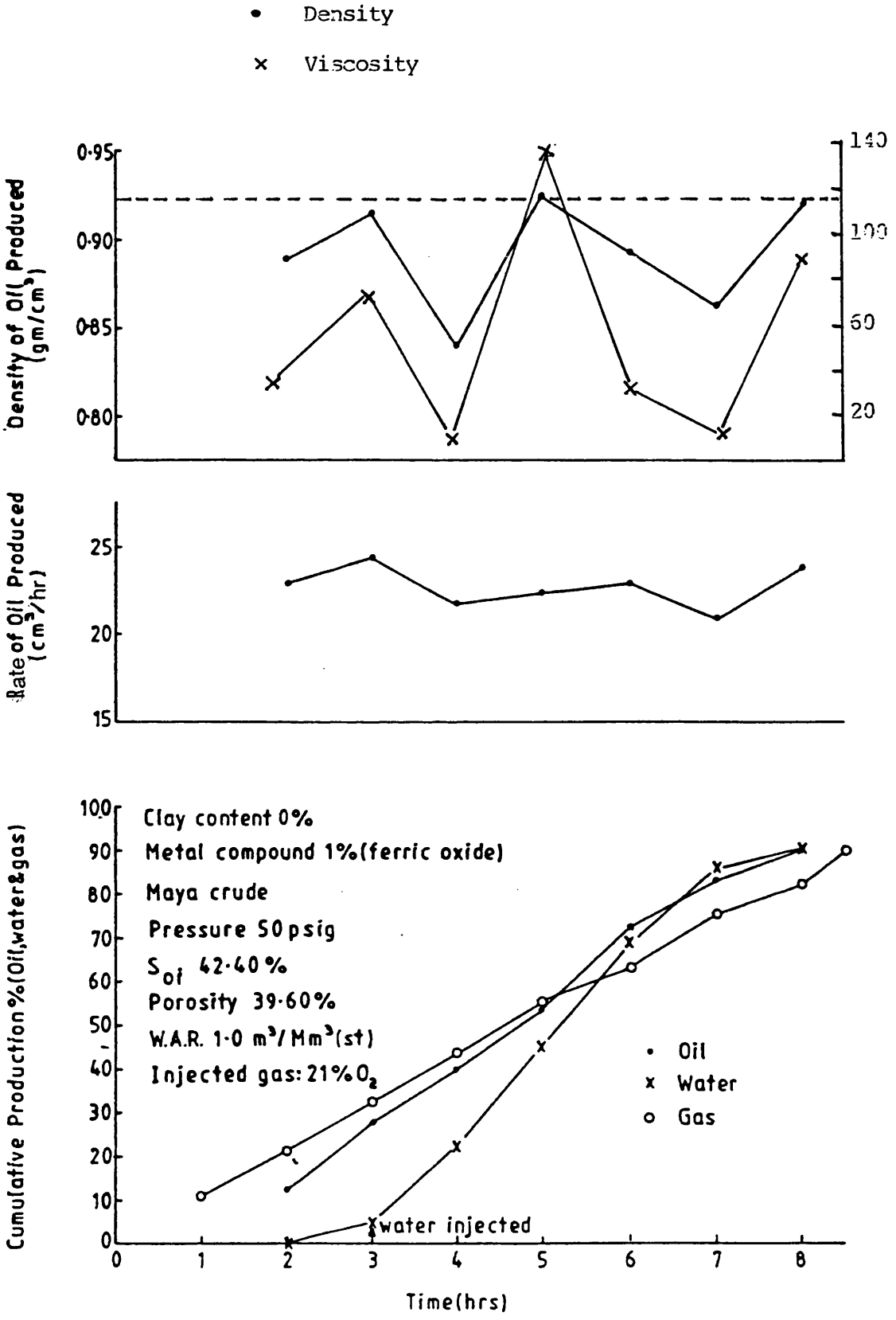

Figure 7.39 Production history (Run 17)

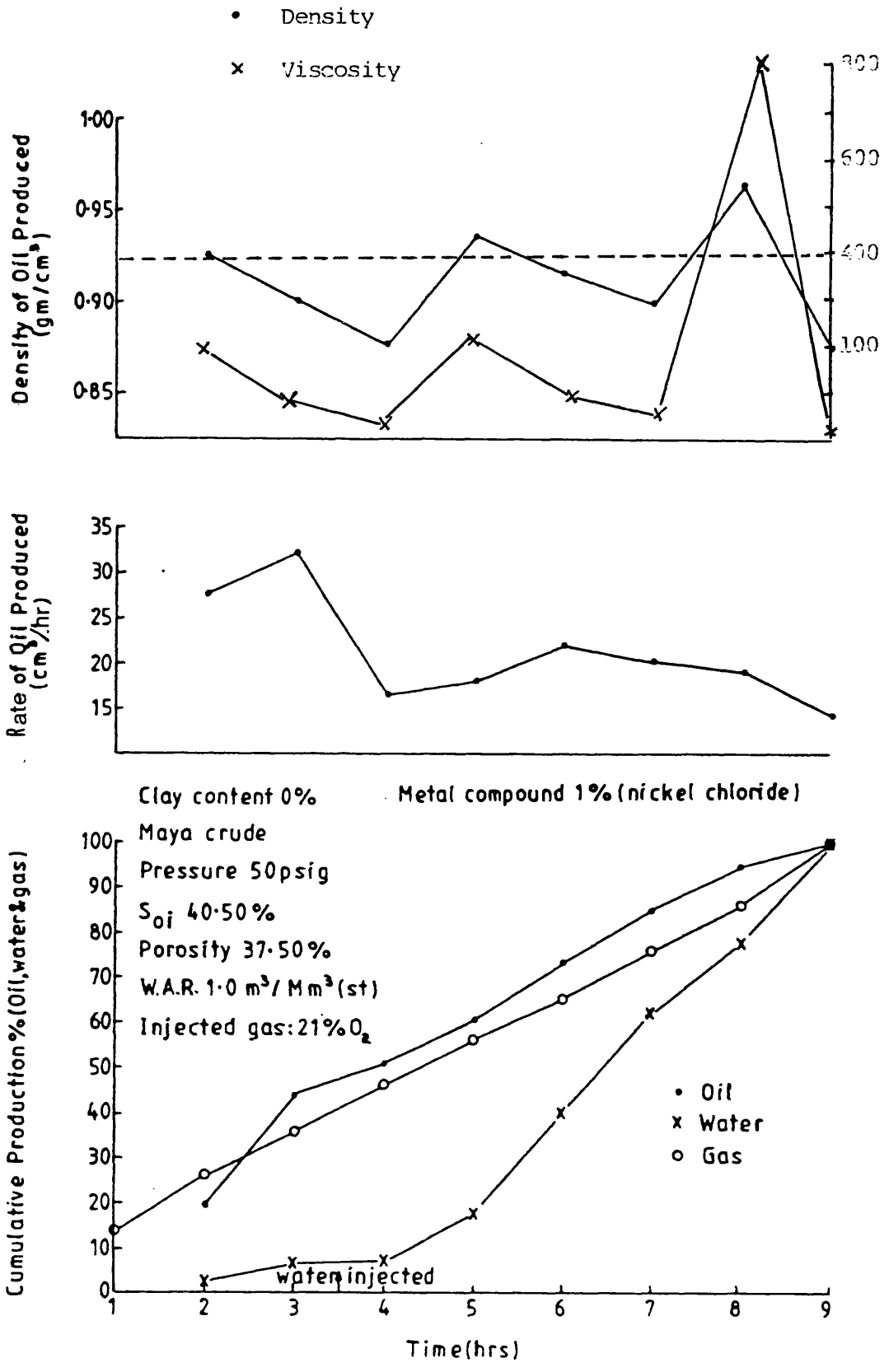

Figure 7.40 Production history (Run 18)

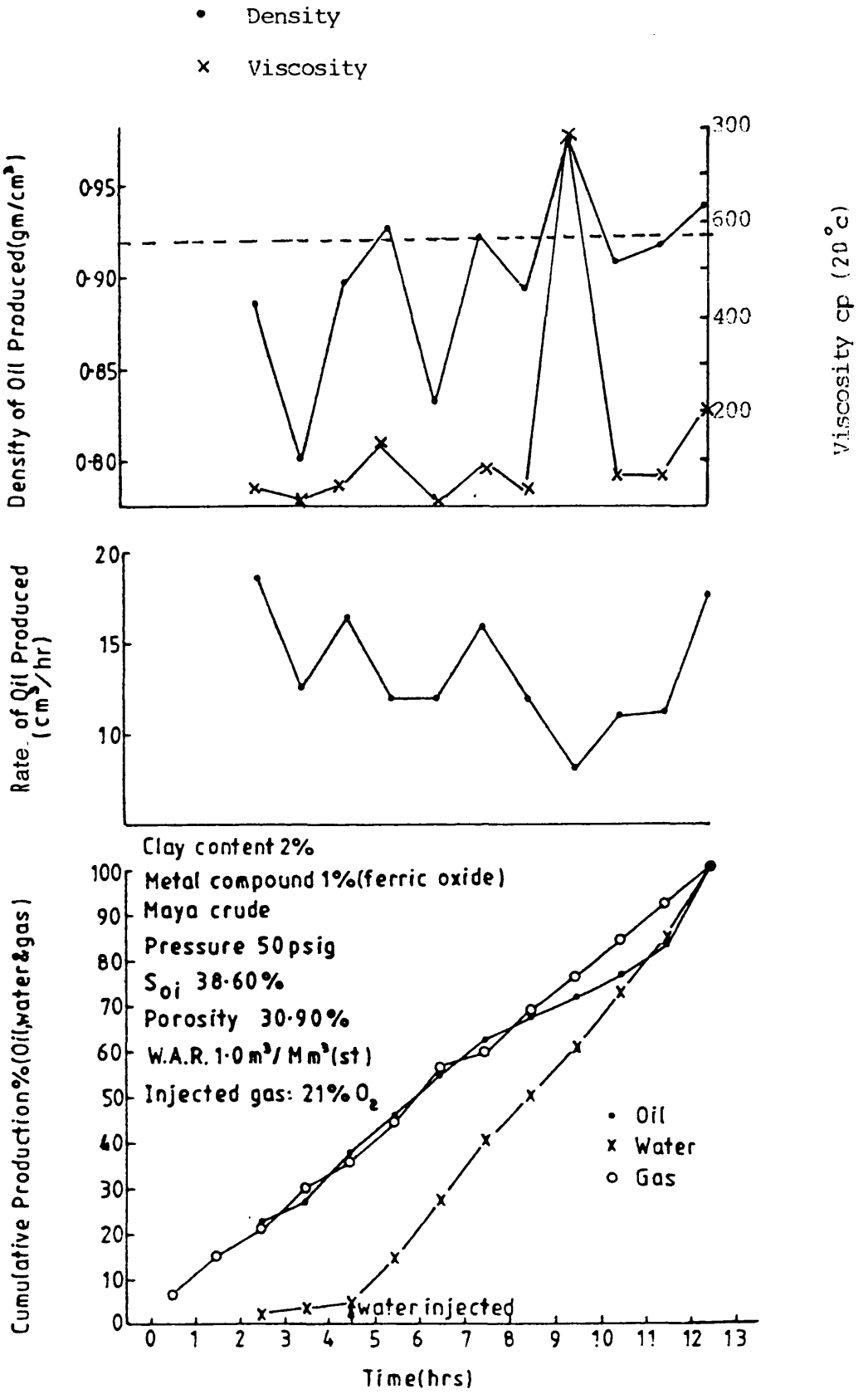

Figure 7.41 Production history (Run 19)

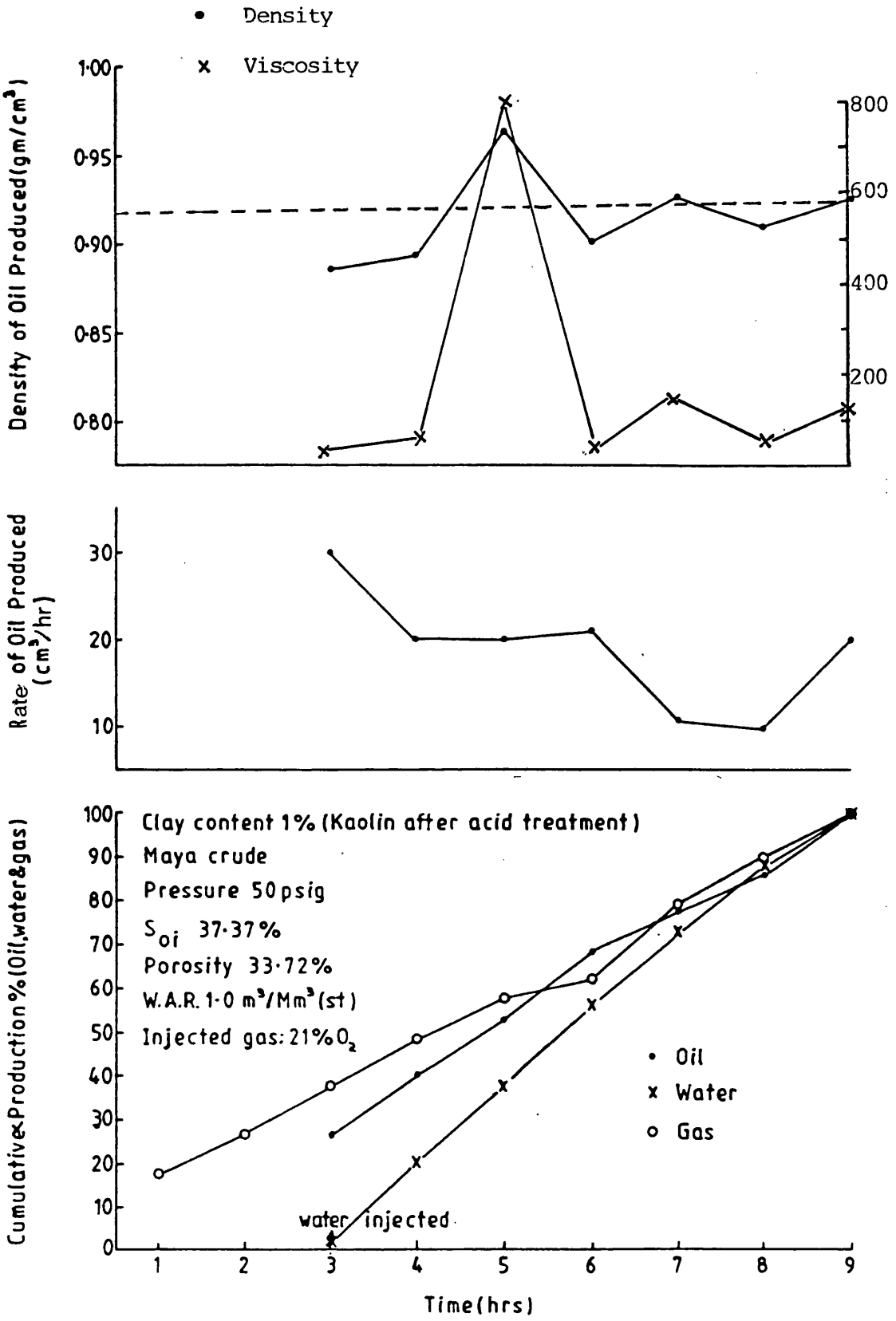

Figure 7.42 Production history (Run 20)

Table 7.6

Physical Properties of Original Crude and Produced Oil

Run No	Crude Oil	Additives Content	Injected Gas $\%O_2$	Original Crude Oil °API	Original Crude Oil Specific Gravity at 20°C	Original Crude Oil Viscosity at 20°C, cp	Produced Oil °API Maximum	Produced Oil °API Average	Produced Oil Specific Gravity at 20°C	Produced Oil Viscosity at 20°C cp +
1	Maya	0%	21	22.1	0.921	203	34	24	0.91	68
2	Maya	2% Kaolin	21	22.1	0.921	203	38	26.6	0.895	38
3	Maya	5% Kaolin	21	22.1	0.921	203	29	25.5	0.901	50
4	Maya	10% Kaolin	21	22.1	0.921	203	33	24.3	0.908	56
5	Maya	15% Kaolin	21	22.1	0.921	203	42	26.3	0.897	42
6	Maya	2% amorphous silica	21	22.1	0.921	203	28.5	24	0.91	68
7	Maya	5% amorphous silica	21	22.1	0.921	203	35	22.3	0.92	88
8	Maya	10% amorphous silica	21	22.1	0.921	203	32	23.1	0.915	80
9	Maya	13.75% amorphous silica	21	22.1	0.921	203	45	23.2	0.914	80
10	Maya Isthmus	3% Kaolin	21	32.4	0.863	65.5*	38	33.8	0.856	6
11	Cold Lake	0%	21	10.2	0.998	200,000	25	21.5	0.925	45
12	Lower Fars	5% additives from L. Fars	21	18.0	0.946	300 +	45	30.3	0.874	92
13	Maya	1% additives from L. Fars	21	22.1	0.921	203	34	24.2	0.909	65
14	Maya	5% Kaolin	21	22.1	0.921	203	25	22.6	0.918	85
15	Cold Lake	0%	35	10.2	0.998	200,000	25	16.8	0.954	650
16	Maya	1% additives from L. Fars	35	22.1	0.921	203	25	22.8	0.917	82
17	Maya	1% Ferric Oxide	35	22.1	0.921	203	37	26.4	0.896	40
18	Maya	1% Nickel Chloride	21	22.1	0.921	203	30	23.5	0.913	74
19	Maya	1% Ferric Oxide +2% Kaolin	21	22.1	0.921	203	44	25.0	0.904	55
20	Maya	1% Acidised Kaolin	21	22.1	0.921	203	28	22.8	0.915	82

* Oil and Gas J. V.81,N.43, Oct 1983

\+ Fig. 7.43

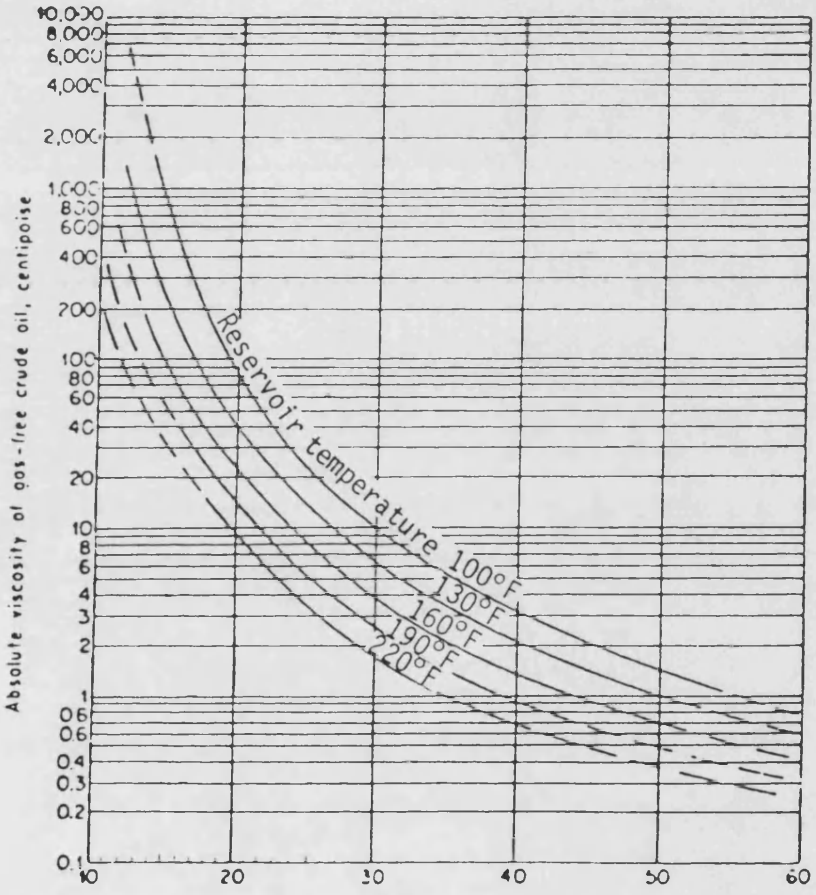

FIGURE 7.43 VISCOSITY OF GAS-FREE CRUDE OIL AS A FUNCTION OF RESERVOIR TEMPERATURE AND STOCK-TANK GRAVITY.(H.K. Van Poolen "Basic Reservoir Engg.")

viscosity of the produced oil. However, for those cases exhibiting a produced oil density less than that of the original crude, there is confidence that the observed variation in predicted viscosity is genuine.

Figures 7.23, 7.25, 7.32, 7.34 and 7.38 show generally similar trends. The density and viscosity of the produced oil increases to a level higher than the original crude density and then decreases towards the end of the run.

In Figures 7.24, 7.28, 7.29, 7.30,7.36 and 7.42, the produced oil density increases gradually to reach a higher level than the original crude density at the end of the run. The indicated viscosity in these cases averages 38, 68, 88, 80, 85 and 82 cp respectively.

In Run 4 (Figure 7.26), the density and viscosity of the produced oil shows a decreased trend over the combustion period.

The density and viscosity of the produced oil tend to increase generally over the combustion period in Figures 7.27, 7.31, 7.33,7.37, 7.39, 7.40 and 7.41. At the midpoint of the combustion period, both density and viscosity curves dropped to low values of 0.81 gm/cm^3 and 10 cp, respectively. Later on, they start to increase and reach a level of 0.975 gm/cm^3 and 200 cp, then decline to 0.92 gm/cm^3 and 80 cp.

However, Bennion *et al.* (1978) separated the produced oil and water by heating and centrifuging. Heating the sample increased the density difference between the oil and water. The density of the produced oil was measured with a digital density meter and is shown in Figure 7.44(a). On the other hand, no production history is presented by Guvenir (1980), due to difficulties in separating the viscous oil-water clay emulsions.

Al-Shalabe (1985) also experienced difficulties in separating the water from the oil-clay emulsion produced, which had been measured. These gave a produced oil density higher than that of the original oil densities as shown in Figure 7.44(b). She found that the production was worse at high water injection rate and as the clay content increased, so did the migration of fines.

Moore *et al.* (1984) conducted laboratory tests on a number of different reservoirs and showed that some oils display sharp changes in density at the end of the test. Figure 7.44(c) demonstrates higher density of the produced oil than the original oil of their work.

The viscosity and specific gravity of the produced oil follow a similar trend and vary over the combustion period. Generally, the oil produced is lighter and less viscous than the original crude (Table 7.6), due to the increase in the light products and decrease of heavy fractions. Heavy components such as asphaltenes are converted to coke which is consumed in the combustion process.

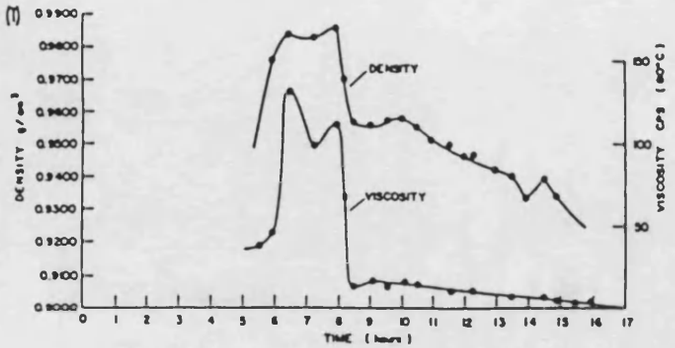

(a) Bennion *et al.* (1978)

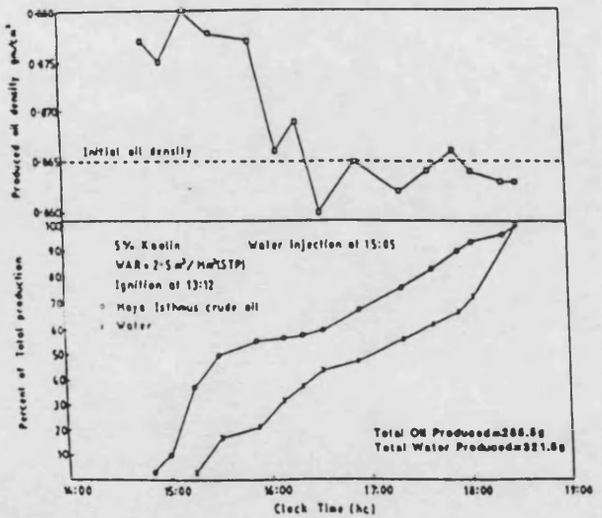

(b) Al-Shalabe (1985)

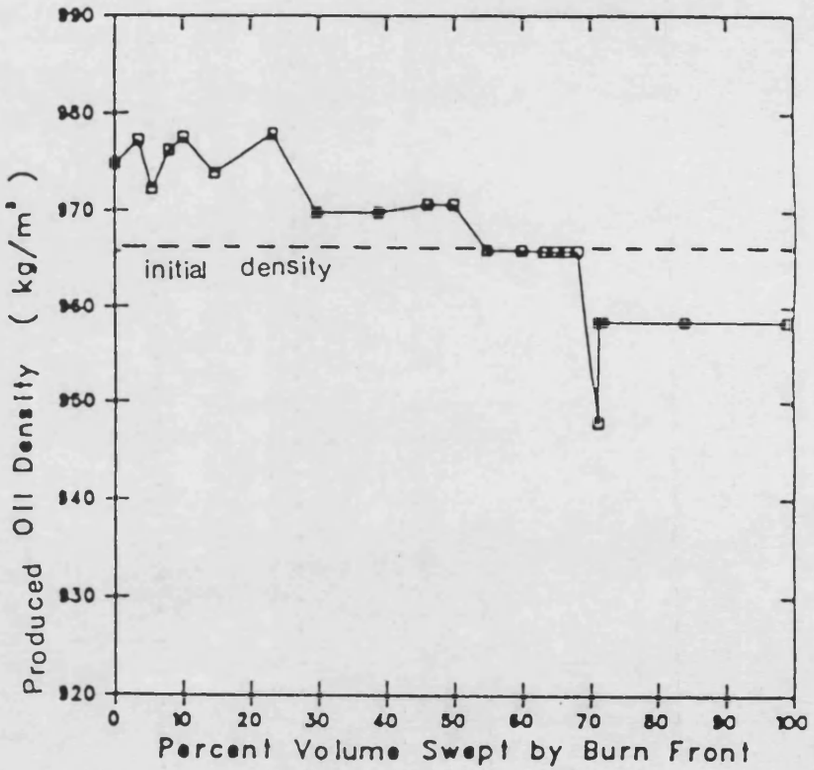

(c) Moore *et al.* (1984)

Figure 7.44 Variation of produced oil density

Other investigators have observed similar behaviour of the produced oil. Penberthy (1965) reported that the viscosity of the oil produced near the end of the tube had a viscosity one third that of the original crude. Thomas et al (1983) observed the following reductions in the properties of the final oil products from *in situ* combustion experiments with Utah tar sand: specific gravity, molecular weight, and percentage of wax, nickel and sulphur content. Burger et al (1985) reported that the oil produced from combustion process had reduced nickel, vanadium and sulphur contents. On the other hand, it was richer in oxidised products and olefins. Adewusi (1986) also noticed that the produced oil had a higher API gravity but lower viscosity and density than the original crude. Figure 7.45 and Table 7.7 show the GC analysis for the Maya crude and the produced oil. The 49 components of the Maya crude oil had reduced to 30 components for the produced oil.

As shown in Table 7.6, the viscosity values of the produced oil for Kaolin runs (Runs 2, 3, 4 and 5) are lower than that with no Kaolin (Run 1). This is attributed to the higher combustion temperature achieved with Kaolin which produces more light components of oil and hence reduces the viscosity of the produced oil. When clay content is increased in the sand matrix by 2, 5, and 10% Kaolin, the viscosity of the produced oil increases by 38, 50 and 56 cp (20°C), respectively, probably due to LTO reaction which occurs ahead of the combustion front. This will lead to the production of light component which some of will be carried with the combustion gases. Therefore, the amount of light oil fractions in the produced oil will decrease and hence, the viscosity will slightly increases. However, with 15% Kaolin (Run 5) the viscosity of the produced oil decreases to 42 cp (20°C), possibly due to the higher combustion temperature achieved comparing with Runs 2, 3, and 4 (2, 5 and 10% Kaolin).

Maya Crude

Produced Oil (Run No.1)

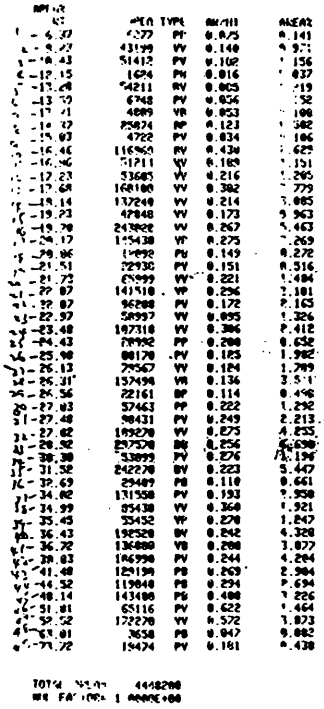

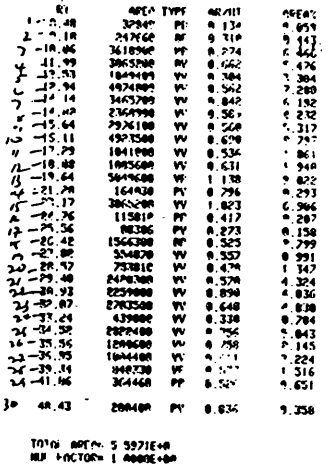

Table 7.7 GC analysis for original crude and produced oil (Adewusi, 1985)

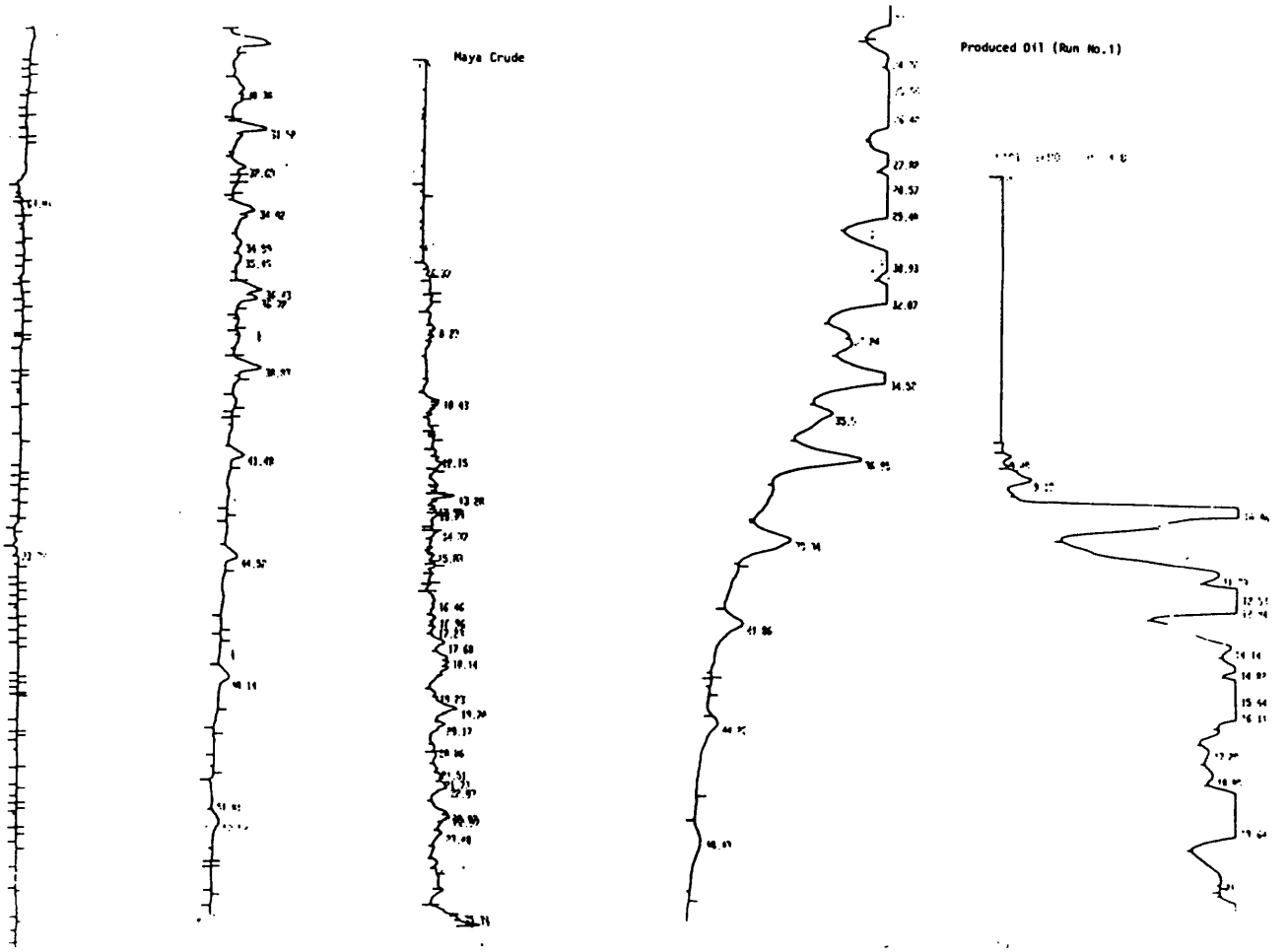

Figure 7.45 GC analysis for original crude and produced oil (Adewusi, 1985)

Table 7.6 represents a significant reduction in the viscosity of the produced oil for the Cold Lake crude cases (Runs 11 and 15). Comparing Run 1 (Maya) with Run 11 (Cold Lake) in which the same operational conditions were used, the viscosity of the produced oil for Run 1 is higher than Run 11. It is expected that for heavy crudes the visbreaking reactions to take place at temperature as low as 260°C (Shu and Hartman, 1986) due to higher asphaltene content, which is 15.9 wt % for Cold Lake and only 9.4 wt % for Maya crude. The higher asphaltene content leads to larger fuel consumption with Cold Lake (15.2 kg/m^3) than with Maya (12.4 kg/m^3), as presented in Table 4.3, and hence lower viscosity of the produced oil. The traces of methane and hydrogen observed in Run 1 (Table 7.1) confirms the occurrence of visbreaking reaction.

Oxygen enrichment experiments (Runs 14, 15, and 16) demonstrate higher viscosity values of the produced oil than the normal air tests (Runs 3, 11, and 13). This is possibly due to the larger steam zone occuring with oxygen enrichment. The enlarged steam zone improves oil displacement which therefore reduces the effect of distillation and cracking processes.

Hansel *et al* (1984) also observed higher viscosity of the produced oil by 10 cp (22°C) than the original crude oil with 40 to 95% oxygen. Adewusi (1986) reported a slight increase of 1.5 cp (38°C) in the viscosity of the produced oil when 35% oxygen was used compared to 21% oxygen for Maya crude oil.

Moreover, with oxygen enrichment early production of oil and water was achieved as shown in Figures 7.37 to 7.38. However, Figure 7.36 (Run 14) show a delay of half hour of oil and water production than in Run 3 (Figure 7.24), due to the dry combustion involved in Run

14. Comparing the overall oil production time for Run 15 (35% O_2) with Run 11 (21%), it is 7 hours for the latter and only 4 hours for the former. On the other hand, Runs 13 (21% O_2) and 16(35% O_2) represent same oil production time. While in Run 3 (21% O_2) the oil production time is lower by 2 hours than in Run 14(35% O_2).

Table 7.8 shows the %OOIP recovered and fuel consumption. As shown in Figure 7.46, the amount of oil recovered decreases with fuel consumption. An increase in fuel consumption will lead to a reduction in the oil ahead of the combustion front. Hence, the ultimate recovery of oil will be lower. This is consistent with Alderman and Osoba (1971) work which found that an increase in oil production corresponded to a decrease in fuel consumption. Adewusi (1986) also found that the decrease in fuel concentration is the main factor affecting oil production during wet combustion. On the other hand, no comment can be made regarding the effect of clay on oil recovery (%OOIP), since oil recovery varies in a random manner. However, a low oil recovery and a high fuel consumption (%OOIP) with Lower Fars core material (Run 12) is due to the low initial oil saturation (Soi 20%).

7.5 Conclusions

(1) Generally, CO_2 production from the *in situ* combustion process increases as the additives content of Kaolin, amorphous silica, natural core, ferric oxide and nickel chloride in the sand pack increases. There is also a corresponding decrease in the CO/CO_2 ratio. With Kaolin content, the apparent H/C ratio of the fuel decreases. This is attributed mainly to an increase in the fuel consumption and resulting higher combustion temperatures.

Table 7.8

Oil Recovery and Fuel Consumption

Run No	Crude Oil	Method of Combustion	Additives Content	Injected Gas $\%O_2$	% OOIP	
					Oil Recovery	Fuel Consumpti
1	Maya	Wet	0%	21	75.4	10.3
2	Maya	Wet	2% Kaolin	21	73.9	12.3
3	Maya	Wet	5% Kaolin	21	81.1	10.3
4	Maya	Wet	10% Kaolin	21	81.3	15.5
5	Maya	Wet	15% Kaolin	21	69.1	12.8
6	Maya	Wet	2% amorphous silica	21	70.4	12.7
7	Maya	Wet	5% amorphous silica	21	74.2	12.4
8	Maya	Wet	10% amorphous silica	21	75.5	14.0
9	Maya	Wet	13.75% amorphous silica	21	64.8	18.6
10	Maya Isthmus	Dry	3% Kaolin	21	78.4	16.7
11	Cold Lake	Wet	0% Kaolin	21	68.7	11.7
12	Lower Fars	Wet	5% additives from L. Fars	21	51.2	34.6
13	Maya	Wet	1% additives from L. Fars	21	65.7	10.0
14	Maya	Dry	5% Kaolin	35	63.1	20.4
15	Cold Lake	Wet	0%	35	60.3	12.9
16	Maya	Wet	1% additives from L. Fars	35	54.8	17.5
17	Maya	Wet	1% Ferric Oxide	21	65.5	12.5
18	Maya	Wet	1% Nickel Chloride	21	68.0	13.5
19	Maya	Wet	1% Ferric Oxide +2% Kaolin	21	58.9	20.3
20	Maya	Wet	1% Acidised Kaolin	21	59.2	14.1

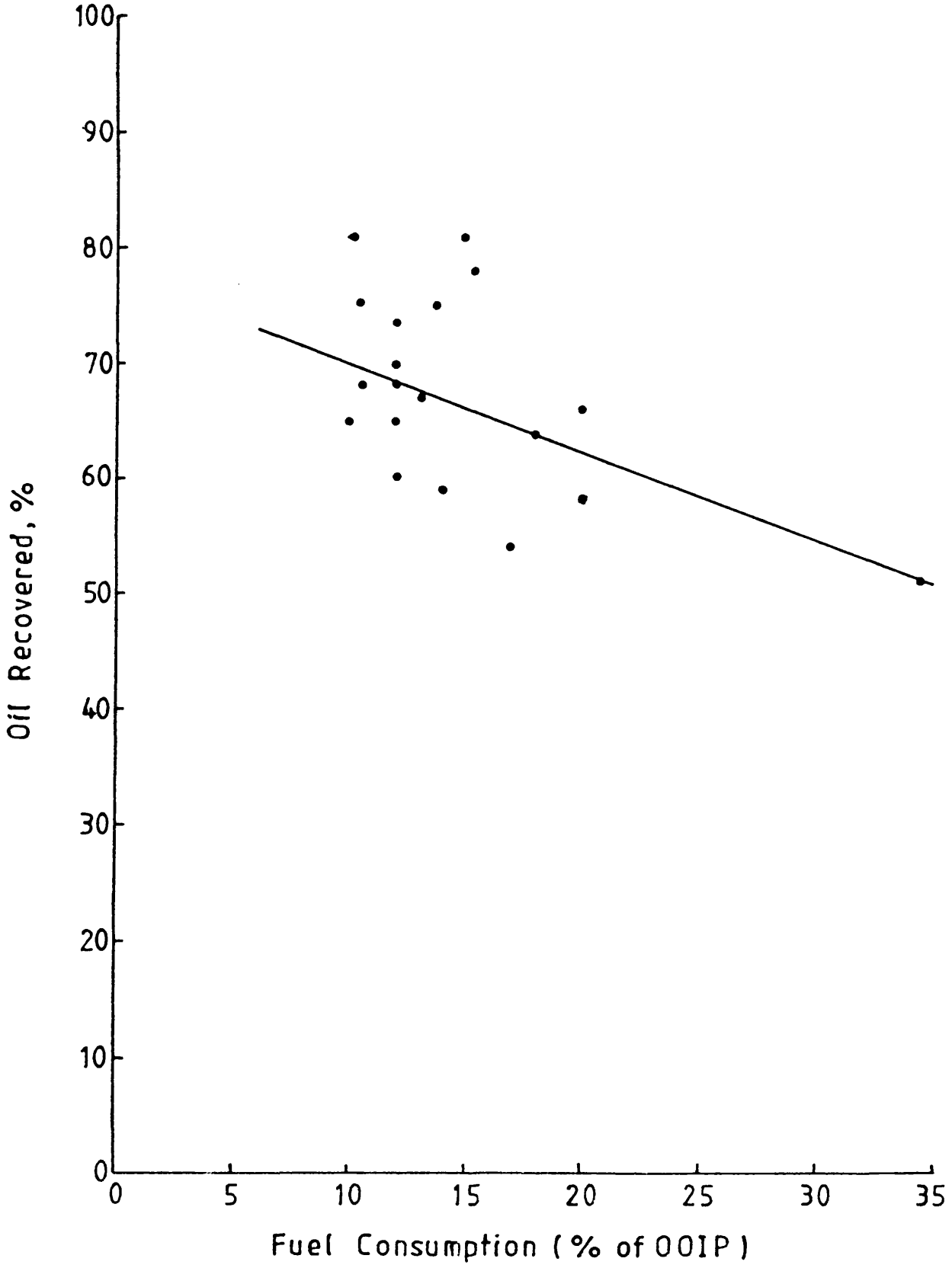

Figure 7.46 Relationship between oil recovered and fuel consumed (as per Table 7.8)

(2) The Chemical composition of the crude oil is altered during combustion process, and this is indicated by significant change in the viscoity of the produced oil. The combustion of crude oil in the presence of Kaolin and amorphous silica leads to higher API gravity, reduced viscosity, and an increase in the lighter components of produced oil.

(3) Oxygen enrichment to 35% oxygen results in a higher concentration of CO and CO_2 in the produced gas than with air combustion. It also leads to faster oil production.

CHAPTER 8

RECOMMENDATIONS

1. Further combustion tube experiments should be made to investigate other types of common clay materials, such as montmorillonite and illite, which have a larger and more reactive surface than the Kaolin.

2. Combustion tube experiments should be supported by TGA and DSC techniques to enable identification of catalytic activity through a study of reaction parameters, i.e. activation energy and reaction activity constant.

3. The effect of sand grain specific surface area on the *in situ* combustion shoud be investigated using particles of different size. However, it will be necessary to use a heavy crude oil which will deposit sufficient fuel to sustain the combustion front.

4. If fresh natural core material from a reservoir is available, further studies should explore its effect on combustion parameters. In order to compare results with other types of sand matrix, the detailed mineral content of the natural core material should be analysed using Mass-Spectrometry.

5. Higher oxygen enrichment levels, extending to use of pure oxygen injection could be investigated. This type of study should also be extended to include the effect of metal compound additives and natural core material under oxygen enrichment conditions.

6. High pressure studies will be useful for investigating the influence that material additives have on the vaporisation and fuel deposition processes.

7. The combustion tube should be modified to incorporate a higher density arrangement of band heaters, preferably achieving full coverage of the tube length, in order to minimise heat losses and to achieve an improved degree of adiabatic control. Attention should also be given to insulating the bottom flange from the combustion tube, since excessive heat losses occur when the combustion front reaches the end of the tube.

8. LTO reaction was responsible for some variation in produced gas composition and other adverse effects. Therefore, the effects of LTO of the crude oil on the performance of the *in situ* combustion process needs to be studied.

9. Investigation of minimum clay content to achieve self-sustained combustion can be extended for lighter crude oil, such as North Sea Forties (36.6° API).

10. Part of the measurement of the combustion front velocities problem is the spacing between the thermocouples (3" distance) through the axial probe. More thermocouples should be fixed along the axial probe.

REFERENCES

Adewusi, V.A. (1986) "Heavy oil recovery by forward *in situ* combustion", PhD thesis, University of Bath.

Alexander, J.D., Martin, W.L. and Dew, J.N. (1962) "Factors affecting fuel availability and composition during *in situ* combustion", J.P.T., October, pp.1154-1163.

Alderman, J.H. and Osaba, J.F. (1971) "A study of oil recovery by *in situ* combustion with the addition of water", SPE 3684, 42nd California regional meeting, L.A., November 4-5th.

Al-Shalabe, M.I. (1985) "Experimental studies of forward *in situ* combustion", PhD thesis, University of Bath.

Bae, J.H. (1977) "Characterisation of crude oil for fire flooding using thermal analysis methods", *SPEJ*, June, pp.211-218.

Bardon, C. and Gadelle, C. (1977) "Essais de laboratoire pour l'etude de la combustion *in situ*" presented at French/Soviet symposium on EOR, Moscow, May.

Berry, V.J. and Parrish, D.R. (1960) "A theoretcial analysis of heat flow in reverse combustion", *Pet. Trans. AIME*, Vol.219, pp.124-131.

Bousaid, I.S. (1967) "Oxidation of crude oil in porous media", PhD thesis, Texas A & M University.

Buchwald, R.W., Hardy, W.C. and Neinast, G.S. (1973) "Case histories of three *in situ* combustion projects", *J.P.T.*, July, pp 784-792.

Buesse, H. (1971) "Experimental investigations of fuel recovery by underground partial combustion of petroleum reservoirs", *Erdoel, Erdgas A.*, 87, No.12.

Burger, J.G. and Sahuquet, B.C. (1972) "Chemical aspects of *in situ* combustion, heat of combustion and kinetcs", *SPEJ*, October, pp.410-422.

Burger, J.G. and Sahuquet, B.C. (1973) "Laboratory research on wet combustion", *JPT*, October, pp.1137-1146.

Burger, J., Souriean, P., Combarnous, M. and Ramey, H.J. (1985), "Thermal methods of oil recvoery", *Ed. Technip,* Paris.

Cady, G.V., Hoffman, S.J. and Scarborough, R.M. (1980) "Silverdale combustion thermal drive project", SPE 8904, 50th meeting, Los Angeles, April 9-11.

Clark, G.A., Jones, R.G., Kinney, W.L., Schilson, R.E., Surkalo, H. and Wilson, R.S. (1965) "The Fry *in situ* combustion test field operations", *JPT*, March, pp.343-347.

Computer Modelling Group (1982) "Computer simulation of thermal EOR schemes", Dorchester, Dorset, England, June 8-10.

Crawford, P.B. (1968) "Underground combustion of hydrocarbons", *Producers Monthly,* June, p.15.

Crookston, R.B., Culham, W.E. and Chen, W.H. (1979) "A numerical simulation model for thermal recovery processes", *SPEJ,* February, pp.37-58.

Dabbous, M.K. and Fulton, P.F. (1974) "Low temperature oxidation reaction kinetics and effects on the *in situ* combustion process", *SPEJ,* June, pp.253-262.

Decroocq, D. (1984) "Catalytic cracking of heavy petroleum fractions", *Ed. Technip,* Paris.

Dew, J.N. and Martin, W.L. (1965) "Air requirements for forward combustion". *Pet. Engineer,* January, pp.82-85.

Dietz, D.N. and Weijdema, J. (1968) "Wet and partially quenched combustion", *JPT,* April, pp.411-415.

Drici, O. and Vossoughi, S. (1985) "Study of the surface area effect on crude oil combustion by thermal analysis techniques", *JPT,* April, pp.731-735.

Ejiogu, G.C., Bennion, D.W., Moore, R.G. and Donnelly, J.K. (1978) "Wet combustion - a tertiary recovery process for the Pambina Cardium reservoir", paper 78-29-32, 29th meeting of CIM, Calgary, June 13-16.

El-Shoubary, Y.M. (1981) "Study of the clay effect on crude oil combustion using TGA and DSC", MSc thesis, University fo Kansas.

Eltantawy, I.M. and Arnold, P.W. (1973) "Catalytic decomposition of organic molecules by clays", *Nature Physical Sci.*, 244, August 27.

Farouq Ali, S.M. (1967) "Forward combustion - state of the art", *Producer Monthly*, November, pp.4-8.

Fassihi, M.R. and Brigham, W.E. (1981) "Analysis of fuel oxidation in *in situ* combustion oil recovery", DOE/ET/12056-26, June.

Fassihi, M.R., Brigham, W.E., and Ramey, H.J. (1980) "The reaction kinetics of *in situ* combustion", SPE 9454, 55th Conference and Exhibition of AIME, Dallas, September, 21-24.

Fassihi, M.R., Brigham, W.E., and Ramey, H.J. (1984) "Reaction kinetics of *in situ* combustion: Part (1) Observation, Part (2) Modelling", *SPEJ*, August, pp. 399-416.

Fassihi, M.R., Ramey, H.J., and Brigham, W.E. (1980) "The frontal behaviour of *in situ* combustion", SPE 8907, 50th California regional meeting, Los Angeles, April 9-11.

Garon, A.M., Kumar, M., Lau, K.K., and Sherman, M.D. (1986) "A laboratory investigation of sweep during oxygen and air fire flooding", SPE Reservoir Engineering, November, pp.565-574.

Gates, C.F. and Ramey, H.J. (1958) "Field results of South Belridge thermal recovery experiments", *Pet. Trans. AIME*, 213, pp.236-244.

Gottfried, B.s. (1965) "A mathematical model of thermal oil recovery in linear system", *SPEJ*, September, pp.196-210.

Grant, B.F. and Szasz, S.E. (1954) "Development of an underground heat wave for oil recovery", *Pet Trans.AIME*, 201, pp.108-118.

Grim, R.E. (1959) "Clay mineralogy", McGraw-Hill.

Grim, R.E. (1962) "Applied clay mineralogy", McGraw-Hill.

Guvenir, I.M. (1980) "The development of an automated *in situ* combustion assembly to study effects of clay on the dry forward *in situ* combustion process", PhD thesis, University of Kansas.

Hansel, J.G., Benning, M.A. and Fernbanher, J.M. (1984) "Oxygen *in situ* combustion for oil recovery: combustion tube tests", *JPT*, July, pp. 1139-1144.

Hardy, W.C., Fletcher, P.B., Shepard, J.C., Dittman, E.W., and Zadow, D.W. (1972) "*In situ* combustion in a thin reservoir containing high gravity oil", *JPT*, February, pp.199-208.

Hardy, T.G., Moore, R.G., Bennion, D.W. and Donnelly, J.K. (1976) "Adiabatic combustion tube evaluation of *in situ* combustion for oil sands", *Proc. Symp. Tar Sands*, 26th Canadian Chem. Eng. Conference , Torento, October, 3-6.

Hobson, G.D. (1984) "Modern Petroleum Technology", John Wiley & Sons.

Hower, W.F. (1974) "Influence of clays on the production of hydrocarbons", SPE 4785, Symp. formation damage control, New Orleans, February 7-8.

Hughes, D.S. (1985) "A numerical assessment of oxygen supported *in situ* combustion as an EOR process in a water flooding North Sea reservoir", 3rd European meeting of improved oil recovery, Rome, April 16-18.

Hvizdos, L.J., Howard, J.V., and Roberts, G.W. (1983) "EOR through oxygen-enriched *in situ* combustion: test results from the Forest Hill field in Texas", *JPT*, June, pp. 1061-1070.

Jacobson, J.M. and Murray, R.G. (1987) "Structural group analysis of changes in Peace River bitumen caused by thermal recovery", *Fuel*, 66, June, pp.753-757.

Kharrat, R. and Vossoughi, S. (1985) "Feasibility study of the *in situ* combustion process using TGA/DSC techniques", *JPT*, August, pp.1441-1445.

Langnes, G.L. and Beeson, C.M. (1965) "*In situ* combustion combined with water flooding", *Pet. Engineer*, July, pp.92-101.

Leaute, R.R. and Collyer, C.J. (1984) "Laboratory studies of *in situ* combustion with Cold Lake crude", 5th Annual Conference, Calgary, Canada, June 14-15.

Lee, S.T., Jacoby, R.H., Chen, W.H., and Culham, W.E. (1981) "Experimental and theoretical studies on the fluid properties required for simulation of thermal prcoesses", *SPEJ*, October, pp.535-550.

Lerner, S.L., Fleming, G.C., and Lara, P.F. (1985) "Dominant processes in *in situ* combustion of light oil reservoirs", *JPT*, May, pp.889-900.

Levenspiel, O. (1972) "Chemical Reaction Engineering", 2nd Edition, Wiley Inter.

Martin, W.L., Alexander, J.D., and Dew, J.N. (1958) "Process variables of *in situ* combustion", *Pet. Trans. AIME*, 213, pp.28-35.

McKay, W.N. (1982) "A discussion of fire flooding", Petroleum Recovery Institute, Calgary, Canada, December.

Milliken, T.H., Oblad, A.G., and Mills, G.A. (1955) "Use of clays as petroleum cracking catalysts", Clays and Clay Technology, Calif. Div. Mines, Bulletin 169, pp.314-326.

Medley, H.D. and Cooley, S.D. (1960) "Hydrocarbon oxidation", *Adv. Pet. Chem. and Refinery*, pp.309-369.

Mills, G.A. (1949) "Process of activating kaolin clay", U.S. Patent 2,477,639, August 2.

Nelson, T.W. and McNeil, J.S. (1961) "How to engineer an *in situ* combustion project", *OGJ*, June 5, pp.58-65.

Okandan, E., Bagci, S., Demiral, B., Parlaktun, M., Topkaya, I. and Curpinar, O. (1982) "Laboratory dry combustion tests for limestone containing light crude oil", 2nd European Symp. EOR, Paris, November 8-10.

Parker, H.W. (1963) "*In situ* combustion using iron catalysts", U.S. Patent 3,087,540, April 30.

Parrish, D.R. and Craig, F.F. (1969) "Laboratory study of a combination of forward combustion and water flooding: The COFCAW process", *JPT*, June, pp.753-761.

Parrish, D.R., Pollock, C.B. and Craig, F.F. (1974) "Evaluation of COFCAW as a tertiary recovery method, Sloss field, Nebraska", *JPT*, June, pp.676-686.

Penberthy, W.L. (1965) "The design and operation of a combustion tube for investigation of combustion oil recovery", MSc thesis, Texas A & M University.

Poettmann, F.H., Schilson, R.E. and Surkalo, H. (1967) "Philosophy and technology of *in situ* combustion in light oil reservoirs", 7th World Petroleum Congress, Mexico, 3, pp.487-498.

Probstein, R.F. and Hicks, R.E. (1982) "Synthetic fuels" McGraw-Hill.

Showalter, W.C. (1963) "Combustion drive tests", *SPEJ*, March, pp.53-58.

Shu, W.R. and Lu, H.S. (1984) "Potential benefit of CO_2 in oxygen combustion" *JPT*, July, pp.1137-1138.

Shu, W.R. and Hartman, K.J. (1986) "Thermal visbreaking of heavy oil during steam recovery processes", *SPE Reservoir Engineering*, September, pp.474-482.

Shu, W.R. and Venkatesan, V.N. (1983) "Kinetics of thermal visbreaking of a Cold Lake bitumen", Paper 83-34-29, 34th Annual Meeting of CIM, May 10-13.

Speight, J.G. (1980) "The chemistry and technology of petroleum", Marcel Dekker Inc.

Sterner, T.E. and Wertman, W.T. (1967) "Laboratory investigation of the *in situ* combustion process for recovering Pennsylvania Grade crude oil", Report 7044, Bureau of Mines, November.

Tadema, H.J. (1959) "Mechanisms of oil production underground combustion", 5th World Petroleum Congress, New York, June 1-5; Section 2, pp.279-287.

Thomas, K.P., Barbour, R.V., Branthaver, J.F. and Dorrence, S.M. (1983) "Composition of oils produced during an echoing *in situ* combustion of Utah tar sand", *Fuel*, 62, April, pp.438-444.

Thomas, G.W., Buthod, A.P., and Omar Allag (1979) "An experimental study of the kinetics of dry forward combustion - final report", U.S. DOE Report BETC-1820-1, February.

Venuto, P.B. and Habib, E.T. (1979) "Fluid catalytic cracking with zeolite catalysts", Marcel Dekker.

Vossoughi, S., Bartlett, G.W. and Willhite, G.P. (1985) "Prediction of *in situ* combustion process variables by use of TGA/DSC techniques and the effect of sand grain specific surface area on the process", *SPEJ*, October, pp.656-664.

Vossoughi, S. and Willhite, G. (1982) "Effect of the sand grain specific surface area on the performance of the tube *in situ* combustion process", SPE 11072.

Vossoughi, S., Willhite, G., El-Shoubary, Y., and Bartlett, G. (1985) "Study of the clay effect on crude oil combustion by thermogravimetry and differential scanning calorimetry", *J. Thermal Analysis*, 27.

Walter, H. (1957) "Application of heat for recovery of oil: field test results and possibility of profitable operation", *JPT*, February, pp.16-22.

Wilson, L.A., Wygal, R.J., Reed, D.W., Gergins, R.L., and Henderson, J.H. (1958) "Fluid dynamics during an underground combustion process", *Pet. Trans. AIME*, 213, pp.146-154.

White, P.D. (1985) "*In situ* combustion appraisal and status", *JPT*, November, pp.1943-1949.

APPENDIX A

Table A.1 Axial Temperature (°C): Run 1

Time (h)	Thermocouple No: 1	2	3	4	5	6	7	8	9	10	11
0	277	369	340	222	112	73	51	41	38	37	33
½	306	395	433	267	139	84	59	46	39	35	31
1	319	400	440	304	168	97	67	52	41	35	31
1½	324	403	442	343	222	119	91	72	58	49	43
2	326	404	449	389	269	161	106	105	91	78	64
2½	314	354	410	447	317	213	139	110	108	107	107
3	301	339	406	449	359	253	175	131	125	124	122
3½	293	346	410	433	408	318	215	158	124	120	121
4	275	319	380	419	432	376	259	193	150	127	123
4½	270	313	379	433	462	467	336	262	207	171	138
5	271	319	371	441	471	485	447	328	264	219	180
5½	259	287	342	442	472	478	478	412	319	262	215
6	246	286	302	423	464	477	477	443	414	316	252
6½	235	263	291	415	457	475	478	481	498	363	276
7	215	248	282	397	446	471	477	477	482	455	315
7½	198	217	263	389	438	468	475	476	477	489	340
8	172	187	288	369	399	455	464	464	462	468	367
8½	140	163	211	275	298	353	366	367	356	326	261

Table A.2 Axial Temperature (°C): Run 2

Time (h) Thermocouple No:	1	2	3	4	5	6	7	8	9	10	11
0	280	362	366	199	110	73	48	39	36	34	30
½	307	392	405	239	132	87	63	44	36	34	30
1	324	409	445	300	180	117	95	81	61	51	45
1½	329	409	457	346	228	139	114	99	92	77	61
2	330	408	461	381	275	182	135	118	105	96	86
2½	331	408	461	392	289	200	143	125	112	101	88
3	331	407	461	407	312	230	167	135	121	111	94
3½	315	358	434	414	328	255	194	154	131	123	117
4	288	351	387	409	340	278	209	162	134	128	123
4½	268	320	373	462	388	316	249	199	161	139	132
5	273	322	362	446	424	358	288	234	191	161	140
5½	256	300	366	438	448	401	321	266	221	186	154
6	235	275	348	421	452	449	368	301	251	211	170
6½	212	253	327	411	450	472	416	347	290	243	193
7	202	236	303	399	443	477	456	388	325	272	213
7½	184	206	294	392	441	473	478	442	366	305	239
8	174	211	296	385	435	464	473	483	426	344	268
8½	174	212	299	381	428	458	468	470	466	394	308
9	162	187	287	383	436	463	475	477	474	460	360
10	151	179	270	367	416	454	466	469	464	462	389
11	125	148	198	252	276	319	331	332	323	296	242

Table A.3 Axial Temperature (°C): Run 3

Time (h)	Thermocouple No: 1	2	3	4	5	6	7	8	9	10	11
0	333	424	457	307	189	117	112	105	99	96	91
½	364	451	493	358	233	148	114	111	108	102	93
1	372	453	500	397	265	179	120	113	112	106	96
1½	375	454	502	424	293	207	146	115	113	109	99
2	377	454	503	442	313	232	168	128	114	111	101
2½	373	432	488	455	331	258	190	147	119	113	105
3	366	424	478	459	351	279	210	165	133	117	110
3½	367	428	481	464	366	302	232	184	151	127	113
4	364	422	478	468	380	325	251	202	167	140	118
4½	361	421	472	475	398	332	264	216	179	151	125
5	350	407	456	470	431	372	286	234	196	165	134
5½	336	363	410	455	444	445	318	258	216	183	150
6	297	309	367	444	464	481	365	297	249	211	174
6½	285	302	356	438	471	492	405	340	290	248	203
7	252	259	323	427	471	507	454	380	329	286	235
7½	217	224	287	406	465	499	524	435	374	331	277
8	205	218	281	399	475	495	525	495	437	394	346
8½	183	189	266	397	476	503	524	522	483	443	387
9	174	195	264	390	472	506	525	536	517	513	443
10	137	161	215	375	302	357	373	374	361	329	265
11	119	137	183	275	267	313	330	333	322	244	235

Table A.4 Axial Temperature (°C): Run 4

Time (h) Thermocouple No:	1	2	3	4	5	6	7	8	9	10	11
0	284	382	385	234	127	86	67	53	46	40	34
½	292	378	402	273	172	103	85	72	60	51	43
1	292	370	414	318	223	139	108	98	93	83	66
1½	311	398	454	362	268	179	138	118	106	100	93
2	320	401	478	420	310	221	200	141	127	113	96
2½	321	397	476	443	350	262	232	163	143	130	109
3	320	378	476	457	377	297	285	189	160	141	120
3½	297	326	439	453	408	344	312	238	201	171	146
4	296	339	441	444	419	363	339	265	227	193	160
4½	294	347	449	459	435	384	370	298	258	220	178
5	275	313	410	452	457	411	410	332	294	254	206
5½	236	266	360	446	478	449	429	375	339	299	242
6	217	247	335	431	481	467	464	395	360	319	262
6½	200	226	321	416	482	490	467	425	390	350	294
7	161	187	286	394	453	483	469	435	399	359	299
7½	109	144	259	365	440	473	476	452	429	398	332
8	113	132	243	356	432	472	481	467	467	438	345
8½	108	116	217	347	425	471	481	477	470	459	371
9	106	112	194	334	417	467	480	480	473	461	377
9½	97	107	180	317	409	461	485	485	484	474	404
10	92	104	170	308	396	462	453	494	493	480	431
10½	88	98	153	278	347	429	410	463	462	446	404
11	83	92	133	240	304	383	290	421	421	404	364
12	72	81	109	169	210	265	280	300	318	298	280

Table A.5 Axial Temperature (°C): Run 5

Time (h)	Thermocouple No: 1	2	3	4	5	6	7	8	9	10	11
0	234	266	448	293	197	117	101	97	94	94	93
½	237	364	494	328	232	158	116	107	103	98	94
1	239	362	505	351	260	191	141	119	113	108	99
1½	239	341	506	371	284	223	170	139	122	117	103
2	238	305	493	457	305	253	196	162	141	128	107
2½	160	211	444	485	331	265	229	196	166	151	125
3	150	141	383	493	350	312	254	214	187	167	140
3½	153	143	341	495	375	340	279	235	205	182	152
4	151	146	282	459	382	358	301	254	221	196	163
4½	150	155	267	375	386	367	315	269	234	205	170
5	151	154	239	375	383	371	327	281	246	216	176
5½	137	147	208	369	377	374	334	290	254	223	181
6	136	151	185	351	376	389	342	299	264	231	187
6½	134	153	165	326	373	465	355	311	275	241	195
7	127	149	130	310	370	410	370	322	285	250	201
7½	125	142	122	297	359	509	389	334	296	259	206
8	126	148	120	284	357	461	454	351	322	266	212
8½	122	146	124	233	347	431	476	391	341	275	221
9	121	144	134	228	330	430	488	413	359	283	225
9½	115	142	130	170	316	380	464	423	374	293	231
10	113	138	127	148	298	345	429	422	418	300	235
10½	112	143	129	141	283	333	402	471	462	381	236
11	115	140	129	139	263	314	367	498	489	407	236
11½	104	129	128	151	252	300	344	382	505	458	238

Table A.6 Axial Temperature (°C): Run 6

Time (h)	Thermocouple No: 1	2	3	4	5	6	7	8	9	10	11
0	245	342	384	220	114	81	56	44	40	39	34
½	265	351	403	254	133	89	66	49	40	38	33
1	273	349	405	277	165	102	74	57	45	40	34
1½	278	349	410	313	208	121	107	85	72	61	50
2	279	349	414	342	246	155	111	114	102	93	73
2½	280	348	416	360	274	190	126	114	111	102	99
3	266	317	412	388	302	221	162	125	123	119	120
3½	252	292	397	430	321	242	184	141	125	121	122
4	242	275	387	474	357	266	206	164	131	123	120
4½	230	266	379	449	388	297	227	182	151	129	125
5	222	263	362	416	409	337	252	201	167	140	121
5½	217	262	359	401	426	402	292	230	190	159	123
6	204	237	342	401	438	492	361	285	237	197	154
7	182	206	300	372	421	443	457	383	317	263	198
7½	174	204	296	379	441	457	467	449	391	350	255
8	159	192	275	365	411	451	463	497	421	353	273
8½	154	176	269	357	415	451	468	486	480	385	301
9	152	177	265	348	419	444	463	476	499	456	327
9½	144	165	261	344	377	439	459	450	482	462	367
10	133	163	231	302	321	390	409	419	422	397	319

Table A.7 Axial Temperature (°C): Run 7

Time (h) Thermocouple No:	1	2	3	4	5	6	7	8	9	10	11
0	258	350	379	239	141	106	92	82	76	74	67
½	271	359	405	269	160	110	90	82	76	72	62
1	273	351	408	282	176	116	91	80	74	70	59
1½	275	349	411	313	220	143	110	99	89	87	77
2	274	346	416	341	253	175	125	119	109	102	96
2½	269	339	410	357	279	205	147	119	120	115	102
3	261	324	430	366	300	234	174	137	122	120	106
3½	247	307	377	363	311	258	196	156	130	122	109
4	244	305	374	366	321	280	219	175	146	127	111
4½	218	255	349	370	336	296	239	193	162	139	123
5	183	184	330	465	344	298	251	209	176	151	128
5½	172	171	345	486	356	304	259	219	187	161	135
6½	133	150	331	443	416	349	284	240	207	180	147
7	180	214	315	390	421	383	310	259	222	192	156
7½	163	144	298	374	412	417	338	280	238	204	165
8	117	123	263	354	399	443	365	301	253	215	173
8½	114	123	255	339	385	483	393	322	269	227	181
9	113	127	245	328	372	439	420	346	285	239	190
9½	115	124	241	320	361	414	488	372	302	251	199
10	102	109	210	306	349	392	427	399	321	264	207
10½	97	104	203	298	358	390	417	432	355	294	231
11	95	113	204	301	359	397	421	480	391	331	263
11½	84	91	180	292	353	393	415	428	407	354	288
12	79	87	168	278	335	387	408	410	445	367	305
12½	91	111	168	250	291	351	371	375	362	324	260
13	89	111	163	229	265	321	340	344	329	295	236

Table A.8 Axial Temperature (°C): Run 8

Time (h) Thermocouple No:	1	2	3	4	5	6	7	8	9	10	11
0	260	359	406	246	136	99	85	79	75	72	66
½	270	353	415	278	160	104	85	76	72	69	62
1	274	352	414	317	210	130	106	93	86	84	81
1½	278	350	445	349	247	164	119	111	102	96	91
2	279	350	465	371	277	197	104	120	114	107	97
2½	279	350	484	385	300	225	166	130	120	113	99
3	280	349	413	396	319	252	189	151	129	119	103
3½	257	307	359	395	332	282	215	173	145	127	115
4	252	315	301	405	347	290	231	189	159	139	120
4½	248	303	309	436	359	295	243	202	172	149	124
5	228	278	305	413	389	309	253	213	182	158	126
5½	222	275	312	393	398	334	267	223	191	165	131
6	204	244	301	379	398	365	286	235	200	172	136
6½	189	234	282	357	384	398	309	249	209	178	140
7½	160	179	273	334	363	467	363	283	230	192	150
8	136	147	220	334	371	411	410	326	267	223	172
8½	135	153	209	321	377	399	421	356	297	250	191
9	127	140	203	329	375	417	480	403	350	308	234
9½	126	141	204	321	377	410	429	416	371	335	256
10	116	127	192	313	371	405	424	428	393	362	280
10½	112	124	189	305	365	401	420	484	411	384	300
11	114	122	188	299	358	396	415	433	424	402	317
11½	106	111	181	295	354	392	413	434	437	414	327
12	97	104	166	282	347	388	410	434	482	425	336
12½	91	96	158	269	330	380	405	432	451	412	335
13½	90	110	155	213	246	301	325	337	334	305	247

Table A.9 Axial Temperature (°C): Run 9

Time (h)	Thermocouple No: 1	2	3	4	5	6	7	8	9	10	11
0	247	341	406	291	194	122	104	97	94	92	88
½	255	343	422	325	232	158	119	110	106	102	93
1	254	336	427	355	263	191	145	122	115	112	100
1½	252	330	427	378	289	220	170	142	128	120	103
2	248	323	421	393	311	246	192	161	142	128	106
2½	246	321	418	406	334	273	214	180	157	139	112
3	245	319	416	416	351	300	238	199	172	150	118
3½	245	318	413	425	365	320	259	216	185	159	123
4	245	317	411	431	378	338	278	233	199	168	128
4½	240	309	401	430	387	352	294	248	210	177	133
5	239	309	397	429	393	364	308	262	221	184	138
5½	153	172	337	408	395	371	323	279	237	195	150
6	147	185	297	372	402	386	345	312	271	217	172
6½	149	212	288	354	394	390	362	341	304	239	186
7	144	178	281	352	386	392	375	364	331	259	198
7½	149	193	266	353	382	398	381	376	346	276	208
8	141	165	258	352	379	387	384	383	356	290	219
8½	149	177	254	350	376	386	387	387	362	301	228
9	147	180	251	347	372	383	386	387	365	309	234
9½	150	185	243	343	369	380	385	386	366	315	240
10	149	176	231	342	379	386	392	394	376	328	254
10½	137	167	222	335	370	384	393	394	379	335	259
11	136	167	213	326	363	379	389	389	376	337	261
11½	134	166	211	320	357	372	384	383	372	338	263
12	122	160	201	317	362	373	385	384	374	344	270

Table A.10 Axial Temperature (°C): Run 10

Time (h) Thermocouple No:	1	2	3	4	5	6	7	8	9	10	11
0	261	345	419	299	195	121	95	83	74	67	59
½	265	341	448	337	238	151	118	106	94	87	76
1	268	342	477	363	270	186	134	116	111	101	97
1½	264	336	473	406	307	223	164	130	119	115	103
2	261	330	465	463	334	262	197	157	133	122	108
2½	257	324	430	472	353	293	226	181	152	132	111
3	252	318	391	474	367	319	256	206	172	146	118
3½	246	308	385	453	378	339	284	228	189	159	126
4	240	302	374	403	384	355	306	249	205	170	133
4½	238	301	371	394	387	368	325	269	221	182	139
5	237	298	369	387	388	378	338	286	235	191	145
5½	226	283	352	376	385	386	349	302	305	201	151
6	225	282	348	368	380	391	358	316	263	211	157
6½	213	265	332	358	373	442	365	325	275	221	163
7	210	264	325	349	366	480	369	335	287	230	169
7½	206	258	320	343	359	484	374	343	298	240	174
8	203	256	316	338	358	450	399	357	314	254	184
8½	198	248	308	334	355	397	435	371	329	269	194
9	196	246	306	330	351	373	485	381	344	285	204
9½	196	246	305	328	347	368	462	467	359	301	215
10	190	239	298	323	343	363	437	486	371	315	226
10½	190	238	296	319	339	358	392	462	387	329	239
11	179	223	281	312	332	354	366	385	373	338	256

Table A.11 Axial Temperature (°C): Run 11

Time (h)	Thermocouple No: 1	2	3	4	5	6	7	8	9	10	11
0	237	323	338	186	88	49	25	19	18	18	18
½	242	317	353	230	124	72	47	28	23	22	22
1	256	331	376	273	177	101	78	63	48	42	39
1½	258	329	384	311	223	134	102	86	79	74	63
2	260	332	422	349	273	180	124	90	89	98	95
2½	251	317	422	361	296	214	159	123	102	94	93
3	249	314	412	399	319	242	188	150	127	110	94
3½	250	313	400	443	342	266	211	173	147	127	103
4	250	313	391	476	367	287	233	193	164	141	112
4½	249	302	346	441	395	313	254	213	182	156	131
5	160	308	327	406	417	340	275	231	197	170	144
5½	160	169	304	384	415	383	297	248	212	183	154
6	151	203	271	372	401	436	322	264	224	193	162
6½	154	201	232	358	388	455	356	282	236	202	168
7	157	175	225	346	375	428	405	305	250	212	174
7½	155	176	219	330	362	404	443	338	267	221	180
8	163	179	211	316	350	387	436	376	287	234	188
8½	150	176	208	307	340	373	411	413	315	248	195
9	148	167	205	292	330	362	394	426	343	265	204
9½	150	169	201	274	320	351	376	419	369	283	216
10	146	160	200	270	310	341	366	402	384	301	228
10½	140	162	192	220	303	332	356	385	390	318	241
11	145	163	168	205	289	326	349	376	387	324	245

Table A.12 Axial Temperature (°C): Run 12

Time (h)	Thermocouple No: 1	2	3	4	5	6	7	8	9	10	11
0	277	357	380	246	132	76	57	37	31	30	29
½	277	349	391	288	185	101	74	58	45	41	40
1	277	346	396	326	230	138	95	85	82	68	63
1½	272	338	392	351	264	182	121	96	92	96	90
2	268	332	387	366	288	216	151	115	99	97	88
2½	264	329	380	376	306	247	178	137	115	103	91
3	218	300	313	362	320	283	209	162	136	121	110
3½	159	183	293	347	334	313	240	186	153	132	119
4	154	173	303	355	351	327	261	206	168	144	127
4½	162	176	294	368	369	336	274	222	184	155	135
5	154	166	278	390	387	340	284	236	197	167	143
5½	153	166	270	414	393	352	299	252	213	181	154
6	146	165	262	409	392	360	310	265	227	194	163
6½	140	160	246	387	395	367	319	276	238	204	170
7	128	152	220	358	398	381	328	285	247	212	176
7½	128	151	209	336	392	399	340	294	256	220	181
8	126	152	204	322	381	421	254	304	263	226	186
8½	128	156	196	312	370	422	370	314	271	232	190
9	133	158	175	294	360	453	391	325	278	237	193
9½	131	156	167	292	348	437	418	341	287	243	197
10	130	155	165	286	340	416	436	358	296	249	201
10½	131	158	177	283	332	396	445	377	307	255	205
11	132	158	167	278	325	379	435	400	320	263	211
11½	125	147	154	274	317	363	408	420	336	273	219
12	127	154	166	271	310	351	386	427	355	284	225
12½	127	153	172	268	304	341	370	410	377	297	234
13	123	157	172	265	299	337	360	394	395	309	242

Table A.13 Axial Temperature (°C): Run 13

Time (h)	Thermocouple No: 1	2	3	4	5	6	7	8	9	10	11
0	267	336	358	279	214	150	121	114	110	107	103
½	262	332	359	293	236	175	141	124	117	114	105
1	261	329	354	302	253	196	160	141	129	121	106
1½	263	333	368	313	271	214	178	155	140	128	109
2	263	333	371	328	293	291	204	179	160	143	117
2½	258	324	371	339	302	256	219	192	171	151	122
3	248	315	382	368	327	281	240	211	187	163	129
3½	235	296	268	381	344	302	259	227	200	172	135
4	225	281	355	386	355	316	273	240	210	180	140
4½	220	278	348	387	363	329	287	252	220	187	145
5	193	248	278	375	373	339	299	265	233	198	160
5½	203	243	278	376	379	346	307	275	242	207	171
6	201	242	287	381	380	352	313	282	249	215	178
6½	195	244	272	257	378	358	319	288	256	225	185
7	205	252	283	365	377	364	325	294	262	229	189
7½	202	247	260	350	376	371	331	301	269	235	195
8	197	240	262	346	381	388	352	322	290	257	207
8½	192	233	250	322	374	418	357	319	288	252	203
9	190	229	245	320	371	415	360	325	289	259	209
9½	190	225	240	318	370	400	370	330	290	260	210
10	186	221	235	315	365	390	390	340	300	265	217
10½	182	218	228	311	361	382	391	358	309	268	220
11	179	211	221	310	358	370	389	370	305	264	218
11½	174	205	217	304	352	360	375	365	301	261	214

Table A.14 Axial Temperature (°C): Run 14

Time (h)	Thermocouple No: 1	2	3	4	5	6	7	8	9	10	11
0	256	342	414	282	194	128	114	108	104	103	99
½	257	330	430	327	238	167	131	123	118	113	106
1	251	317	429	371	292	215	169	148	137	132	122
1½	245	309	421	412	327	265	212	181	165	153	132
2	241	303	415	447	364	316	256	219	196	177	148
2½	238	300	405	455	385	348	287	245	216	190	155
3	237	298	398	456	401	373	311	267	233	201	160
3½	235	295	391	453	415	400	335	289	252	213	165
4	233	292	383	452	427	427	359	312	271	227	173
4½	230	288	375	443	432	440	381	330	288	238	178
5	226	282	366	429	437	447	400	347	303	249	184
5½	223	279	361	417	443	458	424	372	326	269	196
6	223	279	358	407	439	461	433	386	338	278	201
6½	223	278	355	397	429	459	438	398	350	288	207
7	222	278	352	389	416	456	444	410	362	298	212
7½	223	278	350	382	405	448	447	419	375	307	219
8	223	278	349	377	402	435	450	428	389	319	228
8½	218	271	344	375	400	430	455	443	411	338	244
9	213	263	334	370	396	424	455	454	426	359	262
9½	209	259	329	365	391	419	450	458	433	374	277
10	205	255	325	360	390	415	445	450	430	370	275

Table A.15 Axial Temperature (°C): Run 15

Time (h) Thermocouple No:	1	2	3	4	5	6	7	8	9	10	11
0	240	330	421	266	175	115	102	98	95	92	88
½	246	320	438	297	221	132	119	112	105	105	107
1	252	321	406	460	296	200	151	133	126	121	111
1½	253	322	397	482	326	219	169	144	133	125	107
2	255	321	377	438	423	279	208	174	155	140	113
2½	185	281	276	404	430	376	270	220	180	158	131
3	191	267	288	364	417	483	324	244	203	176	148
3½	190	238	274	328	399	454	429	291	229	193	159
4	195	201	272	297	378	426	475	358	264	212	170
4½	200	193	270	292	363	409	447	443	300	231	179
5	180	181	279	292	345	390	421	471	380	266	195
5½	178	162	271	293	329	374	402	427	437	310	215
6	176	178	258	295	333	371	398	420	449	360	249
6½	173	174	254	293	331	370	394	410	429	360	250
7	170	170	250	288	330	366	396	401	417	358	248

Table A.16 Axial Temperature (°C): Run 16

Time (h)	Thermocouple No: 1	2	3	4	5	6	7	8	9	10	11
0	240	326	371	230	148	104	92	90	90	90	89
½	254	342	394	276	191	130	107	104	104	101	92
1	263	341	420	318	230	164	130	115	110	111	101
1½	256	324	415	349	263	196	153	132	119	116	106
2	250	315	409	375	301	234	182	154	139	129	113
2½	242	303	401	400	326	271	212	176	156	142	120
3	236	296	389	414	348	306	247	200	173	153	127
3½	234	295	386	423	366	332	278	225	189	164	133
4	193	237	319	397	387	386	300	246	208	178	149
4½	170	180	277	397	422	393	315	262	221	189	159
5	162	177	278	409	438	403	328	274	233	199	166
5½	150	159	271	403	434	430	341	283	241	205	170
6	142	159	268	389	417	466	367	295	249	211	174
6½	145	162	269	365	398	452	427	316	259	217	177
7	143	163	264	332	380	423	507	353	276	225	182
7½	140	158	245	350	423	432	463	451	344	281	230
8	141	158	233	370	427	427	434	468	422	350	296
8½	140	155	236	364	423	420	417	434	442	370	299
9	138	152	227	361	419	398	407	410	445	370	298

Table A.17 Axial Temperature (°C): Run 17

Time (h)	Thermocouple No: 1	2	3	4	5	6	7	8	9	10	11
0	242	325	379	283	194	115	99	88	77	69	62
½	241	317	383	321	246	158	118	114	106	99	92
1	236	309	380	340	277	195	143	117	116	112	100
1½	234	305	382	359	308	229	175	140	122	121	111
2	233	302	386	380	334	261	204	167	144	132	117
2½	230	297	385	395	351	286	229	190	164	145	121
3	226	290	382	407	363	304	249	209	180	156	126
3½	148	167	319	399	369	319	272	231	197	170	138
4	142	156	267	391	377	332	287	247	212	183	151
4½	144	170	234	379	397	351	306	266	230	220	165
5	145	161	221	381	416	383	334	293	257	224	184
5½	141	154	202	382	421	422	367	322	286	252	205
6	139	161	182	363	399	446	375	325	288	252	204
6½	132	151	188	343	377	422	414	338	290	250	201
7	135	152	192	330	360	396	420	359	297	251	200
7½	127	144	185	319	347	375	391	376	312	260	203
8	121	138	183	315	343	366	375	379	325	271	210
8½	119	132	180	308	340	360	371	375	355	280	220
9	115	130	171	295	331	340	358	368	360	283	222
9½	111	127	165	283	324	329	342	360	348	280	218

Table A.18 Axial Temperature (°C): Run 18

Time (h)	Thermocouple No: 1	2	3	4	5	6	7	8	9	10	11
0	248	331	384	270	179	119	106	100	96	95	86
½	254	330	394	306	216	140	116	109	103	100	101
1	254	323	397	333	248	175	129	117	111	107	103
1½	251	318	396	354	273	205	154	126	119	113	105
2	249	316	396	367	293	231	177	144	128	120	107
2½	246	309	393	381	315	260	202	166	145	130	110
3	241	304	388	389	331	287	229	188	162	142	117
3½	237	298	382	393	343	309	253	209	177	153	122
4	236	297	380	395	352	326	273	228	192	162	127
4½	206	193	365	391	358	342	297	252	208	172	137
5	199	228	328	372	369	351	327	287	227	187	149
5½	161	175	305	374	382	397	396	317	265	222	178
6	157	178	294	362	375	424	389	322	274	230	182
6½	153	172	279	354	376	419	399	323	278	234	185
7	158	180	279	352	380	408	399	326	281	237	187
7½	155	171	268	350	381	396	389	332	283	239	189
8	139	152	252	347	380	387	400	342	287	241	190
8½	144	166	247	342	375	379	380	354	292	243	191
9	139	154	236	332	358	374	378	361	296	244	191
9½	129	149	224	328	353	370	368	370	302	250	199
10	120	138	213	312	340	358	365	368	300	246	195

Table A.19 Axial Temperature (°C): Run 19

Time (h)	Thermocouple No: 1	2	3	4	5	6	7	8	9	10	11
0	238	329	391	266	171	111	96	90	87	86	85
½	249	338	409	306	213	141	112	104	98	95	88
1	256	341	422	338	248	175	133	116	110	105	97
1½	256	338	424	363	277	207	159	133	119	113	103
2	251	328	418	378	302	234	182	152	134	121	104
2½	247	323	415	392	324	263	208	173	150	133	111
3	244	318	411	403	341	288	233	194	166	145	117
3½	235	303	397	409	355	310	256	214	182	156	125
4	231	299	390	410	366	329	278	234	198	167	130
4½	230	298	388	411	373	343	294	251	211	176	136
5	150	146	360	400	379	358	316	275	232	190	148
5½	125	197	332	379	374	360	302	297	246	204	163
6	121	156	324	361	369	363	356	316	264	220	177
6½	125	145	300	351	373	401	365	319	273	231	186
7	125	153	248	335	388	412	362	321	281	240	119
7½	121	146	221	344	407	411	361	326	288	248	199
8	121	155	220	332	412	416	364	329	294	255	205
8½	119	153	219	324	400	424	370	329	294	256	206
9	118	154	190	305	380	435	390	339	293	255	205
9½	111	146	191	282	360	416	420	349	298	255	205
10	112	146	175	273	342	393	437	369	309	259	205
10½	111	149	172	258	327	374	424	392	323	267	208
11	109	135	143	251	313	357	399	417	342	279	213
11½	108	129	137	231	304	345	382	428	360	292	221
12	110	133	137	233	294	333	366	415	382	307	230
12½	107	129	132	226	286	325	356	396	402	320	237

Table A.20 Axial Temperature (°C): Run 20

Time (h) Thermocouple No:	1	2	3	4	5	6	7	8	9	10	11
0	265	347	386	283	196	123	106	94	89	88	85
½	270	344	394	314	233	155	113	109	103	98	93
1	270	342	399	335	262	186	128	116	112	107	97
1½	268	337	400	355	293	221	164	132	124	121	110
2	262	328	396	369	316	254	195	161	140	130	118
2½	260	320	391	377	330	275	220	180	155	145	120
3	253	317	385	382	244	304	245	205	177	155	127
3½	237	274	364	382	374	332	275	235	204	177	147
4	163	188	327	378	379	353	304	266	232	201	166
4½	145	155	314	410	393	365	327	292	259	226	188
5	139	157	278	420	386	363	332	300	268	234	192
5½	135	155	263	419	388	360	329	301	271	237	194
6	135	153	254	403	396	367	330	301	272	239	196
6½	125	141	252	381	402	384	337	303	273	240	197
7	126	155	248	367	399	400	349	309	276	242	198
7½	128	148	243	356	391	416	363	316	279	243	198
8	129	154	226	346	382	425	375	323	282	245	199
8½	119	146	222	335	370	423	387	335	290	249	200
9	124	141	222	325	357	397	392	356	296	252	202
9½	118	132	213	314	338	379	402	359	300	257	205
10	107	124	205	306	327	361	400	359	301	255	202
10½	100	115	199	296	312	348	389	358	300	252	200

APPENDIX B

Table B.1 (Run 1)

Time (h)	Produced Gas Mole Fraction (%)						Gas produced	CO/CO_2 ratio	fuel burned (gm)	air injected m^3 (st)	cumulative carbon burned (gm)
	N_2	O_2	CO_2	CO	CH_4	H_2					
2.50	79.97	6.94	10.73	2.36	0.0	0.0	0.0436	0.22	3.08	0.0441	2.90
3.	78.88	4.46	13.70	2.97	0.0	0.0	0.0200	0.22	1.74	0.0120	4.59
3.25	79.86	1.07	14.97	4.10	0.0	0.0	0.0137	0.27	1.40	0.0139	5.92
3.50	79.77	1.75	14.69	3.79	0.0	0.0	0.0138	0.26	1.36	0.0139	7.21
3.75	79.45	2.83	14.53	3.18	0.0	0.0	0.0114	0.22	1.07	0.0115	8.24
4.	78.50	3.12	15.41	2.97	0.0	0.0	0.0115	0.19	1.08	0.0114	9.31
4.25	77.91	2.36	16.38	3.30	0.05	0.0	0.0114	0.20	1.14	0.0112	10.45
4.50	79.57	1.44	14.53	4.42	0.04	0.0	0.0114	0.30	1.15	0.0115	11.54
4.75	79.25	1.32	14.67	4.63	0.05	0.08	0.0114	0.32	1.17	0.0114	12.66
5.	79.18	1.40	15.07	4.28	0.03	0.04	0.0114	0.284	1.17	0.0114	13.78
5.25	77.20	1.59	17.24	3.97	0.0	0.0	0.010	0.230	1.07	0.0098	14.85
5.50	78.88	1.54	16.01	3.57	0.0	0.0	0.010	0.223	1.02	0.010	15.85
5.75	80.12	1.19	14.70	4.0	0.0	0.0	0.0134	0.27	1.34	0.0135	17.12
6.	79.06	1.36	15.96	3.62	0.0	0.0	0.0133	0.23	1.37	0.0134	18.44
6.25	77.71	1.22	16.91	4.17	0.0	0.0	0.0112	0.25	1.20	0.0110	19.63
6.50	79.42	1.22	14.76	4.61	0.0	0.0	0.0111	0.31	1.15	0.0112	20.73
6.75	78.92	1.18	15.34	4.55	0.0	0.0	0.0115	0.30	1.20	0.0115	21.89
7.	79.30	1.13	15.15	4.42	0.0	0.0	0.0115	0.29	1.19	0.0115	23.03
7.25	79.54	1.59	14.95	3.93	0.0	0.0	0.0103	0.26	1.03	0.0103	24.02
7.50	78.54	3.38	14.95	3.13	0.0	0.0	0.0102	0.21	0.96	0.0102	24.96

Table B.2 (Run 2)

Time (h)	Produced Gas Mole Fraction (%) N_2	O_2	CO_2	CO	CH_4	H_2	Gas produced	CO/CO_2 ratio	fuel burned (gm)	air injected m^3 (st)	cumulative carbon burned (gm)
4.	84.71	5.05	7.60	2.59	0.01	0.03	0.0490	0.34	3.25	0.0525	2.53
4.25	84.32	5.55	7.65	2.47	0.0	0.0	0.0475	0.32	3.08	0.0507	4.98
5.	76.76	3.08	16.96	3.21	0.0	0.0	0.01950	0.19	1.96	0.0189	6.97
5.25	75.49	0.92	19.51	3.98	0.10	0.01	0.0127	0.20	1.47	0.0122	8.49
5.50	75.72	0.94	19.42	3.92	0.0	0.0	0.0128	0.20	1.46	0.0122	10.00
5.75	75.73	1.45	19.04	3.78	0.0	0.0	0.0117	0.20	1.32	0.0113	11.36
6.	77.20	1.37	17.53	3.89	0.0	0.0	0.0118	0.22	1.27	0.0115	12.64
6.25	76.22	0.94	19.00	3.84	0.0	0.0	0.009	0.20	1.02	0.0087	13.68
6.50	76.18	1.24	18.82	3.76	0.0	0.0	0.009	0.20	1.01	0.0087	14.72
6.75	76.00	1.02	19.21	3.74	0.02	0.0	0.0105	0.19	1.19	0.0101	15.94
7.	76.67	0.95	18.93	3.44	0.0	0.0	0.0105	0.18	1.17	0.0102	17.13
7.25	76.39	1.08	19.05	3.41	0.02	0.05	0.0106	0.19	1.86	0.0103	18.35
7.50	76.00	1.08	19.64	3.28	0.0	0.0	0.0107	0.17	1.26	0.0102	19.58
7.75	75.73	0.96	19.76	3.55	0.0	0.0	0.0121	0.18	1.38	0.0116	21.02
8.	75.83	1.31	19.28	3.58	0.0	0.0	0.0121	0.19	1.36	0.0116	22.42
8.25	76.26	1.61	18.55	3.58	0.0	0.0	0.0127	0.19	1.38	0.0122	23.84
8.50	78.07	3.31	15.43	3.06	0.12	0.01	0.0126	0.20	1.20	0.0125	25.03
8.75	79.31	3.91	14.30	2.48	0.0	0.0	0.0121	0.17	1.06	0.0121	26.06
9.	79.86	2.93	14.22	2.98	0.0	0.0	0.0121	0.21	1.11	0.0122	27.11
9.50	80.28	2.74	14.10	2.89	0.0	0.0	0.023	0.20	2.10	0.0234	29.10

Table B.3 (Run 3)

Time (h)	Produced Gas Mole Fraction (%) N_2	O_2	CO_2	CO	CH_4	H_2	Gas produced	CO/CO_2 ratio	fuel burned (gm)	air injected m^3 (st)	cumulative carbon burned (gm)
4.	79.27	4.09	13.62	2.98	0.05	0.0	0.0211	0.22	1.84	0.0213	1.78
4.25	77.41	1.43	17.20	3.88	0.08	0.0	0.0098	0.23	1.05	0.0096	2.83
4.50	75.88	3.12	17.08	3.86	0.07	0.0	0.0098	0.23	1.01	0.0096	3.87
4.75	76.29	3.73	15.59	4.30	0.09	0.0	0.016	0.28	1.58	0.0154	5.48
5.	76.41	4.17	15.16	4.17	0.09	0.0	0.016	0.27	1.54	0.0155	7.05
5.25	77.98	3.11	14.88	3.94	0.09	0.01	0.0159	0.26	1.54	0.0157	8.57
5.50	78.24	3.48	14.48	3.7	0.05	0.0	0.0159	0.26	1.49	0.0158	10.04
5.75	76.91	3.31	16.00	3.71	0.06	0.0	0.0145	0.23	1.43	0.0141	11.49
6.	76.96	3.72	15.15	4.08	0.08	0.01	0.0147	0.27	1.42	0.0143	12.92
6.25	75.67	3.54	16.30	4.38	0.10	0.01	0.011	0.27	1.12	0.0105	14.08
6.50	74.92	3.83	16.73	4.42	0.09	0.01	0.011	0.26	1.13	0.0104	15.26
6.75	74.88	4.19	16.45	4.31	0.14	0.03	0.0155	0.26	1.56	0.0147	16.89
7.	78.09	3.23	14.54	4.03	0.10	0.01	0.0155	0.28	1.49	0.0153	18.35
7.25	80.22	3.23	12.88	3.54	0.11	0.02	0.0177	0.27	1.58	0.0180	19.83
7.50	79.62	3.30	13.36	3.58	0.11	0.02	0.0177	0.27	1.60	0.0178	21.35
7.75	79.82	3.64	12.87	3.40	0.21	0.06	0.0203	0.26	1.78	0.0205	23.02
8.	81.18	3.71	12.40	2.42	0.22	0.07	0.0203	0.20	1.67	0.0209	24.55
8.50	79.45	4.14	12.78	3.35	0.21	0.07	0.033	0.26	2.84	0.0332	27.25
9.	75.76	2.54	16.84	4.41	0.37	0.08	0.0235	0.26	2.48	0.0225	29.79
9.50	75.42	2.41	17.31	4.48	0.33	0.05	0.018	0.27	1.93	0.0171	31.77

Table B.4 (Run 4)

Time (h)	Produced Gas Mole Fraction (%) N_2	O_2	CO_2	CO	CH_4	H_2	Gas produced	CO/CO_2 ratio	fuel burned (gm)	air injected m^3 (st)	cumulative carbon burned (gm)
2.	81.01	5.23	9.97	3.28	0.0	0.0	0.02	0.33	1.51	0.0206	1.34
2.50	78.78	3.75	13.73	3.44	0.0	0.0	0.0109	0.25	0.98	0.0109	2.29
3.	78.70	3.79	13.83	3.37	0.0	0.0	0.0156	0.24	1.40	0.0155	3.65
3.50	80.32	5.72	10.82	2.85	0.0	0.0	0.0256	0.26	1.92	0.0260	5.42
4.	77.31	2.83	16.24	2.97	0.0	0.0	0.0226	0.18	2.21	0.0223	7.63
4.50	77.42	3.54	15.56	2.93	0.0	0.0	0.0238	0.19	2.24	0.0234	9.86
5.	77.0	2.67	16.47	3.28	0.0	0.0	0.0285	0.20	2.84	0.0278	12.72
5.50	77.24	3.41	14.97	3.24	0.0	0.0	0.0214	0.22	2.00	0.0210	14.69
6.	77.0	3.20	14.37	3.54	0.0	0.0	0.0085	0.25	0.79	0.0083	15.46
6.50	78.10	4.48	12.31	3.25	0.0	0.0	0.0296	0.26	2.46	0.0295	17.79
7.	79.04	4.46	12.26	3.29	0.0	0.0	0.0388	0.27	3.24	0.0389	20.86
7.50	77.50	3.48	13.68	3.30	0.0	0.0	0.0099	0.24	0.88	0.0098	21.71
8.	77.02	3.83	14.09	3.41	0.0	0.0	0.0475	0.24	4.31	0.0469	25.93
8.50	76.0	3.06	16.59	3.75	0.0	0.0	0.0304	0.23	3.07	0.0292	29.06
9.	74.01	2.06	18.48	3.78	0.0	0.0	0.0277	0.20	3.01	0.0263	32.19
9.50	76.32	2.40	17.51	3.41	0.0	0.0	0.021	0.19	2.18	0.0203	34.42
10.	77.0	2.15	17.40	3.32	0.0	0.0	0.0383	0.19	3.97	0.0373	38.44
10.50	79.16	2.98	15.02	2.84	0.0	0.0	0.0164	0.19	1.53	0.0164	39.92
11.	80.17	3.40	13.97	2.46	0.0	0.0	0.0192	0.18	1.69	0.0195	41.52

Time (h)	Produced Gas Mole Fraction (%) N_2	O_2	CO_2	CO	CH_4	H_2	Gas produced	CO/CO_2 ratio	fuel burned (gm)	air injected m^3 (st)	cumulative carbon burned (gm)
4.	78.55	1.75	16.43	3.27	0.0	0.0	0.0205	0.20	2.09	0.0204	2.05
4.25	79.02	1.64	16.04	3.30	0.0	0.0	0.0102	0.21	1.03	0.0102	3.05
4.50	78.96	1.58	16.11	3.35	0.0	0.0	0.0103	0.21	1.05	0.0103	4.07
4.75	78.51	1.50	16.60	3.40	0.0	0.0	0.011	0.20	1.14	0.0109	5.18
5.	78.56	1.53	16.59	3.29	0.0	0.0	0.010	0.20	1.03	0.0099	6.19
5.25	78.39	1.60	16.41	3.25	0.0	0.0	0.0102	0.20	1.04	0.0102	7.21
5.50	78.50	1.66	16.70	3.14	0.0	0.0	0.0103	0.19	1.05	0.0102	8.25
5.75	78.26	1.88	16.79	3.07	0.0	0.0	0.011	0.18	1.12	0.0109	9.36
6.	78.50	1.97	16.48	3.05	0.0	0.0	0.01	0.18	1.01	0.0099	10.35
6.25	77.89	1.65	17.33	3.13	0.0	0.0	0.01	0.18	1.04	0.0099	11.39
6.50	77.53	1.61	17.69	3.18	0.0	0.0	0.01	0.18	1.05	0.0098	12.45
6.75	76.97	1.69	18.18	3.18	0.0	0.0	0.01	0.17	1.07	0.0097	13.53
7.	77.82	1.75	17.24	3.19	0.0	0.0	0.011	0.18	1.14	0.0108	14.67
7.50	78.18	2.42	16.44	2.96	0.0	0.0	0.0211	0.18	2.09	0.0209	16.75
8.	79.09	1.69	16.20	3.01	0.0	0.0	0.020	0.19	2.01	0.0200	18.70
8.50	78.90	1.20	16.64	3.25	0.0	0.0	0.0205	0.20	2.12	0.0205	20.77
9.	79.17	1.10	16.20	3.53	0.0	0.0	0.0205	0.22	2.12	0.0205	22.82
9.50	78.60	1.09	16.69	3.61	0.0	0.0	0.021	0.22	2.21	0.0209	24.98
10.	77.52	1.07	17.78	3.63	0.0	0.0	0.021	0.20	2.28	0.0206	27.27
10.50	77.05	1.03	17.91	4.01	0.0	0.0	0.021	0.22	2.32	0.0205	29.60
11.	77.25	1.24	17.96	3.55	0.0	0.0	0.0215	0.20	2.33	0.0210	31.95
11.50	77.31	1.58	17.59	3.52	0.0	0.0	0.0205	0.20	2.18	0.0201	34.15

Table B.6 (Run 6)

Time (h)	Produced Gas Mole Fraction (%) N_2	O_2	CO_2	CO	CH_4	H_2	Gas produced	CO/CO_2 ratio	fuel burned (gm)	air injected m^3 (st)	cumulative carbon burned (gm)
3.50	78.19	5.10	14.52	2.19	0.0	0.0	0.048	0.15	4.08	0.0475	4.07
3.75	78.10	2.55	15.46	3.86	0.0	0.0	0.0121	0.25	1.20	0.0120	5.26
4.	77.85	1.34	16.65	4.17	0.0	0.0	0.0121	0.25	1.29	0.0119	6.54
4.25	76.73	1.21	17.99	4.07	0.0	0.0	0.0122	0.23	1.35	0.0118	7.90
4.50	77.98	1.12	16.85	4.05	0.0	0.0	0.0122	0.24	1.31	0.0120	9.2
4.75	76.75	1.30	18.11	3.84	0.0	0.0	0.0126	0.21	1.38	0.0122	10.60
5.	77.76	1.31	17.10	3.83	0.0	0.0	0.0126	0.22	1.35	0.0124	11.94
5.25	80.17	2.25	14.60	2.82	0.09	0.05	0.0126	0.19	1.18	0.0128	13.05
5.50	79.39	2.22	15.45	2.94	0.0	0.0	0.0126	0.19	1.22	0.0127	14.23
5.75	78.25	1.37	16.49	3.89	0.0	0.0	0.0120	0.24	1.26	0.0119	15.47
6.	77.85	1.39	16.63	4.13	0.0	0.0	0.0120	0.25	1.28	0.0118	16.74
6.25	77.29	1.66	16.46	4.47	0.10	0.01	0.0120	0.27	1.28	0.0117	18.01
6.75	77.31	3.01	15.91	3.73	0.04	0.0	0.012	0.23	1.19	0.0117	19.21
7.	77.96	5.19	14.35	2.42	0.06	0.02	0.016	0.17	1.36	0.0158	20.57
7.25	78.46	5.21	13.44	2.38	0.0	0.0	0.010	0.17	0.84	0.0099	21.4
7.50	78.57	1.24	16.77	3.17	0.16	0.09	0.016	0.19	1.65	0.0159	23.02
7.75	78.25	1.45	16.80	3.13	0.23	0.15	0.012	0.19	1.23	0.0119	24.23
8.	78.81	1.09	16.34	4.07	0.06	0.03	0.013	0.25	1.38	0.0129	25.58
8.25	78.01	1.06	16.35	4.36	0.20	0.02	0.012	0.27	1.28	0.0118	26.84
8.50	76.70	1.0	17.31	4.87	0.07	0.05	0.012	0.28	1.34	0.0117	28.19
8.75	77.24	1.06	16.91	4.72	0.04	0.03	0.0225	0.28	2.48	0.022	30.66
9.	77.47	1.01	16.53	4.67	0.29	0.03	0.0113	0.28	1.23	0.0111	31.87
9.50	77.59	1.11	16.72	4.45	0.09	0.03	0.0113	0.27	1.23	0.0111	33.09

Table B.7 (Run 7)

Time (h)	Produced Gas Mole Fraction (%) N_2	O_2	CO_2	CO	CH_4	H_2	Gas produced	CO/CO_2 ratio	fuel burned (gm)	air injected m^3 (st)	cumulative carbon burned (gm)
5.	80.13	2.99	14.58	2.30	0.0	0.0	0.0255	0.16	2.30	0.0259	2.18
5.50	76.93	1.56	18.07	3.44	0.0	0.0	0.0105	0.19	1.13	0.0102	3.33
5.50	76.82	1.1	18.22	3.86	0.0	0.0	0.0105	0.21	1.16	0.0102	4.51
5.75	77.35	1.26	17.61	3.77	0.0	0.0	0.0140	0.21	1.52	0.0137	6.03
6.25	79.92	1.41	15.12	3.55	0.0	0.0	0.0210	0.23	2.09	0.0212	8.02
6.50	78.32	1.12	16.27	4.29	0.0	0.0	0.0150	0.26	1.60	0.0149	9.58
6.75	77.93	1.09	16.71	4.27	0.0	0.0	0.0110	0.26	1.19	0.0109	10.75
7.	77.77	1.09	16.89	4.24	0.0	0.0	0.0110	0.25	1.19	0.0108	11.93
7.25	77.70	1.0	16.94	4.36	0.0	0.0	0.0113	0.26	1.23	0.0111	13.15
7.50	77.81	1.0	16.88	4.31	0.0	0.0	0.0115	0.26	1.25	0.0113	14.39
7.75	78.56	1.02	16.21	4.21	0.0	0.0	0.0108	0.26	1.15	0.0107	15.51
8.	77.57	0.96	17.24	4.23	0.0	0.0	0.0107	0.25	1.17	0.0105	16.68
8.25	77.60	1.01	17.24	4.15	0.0	0.0	0.0110	0.24	1.20	0.0108	17.87
8.50	77.86	0.95	17.04	4.14	0.0	0.0	0.0110	0.24	1.20	0.0108	19.05
8.75	78.08	1.0	16.82	4.10	0.0	0.0	0.0115	0.24	1.24	0.0114	20.27
9.	78.26	1.09	16.70	3.95	0.0	0.0	0.0115	0.24	1.23	0.0114	21.48
9.25	79.52	1.64	15.15	3.69	0.0	0.0	0.0105	0.24	1.05	0.0106	22.48
9.50	79.55	1.67	15.09	3.68	0.0	0.0	0.0105	0.24	1.05	0.0106	23.48
9.75	79.28	2.13	15.03	3.56	0.0	0.0	0.0113	0.24	1.11	0.0113	24.55
10.	79.20	2.69	14.63	3.48	0.0	0.0	0.0112	0.24	1.07	0.0112	25.58
10.50	79.62	3.51	13.58	3.29	0.0	0.0	0.0225	0.24	2.02	0.023	27.51
11.	77.97	4.61	14.45	2.96	0.0	0.0	0.0215	0.24	1.91	0.021	29.41
11.50	77.04	6.98	13.87	2.11	0.0	0.0	0.0215	0.15	1.69	0.0210	31.15
12.	79.07	8.03	11.07	1.82	0.0	0.0	0.019	0.16	1.28	0.0190	32.39

Table B.8 (Run 8)

Time (h)	Produced Gas Mole Fraction (%) N_2	O_2	CO_2	CO	CH_4	H_2	Gas produced	CO/CO_2 ratio	fuel burned (gm)	air injected m^3 (st)	cumulative carbon burned (gm)
5.	75.98	1.68	18.39	3.94	0.0	0.0	0.0443	0.21	4.88	0.0426	5.02
5.50	77.25	1.41	17.20	4.15	0.0	0.0	0.0227	0.24	2.45	0.0222	7.48
5.75	77.12	0.95	17.77	4.16	0.0	0.0	0.0111	0.23	1.23	0.0108	8.72
6.	77.28	1.04	17.62	4.06	0.0	0.0	0.0112	0.23	1.23	0.0110	9.95
6.25	76.96	0.97	17.99	4.08	0.0	0.0	0.0113	0.23	1.26	0.0110	11.21
6.50	77.0	0.97	18.06	3.98	0.0	0.0	0.0112	0.22	1.24	0.0109	12.47
6.75	77.18	1.12	17.75	3.95	0.0	0.0	0.0140	0.22	1.53	0.0137	14.01
7.25	77.88	2.32	16.47	3.33	0.0	0.0	0.0140	0.20	1.41	0.0138	15.42
7.50	77.8	2.31	16.54	3.35	0.0	0.0	0.0140	0.020	1.42	0.0138	16.83
7.75	79.68	3.10	14.02	3.19	0.0	0.0	0.0113	0.23	1.03	0.0114	17.82
8.	78.94	3.65	14.26	3.15	0.0	0.0	0.0112	0.22	1.02	0.0112	18.81
8.25	81.42	2.92	12.82	2.84	0.0	0.0	0.0112	0.22	0.98	0.0115	19.70
8.50	78.25	3.61	15.87	2.27	0.0	0.0	0.0111	0.14	1.03	0.0110	20.72
8.75	80.01	3.16	14.74	2.09	0.0	0.0	0.0105	0.14	0.94	0.0106	21.61
9.	79.75	3.62	14.53	2.11	0.0	0.0	0.0105	0.15	0.92	0.0106	22.50
9.25	80.06	3.35	14.48	2.11	0.0	0.0	0.0108	0.15	0.95	0.0109	23.41
9.50	82.21	2.97	12.76	2.06	0.0	0.0	0.0109	0.16	0.91	0.0113	23.23
9.75	82.36	2.95	12.66	2.03	0.0	0.0	0.0105	0.16	0.88	0.0109	25.01
10.	81.04	3.67	13.09	2.20	0.0	0.0	0.0105	0.17	0.88	0.0108	25.83
10.25	79.98	3.48	14.25	2.30	0.0	0.0	0.0110	0.16	0.97	0.0111	26.75
10.50	78.4	3.06	16.13	2.41	0.0	0.0	0.0110	0.15	1.04	0.0109	27.79
11.	78.92	2.95	15.71	2.42	0.0	0.0	0.0205	0.15	1.92	0.0205	29.67
11.50	80.33	3.80	12.86	3.00	0.0	0.0	0.0195	0.23	1.68	0.0198	31.24
12.	75.64	3.27	17.85	3.25	0.0	0.0	0.0220	0.18	2.26	0.0211	33.60
12.50	76.13	3.47	17.19	3.21	0.0	0.0	0.0200	0.19	2.00	0.0193	35.67

Table B.9 (Run 9)

Time (h)	Produced Gas Mole Fraction (%) N_2	O_2	CO_2	CO	CH_4	H_2	Gas produced	CO/CO_2 ratio	fuel burned (gm)	air injected m^3 (st)	cumulative carbon burned (gm)
0.	78.99	5.84	12.50	2.61	0.0	0.05	0.0285	0.21	2.25	0.0285	2.19
.50	77.69	5.60	14.03	2.66	0.0	0.02	0.022	0.19	1.85	0.0216	4.05
1.	76.75	5.25	15.31	2.68	0.01	0.01	0.0215	0.17	1.91	0.0209	6.01
1.50	78.47	4.72	14.20	2.61	0.0	0.0	0.0215	0.18	1.86	0.0214	7.85
2.	77.86	5.32	14.22	2.60	0.0	0.0	0.022	0.18	1.87	0.0217	9.72
2.50	78.19	5.36	13.93	2.52	0.0	0.0	0.0215	0.18	1.80	0.0213	11.52
3.	78.06	5.04	14.25	2.65	0.0	0.0	0.022	0.19	1.89	0.0217	13.41
3.50	77.76	4.67	14.79	2.78	0.0	0.0	0.022	0.19	1.95	0.0217	15.37
4.	77.39	4.45	15.25	2.91	0.0	0.0	0.022	0.19	2.01	0.0216	17.39
4.50	76.91	4.15	15.95	2.99	0.0	0.0	0.022	0.19	2.07	0.0214	19.51
5.	76.70	4.32	15.94	3.04	0.0	0.0	0.027	0.19	2.54	0.0262	22.11
5.50	75.19	5.96	16.40	2.45	0.0	0.0	0.0185	0.15	1.66	0.0176	23.88
6.	77.70	5.61	14.62	2.07	0.0	0.0	0.0215	0.14	1.80	0.0211	25.70
6.50	79.95	3.98	13.67	2.40	0.0	0.0	0.0215	0.18	1.84	0.0218	27.46
7.	79.73	3.44	14.23	2.59	0.0	0.0	0.0215	0.18	1.92	0.0217	29.29
7.50	80.30	2.13	14.51	3.06	0.0	0.0	0.022	0.21	2.08	0.0224	31.25
8.	77.44	2.01	17.53	3.02	0.0	0.0	0.0215	0.17	2.23	0.0211	33.50
8.50	79.56	2.06	15.15	3.23	0.0	0.0	0.022	0.21	2.14	0.0222	35.55
9.	78.99	2.22	15.57	3.23	0.0	0.0	0.0225	0.21	2.21	0.0225	37.69
9.50	79.73	2.26	14.74	3.28	0.0	0.0	0.022	0.22	2.11	0.0222	39.71
10.	79.36	2.67	14.89	3.09	0.0	0.0	0.022	0.21	2.08	0.0221	41.71
10.50	79.00	2.97	14.92	3.11	0.0	0.0	0.023	0.21	2.16	0.023	43.82
11.	79.23	2.42	15.38	2.98	0.0	0.0	0.023	0.19	2.21	0.0231	45.96
11.50	77.37	3.77	16.11	2.76	0.0	0.0	0.0225	0.17	2.13	0.0220	48.11
12.	80.48	3.28	13.76	2.49	0.0	0.0	0.0215	0.18	1.89	0.0219	49.89

Table B. 10 (Run 10)

Time (h)	Produced Gas Mole Fraction (%) N_2	O_2	CO_2	CO	CH_4	H_2	Gas produced	CO/CO_2 ratio	fuel burned (gm)	air injected m^3 (st)	cumulative carbon burned (gm)
0.	89.38	3.6	7.56	0.0	0.0	0.0	0.037	0.0	2.24	0.0418	1.42
.50	78.04	8.15	11.92	1.89	0.0	0.0	0.0205	0.16	1.43	0.0203	2.86
1.	81.49	5.30	11.46	1.75	0.0	0.0	0.0200	0.15	1.48	0.0206	4.20
1.50	81.79	5.52	10.82	1.87	0.0	0.0	0.0205	0.17	1.48	0.0212	5.52
2.	81.99	5.14	10.95	1.91	0.0	0.0	0.0210	0.17	1.54	0.0218	6.89
2.50	81.58	4.89	11.50	2.02	0.0	0.0	0.0215	0.18	1.63	0.0222	8.37
3.	80.55	5.00	12.25	2.20	0.0	0.0	0.0210	0.18	1.65	0.0214	9.91
3.50	79.35	4.54	13.63	2.48	0.0	0.0	0.0205	0.18	1.73	0.0206	11.58
4.	78.83	3.70	14.80	2.68	0.0	0.0	0.0210	0.18	1.90	0.0210	13.44
4.50	77.60	4.08	15.56	2.76	0.0	0.0	0.0200	0.18	1.85	0.0196	15.30
5.	77.43	3.98	15.81	2.78	0.0	0.0	0.0210	0.18	1.96	0.0206	17.28
5.50	76.48	4.60	16.13	2.79	0.0	0.0	0.0210	0.17	1.95	0.0203	19.30
6.	76.48	4.60	16.13	2.79	0.0	0.0	0.0210	0.17	1.95	0.0203	21.32
6.50	76.36	4.43	16.37	2.84	0.0	0.0	0.0190	0.17	1.79	0.0184	23.17
7.	76.33	4.34	16.52	2.81	0.0	0.0	0.0210	0.17	1.99	0.0203	25.23
7.50	78.49	4.56	14.19	2.76	0.0	0.0	0.0205	0.19	1.79	0.0204	27.00
8.	77.72	3.85	15.46	2.98	0.0	0.0	0.0210	0.19	1.96	0.0207	28.96
8.50	76.67	3.74	16.41	3.18	0.0	0.0	0.0210	0.19	2.04	0.0204	31.05
9.	75.16	3.81	17.59	3.44	0.0	0.0	0.021	0.20	2.13	0.0200	33.29
9.50	74.93	3.55	17.98	3.55	0.0	0.0	0.021	0.20	2.17	0.0199	35.58
10.	77.46	3.62	15.15	3.78	0.0	0.0	0.0215	0.25	2.06	0.0211	37.65
10.50	76.56	3.23	16.22	3.99	0.0	0.0	0.0215	0.25	2.17	0.0208	39.85
11.	76.29	3.64	16.15	3.91	0.0	0.0	0.0215	0.24	2.14	0.0208	42.04

Time (h)	Produced Gas Mole Fraction (%) N_2	O_2	CO_2	CO	CH_4	H_2	Gas produced	CO/CO_2 ratio	fuel burned (gm)	air injected m^3 (st)	cumulative carbon burned (gm)
3.	78.08	2.10	15.38	4.4	0.25	0.01	0.0210	0.29	2.15	0.0208	2.11
3.50	79.06	1.73	14.24	4.97	0.18	0.0	0.0210	0.35	2.14	0.0210	4.16
4.	76.47	1.33	17.07	5.12	0.16	0.0	0.0215	0.30	2.40	0.0208	4.58
4.50	77.37	1.19	16.17	5.26	0.15	0.0	0.0210	0.33	2.30	0.0206	8.86
5.	76.47	1.23	17.65	4.64	0.32	0.01	0.0220	0.26	2.46	0.0213	11.35
5.50	76.39	1.12	17.48	4.51	0.27	0.01	0.0140	0.25	1.57	0.0135	12.95
5.75	77.19	1.09	17.26	4.47	0.3	0.01	0.0135	0.26	1.49	0.0132	14.44
6.	77.33	1.02	17.24	4.41	0.54	0.1	0.045	0.26	1.60	0.0142	16.03
6.25	77.15	1.01	17.58	4.27	0.89	0.66	0.0103	0.24	1.14	0.0101	17.18
6.50	77.56	0.99	17.12	4.33	0.84	0.21	0.0102	0.25	1.12	0.0100	18.29
6.75	77.90	1.0	16.80	4.30	0.81	0.2	0.0102	0.26	1.11	0.0101	19.38
7.	78.49	0.98	16.29	4.24	0.85	0.14	0.0103	0.26	1.10	0.0102	20.45
7.25	77.54	0.99	17.24	4.22	0.51	0.2	0.0100	0.24	1.09	0.0098	21.54
7.50	77.41	1.05	17.55	3.99	0.48	0.07	0.0105	0.23	1.15	0.0103	22.69
7.75	78.95	1.07	15.91	4.07	0.53	0.07	0.0105	0.26	1.10	0.0105	23.75
8.	78.23	1.06	16.63	4.08	0.16	0.11	0.0105	0.25	1.12	0.0104	24.86
8.25	78.41	1.10	16.42	4.07	0.10	0.0	0.0105	0.25	1.11	0.0104	25.95
8.50	78.71	1.39	16.02	3.87	0.0	0.0	0.0105	0.24	1.09	0.0105	27.01
8.75	80.31	1.55	14.14	4.00	0.0	0.0	0.0102	0.28	1.00	0.0104	27.95
9.	78.83	1.81	15.60	3.75	0.0	0.0	0.0103	0.24	1.04	0.0103	28.96

Table B. 12 (Run 12)

Time (h)	Produced Gas Mole Fraction (%) N_2	O_2	CO_2	CO	CH_4	H_2	Gas produced	CO/CO_2 ratio	fuel burned (gm)	air injected m^3 (st)	cumulative carbon burned (gm)
1.50	80.45	8.63	9.23	1.69	0.0	0.0	0.023	0.18	1.38	0.0234	1.27
2.	80.65	8.37	9.24	1.74	0.0	0.0	0.0225	0.19	1.37	0.0230	2.53
2.50	80.88	7.71	9.69	1.91	0.0	0.0	0.0220	0.20	1.41	0.0225	3.82
3.	80.90	7.22	9.82	2.07	0.0	0.0	0.0225	0.21	1.49	0.023	5.18
3.50	81.88	6.94	9.64	1.54	0.0	0.0	0.0215	0.16	1.38	0.0223	6.40
4.	82.70	4.69	10.70	1.91	0.0	0.0	0.0220	0.18	1.62	0.0230	7.81
4.50	79.80	1.54	15.43	3.23	0.0	0.0	0.022	0.21	2.18	0.0222	9.89
5.	78.04	1.61	16.67	3.68	0.0	0.0	0.0235	0.22	2.45	0.0232	12.32
5.50	75.42	1.28	19.44	3.86	0.0	0.0	0.0225	0.20	2.56	0.0215	14.98
6.	76.03	1.17	18.83	3.96	0.0	0.0	0.0245	0.21	2.76	0.0236	17.82
6.50	75.79	1.15	19.16	3.89	0.0	0.0	0.0205	0.20	2.33	0.0197	20.21
7.	75.87	1.10	19.23	3.80	0.0	0.0	0.0215	0.20	2.44	0.0206	22.73
7.50	75.68	1.05	19.34	3.93	0.0	0.0	0.0215	0.20	2.46	0.0206	25.27
8.	77.18	0.99	17.75	4.08	0.0	0.0	0.0214	0.23	2.32	0.0205	27.59
8.50	75.88	0.87	19.10	4.06	0.0	0.0	0.0210	0.21	2.46	0.0202	30.06
9.	76.29	0.99	18.72	4.01	0.0	0.0	0.0215	0.21	2.43	0.0208	32.54
9.50	78.20	1.01	16.67	4.12	0.0	0.0	0.0215	0.25	2.31	0.0213	34.81
10.	75.14	1.01	19.93	3.92	0.0	0.0	0.0200	0.20	2.32	0.0190	37.23
10.50	76.84	1.04	18.22	3.90	0.0	0.0	0.0210	0.21	2.33	0.0204	39.59
11.	77.18	1.17	17.92	3.73	0.0	0.0	0.0210	0.21	2.29	0.0205	41.90
11.50	77.86	1.35	17.24	3.55	0.0	0.0	0.0200	0.21	2.12	0.0197	44.01
12.	78.53	2.94	15.76	2.77	0.0	0.0	0.0200	0.18	1.91	0.0199	45.90
12.50	78.28	2.64	15.96	3.11	0.0	0.0	0.0205	0.20	2.01	0.0203	47.87

Table B. 13 (Run 13)

Time (h)	Produced Gas Mole Fraction (%) N_2	O_2	CO_2	CO	CH_4	H_2	Gas produced	CO/CO_2 ratio	fuel burned (gm)	air injected m^3 (st)	cumulative carbon burned (gm)
0.	85.41	3.29	10.55	0.75	0.0	0.0	0.0075	0.07	0.54	0.0081	0.43
.50	83.47	1.42	10.51	4.60	0.0	0.0	0.0060	0.44	0.54	0.0063	0.89
1	82.87	1.54	11.55	4.04	0.0	0.0	0.0015	0.35	0.14	0.0016	1.01
1.50	79.96	1.04	15.16	3.83	0.0	0.0	0.0045	0.25	0.46	0.0046	1.44
2.	80.46	1.23	14.56	3.75	0.0	0.0	0.0035	0.26	0.35	0.0036	1.77
2.50	80.06	0.99	15.11	3.85	0.0	0.0	0.007	0.25	0.71	0.0071	2.44
3.	80.34	4.06	12.98	2.62	0.0	0.0	0.0205	0.20	1.73	0.0208	4.06
3.50	79.78	4.32	13.29	2.61	0.0	0.0	0.0215	0.20	1.82	0.0217	5.8
3.75	79.50	4.41	13.45	2.64	0.0	0.0	0.0110	0.20	0.93	0.0111	6.70
4.	79.12	4.36	13.88	2.64	0.0	0.0	0.0110	0.19	0.95	0.0110	7.62
4.25	78.62	4.39	14.23	2.67	0.0	0.0	0.0110	0.19	0.96	0.0110	8.56
4.50	77.94	4.25	15.12	2.69	0.0	0.0	0.0110	0.18	0.99	0.0109	9.56
4.75	77.81	4.35	15.15	2.69	0.0	0.0	0.0110	0.18	0.99	0.0108	10.55
5.	76.07	4.97	16.55	2.42	0.0	0.0	0.0110	0.15	1.01	0.0106	11.61
5.25	78.41	4.13	14.78	2.68	0.0	0.0	0.0110	0.18	0.99	0.0109	12.59
5.50	77.48	3.77	15.99	2.77	0.0	0.0	0.0110	0.17	1.04	0.0108	13.63
5.75	77.38	3.67	16.18	2.77	0.0	0.0	0.0110	0.17	1.05	0.0108	14.69
6.	76.57	3.20	17.48	2.75	0.0	0.0	0.0110	0.16	1.10	0.0107	15.82
6.25	76.60	3.43	17.23	2.73	0.0	0.0	0.0120	0.16	1.18	0.0116	17.04
6.50	76.79	3.42	17.05	2.73	0.0	0.0	0.0120	0.16	1.18	0.0117	18.24
7.	77.12	4.11	16.17	2.59	0.0	0.0	0.0215	0.16	2.01	0.0210	20.29
7.50	80.11	3.09	14.53	2.27	0.0	0.0	0.0225	0.16	2.01	0.0228	22.21
8.	79.22	3.26	15.34	2.18	0.0	0.0	0.0215	0.14	1.96	0.0216	24.12
8.50	81.37	3.02	13.29	2.31	0.0	0.0	0.022	0.17	1.90	0.0227	25.86

Table B. 14 (Run 14)

Time (h)	Produced Gas Mole Fraction (%) N_2	O_2	CO_2	CO	CH_4	H_2	Gas produced	CO/CO_2 ratio	fuel burned (gm)	air injected m^3 (st)	cumulative carbon burned (gm)
0.	69.60	1.92	23.52	4.88	0.0	0.08	0.0195	0.21	3.13	0.021	2.81
.50	68.69	2.01	24.69	4.59	0.0	0.02	0.018	0.19	2.92	0.0190	5.49
1.	69.16	2.03	24.49	4.26	0.0	0.06	0.0185	0.17	2.97	0.0197	8.19
1.50	70.04	2.08	23.83	4.10	0.0	0.01	0.018	0.17	2.85	0.0194	10.74
2.	68.80	1.99	24.70	4.37	0.0	0.06	0.019	0.18	3.06	0.0201	13.54
2.50	67.52	1.96	25.61	4.82	0.0	0.08	0.018	0.19	2.97	0.0187	16.32
3.	65.53	1.81	27.15	5.12	0.16	0.09	0.0185	0.19	3.14	0.0187	19.35
3.50	69.18	1.69	28.58	5.18	0.17	0.08	0.0185	0.18	3.22	0.0183	22.52
4.	65.91	1.06	26.95	5.21	0.17	0.09	0.0185	0.19	3.15	0.0188	25.54
4.25	64.63	1.18	28.85	5.16	0.21	0.08	0.0092	0.18	1.63	0.0092	27.14
4.50	64.66	0.99	28.90	5.03	0.16	0.05	0.0093	0.17	1.63	0.0092	28.73
4.75	64.26	1.02	29.67	4.89	0.13	0.02	0.0095	0.16	1.69	0.0094	30.39
5.	63.77	1.20	30.15	4.92	0.13	0.05	0.0095	0.16	1.70	0.0094	32.08
5.25	64.23	1.20	29.81	4.70	0.0	0.05	0.0095	0.16	1.68	0.0093	33.75
5.50	63.86	0.78	30.23	4.72	0.0	0.04	0.0095	0.16	1.69	0.0093	35.43
5.75	63.08	0.98	31.49	4.61	0.0	0.06	0.0095	0.15	1.73	0.0092	37.18
6.	62.90	1.21	31.45	4.61	0.0	0.05	0.0095	0.15	1.72	0.0091	38.91
6.25	62.90	1.44	31.23	4.60	0.0	0.04	0.0095	0.15	1.71	0.0092	40.64
6.50	62.85	1.59	31.13	4.55	0.0	0.0	0.0095	0.15	1.70	0.0092	42.36
6.75	63.07	0.77	30.80	4.55	0.0	0.0	0.0098	0.15	1.73	0.0095	44.11
7.	63.12	1.86	31.48	4.63	0.0	0.0	0.0097	0.15	1.78	0.0095	45.90
7.25	62.61	2.00	30.97	4.56	0.0	0.0	0.0098	0.15	1.73	0.0094	47.66
7.50	62.25	2.08	31.13	4.63	0.0	0.0	0.0097	0.15	1.74	0.0093	49.42
7.75	61.53	2.10	31.83	4.56	0.0	0.0	0.0095	0.14	1.71	0.0089	51.18
8.	62.00	1.89	31.32	4.57	0.0	0.0	0.0095	0.15	1.69	0.0091	52.91
8.25	62.35	1.91	31.20	4.55	0.0	0.0	0.0100	0.15	1.78	0.0096	54.73
8.50	62.45	2.01	31.04	4.60	0.0	0.0	0.0100	0.15	1.78	0.0096	56.53
8.75	61.72	1.82	31.56	4.72	0.0	0.0	0.0100	0.15	1.80	0.0095	58.38
9.	61.60	1.82	31.83	4.75	0.0	0.0	0.0100	0.15	1.81	0.0095	60.23
9.25	61.85	1.89	31.68	4.59	0.0	0.0	0.0100	0.14	1.80	0.0095	62.07
9.50	61.55	1.84	32.05	4.56	0.0	0.0	0.0100	0.14	1.81	0.0095	63.93

Table B.15 (Run 15)

Time (h)	Produced Gas Mole Fraction (%) N_2	O_2	CO_2	CO	CH_4	H_2	Gas produced	CO/CO_2 ratio	fuel burned (gm)	air injected m^3 (st)	cumulative carbon burned (gm)
.50	68.21	1.30	25.46	5.03	0.0	0.0	0.0305	0.20	5.10	0.032	4.72
1.	64.64	0.33	28.56	6.46	0.0	0.0	0.0125	0.23	2.27	0.012	6.94
1.25	60.98	0.06	30.44	8.24	0.19	0.09	0.0125	0.27	2.42	0.011	9.39
1.50	61.57	0.08	30.31	7.77	0.19	0.08	0.0125	0.26	2.39	0.012	11.81
1.75	61.60	0.08	29.75	8.50	0.0	0.08	0.0095	0.29	1.83	0.009	13.66
2.	60.78	0.08	30.18	8.70	0.19	0.08	0.0095	0.29	1.84	0.008	15.55
2.25	61.57	0.41	29.41	8.54	0.6	0.06	0.0100	0.29	1.91	0.009	17.45
2.50	62.62	0.32	29.90	6.88	0.19	0.08	0.0100	0.23	1.87	0.010	19.32
2.75	64.52	0.79	28.22	6.18	0.21	0.09	0.0093	0.22	1.66	0.009	20.94
3.	63.79	0.38	28.76	6.71	0.25	0.11	0.0092	0.23	1.69	0.009	22.60
3.25	62.56	0.14	29.78	7.14	0.28	0.11	0.0095	0.24	1.78	0.009	24.38
3.50	62.23	0.09	29.69	7.57	0.30	0.12	0.0095	0.25	1.79	0.009	26.18
3.75	62.13	0.12	29.61	7.76	0.28	0.11	0.0085	0.26	1.61	0.008	27.79
4.	61.50	0.09	30.33	7.72	0.25	0.11	0.0085	0.25	1.62	0.008	29.45
4.25	60.93	0.06	31.04	7.66	0.23	0.09	0.0093	0.25	1.78	0.008	31.25
4.50	61.39	0.08	30.62	7.58	0.23	0.09	0.0092	0.25	1.77	0.009	33.04
4.75	62.36	0.27	29.70	7.39	0.20	0.08	0.0090	0.25	1.69	0.008	34.74
5.	62.57	0.28	29.42	7.43	0.22	0.08	0.0090	0.25	1.68	0.008	36.42
5.25	62.73	0.32	29.27	7.43	0.17	0.08	0.0075	0.25	1.40	0.007	37.82
5.50	62.94	0.44	28.98	7.36	0.19	0.08	0.0075	0.25	1.39	0.007	39.26
5.75	57.56	0.46	34.28	7.63	0.0	0.07	0.07	0.22	1.50	0.006	40.80
6.	64.08	0.48	28.20	6.99	0.18	0.07	0.07	0.25	1.37	0.007	42.13

Table B. 16 (Run 16)

Time (h)	Produced Gas Mole Fraction (%) N_2	O_2	CO_2	CO	CH_4	H_2	Gas produced	CO/CO_2 ratio	fuel burned (gm)	air injected m^3 (st)	cumulative carbon burned (gm)
.50	69.16	1.94	25.67	3.23	0.0	0.0	0.025	0.13	4.01	0.0266	3.67
1.	67.30	1.93	27.16	3.61	0.0	0.0	0.019	0.13	3.14	0.0197	6.63
1.50	66.55	2.02	28.04	3.39	0.0	0.0	0.021	0.12	3.49	0.0215	9.98
2.	65.88	2.02	29.33	2.78	0.0	0.0	0.019	0.09	3.18	0.0193	13.08
2.50	68.46	1.95	26.26	3.30	0.0	0.03	0.019	0.13	3.07	0.02	15.93
3.	72.00	2.07	21.55	4.35	0.0	0.04	0.018	0.20	2.76	0.0199	18.30
3.50	70.85	2.04	22.58	4.49	0.0	0.04	0.019	0.20	2.97	0.0207	20.91
3.75	68.61	1.99	24.61	4.75	0.0	0.04	0.0095	0.19	1.54	0.0100	22.32
4.	67.25	1.85	26.07	4.78	0.0	0.05	0.0095	0.18	1.58	0.0098	23.81
4.50	62.07	0.71	30.21	6.76	0.13	0.09	0.0100	0.20	1.76	0.0098	25.55
4.75	60.76	0.44	31.53	7.06	0.16	0.07	0.0095	0.22	1.86	0.0095	27.43
5.	60.49	0.32	32.30	6.87	0.0	0.03	0.0095	0.22	1.82	0.0088	29.29
5.25	60.08	0.36	33.02	6.54	0.0	0.0	0.0105	0.20	1.83	0.0088	31.18
5.50	61.41	0.20	31.27	6.68	0.44	0.0	0.0105	0.21	2.03	0.0097	33.29
5.75	61.47	0.28	31.20	6.62	0.42	0.0	0.0103	0.21	1.99	0.0099	35.31
6.	61.12	0.20	31.38	6.88	0.37	0.0	0.0102	0.22	1.95	0.0097	37.29
6.25	61.14	0.21	31.24	7.05	0.0	0.0	0.0102	0.23	1.94	0.0096	39.27
6.50	61.04	0.16	31.42	7.32	0.0	0.07	0.0103	0.23	1.95	0.0096	41.25
6.75	59.33	0.20	33.21	7.26	0.0	0.0	0.0103	0.22	1.98	0.0097	43.27
7.	60.10	0.80	32.00	7.07	0.0	0.03	0.0102	0.22	2.03	0.0094	45.39
7.25	61.55	0.98	30.64	6.81	0.0	0.03	0.0100	0.22	1.95	0.0094	47.41
7.50	63.59	1.06	29.21	6.12	0.0	0.03	0.0100	0.21	1.87	0.0095	49.31
7.75	65.47	1.08	28.19	5.21	0.0	0.05	0.0100	0.18	1.81	0.010	51.10
8.	66.36	1.96	26.69	4.76	0.13	0.10	0.0100	0.18	1.76	0.010	54.39

Table B. 17 (Run 17)

Time (h)	Produced Gas Mole Fraction (%) N_2	O_2	CO_2	CO	CH_4	H_2	Gas produced	CO/CO_2 ratio	fuel burned (gm)	air injected m^3 (st)	cumulative carbon burned (gm)
.50	86.51	3.99	8.09	1.40	0.0	0.0	0.0505	0.17	3.31	0.0553	2.43
1.	83.49	4.62	10.12	1.77	0.0	0.0	0.0195	0.17	1.39	0.0206	3.61
1.50	83.88	3.65	10.52	1.92	0.0	0.0	0.0180	0.19	1.36	0.0191	4.75
2.	81.76	2.99	12.83	2.43	0.0	0.0	0.0190	0.19	1.62	0.0197	6.22
2.50	78.77	2.52	15.82	2.89	0.0	0.0	0.0185	0.18	1.79	0.0184	7.98
3.	78.87	2.88	15.02	3.22	0.0	0.0	0.0195	0.21	1.85	0.0195	9.78
3.50	77.08	2.60	16.93	3.39	0.0	0.0	0.0210	0.20	2.14	0.0205	11.95
3.75	74.56	2.80	19.63	3.01	0.0	0.0	0.0100	0.15	1.08	0.0094	13.10
4.	75.75	2.84	18.88	2.54	0.0	0.0	0.0100	0.13	1.04	0.0096	14.18
4.50	74.48	2.21	19.94	3.37	0.0	0.0	0.0102	0.17	1.14	0.0096	15.39
4.50	74.47	2.41	19.75	3.38	0.0	0.0	0.0103	0,17	1.14	0.0097	16.60
4.75	74.13	2.45	20.05	3.37	0.0	0.0	0.0103	0.17	1.15	0.0097	17.82
5.	73.91	2.39	20.29	3.41	0.0	0.0	0.0102	0.17	1.15	0.0095	19.05
5.25	72.98	2.61	20.82	3.58	0.0	0.0	0.0105	0.17	1.20	0.0097	20.35
5.75	74.55	2.16	19.48	3.80	0.0	0.0	0.0100	0.20	1.12	0.0094	21.53
6.	75.74	1.29	19.05	3.93	0.0	0.0	0.0100	0.21	1.13	0.0096	22.70
6.25	75.69	1.09	19.34	3.89	0.0	0.0	0.0102	0.20	1.16	0.0098	23.90
6.50	75.43	1.12	19.71	3.73	0.0	0.0	0.0103	0.19	1.18	0.0098	25.12
6.75	75.56	1.34	19.38	3.73	0.0	0.0	0.0098	0.19	1.10	0.0093	26.27
7.	75.81	2.15	18.58	3.46	0.0	0.0	0.0077	0.19	1.05	0.0094	27.36
7.25	75.97	2.51	18.45	3.07	0.0	0.0	0.0097	0.17	1.03	0.0094	28.42
7.50	77.27	3.19	16.82	2.72	0.0	0.0	0.0098	0.16	0.95	0.0095	29.39
7.75	78.53	3.40	15.58	2.49	0.0	0.0	0.0100	0.16	0.93	0.0099	30.31
8.	79.55	3.47	15.03	1.95	0.0	0.0	0.0100	0.13	0.89	0.0101	31.17
8.50	79.25	3.46	15.26	2.02	0.0	0.0	0.0105	0.13	0.94	0.0105	32.09

Table B. 18 (Run 18)

Time (h)	Produced Gas Mole Fraction (%) N_2	O_2	CO_2	CO	CH_4	H_2	Gas produced	CO/CO_2 ratio	fuel burned (gm)	air injected m^3 (st)	cumulative carbon burned (gm)
.50	79.38	5.77	13.38	1.47	0.0	0.0	0.0435	0.11	3.37	0.0437	3.28
1.	79.09	4.66	14.69	1.56	0.0	0.0	0.0185	0.11	1.55	0.0185	4.80
1.50	78.97	4.58	14.88	1.57	0.0	0.0	0.0195	0.11	1.65	0.0195	6.43
2.	79.20	4.47	14.80	1.54	0.0	0.0	0.0190	0.10	1.61	0.0190	8.01
2.50	79.21	4.07	15.12	1.59	0.0	0.0	0.0190	0.11	1.65	0.0191	9.62
3.	78.33	4.11	15.82	1.75	0.0	0.0	0.0195	0.11	1.74	0.0193	11.36
3.50	78.25	3.56	16.43	1.76	0.0	0.0	0.0195	0.11	1.80	0.0193	13.16
4.	78.17	2.90	17.00	1.93	0.0	0.0	0.0190	0.11	1.82	0.0188	14.98
4.50	77.92	2.50	17.65	1.93	0.0	0.0	0.0200	0.11	1.97	0.0197	19.97
5.	76.85	2.29	18.32	2.54	0.0	0.0	0.0190	0.14	1.96	0.0185	18.98
5.25	77.42	2.23	17.78	2.57	0.0	0.0	0.0100	0.14	1.02	0.0098	20.01
5.50	77.19	1.46	16.18	3.16	0.0	0.0	0.0100	0.20	1.01	0.0100	21.00
5.75	77.25	1.12	17.85	3.73	0.0	0.05	0.0098	0.21	1.06	0.0095	22.06
6.	77.26	1.17	17.72	3.79	0.0	0.06	0.0097	0.21	1.06	0.0095	23.13
6.25	78.67	1.16	16.20	3.90	0.0	0.06	0.0105	0.24	1.08	0.0103	24.18
6.50	78.78	1.11	16.25	3.85	0.0	0.0	0.0102	0.24	1.07	0.0102	25.22
6.75	78.73	1.10	16.40	3.77	0.0	0.0	0.0100	0.23	1.05	0.0100	26.24
7.	78.57	1.12	16.59	3.73	0.0	0.0	0.0100	0.22	1.05	0.0099	27.27
7.25	78.61	1.10	16.71	3.58	0.0	0.0	0.0100	0.21	1.05	0.0100	28.30
7.50	77.93	1.01	17.51	3.54	0.0	0.0	0.0100	0.20	1.08	0.0099	29.37
7.75	77.95	1.03	17.52	3.49	0.0	0.0	0.0100	0.20	1.07	0.0099	30.44
8.	77.44	1.01	18.15	3.41	0.0	0.0	0.0100	0.19	1.09	0.0098	31.53
8.25	77.53	0.95	18.11	3.40	0.0	0.0	0.0098	0.19	1.06	0.0096	32.66
8.50	77.90	1.00	17.72	3.38	0.0	0.0	0.0097	0.19	1.05	0.0096	33.64
8.75	78.93	1.01	17.70	2.36	0.0	0.0	0.0100	0.13	1.04	0.0100	34.66
9.	78.61	0.99	17.08	3.32	0.0	0.0	0.0100	0.19	1.06	0.0100	35.69

Table B. 19 (Run 19)

Time (h)	Produced Gas Mole Fraction (%) N_2	O_2	CO_2	CO	CH_4	H_2	Gas produced	CO/CO_2 ratio	fuel burned (gm)	air injected m^3 (st)	cumulative carbon burned (gm)
.50	78.72	5.00	13.72	2.56	0.0	0.0	0.0445	0.19	3.75	0.0443	3.68
1.	80.87	4.12	12.72	2.29	0.0	0.0	0.0215	0.18	1.77	0.0220	5.31
1.50	79.67	4.56	13.47	2.30	0.0	0.0	0.0215	0.17	1.79	0.0217	7.03
2.	79.85	4.47	13.42	2.26	0.0	0.0	0.0215	0.17	1.79	0.0217	8.75
2.50	79.37	4.95	13.46	2.22	0.0	0.0	0.0220	0.16	1.81	0.0221	10.50
3.	79.44	4.72	13.58	2.25	0.0	0.0	0.0215	0.17	1.79	0.022	12.22
3.50	79.37	4.17	14.13	2.33	0.0	0.0	0.0215	0.17	1.86	0.0216	14.02
4.	78.05	5.57	14.03	2.34	0.0	0.0	0.0220	0.17	1.83	0.0217	15.85
4.50	77.83	5.36	14.39	2.42	0.0	0.0	0.0215	0.17	1.82	0.0212	17.68
5.	77.41	4.73	15.35	2.52	0.0	0.0	0.0230	0.16	2.06	0.0225	19.77
5.50	81.25	3.41	13.20	2.14	0.0	0.0	0.0205	0.16	1.73	0.0211	21.36
6.	80.50	2.28	14.80	2.40	0.0	0.0	0.0205	0.16	1.90	0.0209	23.15
6.50	78.67	1.65	17.03	2.65	0.0	0.0	0.0225	0.16	2.28	0.0224	25.40
6.75	79.25	1.42	16.27	3.06	0.0	0.0	0.0113	0.19	1.14	0.0113	26.51
7.	78.16	1.12	17.02	3.70	0.0	0.0	0.0112	0.22	1.19	0.0111	27.69
7.25	79.19	1.19	15.86	3.77	0.0	0.0	0.0115	0.24	1.19	0.0115	28.83
7.50	78.49	1.15	16.62	3.74	0.0	0.0	0.0115	0.22	1.21	0.0114	30.02
7.75	77.53	1.15	17.71	3.61	0.0	0.0	0.0118	0.20	1.28	0.0116	31.30
8.	76.44	1.05	19.00	3.51	0.0	0.0	0.0117	0.18	1.31	0.0113	32.63
8.25	76.97	1.08	18.45	3.51	0.0	0.0	0.0117	0.19	1.29	0.0114	33.94
8.50	76.40	0.97	19.09	3.54	0.0	0.0	0.0118	0.19	1.32	0.0114	35.26
9.	77.08	1.07	18.37	3.48	0.0	0.0	0.0235	0.19	2.58	0.0229	37.90
9.50	78.39	0.94	17.02	3.65	0.0	0.0	0.0230	0.21	2.45	0.0228	40.31
10.	78.91	1.08	16.41	3.60	0.0	0.0	0.0230	0.22	2.40	0.0230	42.65
10.50	80.44	1.04	14.74	3.78	0.0	0.0	0.0225	0.26	2.26	0.0229	44.76
11.	80.00	1.32	15.14	3.54	0.0	0.0	0.0205	0.23	2.05	0.0208	46.71
11.50	80.49	1.42	14.56	3.53	0.0	0.0	0.0230	0.24	2.25	0.0234	48.82
12.	80.75	1.47	14.16	3.63	0.0	0.0	0.0230	0.26	2.23	0.0235	50.89
12.50	82.84	1.66	11.85	3.65	0.0	0.0	0.0200	0.31	1.80	0.0210	52.47

Table B. 20 (Run 20)

Time (h)	Produced Gas Mole Fraction (%) N_2	O_2	CO_2	CO	CH_4	H_2	Gas produced	CO/CO_2 ratio	fuel burned (gm)	air injected m^3 (st)	cumulative carbon burned (gm)
0.	83.45	5.62	9.22	1.71	0.0	0.0	0.0380	0.19	2.52	0.0401	2.11
.50	83.08	5.74	9.48	1.69	0.0	0.0	0.0210	0.18	1.40	0.0221	3.30
1.	82.91	6.14	9.28	1.68	0.0	0.0	0.0200	0.18	1.31	0.0210	4.41
1.50	82.86	5.74	9.66	1.74	0.0	0.0	0.0205	0.18	1.39	0.0215	5.60
2.	80.10	7.86	10.21	1.81	0.0	0.0	0.0200	0.18	1.30	0.0203	6.82
2.50	82.37	5.46	10.34	1.83	0.0	0.0	0.0200	0.18	1.41	0.0209	8.06
3.	82.44	4.13	11.31	2.11	0.0	0.0	0.0205	0.19	1.58	0.0214	9.45
3.50	81.59	4.79	11.47	2.15	0.0	0.0	0.0215	0.19	1.64	0.0222	10.94
4.	78.85	2.45	15.65	3.05	0.0	0.0	0.0195	0.19	1.89	0.0195	12.79
4.50	77.63	1.77	17.33	3.27	0.0	0.0	0.0215	0.19	2.24	0.0211	15.04
5.	75.58	1.13	19.23	4.06	0.0	0.0	0.0210	0.211	2.40	0.0201	17.52
5.50	75.90	1.39	18.72	3.99	0.0	0.0	0.0215	0.21	2.41	0.0207	20.00
6.	75.78	1.18	18.89	4.15	0.0	0.0	0.0215	0.22	2.44	0.0206	22.51
6.50	76.54	1.11	18.23	4.12	0.0	0.0	0.022	0.23	2.46	0.0213	25.01
7.	77.19	1.15	17.50	4.16	0.0	0.0	0.0215	0.24	2.36	0.0210	27.37
7.50	77.21	1.37	17.37	4.05	0.0	0.0	0.0220	0.23	2.38	0.0215	29.76
8.	77.04	1.72	17.31	3.93	0.0	0.0	0.0210	0.23	2.25	0.0205	32.02
8.50	77.43	2.67	16.22	3.69	0.0	0.0	0.0205	0.23	2.07	0.0201	34.10
9.	78.32	3.96	15.08	2.64	0.0	0.0	0.0205	0.17	1.86	0.0203	35.94

Appendix C

Gas Material Balance

Table C.1 shows the overall difference between the calculated mol of air injected and the total mols of gas produced. It also shows the difference in oxygen balance since nitrogen is not involved in any of the crude oil oxidation reactions. Example 1 represents a simple calculation of the gas and O_2 material balance for Run 1.

The differences in oxygen balance for all runs vary from -1.8 to 5.5% for Runs 11 and 15, respectively. In the other hand, the overall gas difference for all runs shows variation on the range of -11.8 to 1.7% for Runs 6 and 13, respectively.

The overall gas balance is related to the oxygen balance since oxygen is the main reaction gas in the combustion process. Different factors are responsible for the errors to the gas balances. According to Penberthy (1965) the gas shrinkage is one source of the errors and was measured to be about 4.2%. Ejiogu et al (1978) and Hardy (1976) have also reported a difference of 11.4 and 20% by volume, respectively, between the inlet injected air and the produced gas.

Both manual adjustment of the inlet air flow rate and sampling collection (in order to maintain constant air flux and to collect the produced liquids periodically) introduced some errors. Any approximation in the calculation of the mol fraction of each component will also introduce small errors in the measured data and consequently in the gas and oxygen balances.

Table C.1

Gas Material Balance

Run No	Cumulative air injected (mol)	Original atoms O	Cummulative gas produced (mol)	Produced atoms O	Overall balance difference %	Oxygen balance difference %
1	11.372	4.77	11.313	4.736	0.5	0.7
2	13.44	5.66	13.398	5.988	0.3	-5.8
3	13.815	5.828	14.023	6.304	-1.5	-8.2
4	18.766	7.908	18.933	8.084	-0.9	-2.2
5	13.648	5.744	13.814	6.018	-1.2	-4.8
6	13.607	5.744	13.773	6.42	-1.2	-11.8
7	13.857	5.828	13.981	6.062	-0.9	-4.0
8	15.104	6.326	15.231	6.504	-0.8	-2.8
9	23.011	9.658	23.178	10.036	-0.7	-3.9
10	20.556	8.658	20.598	8.836	-0.2	-2.1
11	11.152	4.662	11.358	5.02	-1.8	-7.7
12	20.43	8.574	20.598	9.042	-0.8	-5.5
13	12.234	5.162	12.233	5.072	0.01	1.7
14	15.771	11.072	15.771	11.238	0	-1.5
15	9.996	6.410	9.450	7.084	5.5	-10.5
16	13.358	9.324	13.233	9.324	0.9	0
17	14.439	6.078	14.481	6.56	-0.3	-7.9
18	15.521	6.494	15.645	6.528	-0.8	-0.5
19	23.968	10.074	23.926	10.028	0.2	0.5
20	17.31	7.242	17.227	7.142	0.5	1.4

Example 1

Density of N_2 = 1.165 kg/m^3 at 20°C and 1 atm. pressure
Density of O_2 = 1.332 kg/m^3 at 20°C and 1 atm. pressure

Injected gas:

volume of air injected = 0.273 m^3 (st)
volume of N_2 injected = 0.273 x 0.79 = 0.216 m^3 (st)
volume of O_2 injected = 0.273 x 0.21 = 0.0573 m^3 (st)

$$\text{no. of mol of } N_2 = \frac{0.216 \times 1165}{28} = 8.987$$

$$\text{no. of mol of } O_2 = \frac{0.0573 \times 1332}{32} = 2.385$$

total air injected (mol) = 8.987 + 2.385 = 11.372
atoms of O = 2.385 x 2 = 4.770

Produced gas:

	mol %
N_2	79.07
O_2	2.1
CO	3.8
CO_2	15.03

volume of gas produced = 0.272 m^3 (st)
volume of N_2 produced = 0.272 x 0.7907 = 0.215 m^3 (st)
volume of O_2 produced = [0.021 + 0.038 + 0.1503] 0.272 = 0.0569 m^3 (st)

$$\text{no. of mol of } N_2 = \frac{0.215 \times 1165}{28} = 8.945$$

$$\text{no. of mol of } O_2 = \frac{0.0569 \times 1332}{32} = 2.368$$

total gas produced (mol) = 8.945 + 2.368 = 4.736
atoms of O = 2.368 x 2 = 4.736

Therefore; error in overall gas balance = $\frac{11.372 - 11.313}{11.372}$ = 0.52%

error in O_2 balance = $\frac{4.77 - 4.736}{4.77}$ = 0.71%

Appendix D

Liquids Material Balances

Table D.1 gives an overall liquid material balance for Runs 1 to 20. An example of the calculation of the liquid mass balance for Run 1 is given in Example 2. The oil material balance is determined from the oil originally in the pack, the fuel consumed, and the residual fuel in the pack. The error in the oil mass balance varies from 1.8% in Run 1 to 11.1% in Run 13. While the differences in the water material balance vary from 2.8 to 14.4% for Runs 2 and 10, respectively.

Discrepancies in the liquid mass balance have several causes. The difficulties in separating the water from the oil-clay emulsion leads to errors in calculation. Water generated by combustion was calculated from the oxygen balance, assuming that all of the oxygen not observed in the produced gases reacted to form water.

Losses due to liquid handling during downstream separation and liquids in lines are another source of errors. Determining oil saturation in the unburned section of the pack is also a source of error in the liquid mass balance because of the very small fractions of the material.

Table D.1

Liquid Material Balance

Run No.	1	2	3	4	5	6	7	8	9	10	11	12	13	14	15	16	17	18	19	20
Oil Balance (gms)																				
Initial oil in pack	250.5	245.9	281.7	272.0	270.4	262.2	266.8	258.1	270.4	258.3	251.4	139.6	265.0	265.7	276.7	264.7	263.1	266.8	266.8	264.6
Oil produced	177.0	168.8	213.8	211.2	169.1	166.3	183.7	183.2	153.9	190.6	153.1	57.6	152.1	155.3	175.7	144.3	152.0	165.9	137.3	134.0
Fuel consumed	25.9	30.2	29.0	42.2	34.5	33.4	33	36.1	50.4	43.0	29.3	48.3	26.5	65.5	42.4	56.0	32.8	36.0	54.1	37.3
Unburned fuel	31.2	20.5	18.5	15.0	25.4	38.3	23.5	21.8	29.7	19.7	37.8	30.3	35.0	25.0	32.7	38.0	39.5	34.5	33.3	45.0
Oil in lines	12.0	13.0	14.7	10.0	17.8	18.2	14.3	11.6	21.4	12.0	19.6	13.8	22.0	12.3	15.4	15.3	20.2	15.5	20.0	22.7
Total	246.1	232.5	276.0	278.4	246.8	256.2	254.5	252.7	255.4	265.3	239.8	150.0	235.6	258.1	266.2	253.6	244.5	251.9	244.7	239
Difference	4.4	13.4	5.7	-6.4	23.6	6	12.3	5.4	15.0	-7.0	11.6	-10.4	29.4	7.6	10.5	11.1	18.6	14.9	22.1	25.6
Error in balance (%)	1.76	5.45	2.02	2.35	8.73	2.29	4.61	2.09	5.5	2.71	4.61	7.45	11.09	2.86	3.79	4.19	7.07	5.58	8.28	9.67
Water Balance (gms)																				
Initial water in pack	71.6	65.6	83.9	68.6	80.0	67.9	68.7	74.8	68.2	75.2	62.5	0.0	50.0	67.1	67.2	62.2	65.7	63.0	63.6	68.2
Water injected	274.4	324.3	349.3	375.8	404	349.3	400.8	474.0	349.3	0.0	349.3	523.9	199.6	0.0	199.6	224.5	250.5	250.5	399.2	299.4
Water formed by combustion	8.5	9.7	6.2	6.4	3.3	2.7	5.4	3.6	5.1	8.9	2.8	3.4	6.0	13.9	2.43	14.1	6.7	3.0	14.91	12.4
Total	354.5	399.6	439.4	450.8	487.3	419.9	474.9	552.4	422.6	84.1	414.6	527.3	255.6	81.0	269.2	300.8	322.9	316.5	477.7	380
Water produced	283.1	320.6	342.0	386.7	380.5	304.2	441.7	534.3	389.0	58.6	386.6	495	183.6	41.0	203.1	247.0	280	248	389.4	311.5
Water as residue	13.8	26.9	19.1	15.0	28.5	27.1	24.4	20.3	25.4	12.6	19.7	20.3	13.6	10.5	13.0	10.5	12.3	30.3	29.9	22.3
Water in lines	40	40.7	37.5	35.0	37.0	40.5	31.5	35.0	32.7	23.1	29.5	31.0	25	21.3	28.8	20.2	17.8	15.0	16.4	18.1
Total	336.9	388.2	398.6	436.7	446.0	371.8	497.6	589.6	447.1	94.3	435.8	546.3	222.2	72.8	244.9	277.7	309.6	293.3	435.7	351.9
Difference	17.6	11.4	40.0	14.1	41.3	48.1	-22.7	-37.2	-13.5	-12.1	-21.2	-19	33.4	8.2	24.3	23.1	13.3	23.2	42	28.1
Error in balance (%)	4.96	2.85	9.28	3.13	8.48	11.46	4.78	6.73	3.11	14.39	5.11	3.60	13.07	10.12	9.04	7.68	4.12	7.33	8.79	7.39

Example 2

(1)	Oil:		(Weight in gm)	
	initial oil content of pack		= 250.5	(1)
	liquid oil produced		= 177.0	
	fuel consumed		= 25.9	
	residual fuel		= 31.2	
	liquid oil from lines		= 12.0	
		total	= 246.1	(2)
		difference: (1)-(2)	= 4.4	
		error in balance (%)	= 1.76	
(2)	Water:			
	initial water content of pack		= 71.6	
	water injected		= 274.4	
	water formed by combustion		= 8.5	
		total	= 354.5	(1)
	liquid water produced		= 283.1	
	residual water		= 13.8	
	liquid water from lines		= 40.0	
		total	= 336.9	(2)
		difference: (1)-(2)	= 17.6	
		error in balance (%)	= 4.96	

University of Bath

Library
Claverton Down
Bath BA2 7AY
Tel: (0225) 826826
Telex: 449097
Fax: (0225) 826229
Janet: library@uk.ac.bath.gdr
BT Gold(Lanet): 79:LLA2051

Sally

Bath. 826084.

with compliments